UNIVERSIDAD POLITÉCNICA DE MADRID
ESCUELA TÉCNICA SUPERIOR DE INGENIEROS INDUSTRIALES

Development of a methodology for nuclear data uncertainty propagation on isotopic evolution calculations for advanced nuclear systems

DOCTORAL DISSERTATION

Carlos Javier Díez de la Obra

Ingeniero Industrial
by Universidad Politécnica de Madrid

2014

DEPARTAMENTO DE INGENIERÍA NUCLEAR
ESCUELA TÉCNICA SUPERIOR DE INGENIEROS INDUSTRIALES

Development of a methodology for nuclear data uncertainty propagation on isotopic evolution calculations for advanced nuclear systems

Carlos Javier Díez de la Obra

Ingeniero Industrial
by Universidad Politécnica de Madrid

Thesis Director:

Dr. Óscar Luis Cabellos de Francisco
Professor of Nuclear Engineering
Universidad Politécnica de Madrid

2014

Tribunal nombrado por el Sr. D. Carlos Conde Lázaro Rector Magnífico de la Universidad Politécnica de Madrid, el de de 2014

Presidente
Secretario
Vocal
Vocal
Vocal
Suplente
Suplente

Realizado el acto de defensa y lectura de la tesis el día de de 2014 en la Escuela Técnica Superior de Ingenieros Industriales.

Calificación:

EL PRESIDENTE

LOS VOCALES

EL SECRETARIO

This work has been partially supported by "Ministerio de Educación, Cultura y Deporte (Ministry of Education)" of Spain with the FPU (Programa de Formación de Profesorado Universitario) teaching and researching formation program under grant AP2009-1801 for the PhD candidate. The research leading to these results has received funding from the European Atomic Energy Community's Seventh Framework Programme [FP7/2007-2013] under grant agreement #249671, (FP7-EURATOM-FISSION-2009:Project ANDES/249671).

Acknowledgements

This thesis will not have been possible with out the help and collaboration of many people and institutions, which I will try to recall in these lines. However, I do not forget any people who, in purpose or not, has helped me to keep on working on this thesis. For all of them, thanks!

First, I would like to mention and to give my sincerest gratitude to my thesis director, Dr. Óscar Cabellos. He accepted me even when I had worked for him before, and he has always trusted on me to perform and carry on any task, work or duty. I would like also to thank the Department of Nuclear Engineering and the Nuclear Fusion Institute, and their respective directors Eduardo Gallego and José Manuel Perlado, for providing me all the means necessary for performing this work.

Without the help and collaboration of the teams which I worked with during my stays abroad, I could have made this thesis real. In particular, I would like to thank Dimitri Rochman and Arjan Koning, from NRG, for hosting me in my first stay abroad, apart from introducing me in the nuclear data world and Linux/cluster field. In my second stay, at SCK·CEN, I would like to thank Alexey Stankovskiy and Gert van den Eynde for all their help and work, and also Peter Schillebeeckx and Jan Heyse from JRC-IRMM. Finally, I would like to thank Oliver Buss and Axel Hoefer for giving me the chance of a last stay abroad at AREVA, and for everything I have learnt from them (Viele Danke!).

I cannot forget all my foreign colleagues which I have worked with shoulder to shoulder to perform parts of this work: Luca Fiorito (SCK·CEN), Dr. Gasper Žerovnik (JSI), Chiara Ceresio (UPM), and my PhD colleague, and wingman, Jesús Salvador Martínez (UPM). And other colleagues who gave a hand checking and correcting this thesis as Dr. Toby Wright (MU), and again, Dr. Gasper Žerovnik (JSI).

Y ahora en español,

quiero agradecer de nuevo a Óscar todo su apoyo durante la tesis, su confianza plena en mi, y darle las gracias por darme todas las oportunidades tanto como para hacer estancias, como para exponer nuestros trabajos.

También quiero agradecer a todos los compañeros del departamento las risas y los buenos momentos vividos allí, que me motivaron para seguir a delante con el trabajo, especialmente a Angelo Ghiglino, Dra. Raquel Ochoa, Dr. Jose Javier Herrero, David Cereceda y de nuevo a Jesús Salvador Martínez. Y también agradecer a todos aquellos que me echaron una mano con el inglés (incluso con el castellano), en especial a: Ana, Rocio y Monse.

Y por último, quiero dedicarle esta tesis a mi familia: a mi padre Carlos y mis hermanos Cristina y Ricardo, por todo su apoyo y ayuda siempre incodicional; y darle las gracias a todos mis amigos, siempre cerca y atentos aún estando a veces tan lejos.

Resumen

Una apropiada evaluación de los márgenes de seguridad de una instalación nuclear, por ejemplo, una central nuclear, tiene en cuenta todas las incertidumbres que afectan a los cálculos de diseño, funcionanmiento y respuesta ante accidentes de dicha instalación. Una fuente de incertidumbre son los datos nucleares, que afectan a los cálculos neutrónicos, de quemado de combustible o activación de materiales. Estos cálculos permiten la evaluación de las funciones respuesta esenciales para el funcionamiento correcto durante operación, y también durante accidente. Ejemplos de esas respuestas son el factor de multiplicación neutrónica o el calor residual después del disparo del reactor. Por tanto, es necesario evaluar el impacto de dichas incertidumbres en estos cálculos.

Para poder realizar los cálculos de propagación de incertidumbres, es necesario implementar metodologías que sean capaces de evaluar el impacto de las incertidumbres de estos datos nucleares. Pero también es necesario conocer los datos de incertidumbres disponibles para ser capaces de manejarlos.Actualmente, se están invirtiendo grandes esfuerzos en mejorar la capacidad de analizar, manejar y producir datos de incertidumbres, en especial para isótopos importantes en reactores avanzados. A su vez, nuevos programas/códigos están siendo desarrollados e implementados para poder usar dichos datos y analizar su impacto. Todos estos puntos son parte de los objetivos del proyecto europeo ANDES, el cual ha dado el marco de trabajo para el desarrollo de esta tesis doctoral.

Por tanto, primero se ha llevado acabo una revisión del estado del arte de los datos nucleares y sus incertidumbres, centrándose en los tres tipos de datos: de decaimiento, de rendimientos de fisión y de secciones eficaces. A su vez, se ha realizado una revisión del estado del arte de las metodologías para la propagación de incertidumbre de estos datos nucleares.

Dentro del Departamento de Ingeniería Nuclear (DIN) se propuso una metodología para la propagación de incertidumbres en cálculos de evolución isotópica, el Método Híbrido. Esta metodología se ha tomado como punto de partida para esta tesis, implementando y desarrollando dicha metodología, así como extendiendo sus capacidades. Se han analizado sus ventajas, inconvenientes y limitaciones. El Método Híbrido se utiliza en conjunto con el código de evolución isotópica ACAB, y se basa en el muestreo por Monte Carlo de los datos

nucleares con incertidumbre. En esta metodología, se presentan diferentes aproximaciones según la estructura de grupos de energía de las secciones eficaces: en un grupo, en un grupo con muestreo correlacionado y en multigrupos. Se han desarrollado diferentes secuencias para usar distintas librerías de datos nucleares almacenadas en diferentes formatos: ENDF-6 (para las librerías evaluadas), COVERX (para las librerías en multigrupos de SCALE) y EAF (para las librerías de activación).

Gracias a la revisión del estado del arte de los datos nucleares de los rendimientos de fisión se ha identificado la falta de una información sobre sus incertidumbres, en concreto, de matrices de covarianza completas. Además, visto el renovado interés por parte de la comunidad internacional, a través del grupo de trabajo internacional de co-operación para evaluación de datos nucleares (WPEC) dedicado a la evaluación de las necesidades de mejora de datos nucleares mediante el subgrupo 37 (SG37), se ha llevado a cabo una revisión de las metodologías para generar datos de covarianza. Se ha seleccionando la actualización Bayesiana/GLS para su implementación, y de esta forma, dar una respuesta a dicha falta de matrices completas para rendimientos de fisión.

Una vez que el Método Híbrido ha sido implementado, desarrollado y extendido, junto con la capacidad de generar matrices de covarianza completas para los rendimientos de fisión, se han estudiado diferentes aplicaciones nucleares. Primero, se estudia el calor residual tras un pulso de fisión, debido a su importancia para cualquier evento después de la parada/disparo del reactor. Además, se trata de un ejercicio claro para ver la importancia de las incertidumbres de datos de decaimiento y de rendimientos de fisión junto con las nuevas matrices completas de covarianza. Se han estudiado dos ciclos de combustible de reactores avanzados: el de la instalación europea para transmutación industrial (EFIT) y el del reactor rápido de sodio europeo (ESFR), en los cuales se han analizado el impacto de las incertidumbres de los datos nucleares en la composición isotópica, calor residual y radiotoxicidad. Se han utilizado diferentes librerías de datos nucleares en los estudios antreriores, comparando de esta forma el impacto de sus incertidumbres. A su vez, mediante dichos estudios, se han comparando las distintas aproximaciones del Método Híbrido y otras metodologías para la porpagación de incertidumbres de datos nucleares: Total Monte Carlo (TMC), desarrollada en NRG por A.J. Koning y D. Rochman, y NUDUNA, desarrollada en AREVA GmbH por O. Buss y A. Hoefer. Estas comparaciones demostrarán las ventajas del Método Híbrido, además de revelar sus limitaciones y su rango de aplicación.

Abstract

For an adequate assessment of safety margins of nuclear facilities, e.g. nuclear power plants, it is necessary to consider all possible uncertainties that affect their design, performance and possible accidents. Nuclear data are a source of uncertainty that are involved in neutronics, fuel depletion and activation calculations. These calculations can predict critical response functions during operation and in the event of accident, such as decay heat and neutron multiplication factor. Thus, the impact of nuclear data uncertainties on these response functions needs to be addressed for a proper evaluation of the safety margins.

Methodologies for performing uncertainty propagation calculations need to be implemented in order to analyse the impact of nuclear data uncertainties. Nevertheless, it is necessary to understand the current status of nuclear data and their uncertainties, in order to be able to handle this type of data. Great efforts are underway to enhance the European capability to analyse/process/produce covariance data, especially for isotopes which are of importance for advanced reactors. At the same time, new methodologies/codes are being developed and implemented for using and evaluating the impact of uncertainty data. These were the objectives of the European ANDES (Accurate Nuclear Data for nuclear Energy Sustainability) project, which provided a framework for the development of this PhD Thesis.

Accordingly, first a review of the state-of-the-art of nuclear data and their uncertainties is conducted, focusing on the three kinds of data: decay, fission yields and cross sections. A review of the current methodologies for propagating nuclear data uncertainties is also performed.

The Nuclear Engineering Department of UPM has proposed a methodology for propagating uncertainties in depletion calculations, the Hybrid Method, which has been taken as the starting point of this thesis. This methodology has been implemented, developed and extended, and its advantages, drawbacks and limitations have been analysed. It is used in conjunction with the ACAB depletion code, and is based on Monte Carlo sampling of variables with uncertainties. Different approaches are presented depending on cross section energy-structure: one-group, one-group with correlated sampling and multi-group. Differences and applicability criteria are presented. Sequences have been developed for using different nuclear data

libraries in different storing-formats: ENDF-6 (for evaluated libraries) and COVERX (for multi-group libraries of SCALE), as well as EAF format (for activation libraries).

A revision of the state-of-the-art of fission yield data shows inconsistencies in uncertainty data, specifically with regard to complete covariance matrices. Furthermore, the international community has expressed a renewed interest in the issue through the Working Party on International Nuclear Data Evaluation Co-operation (WPEC) with the Subgroup (SG37), which is dedicated to assessing the need to have complete nuclear data. This gives rise to this review of the state-of-the-art of methodologies for generating covariance data for fission yields. Bayesian/generalised least square (GLS) updating sequence has been selected and implemented to answer to this need.

Once the Hybrid Method has been implemented, developed and extended, along with fission yield covariance generation capability, different applications are studied. The Fission Pulse Decay Heat problem is tackled first because of its importance during events after shutdown and because it is a clean exercise for showing the impact and importance of decay and fission yield data uncertainties in conjunction with the new covariance data. Two fuel cycles of advanced reactors are studied: the European Facility for Industrial Transmutation (EFIT) and the European Sodium Fast Reactor (ESFR), and response function uncertainties such as isotopic composition, decay heat and radiotoxicity are addressed. Different nuclear data libraries are used and compared. These applications serve as frameworks for comparing the different approaches of the Hybrid Method, and also for comparing with other methodologies: Total Monte Carlo (TMC), developed at NRG by A.J. Koning and D. Rochman, and NUDUNA, developed at AREVA GmbH by O. Buss and A. Hoefer. These comparisons reveal the advantages, limitations and the range of application of the Hybrid Method.

Contents

List of Figures

List of Tables

Abbreviations

Technological

ADS	Accelerator Driven System
ASAP	Adjoint Sensitivity Analysis Procedure
BOC	Beginning of Cycle
BOL	Beginning of Life
C/E	Calculated / Experiment
CFY	Cumulative Fission Yield
ChFY	Chain Fission Yield
CR	Control Rod
CUP	Covariance Uncertainty Propagation
DH	Decay Heat
EAF	European Activation File
EFIT	European Facility for Industrial Transmutation
ENDF	Evaluated Nuclear Data File
EOC	End of Cycle
EOL	End of Life
ESFR	European Sodium Fast Reactor
FA	Fuel Assembly
FP	Fission Product
FPDH	Fission Pulse Decay Heat
FSAP	Forward Sensitivity Analysis Procedure
FY	Fission Yield
GLS	General Least Squares
HFP	Hot Full Power
HM	Hybrid Method

IFY	Independent Fission Yield
JEFF	Joint Evaluated Fission and Fusion
JENDL	Japanese Evaluated Nuclear Data Library
LHS	Latin Hypercube Sampling
LWR	Light Water Reactor
MA	Minor Actinides
MC	Monte Carlo
MFY	Mass Fission Yield
MPP	Most Probable Point
ND	Nuclear Data
ODE	Ordinary Differential Equations
PCE	Polynomial Chaos Expansion
PDF	Probability Density Function
PWR	Pressurised Water Reactor
RDD	Radioactive Decay Data
rel.std.dev.	Relative standard deviation
RRR	Resolved Resonance Region
std.dev.	Standard deviation
SVD	Single Value Decomposition
TAGS	Total Absorption Gamma-ray Spectrometry
TMC	Total Monte Carlo
TMI	Three Mile Island
UAM	Uncertainty Analysis in Modelling
unc.	uncertainty
UQ	Uncertainty Quantification
URR	Unresolved Resonance Region
XS	Cross section

Institutional

ANDES	Accurate Nuclear Data for nuclear Energy Sustainability
BNL	Brookhaven National Laboratory
CCFE	Culham Centre for Fusion Energy
CEGB	Central Electricity Generating Board

CHANDA	CHAllenges in Nuclear DAta
CSEWG	Cross Section Evaluation Working Group
CSN	Consejo de Seguridad Nuclear
DIN	Departamento de Ingeniería Nuclear
EU	European Union
EUROTRANS	EUROpean Research Programme for the TRANSmutation of high level nuclear waste in an accelerator driven system
GRS	Gesellschaft für Anlagen- und Reaktorsicherheit
JAEA	Japan Atomic Energy Agency
JNDC	Japanese Nuclear Data Committee
KIT	Karlsruhe Institute of Technology
LANL	Los Alamos National Laboratory
LLNL	Lawrence Livermore National Laboratory
NEA	Nuclear Energy Agency
NNDC	National Nuclear Data Center
NNL	National Nuclear Laboratory
NRG	Nuclear Research and consultancy Group
OECD	Organisation for Economic Co-operation and Development
ORNL	Oak Ridge National Laboratory
PSI	Paul Scherrer Institute
SCK•CEN	StudieCentrum voor Kernenergie • Centre d'Etude de l'Energie Nucléaire
SNL	Sandia National Laboratory
UKAEA	UK Atomic Energy Authority
UPM	Universidad Politécnica de Madrid
USDOE	United States Department of Energy
WPEC	Working Party on International Nuclear Data Evaluation Co-operation

Chapter 1

Introduction

1.1 Thesis origin

Safety margins guarantee the safe performance of nuclear facilities during operation and after an event. These safety margins are designed to take into account all the uncertainties introduced throughout the designing stage, such as uncertainties on the engineering designs, model uncertainties, data uncertainties used on the design, build-up and operation, etc. The impact of these uncertainties are analysed through Uncertainty Quantification (UQ) studies, which yield a better understanding of uncertainties, identifying weak points that need to be reinforced or reducing the need for very conservative safety assumptions. This produces more realistic analyses and improvements in competitiveness. For these reasons, new methodologies are constantly being developed to yield accurate estimations of safety margins including uncertainties.

Nuclear data uncertainties have an impact on safety margins as they affect core neutronics, fuel depletion and material activation calculations. They may arise from limited measurement precision and/or modelling uncertainties, e.g. in regions where insufficient experimental data are available. This translates into uncertainties in the results of nuclear transport/depletion codes, which are thus only meaningful when being supplemented with uncertainty estimates.

Great efforts are underway to enhance the European capability to analyse/handle/produce covariance data, especially for isotopes which are of importance for advanced reactors, but

also for "the big three" – ^{235}U, ^{238}U and ^{239}Pu, and to address their impact in relevant performance parameters such as the effective neutron multiplication coefficient (k_{eff}), fuel composition throughout depletion/burn-up, radiotoxicity and decay heat during cooling time. These efforts have been translated into European Projects, first with EUROTRANS (EUROpean Research Programme for the TRANSmutation of high level nuclear waste in an accelerator driven system) from 2004 - 2009, followed by ANDES (Accurate Nuclear Data for nuclear Energy Sustainability) between 2009 - 2013, and continuing with CHANDA (CHAllenges in Nuclear DAta) from 2013 to 2016, with all of which Universidad Politécnica de Madrid (UPM) is involved.

In these projects, to analyse the impact of nuclear data uncertainties on isotopic composition, uncertainty propagating methodologies – in particular the Hybrid Method (HM) [García-Herranz et al., 2008], based on Monte Carlo sampling – were initially implemented in the ACAB depletion code [Sanz et al., 2008]. This led to preliminary Uncertainty Quantification (UQ) studies on activation/transmutation/depletion calculations for advanced reactors [Álvarez-Velarde et al., 2009, García-Herranz et al., 2008], where the performance of different nuclear data libraries and their uncertainties were also compared. Uncertainties from other nuclear data apart from cross section: fission yields and decay data, began to be introduced in UQ studies with HM [Cabellos et al., 2011b]. However, these implementations were at an early stage of development, so new capabilities and improvements can be introduced. Further investigations on the applicability of HM are also required.

Finally, in the international nuclear data community, more and more nuclear data libraries are including uncertainty information, which is usually updated with new releases. Keeping track of the content and state-of-the-art of nuclear data uncertainties is of importance, because explanations of the different performance of such libraries and their uncertainties on UQ studies rely on the underlying information.

1.2 Objectives and original contributions

The aim of this thesis is to develop and to improve the Hybrid Method, with the ACAB depletion code, and to analyse its range of applicability and its limitations. This is done by means of comparisons with other methodologies and UQ studies using HM on different applications. In addition, different nuclear data libraries are studied, and their uncertainties

compared, not only at origin but also in their impact on different applications. Lacks of data or inconsistencies in nuclear data uncertainties are investigated, and whenever possible, modifications or solutions are proposed with their corresponding application cases.

This study falls within the framework of the ANDES project, specifically Work Package (WP) 2, and the tasks, milestones, and especially the deliverables of the WP inform this work.

The original contributions of this thesis, with the references where they have been published, are:

- Comparison between cross section uncertainties from EAF-2007, EAF-2010 and SCALE6.0, under different neutron spectra: PWR, ADS and DEMO. [Díez et al., 2012] [Cabellos et al., 2011a]
- Development and implementation of a HM approach using correlated sampling with one-group cross sections, after reviewing HM and identifying issues of applicability to depletion problems with more-than-one depletion/burn-up steps [Díez et al., 2014b, Mills et al., 2013]
- Development and implementation of a HM approach using multi-group cross sections to tackle problems with more-than-one depletion/burn-up steps. [Díez et al., 2014c]
- Development and implementation of a sequence for using the COVERX nuclear data format with HM/ACAB in one-group and in multi-group approaches with a review of the sequences for generating cross section data for ACAB from EAF and ENDF-6 format. [Díez et al., 2013a, Díez et al., 2014c]
- Implementation of a Bayesian/GLS method for fission yield covariance generation, followed by a review of methodologies suitable for generating fission yield data covariances. [Fiorito et al., 2014, Cabellos et al., 2013]
- UQ studies with HM on Fission Pulse Decay Heat (FPDH) problems, propagating fission yield and decay data uncertainties, analysing the major contributors, identifying areas of missing nuclear data uncertainties in the JEFF-3.1.1 nuclear data library and assessing their impact, comparing the performance of different nuclear data libraries: JEFF-3.1.1 and ENDF/B-VII.1. [Díez et al., 2011, Fiorito et al., 2014, Cabellos et al., 2013]
- Evaluation of the effect of fission yield covariance data generated with a Bayesian/GLS method in FPDH calculations with HM. [Fiorito et al., 2014, Cabellos et al., 2013]

- Comparison between the HM and the Total Monte Carlo (TMC) methods for propagating cross section uncertainties in depletion calculations using uncertainties provided within covariance data or uncertainties in nuclear data parameters. [Díez et al., 2013a, Mills et al., 2013]

- Comparison between the HM and the NUDUNA methods, showing the importance of uncertainties in isotopic concentrations in transport calculations and the limitations of HM. [Díez et al., 2014a]

- Application of HM to a hypothetical burn-up case of a fuel pin-cell with large spectrum variations between burn-up steps. [Díez et al., 2014c]

- UQ study with HM for European Facility for Industrial Transmutation (EFIT) fuel cycle on isotopic composition, decay heat and radiotoxicity uncertainties due to cross section, fission yield and decay data uncertainties. [Cabellos et al., 2011b, Díez et al., 2014b, Cabellos et al., 2011a, Mills et al., 2013]

- UQ study with HM for European Sodium Fast Reactor (ESFR) fuel cycle on isotopic composition, due to cross section, fission yield and decay data uncertainties. [Díez et al., 2014b, Mills et al., 2013]

1.3 Structure

Part I presents the state-of-the-art of nuclear data used throughout this thesis, and current methodologies and codes/tools for propagating nuclear data uncertainties in activation/transmutation/depletion/burn-up calculations. Within this part, Chapter 2 shows the different nuclear data used: decay data, fission yield and cross section; with reviews of their state-of-the-art and comparisons between different nuclear libraries used in this thesis. The different formats used for storing nuclear data are also presented. Meanwhile, Chapter 3 presents how nuclear data uncertainties should be considered in depletion calculations, recalling different methodologies for performing UQ studies. Furthermore, detailed descriptions of the approaches applied are provided and compared later with the Hybrid Method.

Part II compiles the implementations and developments performed during this thesis. Chapter 4 reviews the methodology selected for performing UQ studies on depletion calculations – the Hybrid Method – and presents the implementations and developments carried out during

this thesis. The complete HM application sequence is shown, from the processing of nuclear data to the analysis of results, with a description of each stage. Chapter 5 provides a review of different methodologies for generating fission yield covariance data, and justifies their need. One methodology is selected and implemented to generate fission yield covariances, and its applicability is shown by generating examples of covariance data. These examples are used later in UQ studies.

Part III contains all the UQ studies and comparisons of methodologies with HM. Chapter 6 presents the UQ studies performed for: Fission Pulse Decay Heat (FPDH) calculations for ^{235}U and ^{239}Pu thermal fissions, European Facility for Industrial Transmutation (EFIT) fuel cycle and European Sodium Fast Reactor (ESFR) fuel cycle. After presenting the applications, Chapter 7 then shows the comparisons of HM with other methodologies: Total Monte Carlo under the EFIT framework, and NUDUNA under the framework of a typical PWR pin-cell burn-up problem. In addition, an hypothetical burn-up case with large spectrum variations between burn-up steps is studied in order to assess the limitations of HM.

Finally, Chapter 8 summarises the main achievements of this thesis and the main conclusions obtained from the different UQ studies conducted, regarding not only the methodologies applied but also the current status of uncertainty levels in the libraries used.

PART I

STATE-OF-THE-ART

Chapter 2

State-of-the-art of Nuclear Data Uncertainties

Abstract - This Chapter presents the different nuclear data and storing formats addressed and used throughout this thesis. Reviews of the state-of-the-art are performed for different libraries, and comparisons are conducted between libraries to analyse their differences. First, the content of the JEFF-3.1.1 library is reviewed concerning decay data and their uncertainties, and fission yield data and their uncertainties are analysed for major evaluated nuclear data libraries: ENDF/B-VII.1, JEFF-3.1.2 and JENDL-4.0. Finally, cross section data and their uncertainties provided within EAF-2007, EAF-2010 and SCALE6.0 are reviewed. Covariance data supplied within such libraries are processed and compared, and an additional comparison is carried out to show differences between one-group cross sections collapsed with different neutron spectra.

This chapter shows, partially or completely, works already presented in the following references:

- ANDES Deliverable D2.1 [Cabellos et al., 2011a].
- ANDES Deliverable D2.6 [Cabellos et al., 2013].
- International Journal Article [Fiorito et al., 2014].
- Web Conference Journal Article [Díez et al., 2012]

2.1 Introduction to nuclear data libraries

Nuclear data provide the information not only of how sub-atomic particles, for example neutrons and protons, interact with nuclei, but also of how radioactive nuclei decay. All the data involved in such interactions and in such decay processes are considered as nuclear data.

Such data are required, for example, to calculate the propagation of neutrons inside a nuclear reactor through the Boltzmann equation. This equation needs, as problem parameters, cross section data which measure the different interactions, such as scattering or capture, of sub-atomic particles with nuclei. Also, nuclear data are used for calculating the evolution of radioactive nuclei and other nuclei whose nature change due to interaction with sub-atomic particles. This evolution can be solved through the Bateman equations, which requires how nuclei change due to interactions with particles (cross section data) and how radioactive nuclei decay in time and in which mode, given as decay data. When a fission event takes place, because of an interaction between nucleus and particle or because it is the nucleus decay mode, fission yield data supply the formation probability information of possible nuclei, known as fission products.

Nuclear data libraries can store such data, and depending on the purpose of the library or the nuclear data stored, different kinds can be found: general-purpose evaluated nuclear data libraries, activation data libraries, transport data libraries, decay data libraries, etc; which can also use different storing formats. Major general-purpose evaluated nuclear data libraries are usually the most important because great efforts: economical, manpower and time; are spent in order to generate the best evaluations, where the best-estimated values are provided after reviewing experimental data, nuclear models, and the performance of such values on nuclear applications (benchmarks). However, other specific-purpose libraries can provide relevant data in the meantime, or specific for one kind of application, making use of the best what we have until new releases are provided.

Nuclear data are not free of uncertainties, they are evaluated through experimental data and nuclear models. So, therefore, they have a limited accuracy arsing from both limited measurement precision and limited modelling capability. These uncertainties are analysed and evaluated, and then, provided within the nuclear data. However, not always are uncertainty information given within nuclear data libraries and even they could lack in completeness or

provide inconsistent uncertainty data. Such issues can only be found once reviews of the libraries are performed.

Thus, within this thesis the main nuclear data are presented: decay data, fission yield and cross section; with reviews of nuclear data libraries from which data were retrieved during this thesis. Because uncertainties will be later propagated, special emphasis has been on uncertainties provided within libraries. Comparisons are carried out to find differences between libraries, and for later discussions on the performance of the libraries used.

2.2 Nuclear data libraries used

The major general-purpose evaluated nuclear data libraries used throughout this thesis are:

- The JEFF (Joint Evaluated Fission and Fusion) nuclear data library is an evaluated library which is produced by a coordinated group of the Nuclear Energy Agency (NEA) Data Bank, that belongs the Organisation for Economic Co-operation and Development (OECD). This library contains neutron and proton interaction data, radioactive decay data, fission yields, and thermal scattering law data. Its latest update was released in March 2014, with the JEFF-3.2 library [OECD/NEA Data Bank, 2014]. However, it is not included in this study. The JEFF library studied here is JEFF-3.1.2 [OECD/NEA Data Bank, 2012]. The only changes in JEFF-3.1.2 from JEFF-3.1.1 [Koning et al., 2011, Santamarina et al., 2009] are regarding cross section data, so JEFF-3.1.2 keeps the same decay and fission yield data as JEFF-3.1.1. Therefore, the JEFF-3.1.2 and JEFF-3.1.1 terms will be used indistinguishably when decay data or fission yield data coming from JEFF libraries are referenced.

- The ENDF/B evaluated nuclear data libraries is the results of a cooperative effort of the national laboratories, industry, and universities in the United States and Canada denominated The Cross Section Evaluation Working Group (CSEWG).The latest release was in December 2013 with the ENDF/B-VII.1 library [Chadwick et al., 2011], and it contains photonuclear, photo-atomic, radioactive decay, spontaneous fission yields, neutron fission yields, atomic relaxation, thermal scattering, standards, neutron interaction, electro-atomic interaction, proton interaction, deuteron interaction, triton interaction and ^{3}He interaction data. However, in this thesis, only decay, neutron fission yields and neutron interaction data are of interest.

- The JENDL (Japanese Evaluated Nuclear Data Library) nuclear data libraries are produced by the Nuclear Data Centre at the Japan Atomic Energy Agency (JAEA) with the aid of the Japanese Nuclear Data Committee (JNDC). The latest release is the JENDL-4.0 library [Shibata et al., 2011], which contains neutron interaction, fission yield, thermal scattering, photo-atomic and electro-atomic data. This latest release was updated through JENDL-4.0+, which does not exist any longer, and JENDL-4.0u [JAERI, 2013], where JENDL-4.0u provides corrections after nuclear data were partly revised from important and/or trivial error(s). JENDL-4.0 does not provide any Radioactive Decay Data (RDD) by itself, but such data are supplied with the JENDL Fission Product Decay Data File (JENDL/FPD), whose latest release is JENDL/FPD-2011 [Katakura, 2012].

- TENDL (TALYS-based Evaluated Nuclear Data Library) provides nuclear data based on the output of the TALYS nuclear model code system [Koning et al., 2013a] for direct use in both basic physics and applications. The latest version available is TENDL-2013 [Koning and Rochman, 2012, Koning et al., 2013b], the sixth release, which is based mainly on both default and adjusted TALYS calculations. It contains evaluations for seven types of incident particles, for all isotopes living longer than 1 second (about 2600 isotopes), up to 200 MeV, with covariances. TENDL is not a default or shadow library.

Other specific-purpose nuclear data libraries reviewed and used during this thesis are:

- SCALE6.0 cross section libraries, which are aimed to provide cross section data to transport codes within the SCALE6.0 tool suite [ORNL, 2009]. Special interest is in their covariance data, which supply covariance information between different cross section reactions, later called cross-correlations. This information is stored in COVERX format [ORNL, 2009, M18.A.6].

- The ORIGEN decay data library for SCALE6.0 [ORNL, 2009, Vol.III, Sec.M6], which contains nuclear decay data, neutron reaction cross sections, delayed photon yields and neutron emission data for the SCALE6.0 depletion code ORIGEN-S.

- The European Activation File (EAF) nuclear data library is a collection of nuclear data aimed at nuclide inventory calculations due to neutron or charged particle activation. Their latest releases EAF-2007 [Forrest, 2007] and EAF-2010 [Sublet et al., 2010] provide extensive uncertainty data for cross sections.

- The COMMARA-2.0 library [Herman et al., 2011] is aimed to provide cross section covariance data for advanced reactors. It has been developed by BNL-LANL collaboration for Advanced Fuel Cycle Initiative applications over the period of three years, 2008-2010. It contains cross section covariances for 110 materials relevant to fast reactor R&D. The library is to be used together with the ENDF/B-VII.0 [Chadwick et al., 2006] central values. Covariance data are given in 33-energy groups, from 10^{-5} eV to 19.6 MeV, obtained by processing with the NJOY processing code [MacFarlane and Kahler, 2010] using 1/E neutron spectrum. In addition to these 110 files, the library contains 20 files with fission neutron emission $\overline{\nu}$ covariances, 3 files with covariances for prompt fission neutron spectra (for ^{238,239,240}Pu), and 2 files with the average cosine of the elastic scattering angle $\overline{\mu}$ covariances (for ^{23}Na and ^{56}Fe). An important fact of this library is that no covariance data between different cross section reactions are provided.

2.3 Formats for storing nuclear data

The main characteristics for translating tasks of nuclear data formats, used within this thesis, are presented here. Because the COVERX format is converted into user-readable format before being processed or being analysed, it is not described here, but a complete description is provided in Ref. [ORNL, 2009, M18.A.6].

2.3.1 ENDF-6 format

Major evaluated nuclear data libraries supply their data in ENDF-6 format [CSEWG, 2012]. The structure of an ENDF-6 format tape/file is hierarchical and sketched in Fig. 2.1. Each tape/file contains a library which may have several sections representing different materials (MAT). The library type defines the incoming projectile, or if it is a decay data library. Each material section is structured into several so-called files (MF). The most relevant files for the applications studied during this thesis are files 1-8 and 31-35:

- File 1 (MF1) contains general information and the multiplicities of neutrons for prompt and delayed fission reactions, and other fission quantities.
- File 2 (MF2) contains resonance parameters.
- File 3 (MF3) contains background cross sections, which are cross section values that should be added to those provided by the resonance parameters.
- Files 4-6 (MF4-6) are used to store energy and angular distributions of final state particles.
- File 7 (MF7) contains thermal scattering data - S(α,β).
- File 8 (MF8) provides radioactive decay data and fission product yields.
- Files 31-35 (MF31-35) store the covariance information for MF1-5.

Each file contains sections (MT) providing information on a specific reaction type and the sections themselves are structured in several records (MR).

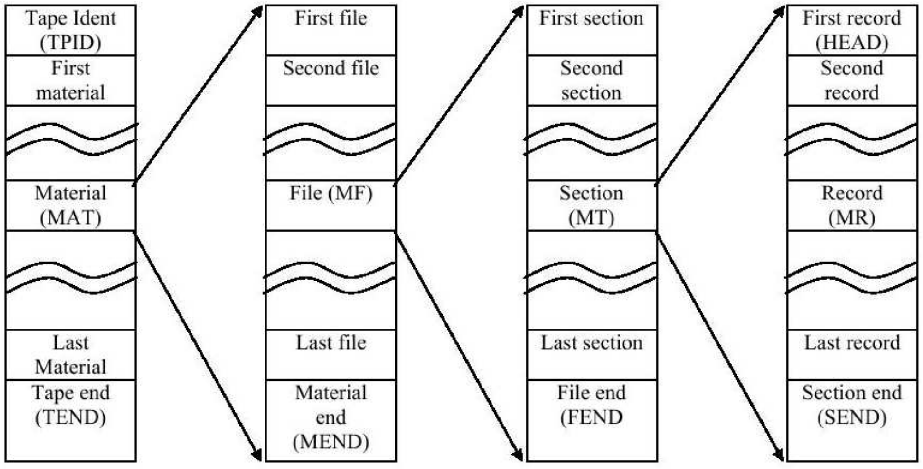

FIGURE 2.1: Structure of an ENDF-6 type tape/file. (From [CSEWG, 2012])

2.3.2 EAF format

There are two types of EAF formats [Sublet et al., 2010] for storing cross section data: point-wise and group-wise. Only the former is reviewed, because it is the only one used in this thesis. It consists essentially of the MF3 file of ENDF-5 format [Kinsey, 1979] (which ENDF-6 format is compatible with), with the following deviations:

- Two comment lines have been added at an earlier stage, stating the origin of data.
- The material number MAT consists of Z and the two last digits of A. To describe isomeric targets A has been increased by 50 or 70, first and second states, respectively.
- The identifiers LIS and LFS are used to indicate the (isomeric) states of the target and final nucleus, respectively. The convention adopted is that LFS = 99 means total production cross section; and LFS = 0, 1, or 2 means production of ground state, first and second isomeric state, respectively.
- The reaction nomenclature is as defined by ENDF, except that reaction numbers leading to isomeric states have been increased by 300 or 600 (again, for first and second isomeric states, respectively). The cross sections for one material number are ordered according to increasing MT numbers, except that cross sections leading to isomeric states follow immediately after the cross section leading to the ground state.

2.4 Decay data

Radioactive Decay Data (RDD) libraries are needed for burn-up/inventory/transmutation/ depletion calculations, because they provide the parameters (decay constants – half-lives, branching ratios, decay energies, etc) that drive the time evolution of radioactive isotopes and their energy release.

Such data carry uncertainties, whose values are usually found in the form of standard deviations (std.dev.) or relative standard deviations (rel.std.dev.). Major evaluated nuclear data libraries usually provide a RDD sub-library, that in ENDF-6 format is referred with `NSUB=4`.

Because of the usage of JEFF-3.1.1 RDD [Kellet et al., 2009] along this work, a review is performed in order to assess the decay data available. In addition, the uncertainty data included in such a library are analysed for further Uncertainty Quantification (UQ) calculations.

Note that there was no update of decay data from JEFF-3.1.1 to JEFF-3.1.2, so both refer to the same data.

2.4.1 Review of JEFF-3.1.1 RDD and their uncertainties

2.4.1.1 Data summary

This decay library contains data for 3852 isotopes, stored in ENDF-6 format, from neutron ($^{1}n_{0}$) to roentgenium ($^{272}Rg_{111}$), where 226 isotopes are stable. Spectral data are provided for 1521 nuclei. It collects every main possible decay mode: β^{+}, β^{-}, α, isomeric transition (IT), p, n, $2\beta^{-}$, $2\beta^{+}$, 2p, 2n, spontaneous fission (SF), and also, all basic nuclear properties of the stable isotopes (spin, parity, atomic weight), within their natural abundances. The total number of neutrons per fission ($\overline{\nu}_{total}$) – fission neutron emission – is included in this library for the 27 major spontaneous fissioning systems.

This library includes total absorption gamma-ray spectrometry (TAGS) measurements which try to avoid the "Pandemonium effect" [Hardy et al., 1977]. This effect provokes inaccurate determinations of the gamma and beta decay components, that leads to differences between simulations of decay heat and experimental data. However, not all decay energy data have been updated with such experiments, and also, last TAGS experimental data available [Algora et al., 2010] have not been yet included in JEFF-3.1.1 RDD.

Concerning which information is provided, the half-life values are supplied with their mean values and their relative uncertainties. Those marked with 100% uncertainty mean that no uncertainty was given in previous versions, so i.e. were a zero value instead. Those marked with "~" mean that their relative uncertainty is smaller than 0.01%. Decay energy values are provided with their mean values and their relative uncertainties as well.

2.4.1.2 Processing decay data libraries

First, half-life uncertainty values in JEFF-3.1.1 are addressed. Differences have been found between the content described in Ref. [Kellet et al., 2009] and the official ENDF-6 file for JEFF-3.1.1 ("JEFF311RDD.out", downloaded from www.oecd-nea.org). The origin of such differences comes from the isotopes whose uncertainties in the former source are of 100% or are not provided, because zero uncertainty is given for such isotopes in the latter source! That provokes also an additional inconsistency problem: the isotopes whose uncertainties are smaller than 0.01% in the former source have also zero uncertainty in the latter.

As mentioned previously, not all isotopes have an uncertainty for their decay energy. A study of which isotopes have no uncertainty data is important because they may change the final results of uncertainty propagation calculations. No uncertainty should be assumed as zero uncertainty, and therefore, uncertainty values will be proposed as a first approximation to quantify the importance of such isotopes. Such a suggestion can be based on the average values found for the decay energy uncertainties of each decay mode.

Then, the first task is to identify which isotopes have no uncertainty for their decay energy. Using a home-made program to read ENDF-6 files, all the information is retrieved and analysed.

Table 2.1 and Fig. 2.2 show the number of isotopes with no uncertainty for their decay energy modes, classified according to their half-lives. The bulk of these isotopes have a half-life between 10^3 s and 10^{-2} s. So, most of them are isotopes with a short half-life. In order to know which values of A and Z these isotopes have and their relationship with half-life values, Fig. 2.3 is presented. It shows in the x-axis the asymmetry $(A/Z - 1)$ and in the y-axis the half-life. Most of isotopes are grouped between 1 and 1.65 of asymmetry and from 10^3 s to 10^{-2} s of half-life. Hence, no uncertainties for decay energy are provided for neutron rich isotopes, which mainly undergo β^- decay.

TABLE 2.1: Number of isotopes with no uncertainty in their decay energy grouped by half-life bins. The upper limit of bins is in the left side, while the lower limit in the right side.

Group	$T_{1/2}$ (s)	Number of isotopes	$T_{1/2}$ (s)
1	a> 10^{7}	27	-
2	a< 10^{7}	7	a> 10^{6}
3	a< 10^{6}	18	a> 10^{5}
4	a< 10^{5}	55	a> 10^{4}
5	a< 10^{4}	113	a> 10^{3}
6	a< 10^{3}	250	a> 10^{2}
7	a< 10^{2}	302	a> 10^{1}
8	a< 10^{1}	360	a> 10^{0}
9	a< 10^{0}	370	a> 10^{-1}
10	a< 10^{-1}	283	a> 10^{-2}
11	a< 10^{-2}	133	a> 10^{-3}
12	a< 10^{-3}	36	a> 10^{-4}
13	a< 10^{-4}	9	a> 10^{-5}
14	a< 10^{-5}	8	a> 10^{-6}
15	a< 10^{-6}	22	a> 10^{-7}
16	a< 10^{-7}	78	-
Total		2071	

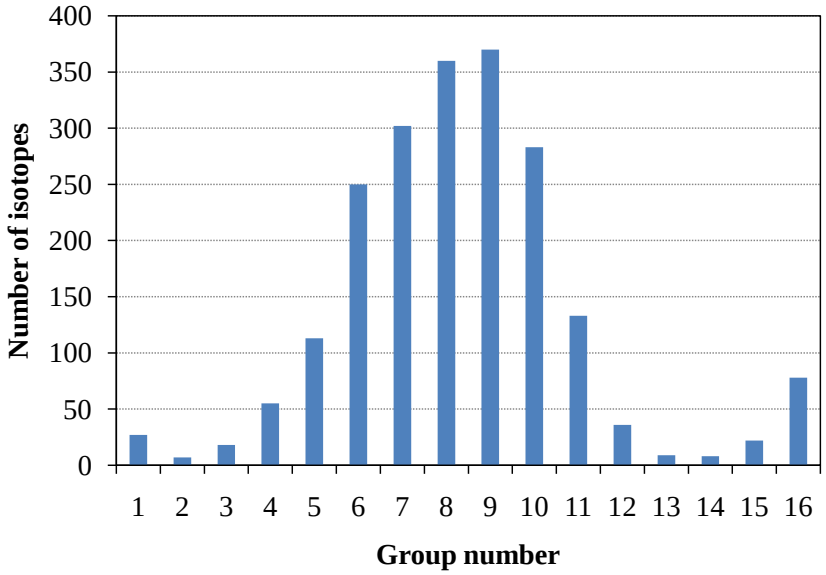

FIGURE 2.2: Number of isotopes with no uncertainty in their decay energy, classified in the groups given in Table 2.1.

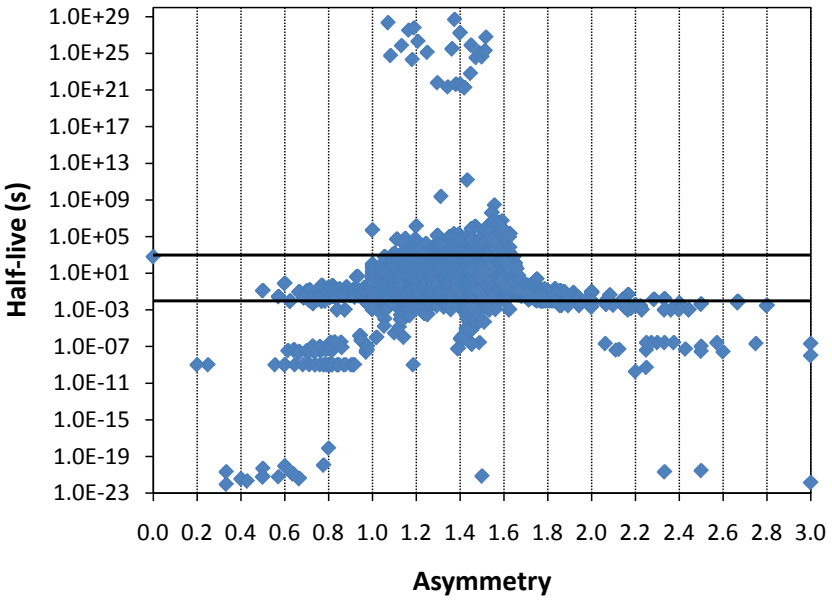

FIGURE 2.3: Distribution of isotopes with no uncertainty in their decay energies, plotted by half-life values and asymmetry (A/Z -1).

2.5 Fission yield data

Different sources/libraries can be used to retrieve fission yield data. Those sources can be completed or not with uncertainty data. Because, later, burn-up/depletion calculations will take place, fission yield data are going to be used. So, in order to understand differences between results from different libraries, comparisons among libraries are held before processing data for depletion/burn-up codes.

This section aims at summarising the main characteristics of the latest release of following main nuclear data libraries: ENDF/B-VII.1, JEFF-3.1.1 (whose data are copied in JEFF-3.1.2 and JEFF-3.2) and JENDL-4. A comparison of the data stored in such libraries, fission yield values and their uncertainties, is performed in this section for the ^{235}U thermal fission.

2.5.1 Fission yield data libraries

Fission Yields (FYs) characterise the probability of a particular nuclide or mass to be formed after fission. Accurate FY measurements and/or predictions, as well as the knowledge of the carried uncertainties, are essential to many applications in nuclear technology, and here in particular for depletion calculations. The most used general-purpose evaluated nuclear data libraries: JEFF, ENDF/B and JENDL, provide these data in the ENDF-6 format along

with their uncertainties as standard deviation. To date, no correlation between FYs is supplied in such libraries, but several institutions/projects are putting a great effort to develop methodologies to generate full covariance matrices.

Fission yield data from the latest release of the following libraries are compared:

- JEFF fission product yields data stored in the JEFF (and previously JEF) database come from the United Kingdom experiments pioneered at Harwell and reported by Crouch [Crouch, 1977]. His work was continued in the UKFY1 library and thus adopted by the first stage of the Joint Evaluated File, JEF1 [James, 1987]. Later on, a new evaluation of independent and cumulative yields has been prepared by James, Mills and Weaver which resulted in the new UKFY2 library, adopted for JEF2 [James et al., 1991]. Further on, in 2005, the completely revised third version JEFF-3.1 was made available and then updated with: Radioactive Decay Data and Fission Yields sublibraries from UKFY3, a database [Mills, 1995] of recent references produced after a thorough search of recent literature, and the international database EXFOR [Otuka et al., 2011]. The most recent release JEFF-3.1.2 (currently JEFF-3.2, but not released at the time when this work was carried out) takes its FY data from the previous JEFF-3.1.1, which is based upon the UKFY3.6A database.

- ENDF/B uses the 1989 LANL evaluation by England and Rider [England and Rider, 1994], initially transmitted to the ENDF/B-VI library. England and B.F. Rider work has been used later in ENDF/B-VII.0 (equal to ENDF/B-VI) [Chadwick et al., 2006]. In the latest version ENDF/B-VII.1, neutron fission yields were reevaluated for ^{239}Pu (fast and 14 MeV) by LANL to correct some errors identified in the England and Rider data [Chadwick et al., 2011]. The others were taken over from ENDF/B-VII.0.

- JENDL decay data for fission products were initially stored in the JENDL Fission Product Decay Data File 2000 (JENDL/FPD-2000) [Katakura et al., 2001]. From 2000 to 2011, the library has been renovated into JENDL/FPD-2011 [Katakura, 2012] with the addition of new measurements. Eventually, fission product yields were revised introducing the ENDF/B-VI Fission Product Yields database into the new library JENDL/FPY-2011 [Katakura, 2012], with modifications to have consistency with JENDL/FPD-2011, and conveyed to the last version JENDL-4. In addition to the extension of the number of independent yields, compared to the original ENDF/B version, to equal the amount

of nuclides present in JENDL/FPD-2011, cumulative fission product yields were calculated as well according to the decay chain of JENDL/FPD-2011.

Table 2.2 lists the data stored in the three libraries according to the fissioning nuclide and neutron energy. ENDF/B-VII.1 includes 60 sets of neutron FY data and provides FYs for heavy nuclides at different neutron energies. JENDL-4 resorts to the same evaluation as ENDF/B-VII.1, covering the same 60 sets of FYs, but includes ternary fission products, not handled in ENDF/B. JEFF-3.1.2 copies its data from JEFF-3.1.1, which stores 41 sets of FYs and includes ternary yields as well.

TABLE 2.2: Fission yield data available in ENDF/B-VII.1, JEFF-3.1.1 and JENDL-4 as function of the incident neutron energy: Thermal (T) (0.0253 eV), Fast (F) (500 keV), High-energy (H) (14 MeV) neutron fission and S for Spontaneous fission.

Nuclide	ENDF/B-VII.1	JEFF-3.1.1	JENDL-4
^{227}Th	T	-	T
^{229}Th	T	-	T
^{232}Th	FH	FH	FH
^{231}Pa	F	-	F
^{232}U	T	-	T
^{233}U	TFH	TFH	TFH
^{234}U	FH	FH	FH
^{235}U	TFH	TFH	TFH
^{236}U	FH	FH	FH
^{237}U	F	-	F
^{238}U	FHS	FH	FHS
^{237}Np	TFH	TF	TFH
^{238}Np	F	TF	F
^{238}Pu	F	TF	F
^{239}Pu	TFH	TF	TFH
^{240}Pu	TFH	F	TFH
^{241}Pu	TF	TF	TF
^{242}Pu	TFH	F	TFH
^{241}Am	TFH	TF	TFH
^{242m}Am	T	TF	T
^{243}Am	F	TF	F
^{242}Cm	F	S	F
^{243}Cm	TF	TF	TH
^{244}Cm	FS	TFS	FS
^{245}Cm	T	TF	T
^{246}Cm	FS	-	FS
^{248}Cm	FS	-	FS
^{249}Cf	T	-	T
^{250}Cf	S	-	S
^{251}Cf	T	-	T
^{252}Cf	S	S	S
^{253}Es	S	-	S
^{254}Es	T	-	T
^{254}Fm	S	-	S
^{255}Fm	T	-	T
^{256}Fm	S	-	S

2.5.2 Modelling

There exist different definitions of FYs:

The *Independent fission yield* (IFY), $y(A, Z, M)$, is defined as the number of atoms of nuclide with mass A, charge Z, and isomeric state M produced directly from one fission, after the emission of prompt neutrons, but before the emission of delayed neutrons. It can be written as the product of three factors:

$$y(A, Z, M) = Y(A)f(A, Z)r(A, Z, M), \tag{2.1}$$

where:

- $Y(A)$ represents the total *mass fission yield* (MFY), that is, the sum of independent fission yields of all fission products with mass number A, before delayed neutron emission.
- $f(A, Z)$ is the *fractional independent yield* of all isomers with mass A and charge Z.
- $r(A, Z, M)$ is called *isomeric yield ratio* and represents the fraction of fission products *(A,Z)* generated as isomeric state M.

To calculate IFYs the said coefficients need to be known for each fission system, but even those chains with the highest coverage of measured data do not provide values for all parameters. It is indeed necessary to resort to semi-empirical models and interpolation/extrapolation methods for both mass and fractional yields.

The *cumulative fission yield* (CFY) $C(A, Z, M)$ is the total number of atoms of nuclide with mass number A, charge Z and isomeric state M produced over all time after one single fission. That is, the total number of atoms of that nuclide generated both through one single direct fission and radioactive decay of all the precursors. CFYs have a strong relationship with fission products decay chains, which means that they can be calculated from IFYs and decay data branching fractions using what is so-called *Q-matrix* approach [James et al., 1991], represented by Eq. 2.2:

$$C_j = \sum_i Q_{i,j} y_i, \tag{2.2}$$

where $Q_{i,j}$ are the decay branching ratios from isotope i to j and y_i represents the IFY of isotope i of for the fission system studied. Therefore, Q, so-called also *Q-matrix*, is the matrix of the decay branching ratios that steers fission products toward stable nuclides.

The *chain fission yield* (ChFY) $Ch(A)$ is defined as the sum of cumulative yields of the last stable or long-lived chain members with same mass A and is obtained in classical mass spectrometric measurements of long lived and stable end products of mass chains. The term *chain yield* has been commonly used to describe both the sum of cumulative yields of the last stable or long-lived chain members, and the isobaric sum of independent yields (*mass yield*). The two definitions, even if slightly, may differ by a few per cent as the second does not include the contribution of delayed-neutron emission [Mills, 1995].

All the three evaluated libraries store the recommended independent and cumulative fission yields with their uncertainties, whereas the chain yields are provided only in the literature.

Because of the lack of a full and complete database of measurements for IFYs, several models and methodologies are used in order to supply such missing data. Empirical models have been developed because predictions using purely theoretical models for the fission process are not sufficiently accurate and reliable for applied purposes [IAEA, 2001]. Models are used in evaluations to obtain numerical values where no yields have been measured, or to check and adjust experimental data to the expected distribution of yields. Information on the models used in the studied evaluations are reported in Table 2.3.

TABLE 2.3: Models and methodologies used in ENDF/B-VII.1, JEFF-3.1.1 and JENDL-4 for generating independent fission yields.

	ENDF/B-VII.1	JEFF-3.1.1	JENDL-4
$Y(A)$	Summation of Gaussian functions	Summation of Gaussian functions	Summation of Gaussian functions
$f(A,Z)$	Z_P model by Wahl + odd/even effect	Z_P model by Wahl + odd/even effect	Z_P model by Wahl + odd/even effect
$r(A,Z,M)$	Madland & England model + 50/50 split	Madland & England model	Madland & England model
Ternary yields	Not treated (Z_P model corrected)	Serot, *et. al* + UKFY3.6A	England & Rider + Mills

Model distribution for $Y(A)$ for MFYs can be fitted approximately by a summation of Gaussian functions [Musgrove et al., 1973]. This technique resorts to the apparent similarity of the mass yield distributions to Gaussian distributions and can be used to predict those fission yields which do not have any experimental value. Good results have been obtained by summing up to a total of five Gaussian functions: two for each peak of probability plus one for the near-symmetric fissions. The modelled functions were fitted to the chain yield experimental values, after having reduced the 15 parameters representing the five Gaussians (strength, mean and width for each Gaussian) to 8 by imposing a set of constraints [Katakura, 2003]. Under some circumstances, it has been demonstrated that this number of parameters can be reduced to two [IAEA, 2001].

Fractional independent yields $f(A, Z)$ are predicted by the empirical Z_P Wahl model [Wahl, 1985, Wahl, 1988], since only a small fraction of the yields have been measured and theoretical models are not sufficiently advanced to give reliable yield estimates [Wahl, 2002]. The model is properly adjusted to take into account the odd-even effect in the fission product distribution, since the yields of nuclides with even atomic and/or neutron number are enhanced. Fractional yields are normalised such that $\sum_Z f(A, Z) = 1$ for all A. In the ENDF/B library, the said model was further modified because ternary fissions are not considered. Thus, the small amount of charge carried away by the ternary products was reintegrated into the system for a correct charge balance [England and Rider, 1994].

The ratio of isomeric yield $r(A, Z, M)$ is modelled with the main predictive model available in [Madland and England, 1976], or its further development in [Rudstam, 1992], which gives the yield of each isomer as a non-linear function of its angular momentum. ENDF/B-VII.1 uses this latter model, except when direct measurements are provided or the angular momentum is not known. In the last case, IFYs are arbitrarily divided equally between the ground state and short half-life metastable states: in several measured cases like ^{133}Xe, ^{135}Xe and ^{133}Te, the short half-life metastable state is favored [England and Rider, 1994].

Only JENDL-4 and JEFF-3.1.1 libraries cover ternary fission product yields. JENDL-4 provides them by consulting the England and Rider compilation [England and Rider, 1994] and Mills' one [Mills, 1995]. The element yields are taken from those of England and Rider compilation and the mass distribution of the element is calculated using the Mills compilation, as stated in [Katakura, 2012]. Meanwhile, JEFF-3.1.1 uses Serot work [Serot et al., 2005] for the evaluation of the principal ternary product yields ^{4}He and ^{3}H, and extends to the other

nuclides including evaluated files from UKFY3.6A database [Kellet et al., 2009]. ENDF/B does not handle the ternary fission and the Wahl Z_P model is corrected accordingly.

2.5.3 Fission yield data comparison

IFYs are provided by every studied library, after measurements and corrections or predictions through models, as recommended values, along with their uncertainties. ENDF/B, JEFF and JENDL nuclear data come from different experimental databases and/or models and approximations, therefore whether the libraries are consistent, or discrepancies occur, is analysed. Here only thermal neutron induced fission yields are studied, referring them with the "thermal fission" term.

For the ^{235}U thermal fission, JENDL-4 and JEFF-3.1.1 IFYs greater than 1% have an average of ∼10% discrepancy between libraries, while for those between 0.5 and 1% the difference (on average) increases up to ∼20%. Lower yields show even higher discrepancies. FPs, which have large fission yield values and large discrepancies between libraries, either have extremely long half-life values, such that in practical applications it is reasonable to discard them, or give a negligible contribution in terms of nuclear operations and computations, e.g. low decay heat or radiotoxicity. Similar conclusions come out when comparing JEFF-3.1.1 and ENDF/B-VII.1, while the latter and the JENDL-4 library generally present a good agreement as they mainly originate from the same source. The average discrepancy between ENDF/B-VII.1 and JENDL-4 IFYs is $< 1\%$, but it increases significantly for FPs with one or more metastable states because of the different methodologies of evaluation. Analogous behaviours arise when comparing IFYs for other fissioning systems or energies.

CFYs in JEFF-3.1.1 are copied from UKFY3.6A, which uses Eq. 2.2 to calculate CFYs from IFYs with decay branching ratios processed from JEFF-3.1.1 RDD [Kellet et al., 2009]. Similarly, CFYs in JENDL-4 are the sum of IFYs and all the precursor nuclides, with branching ratios taken from the JENDL/FPD-2011 file [Katakura, 2012]. ENDF/B calculates CFYs from IFYs by tracing the decay chain of each isotope toward the stable nucleus with consistent decay constants and half-life values as described in [England and Rider, 1994]. However, ENDF/B-VII.1 updated FYs for ^{239}Pu fast and high energy fissions [Chadwick et al., 2011] using a bayesian approach (presented in Chapter 5).

The comparison of IFYs and CFYs, reported in Table 2.4 for a selection of FPs of importance for the standard fission reaction of ^{235}U [IAEA, 2001], shows an example of the differences between evaluations. JENDL and ENDF/B agree for the most of CFYs: large discrepancies occur only in correspondence of isotopes with metastable states. On the contrary, these reference yields show extremely large differences between JEFF-3.1.1 and ENDF/B-VII.1 (or JENDL-4), with two thirds of all the selected yields carrying a relative difference higher than 1%, and relative differences higher than 10% are found for a third. However, the largest discrepancies generally appear for nuclides with very small fission yields. Therefore a good agreement between libraries is reached for largest fission yield values. Meanwhile, for small fission yield values, large differences appear because of the discrepancies between the different experimental data used in each library. Such discrepancies come from the difficulties of measuring very small fission yield values.

TABLE 2.4: Comparison of reference IFYs and CFYs of ^{235}U thermal fission for ENDF/B-VII.1, JEFF-3.1.1 and JENDL-4. Values are reported as relative differences in absolute values. IFYs of ^{129}I, ^{105}Pd, ^{107}Pd, ^{147}Sm are zeros in all the libraries. Only ENDF/B-VII.1 and JENDL-4 provide non-null IFYs for ^{143}Nd.

	ENDF/B-VII.1 fission yields (%)		differences (%) $\frac{\|\text{JEFF}-\text{ENDF/B}\|}{\|\text{ENDF/B}\|}$		$\frac{\|\text{JENDL}-\text{ENDF/B}\|}{\|\text{ENDF/B}\|}$	
Nuclide	IFY	CFY	IFY	CFY	IFY	CFY
^{109}Ag	-	0.03	-	7.87	-	0.31
^{85}As	0.12	0.22	15.98	34.69	0.16	6.44
^{88}Br	1.39	1.78	6.31	2.12	0.15	2.23
^{89}Br	1.04	1.09	24.55	25.11	0.15	0.17
^{90}Br	0.55	0.56	13.84	13.79	0.16	0.12
^{91}Br	0.22	0.22	32.45	32.38	0.13	0.13
^{97}Br	3.44E-10	3.44E-10	108.29	108.29	0.15	0.15
^{144}Ce	0.03	5.50	0.44	0.46	0.15	0.15
^{133}Cs	7.92E-07	6.70	78.87	1.53	0.15	0.14
^{134}Cs	3.85E-06	7.71E-06	33.53	57.35	15.02	0.15
^{135}Cs	2.45E-04	6.54	24.6	1.27	24.01	0.24
^{136}Cs	2.77E-03	0.01	63.08	5.43	25.81	0.15
^{137}Cs	0.06	6.19	20.42	0.53	0.15	0.21
^{153}Eu	2.33E-07	0.16	94.14	6.7	0.15	0.19
^{154}Eu	9.70E-08	1.94E-07	5.91	0.66	5.04	0.15
^{154m}Eu	9.70E-08	1.94E-07	4.59	4.81	5.34	5.34
^{155}Eu	2.63E-06	0.03	11.84	4	0.15	0.18
^{156}Eu	1.62E-05	0.01	1.14	10.2	0.15	0.15
^{155}Gd	4.08E-10	0.03	60.52	4	0.15	0.18

Continued on next page

Table 2.4 – continued from previous page

	ENDF/B-VII.1 fission yields (%)		differences (%) $\frac{\|JEFF-ENDF/B\|}{\|ENDF/B\|}$		differences (%) $\frac{\|JENDL-ENDF/B\|}{\|ENDF/B\|}$	
Nuclide	IFY	CFY	IFY	CFY	IFY	CFY
^{129}I	-	0.54	-	29.97	-	0.02
^{137}I	2.62	3.07	18.12	16.37	0.15	0.2
^{138}I	1.42	1.49	2.98	1.12	0.15	0.17
^{139}I	0.77	0.78	23.59	23.1	0.14	0.03
^{140}La	0.01	6.22	90.12	1.53	0.15	0.18
^{95}Mo	4.94E-10	6.50	66.2	0.02	0.15	0.1
^{97}Mo	2.49E-06	6.00	39.66	0.05	0.15	0.8
^{143}Nd	4.80E-12	5.96	100	0	0.15	0.13
^{145}Nd	5.55E-08	3.93	32.23	0.27	0.15	0.16
^{105}Pd	-	0.96	-	1.94	-	0.62
^{107}Pd	-	0.15	-	4.72	-	0.27
^{147}Pm	2.49E-09	2.25	39.36	0.65	0.15	0.19
^{148}Pm	4.45E-09	4.82E-09	898.52	929.84	15.8	13.88
^{148m}Pm	8.10E-09	8.10E-09	1184.91	1184.91	8.45	8.45
^{93}Rb	3.07	3.55	0.72	0.25	0.15	0.15
^{94}Rb	1.57	1.65	10.74	0	0.15	0.13
^{95}Rb	0.76	0.77	15.11	14.57	0.16	0.35
^{103}Rh	6.38E-11	3.03	217.59	2.39	2.16	0.07
^{101}Ru	1.62E-08	5.17	75.03	81.72	0.15	0.05
^{102}Ru	9.76E-07	4.30	43.34	0.29	0.15	0.52
^{103}Ru	2.36E-05	3.03	57.87	2.39	0.15	0.07
^{104}Ru	3.27E-04	1.88	24.43	0.23	0.15	0.05
^{106}Ru	9.07E-07	0.40	205.7	2.19	0.15	0.15
^{135}Sb	0.15	0.15	22.67	22.43	0.14	0.21
^{79}Se	1.10E-05	0.04	35.58	8.78	0.45	0.13
^{147}Sm	-	2.25	-	0.65	-	0.19
^{149}Sm	1.71E-10	1.08	41.76	2.67	0.15	0.17
^{150}Sm	1.22E-08	3.00E-05	34.39	104.25	0.15	0.11
^{151}Sm	4.75E-07	0.42	9.75	0.38	0.15	0.17
^{152}Sm	9.65E-06	0.27	3.93	5.36	0.15	0.15
^{126}Sn	0.04	0.06	11.09	5.76	0.15	0.57
^{92}Sr	1.08	5.94	7.4	1.62	0.15	0.1
^{99}Tc	1.23E-07	6.11	138.67	0.37	0.13	0.49
^{131}Xe	1.42E-07	2.89	4.73	0.43	0.95	0.01
^{135}Xe	0.08	6.54	11.97	1.15	4.37	0.24
^{98m}Y	1.11	1.11	57.56	78.44	69.35	69.35
^{99}Y	1.95	2.08	1.29	9.67	0.15	0.05

Continued on next page

Table 2.4 – continued from previous page

	ENDF/B-VII.1 fission yields (%)		differences (%) $\frac{\|JEFF-ENDF/B\|}{\|ENDF/B\|}$		$\frac{\|JENDL-ENDF/B\|}{\|ENDF/B\|}$	
Nuclide	IFY	CFY	IFY	CFY	IFY	CFY
^{91}Zr	4.42E-08	5.83	32.84	0.36	0.15	0.21
^{93}Zr	1.37E-04	6.35	74.85	1.4	0.15	0.1
^{95}Zr	0.13	6.50	72.21	0.01	0.08	0.1

2.5.4 Uncertainty data

MFYs from different libraries, intended as sums of independent yields with the same mass number, are in good agreement (Fig. 2.4), but the associated uncertainties show different behaviours. Uncertainties on the total MFYs are calculated by means of simple propagation through the sum of IFYs, assuming no correlation between different IFYs belonging to the same chain:

$$Y(A) = \sum_i y_i(A), \tag{2.3}$$

$$\Delta Y(A) = \sqrt{\sum_i (\Delta y_i(A))^2}. \tag{2.4}$$

The uncertainty in IFYs is a function of the chain yield and the fractional independent yields uncertainties. The small uncertainties assigned by ENDF/B-VII.1 are claimed to be the result of many determinations [England and Rider, 1994]. Meanwhile, for modelled IFYs in any fission system, large uncertainty values are suggested based on the IFY value: 32% uncertainty for IFY values greater than 1%, 64% for those between 0.5% and 1.0%, 100% uncertainty for those<0.5% [England and Rider, 1994]. These small yields (with large uncertainties) occur more frequently in correspondence of the tails and the central valley of the FY distribution, as shown in Fig. 2.4. In contrast, uncertainties in JEFF-3.1.1 are less jagged throughout the whole mass range. JEFF evaluators assessed that for chain yields generated using model parameters a 30% estimate of uncertainty was justified [Mills, 1995]. Fractional independent yield modelling was assumed to have an uncertainty of 30% as well. These uncertainties were subsequently used to calculate uncertainties of the derived parameters [Mills, 1995].

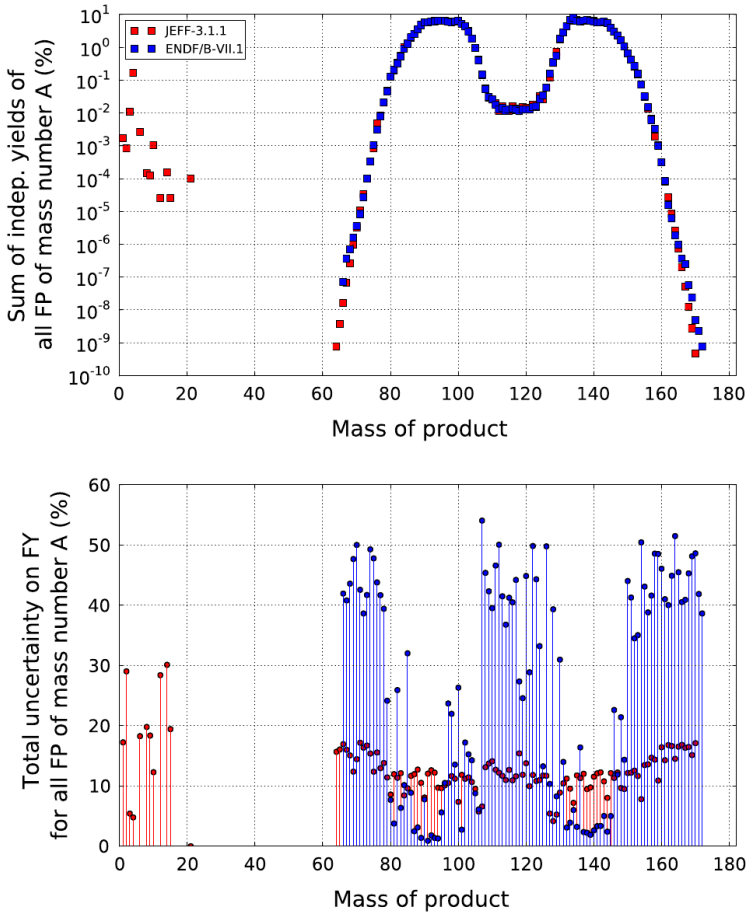

FIGURE 2.4: Mass-Yields distribution and uncertainties for ^{235}U thermal fission products from ENDF/B-VII.1 and JEFF-3.1.1 libraries. (From [Fiorito et al., 2014])

From Fig. 2.4, very different uncertainty values for MFYs are obtained from JEFF-3.1.1 and ENDF/B-VII.1. ENDF/B-VII.1 provides much lower uncertainty values, for the well-determined sets of fission product yields belonging to those reactions regarded as important for nuclear purposes (e.g. ^{235}U and ^{239}Pu thermal fission), than JEFF-3.1.1 in the peaks' regions. However, ENDF/B-VII.1 supplies very large uncertainties for those fissioning systems which give a smaller contribution in terms of maximum fraction of fission rate (e.g. ^{227}Th and ^{245}Cm), when compared with JEFF-3.1.1. The comparison of data stored in ENDF/B-VII.1 and JENDL-4, performed here, shows that JENDL-4 takes its uncertainties for IFYs directly from the ENDF/B-VI database and gives a standard deviation of 80% to those yields that do not belong to ENDF/B-VII.1, but are present in the JENDL Decay Data library.

The uncertainty estimation on the evaluated chain yields (ChFYs) results from Wahl's method upon an empirical exponential function [Wahl, 2002]:

$$PER = 25 \exp\left(-0.25 \ln Y(A)\right), \tag{2.5}$$

where PER is the percentage uncertainty in terms of 100 times the standard deviation divided by the yield. Most experimental chain yields fall within the estimated range of uncertainties, which suggests that most estimated chain yields, calculated from the previous equations, should be reliable to within the estimated uncertainties. Evaluated chain yield uncertainties are compared with their corresponding values calculated with Eq. 2.4. Discrepancies between such uncertainty values show an inconsistency in the evaluation of uncertainties and that suggests the presence of correlations between IFYs.

The uncertainties on cumulative yields ΔC_i provided in JEFF-3.1.1 were determined from the uncertainties on both the adjusted independent yields Δy_i and the experimentally based chain yields ΔCh through a least squares approach [Kellet et al., 2009]:

$$\Delta C_i = \sqrt{\left(\left(1 - \frac{C_i}{Ch}\right)\sum_i Q_{i,j}\Delta y_i\right)^2 + \left(\frac{C_i}{Ch}\Delta Ch\right)^2}. \tag{2.6}$$

In contrast, the uncertainty on CFYs can be calculated resorting to the Q-matrix formula with the assumption that the matrix Q does not carry any uncertainty:

$$\Delta C_i = \sqrt{\sum_j Q_{j,i}^2 var(y_j) + \sum_j \sum_{k \neq j} Q_{j,i} covar(y_j, y_k) Q_{k,i}}. \tag{2.7}$$

The uncertainties provided in JEFF-3.1.1 through Eq. 2.6 are compared with the result of applying Eq. 2.7 to the JEFF-3.1.1 data. The comparison reveals that uncertainties provided with the former equation are much smaller that the ones coming from the latter equation since there is no correlation data between IFYs currently provided within JEFF-3.1.1. Therefore, this difference suggests that negative correlations exist between FYs which are related through decay chains or have the same mass number, which have not been yet addressed in the current major evaluated nuclear data libraries.

2.6 Cross section data

As presented in Sec. 2.1, cross section data are of importance not only for transport calculations, but also for depletion/burn-up calculations. In particular, criticality calculations are very sensitivity to cross section data and they guarantee the safety performance, shutdown and operations of nuclear reactors. Furthermore, for radiation shielding, response function variables, such as radiation doses, depend directly on cross section data through transport calculations. Such reasons make cross section data the core of evaluated nuclear data libraries, and also justify the great efforts committed in order to improve them.

Works have been conducted in the framework of this thesis which were aimed to review the state-of-the-art of cross section data. For example, the sensitivity analysis of most important cross sections for the ADS-like reactor MYRRHA with the comparison of different library performances [Stankovskiy et al., 2014, Díez et al., 2014d] motivated the comparison of the major evaluated nuclear data libraries: ENDF/B-VII.1, JENDL-4.0 and JEFF-3.1.2. In addition, the review of the state-of-the-art of the ^{nat}C thermal capture cross section [Díez et al., 2013c] led to the re-evaluation of such cross section data and the acceptation of the proposed ^{nat}C ENDF-6 format file by the author of this thesis for the JEFF-3.2 library.

More cross section libraries have been reviewed, as shown in Sec. 2.1. However only three are going to be more extensively described, focusing mainly on their uncertainty information. EAF libraries have been selected because of their completeness: their spectrum of reactions covered is one of the largest compared with any other cross section library.They are extensive not only in providing reaction cross sections, but also in supplying uncertainties: all the cross section data provided within such libraries come with uncertainty estimations. Also, such a choice has been based on its usage in previous UQ studies [Álvarez-Velarde et al., 2009]. In contrast, the SCALE6.0 library has been chosen because it is one of the most complete cross section library concerning covariance data: it provides covariance data between different reactions, even between different isotopes. Furthermore, much of the covariance information given in SCALE6.0 has been already included in ENDF/B-VII.1. The last library described is TENDL-2010, because the later comparison done in this thesis between two Monte Carlo sampling methodologies for cross section data propagation: the Hybrid Method and Total Monte Carlo.

2.6.1 EAF-2007 and EAF-2007/UN Nuclear data libraries

EAF-2007 [Forrest, 2007] collects neutron cross sections from low energies (10^{-5} eV) to high energies (60 MeV) for nuclides from Hydrogen (^{1}H) to Fermium (^{257}Fm). There are a total of 816 possible isotopes, including ground states and isomeric states, giving a total of 65565 reaction channels. Within EAF-2007 comes its uncertainty library EAF-2007/UN which provides uncertainties data for all cross sections in EAF-2007. Both libraries are provided in EAF format.

The uncertainty information is provided in the following structure:

- For threshold reactions, there are two energy groups for uncertainties: one from the threshold energy to 20 MeV and another from 20 MeV to 60 MeV.
- For non-threshold reactions, there are four energy groups: the first one from 10^{-5}eV to the end of thermal region E_v, the second one from E_v to the end of resonance region E_H, the third one from E_H to 20 MeV, and the last one from 20 MeV to 60 MeV. E_v is usually determined by the first resonance of the isotope. Meanwhile, the E_H value is 100 keV, but depends on the isotope as well.

The emphasis for EAF-2007 uncertainties has been to include as much experimental information as possible. For threshold reactions, experimental variance information at 14 MeV is available for 1085 reactions. These uncertainties have been estimated from the data scatter around the library excitation curve in EXFOR [Otuka et al., 2011] plots or from the now growing data base of experimental validation (see [Forrest, 2007]). These 14 MeV experimental variances are used for the energy range of the excitation function up to 20 MeV, and because there is no information on uncertainties at other energies, an uncertainty value of three times the experimental uncertainty has been adopted, $\Delta\sigma = 3\Delta\sigma_{exp}$. The same uncertainty is used for the next energy group (from 20 MeV to 60 MeV), however, this can be changed for particular reactions if experimental data exist or systematics are provided.

For non-threshold reactions, for the first two groups (thermal and resonances), available experimental information is used. The third group uses experimental information if available, and the last group assumes the same uncertainty as the third group.

The uncertainty is stored as the squared relative standard deviation (rel.std.dev.) (Δ^2), which is calculated using an error factor, f, defined in Eq. 2.8:

$$f = 1 + \Delta. \tag{2.8}$$

If a scatter plot is used to determine the uncertainty of a cross section, the error factor should satisfy Eq. 2.9, covering all experimental data:

$$\frac{\sigma}{f} < \sigma < f \cdot \sigma. \tag{2.9}$$

When there is no information available (experimental, plots, etc), then, estimations for the error factor are suggested.

Depending on the reaction type, data origin and energy range, uncertainties may vary from less than a few percent to a factor of five in exceptional cases. However, the bulk of uncertainties range from a few percent to a factor of two.

There is no correlations between cross sections from different energy-groups of the energy-group structure provided within EAF-2007/UN and no correlations between different cross section reactions. However, because EAF-2007 provides cross section data in a broader energy-group structure, a 100% correlation have to be assumed for those cross section groups provided in EAF-2007 that lay in the same energy-group given in EAF-2007/UN. This information is very important when uncertainty data are collapsed to a different energy-group structure.

2.6.2 EAF-2010 and EAF-2010/UN Nuclear data libraries

EAF-2010 [Sublet et al., 2010] is the latest release of the EAF libraries. It keeps the amount of targets, 816, but increases the number of excitation functions up to 66256. It has also gained considerably in quality and completeness if compared with EAF-2007 [Sublet et al., 2010]. The wide range of available integral data has been used to improve the library. As EAF-2007, it ranges from low energies (10^{-5}eV) to high energies (60 MeV) for nuclides from hydrogen (^{1}H) to fermium (^{257}Fm). EAF-2010/UN is its uncertainty library, which has the same energy-group structure as EAF-2007/UN for threshold and non-threshold reactions. Experimental data information and information from TALYS [Koning et al., 2009] nuclear

model calculations have been included as much as possible in order to fulfil such completeness, in addition to some normalisation factors.

As in EAF-2007/UN, in cases where no experimental information is available, the uncertainty is extracted from systematics, results of graphical information or from estimates. The new estimations of the error factors show that the error factors adopted in EAF-2007/UN were, for some reactions, unnecessarily conservative and new more realistic values are proposed for important major reactions, as shown in Table 2.5.

TABLE 2.5: Changes in EAF-2010/UN error factors from EAF-2007/UN derived from systematics or estimates based on EAF validations. (From [Sublet et al., 2010])

Reaction	Systematic	Error factor (f)
(n,n′)	Vonach	2.0
(n,2n)	Badikov	1.4
(n,3n)	Estimate	3.0➔1.8 [a]
(n,4n)	Estimate	3.0➔2.0 [a]
(n,n′α)	Estimate	3.0➔2.0 [a]
(n,d)	Forrest	3.0➔2.0 [b]
(n,n′p)	Kopecky	2.0
(n,t)+(n,n′d)	Forrest	1.6
(n,n′t)	Estimate	5.0➔3.0 [a]
(n,n′h)	Estimate	5.0➔3.0 [a]
(n,f)	Estimate	2.0
(n,γ)	Kopecky	2.0➔1.5 [c]
(n,p)	Forrest	1.5
(n,h)	Lishan	1.9

[a] Neutron emission channels have been shown to be in good agreement with the experimental data and therefore more accurate estimates are proposed for (n,xn) reactions.

[b] For (n,d) reactions with targets where asymmetry, $s < 0.1$, the results are in reasonable agreement with experiments with a well defined systematic formula. For heavier targets ($s > 0.1$) the accuracy is less good. However, the (n,n′p) reaction becomes dominant and (n,n′p)+(n,d) can be used as an additional check.

[c] This is extensively discussed in Ref. [Forrest et al., 2008].

Also, a review of the uncertainty assignments for total and partial threshold cross sections, total cross sections and non-threshold cross sections has been performed in EAF-2010/UN. New assignment rules were implemented based on such a review [Sublet et al., 2010].

2.6.3 SCALE 6.0 covariance data

The SCALE6.0 covariance library [ORNL, 2009, Vol.III, Sec.M19] were the most complete and updated compilation, in conjunction with COMMARA-2.0, until the release of ENDF/B-VII.1 and JENDL-4.0. This library is based on several different uncertainty approximations with varying degrees of "fidelity" to the actual nuclear data evaluation. Then, there are two types of uncertainty information:

- "High-fidelity" covariances: These covariances come from evaluated nuclear data libraries: ENDF/B-VI.8 [McLane and CSEWG, 1996], ENDF/B-VII.0 [Chadwick et al., 2006], a pre-release of ENDF/B-VII.1 and JENDL-3.3 [Shibata et al., 2002] for more than 50 nuclides, including the most important ones for LWR applications. In these 50 nuclides, one can find uncertainty data for ^{233,235,238}U, ^{239,240,241,242}Pu, and ^{241}Am.

- "Low-fidelity covariances": These covariances are defined to be those that are estimated independently of a specific data evaluation. They come from a project run by BNL, LANL and ORNL, where ORNL used uncertainties in integral experiment measurements of thermal cross sections, resonance integrals and potential cross sections to approximate the standard deviations of capture, fission and elastic scattering reactions for thermal (<0.5 eV) and resonance ranges (0.5 eV - 5 keV). Full energy correlation was assumed for the covariances within each of these respective ranges. BNL and LANL provided estimates in the fast energy range from 5 keV - 20 MeV for covariances of capture, fission, elastic, inelastic, (n,2n) cross sections and prompt $\overline{\nu}$, using optical model and empirical estimates of nuclear reaction models. The uncertainty data out of the scope of the previous project is approximated by different approaches. These data were so-called the "BLO" [BNL-LANL-ORNL] uncertainty data [Little et al., 2008].

It provides uncertainties for a total of 401 nuclides in the form of covariance matrices for cross sections, fission neutron emission $\overline{\nu}$ and fission neutron spectrum χ, even covariance data between reactions of different isotopes. The energy-group structure used is in 44-groups.

Much of the approximate uncertainty data in this library is based on simplifying approximations that do not depend on any specific ENDF evaluations, and thus the relative uncertainties can be applied to all cross section libraries within the limitations of the assumed methodology. This assumption is partially justified by the fact that different evaluations often use

many of the same experimental measurements. Furthermore, nuclear data evaluations from ENDF/B-VII, ENDF/B-VI and JENDL-3.3 tend to agree rather well for many types of cross sections, so it seems reasonable to assume that the uncertainties in these data are similar. In general, the SCALE covariance library should be viewed as a best-estimate assessment of data uncertainties.

2.6.4 TENDL-2010 nuclear data library

TENDL-2010 [Rochman and Koning, 2010, Koning and Rochman, 2010] is the third version of the TENDL libraries, which is based on both default and adjusted TALYS calculations and data from other sources (previous releases such as TENDL-2009 [Koning and Rochman, 2009a, Koning and Rochman, 2009b] and TENDL-2008 [Koning and Rochman, 2008a] [Koning and Rochman, 2008b]). Currently, the latest release is TENDL-2013, however TENDL-2010 was the one available when part of this work was performed.

This library, TENDL-2010, provides a complete set of neutron reaction data from thermal energies up to 200 MeV from all isotopes from ^{6}Li to ^{281}Ds. All data are completely and consistently evaluated using the TALYS-1.2 [Koning et al., 2009] nuclear reaction code, in combination with resonance data, experimental data and data from existing evaluations, using the ENDF-6 format.

Complete covariance files for resonance parameters, cross sections and angular distributions are provided, stored in MF31-34 of the ENDF-6 format, and also there are covariance data processed in multi-group structure: 15, 30, 33, 44 and 187 groups.

This version of TENDL provides random ENDF files to propagate uncertainties. They are generated using TALYS by running a Monte Carlo technique, denominated Total Monte Carlo (TMC), described later in Chapter 3, Sec. 3.4. Because TALYS is a nuclear model code, its nuclear parameters could be modified in order to introduce variations on the output data. If these parameters are randomised using probability density functions, then random libraries are obtained. Also, after performing statistical analysis, final covariance information could be obtained.

2.6.5 Processing nuclear data libraries and their uncertainties

This section is aimed at processing nuclear data libraries, studying their uncertainties and showing the differences between each other, but only concerning cross section data. Then, EAF-2007/UN, EAF-2010/UN and SCALE6.0 are compared, using EAF-2010 as reference.

There are different ways to compare these libraries, choosing the following two because of their easy implementation and direct extraction of conclusions:

1. EAF-2007/UN and EAF-2010/UN are expanded to SCALE6.0 energy-group structure (44-groups) and their covariances matrices are compared.
2. EAF-2007/UN, EAF-2010/UN and SCALE6.0 are collapsed to one-group, using neutron spectra from different nuclear systems.

2.6.5.1 Comparison of covariance matrices in 44-groups

Due to the large amount of information provided within these libraries, here only ^{235}U and ^{239}Pu isotopes are compared for (n,γ) and (n, fission) reactions. More comparisons of covariance matrices between EAF-2007, EAF-2010 and SCALE6.0, for more reactions and isotopes, can be found in [Cabellos et al., 2011a].

To expand from EAF-2007/EAF-2010 3/4-groups structure to the SCALE6.0 44-groups, 100% correlation is assumed between cross sections that lay in the same energy-group defined in their corresponding uncertainty library, as stated in Sec. 2.6.1. Therefore, the uncertainties in the EAF files take the form of block matrices, where the unity blocks represent the full correlation between energy-groups. When the edge of an energy region in EAF files falls inside a SCALE6.0 energy-group, a weighted average of the cross section and its uncertainty are calculated. These calculations are carried out with NJOY (v99.393) [MacFarlane and Kahler, 2010].

Fig. 2.5 and Fig. 2.6 show the differences between EAF-2010/UN and SCALE6.0 for (n,fission) reaction, while Fig. 2.7 and Fig. 2.8 present (n,γ) covariance matrices.

For the ^{235}U (n,fission) cross section, EAF-2010 provides uncertainties in three energy regions that represent thermal, epithermal and fast energies, while in SCALE6.0 only two regions are presented: thermal-epithermal and fast energies. The energy regions defined in EAF-2010

and SCALE are not the same. Also, at least the uncertainties in EAF-2010 are one order of magnitude higher than SCALE6.0 ones for high energies. In the case of ^{239}Pu, differences are similar to the ^{235}U case, except that EAF uncertainties are 6 times higher the SCALE ones in the fast region.

For the ^{235}U (n,γ) cross sections, differences between EAF-2007 and EAF-2010 are observed only in the epithermal region, which has increased its upper limit in EAF-2010. Whereas SCALE6.0 has only two regions, thermal and fast. Relative uncertainties are quite similar between SCALE6.0 and EAF libraries.

For ^{239}Pu reactions, same differences as in ^{235}U are found.

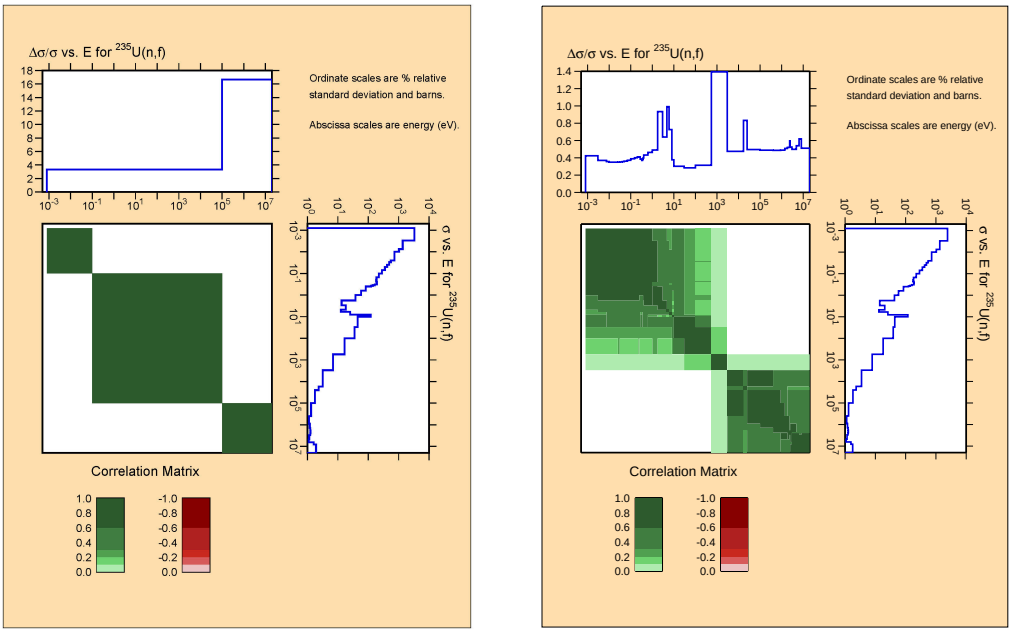

FIGURE 2.5: EAF-2010 (left) and SCALE6.0 (right) covariance matrices for the ^{235}U (n,fission) cross section.

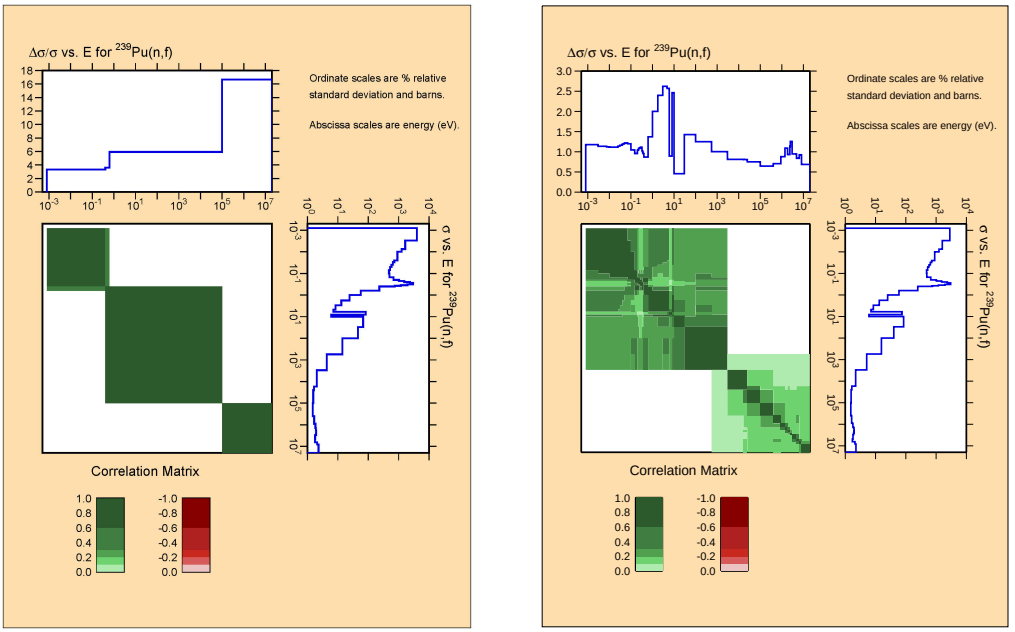

FIGURE 2.6: EAF-2010 (left) and SCALE6.0 (right) covariance matrices for the ^{239}Pu (n,fission) cross section.

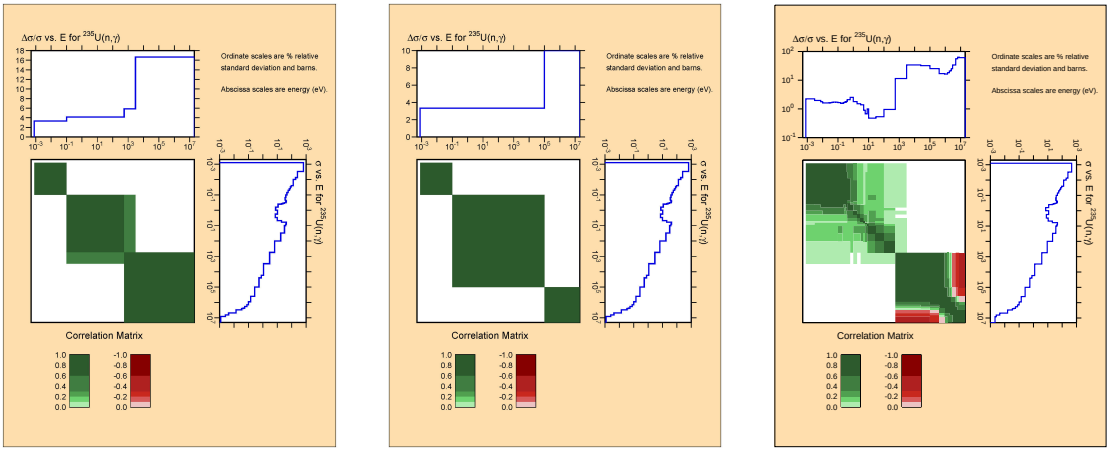

FIGURE 2.7: EAF-2007 (left), EAF-2010 (centre) and SCALE6.0 (right) covariance matrices for the ^{235}U (n,γ) cross section.

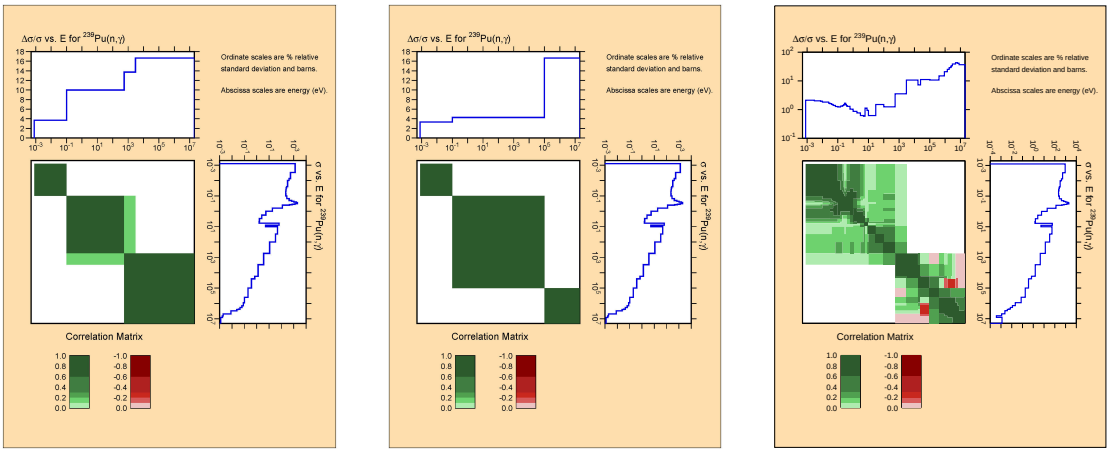

FIGURE 2.8: EAF-2007/UN (left), EAF-2010/UN (centre) and SCALE6.0 (right) covariance matrices for the ^{239}Pu (n,γ) cross section.

An important feature of SCALE6.0 is that it provides covariance matrices between different cross section reactions of one isotope, and even different isotopes. Usually, the main reactions, such as (n,fission) and (n,γ), are correlated. But also, there exist other cross-correlations that relate (n,elastic) to (n,γ) and to (n,fission). Examples are presented in Fig. 2.9. More cross-correlations have been processed, which can be found in [Cabellos et al., 2011a]. Usually, non-zero values appear at low energies (below 10 keV), while at high energies there are no correlations (negligible correlations or zero values are found).

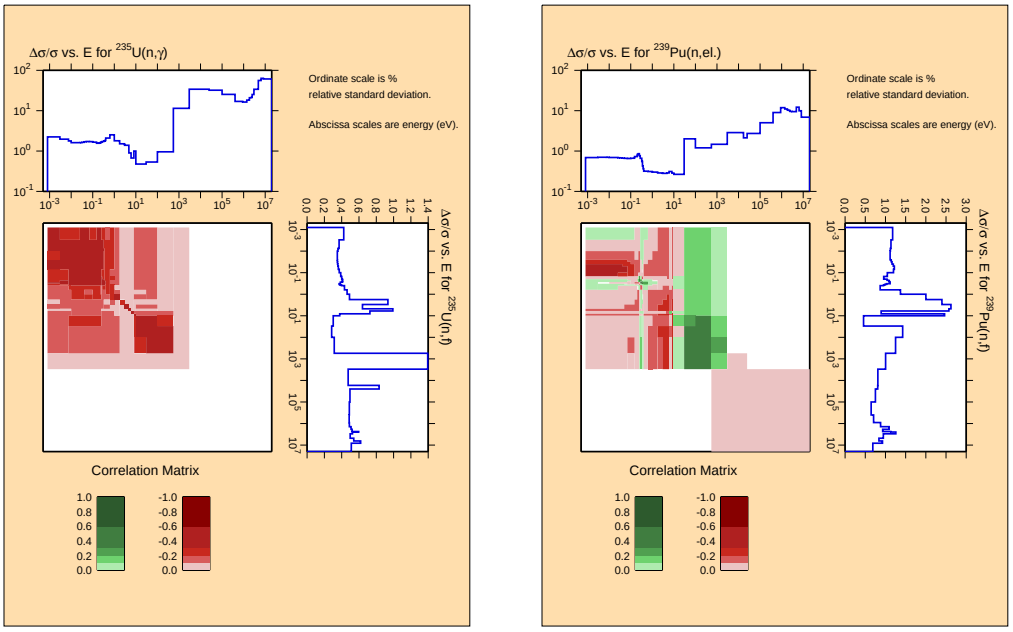

FIGURE 2.9: Covariance matrices between (n,γ) and (n,fission) cross sections for ^{235}U (left), and between (n,fission) and (n,elastic) cross sections for ^{239}Pu (right). Both data have been retrieved from SCALE6.0.

2.6.5.2 Comparison of uncertainties in one-group

Using the collapsing method described in Chapter 4, Sec. 4.2.1, three different neutron spectra are used to compare uncertainties of cross section reactions in one-group.

These spectra are presented in Fig. 2.10 for each application. The ADS spectrum is taken from the EFIT facility design [Artioli, 2006], while the PWR [ORNL, 2009] and the DEMO (fusion application) [Wong et al., 2005] spectra are standard.

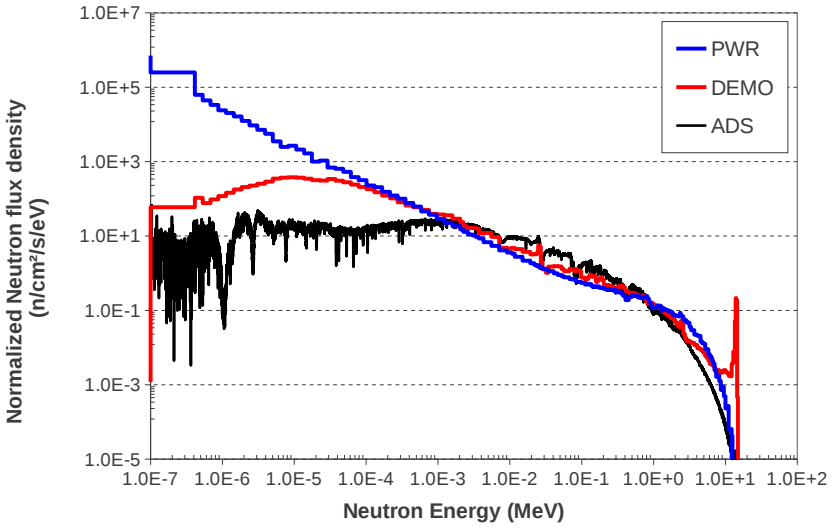

FIGURE 2.10: Normalised neutron spectra for different nuclear applications.

Using ADS neutron spectrum For the ADS spectrum, main transuranic isotopes are studied for (n,fission), (n,γ) and (n,γ-M) reactions: ^{234,235,236,238}U, ^{237}Np, ^{238,239,240,241}Pu, ^{241,242m,243}Am, ^{242,243,244,245,246,247,248}Cm, ^{249}Bk, ^{249,250,251,252}Cf. The (n,γ-M) reaction corresponds to the neutron capture reaction that leaves the nucleus in its first isomeric state (M). Their collapsed uncertainty values are compared with target accuracies provided in [García-Herranz et al., 2010].

Table 2.6 shows one-group uncertainties of the mentioned reactions corresponding to each library. Cells in red mean that there is a target accuracy proposed for the isotope-reaction that such cells represent. If any of the uncertainty values is less than twice the target value, they are written in bold blue while the others in non-bold. These results reveal that SCALE6.0 has not uncertainty information for (n,γ-M) reactions for any isotope. In contrast, it gives the lowest uncertainty values for most of the most important isotopes, such as ^{235,238}U and ^{239,241}Pu. On the contrary, EAF-2010 does not reach such an accuracy level. EAF-2010 shows a trend of reducing uncertainties when compared with EAF-2007. Also, it provides

lower uncertainty values than SCALE-6.0 for heavier isotopes than ^{243}Cm, such as ^{243,246}Cm and ^{249}Cf. Regarding target accuracies for (n,fission) reactions, EAF-2010 achieves two targets: for ^{235}U and ^{241}Pu, while SCALE6.0 fulfils these two and also for ^{239}Pu. For (n,γ), SCALE6.0 is close to achieve eight targets while EAF-2010 is close to achieve 11 targets. In the case of SCALE6.0, targets for U, Np, Pu and two Cm are achieved, while EAF-2010 fulfils requirements for Pu, Cm and Cf. For (n,γ-M) reactions, uncertainties are only supplied by EAF files. Only EAF-2010 achieves one of the target values for such reactions, specifically for ^{243}Cm.

Fig. 2.11 presents one-group cross section uncertainty values for (n,γ) reactions of EAF-2007 and SCALE6.0 divided by EAF-2010 values for all the isotopes in each libraries. For most of isotopes, EAF-2010 has reduced their uncertainty values when compared with EAF-2007. SCALE6.0 provides higher uncertainties than EAF-2010 for light isotopes, but as the ZZAAAM number increases, the number of isotopes with high uncertainties and with low uncertainties become similar. Values at 0.01 indicate that SCALE6.0 does not supply uncertainties for these isotopes.

TABLE 2.6: Comparison of one-group cross section uncertainties (%) among EAF-2007, EAF-2010 and SCALE6.0 libraries for (n,fission), (n,γ) and (n,γ-M) reactions of main transuranic isotopes, collapsed with an ADS spectrum (from the EFIT facility). Cells in red mean that there is a target accuracy proposed for the isotope-reaction that such cells represent. If any of the uncertainty values is less than twice the target value, they are written in bold blue while the others in non-bold.

	(n,fission)				(n,γ)				(n,γ-M)			
Isotope	EAF2007	EAF2010	SCALE6.0	TARGET	EAF2007	EAF2010	SCALE6.0	TARGET	EAF2007	EAF2010	SCALE6.0	TARGET
234U	16.5	16.5	30.0		38.9	26.0	**6.9**	**7.1**	38.9	26.0	-	**7.1**
235U	12.9	**5.5**	**0.4**	**4.2**	11.3	3.2	21.8		-	-	-	
236U	15.9	15.3	27.2		8.9	3.2	3.1		-	-	-	
238U	16.6	16.6	0.5		6.7	3.2	1.4		-	-	-	
237Np	16.7	16.4	6.6		14.3	9.1	**3.3**	**2.8**	-	-	-	
238Pu	12.4	**10.1**	**10.6**	**6.4**	14.5	**3.7**	**6.6**	**5.2**	-	-	-	
239Pu	9.6	7.9	**0.4**	**3.4**	12.5	4.2	4.8		-	-	-	
240Pu	15.8	14.7	0.6		9.3	**3.6**	**1.2**	**4.8**	-	-	-	
241Pu	15.6	**5.6**	**1.2**	**4.2**	15.4	5.2	4.0		-	-	-	
242Pu	16.5	16.5	3.4		12.6	**3.5**	**5.0**	**5.3**	-	-	-	
244Pu	16.5	16.5	19.0		30.4	7.4	24.9		-	-	-	
241Am	16.6	16.6	2.2		15.8	16.7	**4.7**	**2.8**	15.8	16.7	-	**2.9**
242MAm	16.5	5.6	9.8	**2.4**	32.8	13.2	14.5	**6.2**	-	-	-	
243Am	16.6	16.0	5.8		15.3	5.0	4.5		15.3	**3.8**	-	**4.1**
242Cm	16.5	16.5	31.9		30.0	12.9	10.8	**3.4**	-	-	-	
243Cm	16.0	**5.9**	19.7	**3.2**	32.0	**5.2**	14.2	**7.4**	-	-	-	
244Cm	16.4	14.8	37.0		24.6	**3.7**	**7.7**	**4.6**	-	-	-	
245Cm	9.8	11.3	20.2	**4.1**	32.8	**4.1**	**9.8**	**5.5**	-	-	-	
246Cm	16.6	15.2	8.0		28.2	**3.7**	20.3	**4.3**	-	-	-	
247Cm	16.5	16.5	11.3	**4.0**	32.1	**7.7**	20.6	**5.0**	-	-	-	
248Cm	16.2	15.3	16.2		19.2	**3.8**	16.9	**2.5**	-	-	-	
249Bk	16.6	16.6	22.5		31.7	8.8	23.7	**3.2**	-	-	-	
249Cf	16.3	5.8	19.3		32.4	**4.8**	24.5	**4.3**	-	-	-	
250Cf	33.0	33.0	**13.3**	**6.9**	29.3	9.0	16.0	**2.6**	-	-	-	
251Cf	31.6	12.9	21.9	**3.7**	30.0	**3.9**	16.6	**2.4**	-	-	-	
252Cf	15.0	10.7	6.1		31.2	4.0	18.1		-	-	-	

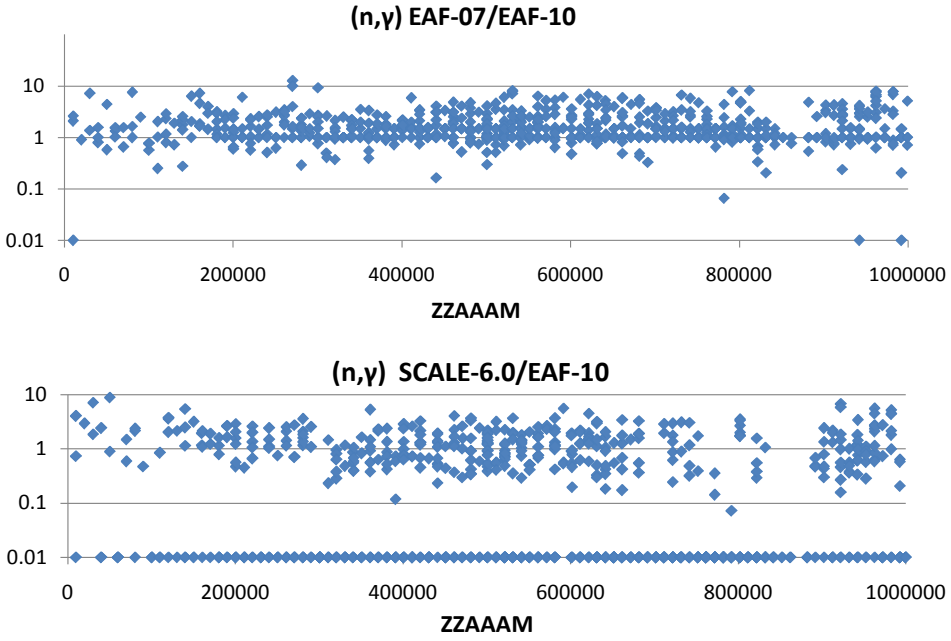

FIGURE 2.11: Ratio of one-group cross section uncertainty values from EAF-2007 and SCALE6.0 to EAF-2010 for (n,γ) reactions, collapsed with an ADS spectrum (from EFIT facility).

Fig. 2.12 shows the ratio of dividing EAF-2007 and SCALE6.0 by EAF-2010 for (n,fission) reaction. EAF-2010 has reduced their uncertainty values, if compared with EAF-2007, except for ^{242}Am. SCALE6.0 has no uncertainties for some isotopes that EAF-2010 provides uncertainties for. In contrast, SCALE6.0 gives lower uncertainty values than EAF-2010, especially for ^{238}U and ^{239,240}Pu. The isotopes with ratios values of 0.01 are again those which SCALE6.0 does not provide uncertainty data for.

Using PWR neutron spectrum For high burn-up PWRs (up to 100 GWd/tU), different response functions are studied in [Salvatores et al., 2008] concerning neutronics calculations. Desired maximum uncertainty values, or target accuracies, were provided in order to establish a framework for nuclear data requirements. Such target accuracies are presented in Table 2.7.

TABLE 2.7: General target accuracies for high burn-up PWRs.

k_{eff}	Doppler reactivity coefficient	Burn-up ($\Delta\rho$)	Transmutation
0.5%	10%	500 pcm	5%

The current state of such general target accuracies is addressed by using the BOLNA cross section covariance data [Salvatores et al., 2008]. Once response function uncertainties are evaluated, a study of how to improve cross section uncertainties in order to satisfy such general

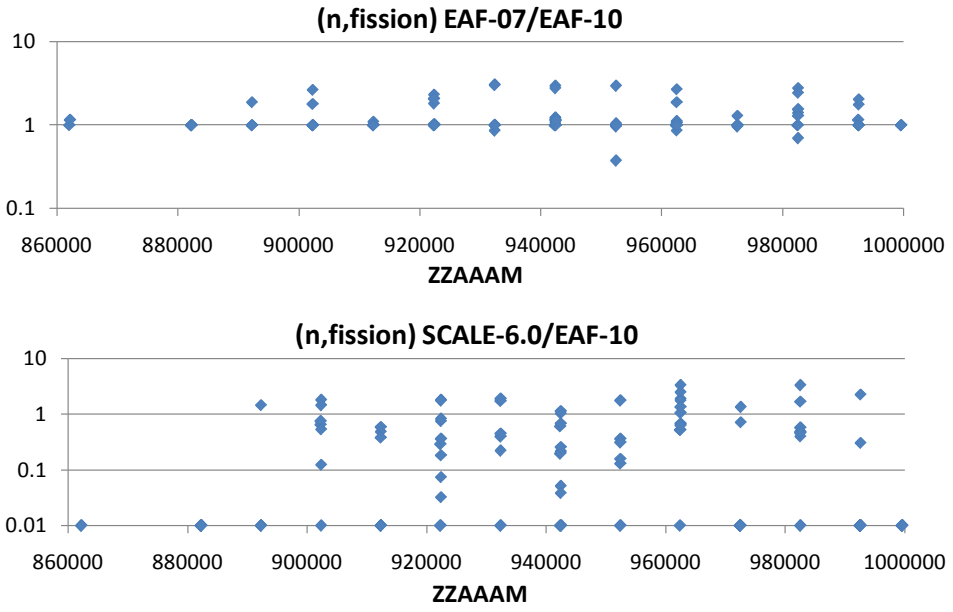

FIGURE 2.12: Ratio of one-group cross section uncertainty values from EAF-2007 and SCALE6.0 to EAF-2010 for (n,fission) reactions, collapsed with an ADS spectrum (from EFIT facility).

target accuracies is performed under two hypothesis: the efforts to improve the uncertainties of one cross section reaction or other are the same ($\lambda = 1$), and the efforts depend on the cross section addressed ($\lambda \neq 1$) [Salvatores et al., 2008]. This provides a set of target accuracies for cross section data that could fulfil the general target accuracies for different neutronics response functions.

These target accuracies for ^{235,238}U, ^{239,240,241,242}Pu and Oxygen are compared with the information in EAF-2007 and EAF-2010 through Table 2.8. Again, it is observed that EAF-2010 has reduced its uncertainties, but this time such a reduction is appreciated at energy-group level. Whether EAF files fulfil or not target accuracies has been marked using a colour legend, where green means the target is achieved, yellow means that not all the energy-group cross sections reach their targets, and, finally, red means that none of the energy-group cross sections achieve any target. For the (n,γ) reactions of ^{235}U and ^{240,241}Pu, requirements are fulfilled with EAF-2010.

TABLE 2.8: Nuclear data uncertainties and target accuracies (%) for U, Pu and O isotopes in high burn-up PWRs.

Using BOLNA covariance matrices

Isotpe		Cross-section	Energy range	Uncertainty			EAF - 2007		EAF - 2010	
				Initial	Required					
					λ=1	λ≠1	Energy Range	Uncertainty	Energy Range	Uncertainty
U	235	(n,γ)	67.4 - 24.8 keV	32.9	19.9	18.5	2.25 keV - 20 MeV	16.67	0.10 eV - 0.10 MeV	3.33
			24.8 - 9.12 keV	43	17.8	16.2				
			9.12 - 2.03 keV	33.9	11.5	10.3				
	238	(n,γ)	24.8 - 9.12 keV	9.4	4.6	4	10 keV - 20 MeV	16.67	0.5 eV - 0.10 MeV	3.33
			9.12 - 2.03 keV	3.1	3.1	2.9	1.0 eV - 10 keV	3.33		
			454 - 2.6 eV	1.7	1.4	1.3				
Pu	239	(n,γ)	0.54 - 0.10 eV	1.4	1	0.9	Thermal - 0.10 eV	3.70	0.10 eV - 0.10 MeV	4.27
		(n,fission)	0.54 - 0.10 eV	0.9	0.9	0.8	Thermal - 30 keV	3.33	Thermal - 0.50 eV	3.33
	240	(n,γ)	0.54 - 0.10 eV	3.2	3.1	3.2	0.10 eV - 4.0 keV	3.57	0.10 eV - 0.10 MeV	3.33
			0.10 eV - thermal	4.8	3.1	4	Thermal - 0.10 eV	3.43	Thermal - 0.10 eV	3.33
	241	(n,γ)	22.6 - 4.00 eV	8.4	7.3	8.4	0.10 eV - 0.30 keV	6.27	0.10 eV - 0.10 MeV	3.33
			0.54 - 0.10 eV	6.8	3	3.8				
		(n,fission)	2.03 - 0.454 keV	12.7	11.2	12.7	Thermal - 30 keV	3.33	Thermal - 0.10 MeV	3.33
			454 - 22.6 eV	19.4	4.7	5.9				
			22.6 - 4.00 eV	4.2	3.3	4.2				
			4.00 - 0.54 eV	26.8	7.7	9.8				
			0.54 - 0.10 eV	2.9	1.7	2.2				
			0.10 eV - thermal	3.3	1.9	2.4				
	242	(n,γ)	4.00 - 0.54 eV	3.8	3.4	3.8	0.05 eV - 1.29 keV	9.10	0.50 eV - 0.10 MeV	3.33
O		(n,γ)	19.6 - 6.07 MeV	100	12.1	10.9	1.0 MeV - 20 MeV	33.33	1.0 MeV - 20 MeV	33.33
			6.07 - 2.23 MeV	100	9.9	8.9				

When main transuranic isotopes are observed using one-group uncertainties for (n,fission) and (n,γ) reaction, as shown in Table 2.9, it can be seen that SCALE6.0 gives the lowest uncertainties for 17 isotopes while EAF-2010 only for 12. In spite of that, uncertainty values for ^{242m}Am, ^{243}Cm and ^{249}Cf are very similar using either EAF-2010 or SCALE-6.0.

TABLE 2.9: One-group uncertainties (%) for main transuranic isotopes collapsing EAF-2007, EAF-2010 and SCALE6.0 data for (n,γ) and (n,fission) reactions with a PWR spectrum.

		(n,fission)			(n,γ)		
ISOTOPE		EAF-2007	EAF-2010	SCALE 6.0	EAF-2007	EAF-2010	SCALE 6.0
U	234	15.86	15.84	24.82	38.87	26.03	5.73
	235	2.39	2.39	0.33	2.64	2.35	1.35
	236	11.67	12.16	19.5	3.85	3.1	2.99
	238	16.65	16.65	0.52	3.15	3.17	1.38
Np	237	16.5	16.41	7	5.72	7.58	2.68
Pu	238	7.23	4.86	6.01	3.73	3.07	1.79
	239	3.32	3.2	0.78	8.21	3.55	1.17
	240	14.94	14.27	2.7	3.3	3.09	1.23
	241	3.3	3.32	0.87	3.9	2.39	0.94
	242	15.81	15.77	4.53	8.51	3.31	9.76
	244	16.56	16.56	21.32	23.48	4.87	35.39
Am	241	21.34	12.44	1.66	6.38	3.89	2.5
	242M	3.31	3.33	3.05	22.36	10.19	23.2
	243	15	14.62	5.12	3.72	4.44	2.41
Cm	242	16.6	10.79	32.83	19.29	9.42	12.05
	243	3.94	2.56	2.71	5.94	2.35	5.58
	244	13.36	12.22	25.8	6.93	3.01	9.99
	245	3.65	5.03	2.45	14.68	2.67	4.28
	246	14.6	13.67	8.37	7.99	3.15	5.63
	247	4.96	5.25	13.04	16.51	7.63	6.33
	248	12.91	13.36	16.33	10.48	3.57	5.5
Bk	249	28.84	14.56	6.47	9.52	7.74	4.96
Cf	249	7.3	2.6	1.76	3.94	2.51	4.39
	250	13.81	41.36	0.6	4.85	5.93	5.91
	251	8.74	5.7	4.37	5.95	2.88	4.73
	252	11.69	4.84	11.5	12.14	2.65	5.13

Fig. 2.13 shows the differences of EAF-2007 and SCALE6.0 to EAF-2010 for the (n,γ) reaction. For a large number of isotopes EAF-2010 has reduced their uncertainties from EAF-2007. For SCALE6.0, the same trend as using an ADS spectrum is observed when it is compared with EAF-2010: it does not give uncertainty values for 54% of the isotopes included in EAF-2010. However, again it provides very low uncertainty values, such as for ^{135}I and ^{79}Se.

Fig 2.14 presents EAF-2007 and SCALE6.0 one-group uncertainty values divided by EAF-2010 for the (n,fission) reaction. At least for 55% of the isotopes in EAF-2007, their uncertainties have been reduced in EAF-2010, except for ^{250}Cf. SCALE6.0 does not provide uncertainties for 42% of the isotopes included in EAF-2010, but 36% of the isotopes have lower uncertainties in SCALE6.0 than in EAF-2010. In addition, very low uncertainty values are provided with SCALE-6.0, for e.g. ^{238}U and ^{250}Cf.

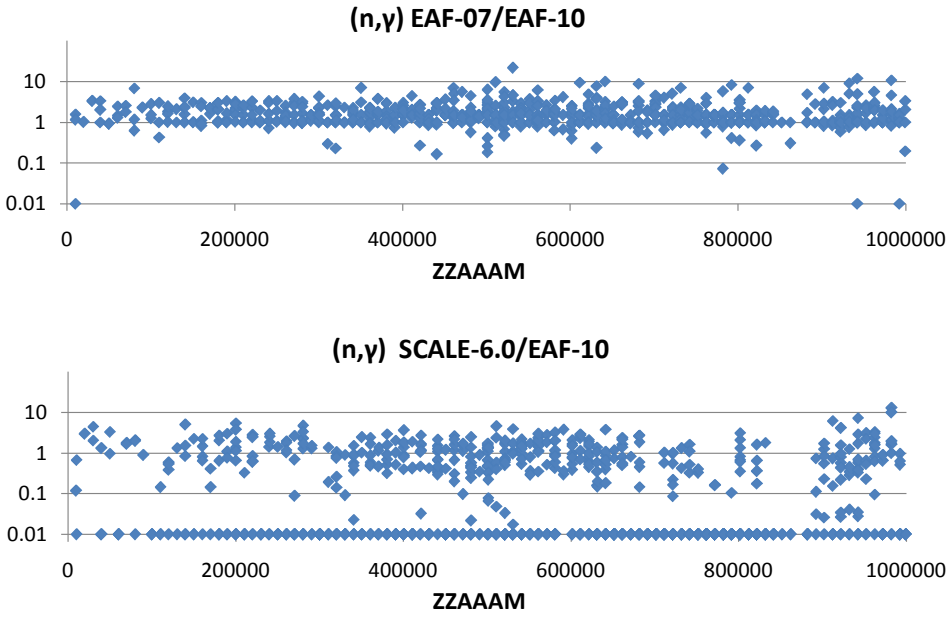

FIGURE 2.13: Ratio of one-group uncertainty values of EAF-2007 and SCALE6.0 divided by EAF-2010 ones for the (n,γ) reaction, collapsed with a PWR spectrum.

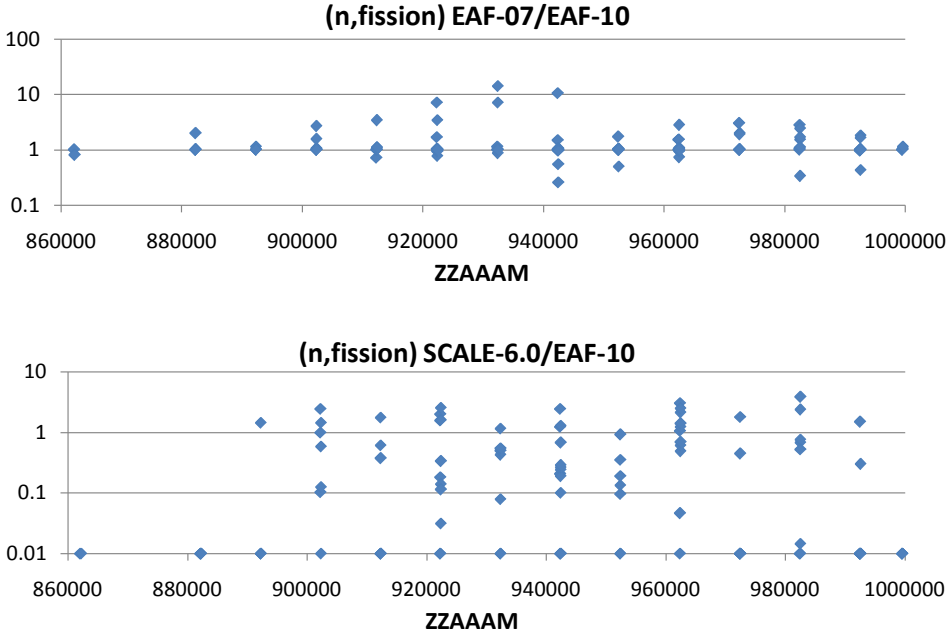

FIGURE 2.14: Ratio of one-group uncertainty values of EAF-2007 and SCALE6.0 divided by EAF-2010 ones for the (n,fission) reaction, collapsed with a PWR spectrum.

Using DEMO neutron spectrum For the DEMO application [Wong et al., 2005], in which a fusion spectrum is obtained, Fig. 2.15 presents (n,γ) one-group cross section uncertainty values for all isotopes included in EAF-2007, EAF-2010 and SCALE6.0. The bulk of uncertainties lay between between 3% and 40%. Although SCALE6.0 provides the lowest uncertainty values, it des not give uncertainties for 54% of the isotopes included in EAF files.

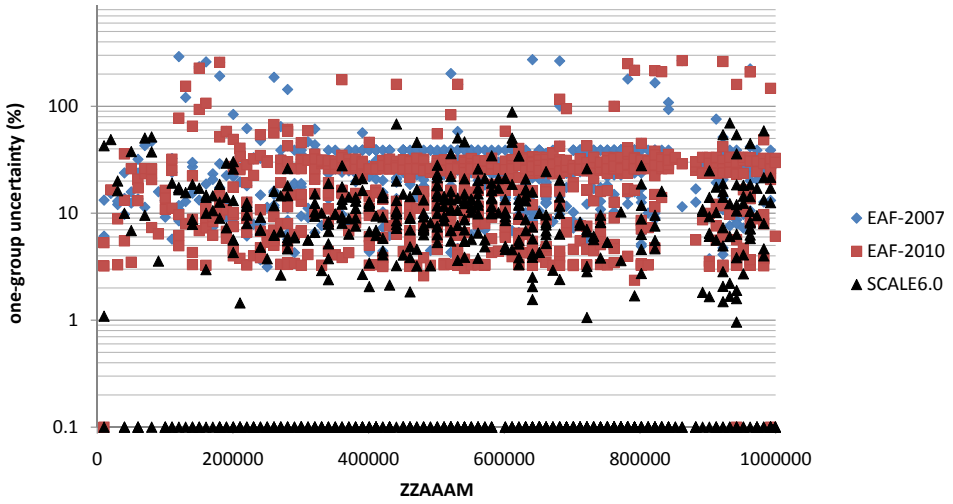

FIGURE 2.15: One-group cross section uncertainties (%) for every isotope included in EAF-2007, EAF-2010 and SCALE6.0 for (n,γ) reactions, collapsed with the DEMO spectrum.

For the (n,γ) reaction, a comparison between libraries is performed and presented in Fig 2.16. The ratios between one-group cross section uncertainty values from EAF-2007 and SCALE6.0 to EAF-2010 are calculated. The same trends are observed as using PWR or ADS spectra: EAF-2007 provides, in general, higher uncertainty values than EAF-2010; SCALE6.0 uncertainties are mainly smaller than EAF-2010 but for large number of isotopes uncertainties are not supplied.

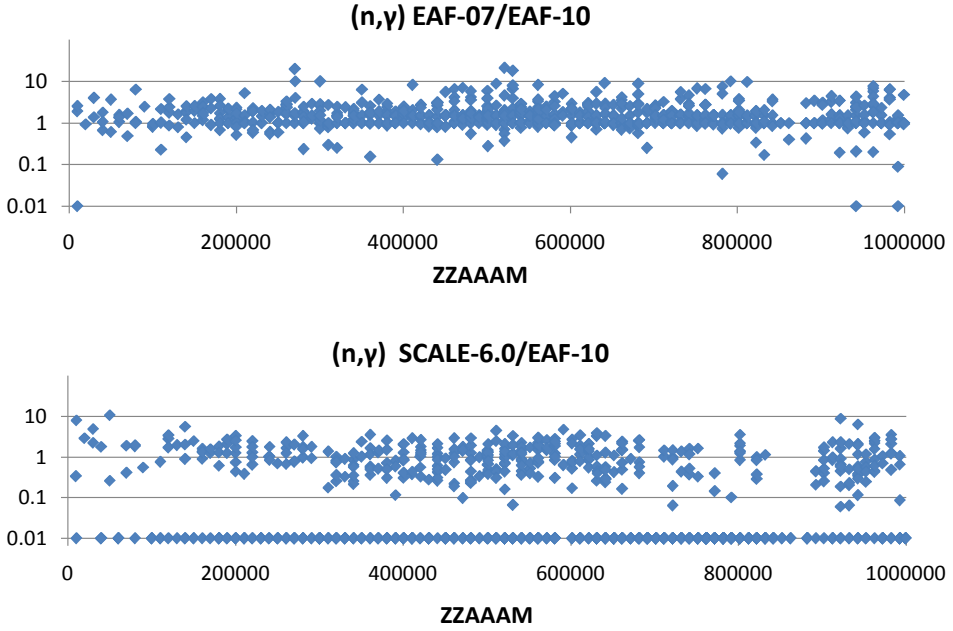

FIGURE 2.16: Ratio of one-group uncertainty values of EAF-2007 and SCALE6.0 divided by EAF-2010 ones for (n,γ) reactions, collapsed with the DEMO spectrum.

Because of the fast neutron spectrum of DEMO, threshold reactions start to be of interest. For such a reason the (n,p) reactions are analysed, comparing the uncertainties provided within the mentioned libraries in Fig. 2.17. In contrast with previous studied reactions, here EAF-2010 has larger uncertainties than EAF-2007. This fact is also observed when other spectra (ADS and PWR) are applied. Here, SCALE6.0 stops to give the lowest uncertainty values, being substituted with EAF-2010.

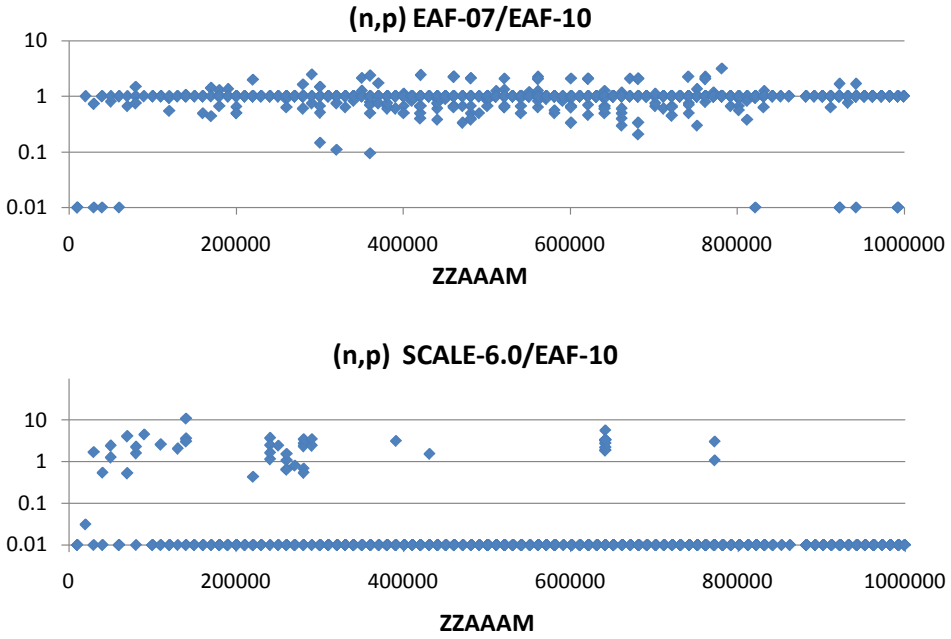

FIGURE 2.17: Ratio of one-group uncertainty values of EAF-2007 and SCALE6.0 divided by EAF-2010 ones for (n,p) reactions, collapsed with the DEMO spectrum.

Analysis of the effect of neutron spectra Table 2.10 and 2.11 are aimed at comparing uncertainties from each library when different neutron spectra are used. Then, only (n,γ) and (n,fission) are studied, and their uncertainty values collapsed into one-group are compared. The colour legend means: green for the lowest uncertainty values among neutron spectra, yellow for the middle values and red for the highest.

For (n,γ) reactions, Table 2.10, EAF-2010 gives the lowest values when the PWR neutron spectrum is used, while the ADS spectrum provokes the highest uncertainties. The DEMO spectrum gives lower uncertainties than the ADS spectrum, but not as small as with the PWR spectrum. SCALE-6.0 gives the highest uncertainty values with the ADS spectrum, while with the PWR and DEMO spectra the lowest values are obtained (more green cells are obtained with the PWR spectrum than with DEMO, although differences between them are rather small). Note that when SCALE6.0 is used for (n,γ) reactions, one-group uncertainty

values obtained for some of the main transuranic isotopes (heavier than ^{243}Cm) with the ADS spectrum can double, or even more, the values obtained with the PWR or DEMO spectra.

TABLE 2.10: Comparison of one-group cross section uncertainties (%) for (n,γ) reactions of main transuranic isotopes among EAF-2007, EAF-2010 and SCALE-6.0 libraries, using PWR, ADS and DEMO spectra.

(n,γ)		EAF-2007			EAF-2010			SCALE 6.0		
ISOTOPE		PWR	ADS	DEMO	PWR	ADS	DEMO	PWR	ADS	DEMO
U	234	38.87	38.87	38.87	26.03	26.03	26.03	5.73	6.93	4.95
	235	2.64	11.28	4.75	2.35	3.23	3.2	1.35	21.8	7.32
	236	3.85	8.9	4.11	3.1	3.2	3.24	2.99	3.11	2.07
	238	3.15	6.67	3.27	3.17	3.17	3.27	1.38	1.44	1.49
Np	237	5.72	14.33	7.63	7.58	9.13	9.79	2.68	3.3	2.21
Pu	238	3.73	14.46	9.99	3.07	3.69	3.27	1.79	6.63	3.84
	239	8.21	12.48	8.64	3.55	4.21	4.18	1.17	4.86	1.59
	240	3.3	9.26	3.52	3.09	3.62	3.28	1.23	1.2	0.96
	241	3.9	15.37	7.99	2.39	5.22	3.27	0.94	4	1.9
	242	8.51	12.62	8.01	3.31	3.51	3.27	9.76	5	6.36
	244	23.48	30.44	23.86	4.87	7.36	5.64	35.39	24.88	35.87
Am	241	6.38	15.81	9.72	3.89	16.65	16.55	2.5	4.67	4.08
	242M	22.36	32.77	27.78	10.19	13.18	10.48	23.2	14.66	12.4
	243	3.72	15.34	7.28	4.44	4.98	4.71	2.41	4.48	2.71
Cm	242	19.29	30.01	24.25	9.42	12.86	13.65	12.05	10.8	6.25
	243	5.94	31.97	20.18	2.35	5.21	3.56	5.58	14.24	10.39
	244	6.93	24.56	8.47	3.01	3.72	3.27	9.99	7.72	7.18
	245	14.68	32.75	25.83	2.67	4.13	3.35	4.28	9.83	8.35
	246	7.99	28.21	13.82	3.15	3.7	3.29	5.63	20.32	8.11
	247	16.51	32.12	23.03	7.63	7.67	8.17	6.33	20.59	7.13
	248	10.48	19.19	10.57	3.57	3.79	3.68	5.5	16.85	5.79
Bk	249	9.52	31.73	20.56	7.74	8.82	8.86	4.96	23.99	9.49
Cf	249	3.94	32.39	23.13	2.51	4.8	3.73	4.39	24.59	13.35
	250	4.85	29.33	8.72	5.93	8.97	9.72	5.91	16.06	4.65
	251	5.95	29.95	12.72	2.88	3.85	3.22	4.73	16.89	3.99
	252	12.14	31.22	23.64	2.65	4.03	3.8	5.13	18.11	8.01

For (n,fission) reactions, Table 2.11, EAF-2010 provides the lowest uncertainties when the PWR spectrum is used, while the highest values are reached with the ADS spectrum. With EAF-2010, the DEMO spectrum does not provide uncertainty values as low as for (n,γ) reactions. Furthermore, the uncertainties obtained with the DEMO spectrum can be as high as with the ADS spectrum for some isotopes such as ^{236}U, when EAF-2010 is used. SCALE-6.0 follows the same trend as for (n,γ) reactions: their highest values are reached when the ADS spectrum is applied. However, with PWR or DEMO spectra same amount of highest values are reached. In particular, the DEMO spectrum gives the highest values for ^{241,243}Am, while the highest uncertainties for ^{237}Np are obtained with the PWR spectrum.

With the ADS spectrum, the highest uncertainties for main transuranic isotopes are reached when (n,γ) and (n,fission) reactions are addressed. The PWR spectrum provokes the lowest uncertainties when EAF-2010 is used. However, with SCALE6.0, it is not easy to distinguish with which spectrum are obtained the lowest uncertainties: DEMO or PWR.

Although one-group uncertainty cross section values from EAF-2007 are presented in Table 2.10 and 2.11, only statements about comparisons between EAF-2010 and SCALE6.0

were made. The reason is the overall performance of EAF-2007 is to carry higher uncertainty values than EAF-2010, except for (n,p) reactions which are only of interest for fast spectra.

Between EAF-2010 and SCALE6.0, one can observe that uncertainty levels for isotopes lighter than ^{242}Pu, SCALE6.0 provides lower uncertainty levels, while EAF-2010 gives lower uncertainties for heavier isotopes than ^{243}Cm.

TABLE 2.11: Comparison of one-group cross section uncertainties (%) for (n,fission) reactions of main transuranic isotopes among EAF-2007, EAF-2010 and SCALE-6.0 libraries, using PWR, ADS and DEMO spectra.

(n,fission)		EAF-2007			EAF-2010			SCALE 6.0		
ISOTOPE		PWR	ADS	DEMO	PWR	ADS	DEMO	PWR	ADS	DEMO
U	234	15.86	16.47	16.43	15.84	16.47	16.43	24.82	29.99	15.37
	235	2.39	12.86	6.99	2.39	5.5	4.7	0.33	0.41	0.3
	236	11.67	15.88	15.68	12.16	15.31	15.63	19.5	27.16	11.42
	238	16.65	16.61	16.66	16.65	16.61	16.66	0.52	0.54	0.55
Np	237	16.5	16.66	16.64	16.41	16.39	16.55	7	6.55	3.81
Pu	238	7.23	12.35	12.5	4.86	10.09	11.21	6.01	10.55	10.75
	239	3.32	9.59	6.02	3.2	7.87	6.48	0.78	0.4	0.58
	240	14.94	15.84	16.16	14.27	14.68	15.87	2.7	0.57	0.59
	241	3.3	15.58	8.79	3.32	5.64	4.3	0.87	1.23	0.75
	242	15.81	16.46	16.52	15.77	16.46	16.52	4.53	3.43	3.61
	244	16.56	16.48	16.6	16.56	16.47	16.59	21.32	18.96	17.29
Am	241	21.34	16.62	16.4	12.44	16.62	16.4	1.66	2.19	2.71
	242M	3.31	16.48	15.1	3.33	5.59	4.28	3.05	9.88	7.28
	243	15	16.61	16.48	14.62	15.95	16.29	5.12	5.76	9.67
Cm	242	16.6	16.52	16.17	10.79	16.51	15.66	32.83	31.85	24.37
	243	3.94	16	10.64	2.56	5.91	4.68	2.71	19.72	9.03
	244	13.36	16.42	15.93	12.22	14.82	15.39	25.8	37.01	21.33
	245	3.65	9.75	7.3	5.03	11.33	12.56	2.45	20.18	9.45
	246	14.6	16.59	16.41	13.67	15.24	15.99	8.37	8.01	8.58
	247	4.96	16.46	14.43	5.25	16.46	14.44	13.04	11.3	11.42
	248	12.91	16.19	15.41	13.36	15.28	15.33	16.33	16.17	16.11
Bk	249	28.84	16.61	16.44	14.56	16.61	16.44	6.47	22.5	20.02
Cf	249	7.3	16.28	12.85	2.6	5.83	4.79	1.76	19.35	7.31
	250	13.81	32.97	29.36	41.36	32.98	30.73	0.6	13.32	12.85
	251	8.74	31.57	17.82	5.7	12.92	9.5	4.37	22.02	9.23
	252	11.69	14.95	14.72	4.84	10.68	9.74	11.5	6.11	12.54

Chapter 3

Uncertainty Quantification in depletion calculations

Abstract - This Chapter discusses briefly different methodologies to propagate uncertainties, focusing on what has been done for uncertainty quantification studies of nuclear data uncertainties on transport/depletion/burn-up problems. A summary of methodologies/codes/tools available is shown, highlighting their capabilities to propagate nuclear data uncertainties in burn-up/depletion calculations. For methodologies/codes/tools applied during this thesis, a more extensive description is provided.

This chapter shows, partially or completely, works already presented in the following references:

- International Conference Proceeding [Díez et al., 2011].
- ANDES Deliverable D2.1 [Cabellos et al., 2011a].
- International Journal Article [Díez et al., 2013b].
- International Journal Article [Díez et al., 2013a].
- International Journal Article [Díez et al., 2014a].

3.1 Introduction to burn-up/depletion calculations and Uncertainty Quantification studies

Transport codes describe the propagation of sub-atomic particles, e.g. neutrons, in matter by solving the Boltzmann equation which includes both the flow and the interaction of the particles with the surrounding material. The interaction rates are usually determined from microscopic cross sections with nuclei. These interactions modify the nature of nuclides, by e.g. adding more neutrons to the nucleus or fissioning the nucleus, so nuclide concentrations change throughout the time. Radioactive nucleus can be obtained through such interactions, or being present at the beginning of the study, and their natures change also throughout the time because they are radioactive.

The material composition time evolution can be tackled by solving the Bateman equation (Eq. 3.1) with depletion codes:

$$\frac{dN_i}{dt} = \begin{array}{rr} -\lambda_i N_i + \sum_j \lambda_j \beta_{ji} N_j + & \text{(decay)} \\ + \sum_j N_j \left(\int \gamma_{j,i}(E) \sigma_{j,f}(E) \phi(E) dE \right) + & \text{(fission yield)} \\ + \sum_j N_j \left(\int \sigma_{j,i}(E) \phi(E) dE \right) - N_i \int \sigma_i(E) \phi(E) dE, & \text{(cross sections)} \end{array} \tag{3.1}$$

where N_i is the concentration of the isotope i, λ_i is its decay constant, β_{ji} is the branching ratio of the isotope j decay mode to the isotope i, $\gamma_{j,i}(E)$ is the fission yield of the isotope j which produces the isotope i, $\sigma_{j,f}(E)$ is the fission cross section as a function of the incident neutron energy E, $\sigma_{j,i}(E)$ is the sum of cross sections of the isotope j that generate directly the isotope i, and $\sigma_i(E)$ is the sum of cross sections that transmute the isotope i. The integrals are over the energy of the neutron spectrum $\phi(E)$, normalised this to the neutron flux level. If the neutron spectrum is normalised to 1, as done commonly, ϕ should be multiplied by the neutron flux level.

Such an equation requires not only interaction rates, neutron flux and spectrum in conjunction with cross section data, but also the decay data which determine how radioactive nuclides decay: mainly to which nuclide and how frequent. Then, nuclide concentrations under an irradiation field can be followed. If nuclide concentrations evolve throughout time, the neutron spectrum and flux (radiation field) have to be re-calculated under new conditions of concentrations. Therefore, transport and depletion calculations are coupled in order to evaluate properly the nuclide concentration and neutron field throughout time. Once these

variables are calculated, other derived functions, such as neutron multiplication factor k_{eff}, power generation or radiation emission, can be addressed. This type of problems are so-called burn-up problems.

As seen in Chapter 2, the required data for such calculations, the nuclear data, are provided with nuclear data libraries, e.g. ENDF/B-VII.1, JEFF-3.1.1 or JENDL-4.0. Nuclear data are then processed in order to serve as input for specific nuclear transport/depletion codes (e.g. SCALE [ORNL, 2009], MCNP [X-5 Monte Carlo Team, 2003], ACAB [Sanz et al., 2008], FISPACT-II [Sublet et al., 2012]). These input data have uncertainties which are translated into uncertainties for the results of nuclear transport/depletion codes.

Fig. 3.1 shows a typical scheme of a burn-up problem, where the coupling between transport and depletion parts is depicted. Transport calculations provide neutron flux level (ϕ) and its energy distribution (spectrum), apart from other responses e.g. k_{eff}, based on the material (isotopic) composition at a given time. Neutron flux and spectrum are fed (blue arrows) to depletion calculations which use such data to calculate interaction rates, and then, the new composition at the end of that burn-up step ($N_i \rightarrow N_{i+1}$) can be determined. The new composition is given to transport (red arrows), in which the same calculations are repeated, providing again new neutron flux level and spectrum to depletion. This iteration of transport/depletion calculations is thus repeated until e.g. a desired irradiation time is achieved or a burn-up (energy extracted from nuclear fuel) is reached.

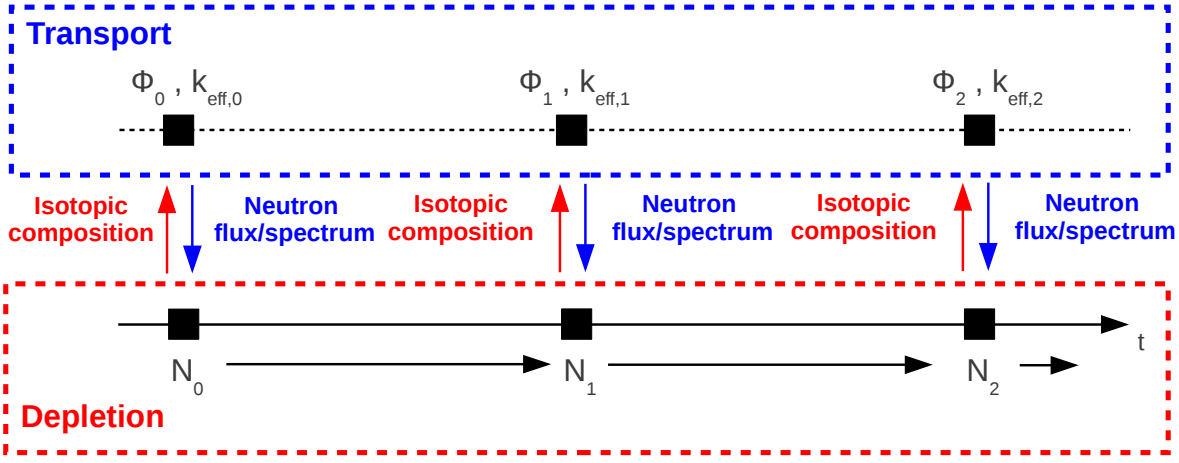

FIGURE 3.1: Typical burn-up scheme, coupling transport and depletion calculations.

Focusing only on nuclear data uncertainties, they affect both parts of a burn-up calculation: transport and depletion, because cross sections data are required by both parts. As stated

before, cross sections provide information how nucleus interact with neutrons and how the nucleus nature changes due to such interactions. Therefore, their uncertainties have to be taken into account in both parts. They first will induce uncertainties on transport calculations, which are then propagated to the depletion part through neutron flux and spectrum. Cross section uncertainties appear again in the depletion part explicitly, apart from being indirectly in neutron flux and spectrum, and affect the evolution of material compositions. In addition, decay data and fission yield data uncertainties have to be taken into account in depletion. After a burn-up step, the new composition carries an uncertainty which is propagated to transport, closing the loop described before for burn-up calculations.

When there is no material irradiation, or there is no relevant neutron field distribution to be calculated, the transport part is omitted from the scheme, and only depletion calculations are addressed. However, the propagation of the uncertainties remains the same, just without transport feedback.

3.2 Uncertainty Quantification general methodologies

An Uncertainty Quantification (UQ) study tries to determine how likely certain outcomes are if some aspects of the system are not exactly known. In other way, an UQ study assesses how uncertainties in input parameters of a model or problem affect the outputs, and tries to quantify the uncertainties on such outputs.

There are several methods to perform a UQ study:

- Local expansion-based methods, like propagation of moments [Cacuci, 2003] which is based on First Order Perturbation theory. With sensitivity coefficients of system responses to the system parameters and uncertainty data on such system parameters, uncertainties on system responses can be estimated.
- Simulation based methods – or Monte Carlo sampling [Gentle, 2003], which considers the system parameters with uncertainties as random variables. Then, after selecting probability density functions (PDFs) for these variables, they are sampled using the uncertainty data available. They are applied to the system model, obtaining random system responses. The uncertainties on system responses are then estimated with an statistical analysis.

- Functional expansion-based methods, like polynomial chaos expansion (PCE) [Ghanem and Red-Horse, 1999], where random quantities are represented by an expansion consisting of functions of random variables multiplied by deterministic coefficients. On these expansions, model functions are applied in order to obtain the dependency of the system responses as functions of such expansions. With the properties of the expansions, the uncertainty on responses can be addressed.

- Most probable point (MPP)-based methods [Haldar and Mahadevan, 2000] – or reliability methods, which are based on probabilistic approaches that compute approximate response function of the system, obtaining distributions of these functions based on specified uncertain variable distributions. These methods are usually applied to estimate uncertainties in the tails of the response distributions, because they are more efficient than sampling based approaches when assessing events with low probability.

Up to now, local expansion-based methods (First Order Perturbation Theory) and simulation based methods (Monte Carlo sampling) are being broadly applied to perform UQ studies of nuclear data uncertainties, but also other methodologies start to be introduced as e.g. PCE [Gilli, 2013, Dossantos-Uzarralde, 2008]. Therefore, only the first two mentioned methodologies are described on the following. These two methodologies are observed in methodologies/tools/codes aimed to perform such studies, such as TSUNAMI-SCALE6.0 [ORNL, 2009], MCNP code series like MCNP5 [X-5 Monte Carlo Team, 2003], ERANOS [Rimpault et al., 2002], Total Monte Carlo (TMC) [Koning and Rochman, 2008c], XSUSA [Zwermann et al., 2009], NUDUNA [Buss et al., 2011], Kiwi [Mattoon et al., 2012] and PSI-NUSS [Wieselquist et al., 2013, Zhu et al., 2014].

3.2.1 First Order Perturbation Theory / Propagation of moments

The propagation of moments [Cacuci, 2003] is a deterministic methodology for uncertainty propagation of uncertainties in system parameters on system responses based on sensitivity analysis, using First Order Perturbation theory. The sensitivity analysis studies the variation of system responses when system parameters change. With such information and the uncertainties in system parameters, given as covariance matrices, the uncertainties on system responses can be calculated. The development of the equations that lead to such result is described on the following.

Let R be the response function of a system that satisfies $R = f(\alpha_1, \alpha_2, \ldots, \alpha_k)$, where the system parameters are $(\alpha_1, \alpha_2, \ldots, \alpha_k)$. If these parameters are defined with a mean value α_i^0 and its uncertainty $\delta\alpha_1$ given as std.dev., α_i can be represented as a linear function of α_i^0 and $\delta\alpha_i$:

$$(\alpha_1, \alpha_2, \ldots, \alpha_k) = (\alpha_1^0, \alpha_2^0, \ldots, \alpha_k^0) + (\delta\alpha_1, \delta\alpha_2, \ldots, \delta\alpha_k) = \alpha^0 + \delta\alpha. \tag{3.2}$$

If the response function is applied to Eq. 3.2, and it is expanded using a Taylor series around the mean value α^0, retaining only the terms up to the second order in the variations of $\delta\alpha_i = (\alpha_i - \alpha_i^0)$, Eq. 3.3 is obtained:

$$\begin{aligned} R(\alpha_1, \alpha_2, \ldots, \alpha_k) = \quad & R(\alpha_1^0, \alpha_2^0, \ldots \alpha_k^0) + \textstyle\sum_{i=1}^{k} \left[\left(\frac{\partial R}{\partial \alpha_i} \right)_{\alpha^0} \cdot \delta\alpha_i \right] && \text{(first order)} \\ & + \textstyle\sum_{i,j=1}^{k} \left[\left(\frac{\partial^2 R}{\partial \alpha_i \delta\alpha_j} \right)_{\alpha^0} \cdot \delta\alpha_i \cdot \delta\alpha_j \right]. && \text{(second order)} \end{aligned} \tag{3.3}$$

Considering the system parameters $(\alpha_1, \alpha_2, \ldots, \alpha_k)$ as random variables distributed according to a Gaussian PDF $p(\alpha_1, \alpha_2, \ldots, \alpha_k)$, the next properties can be described:

$$E\left[\alpha_i\right] = \alpha_i^0, \tag{3.4}$$

$$var\left[\alpha_i, \alpha_i\right] = \int_{S_\alpha} \left(\alpha_i - \alpha_i^0\right)^2 p(\alpha_1, \alpha_2, \ldots, \alpha_k) d\alpha_1 d\alpha_2 \ldots d\alpha_k = \sigma_i^2. \tag{3.5}$$

If only the first terms of the approximation are taken, the results of calculating the mean value and the variance are obtained through Eq. 3.6 and Eq. 3.7, respectively:

$$E\left[R\right] = \int_{S_\alpha} \left[R(\alpha_1^0, \ldots, \alpha_k^0) + \sum_{i=1}^{k} \left(\frac{\partial R}{\partial \alpha_i} \right)_{\alpha^0} \cdot \delta\alpha_i \right] p(\alpha_1, \ldots, \alpha_k) d\alpha_1 \ldots d\alpha_k = R\left(\alpha^0\right), \tag{3.6}$$

$$\begin{aligned} var\left(R\right) = E\left[\left(R - R_0\right)^2\right] = \textstyle\int_{S_\alpha} \left[\sum_{i=1}^{k} \left(\frac{\partial R}{\partial \alpha_i} \right)_{\alpha^0} \cdot \delta\alpha_i \right]^2 p(\alpha_1, \ldots, \alpha_k) d\alpha_1 \ldots d\alpha_k = \\ = \textstyle\sum_{i=1}^{k} \left[S_i^2 var(\alpha_i) \right] + \sum_{i,j=1}^{k} \left[S_i S_j covar(\alpha_i, \alpha_j) \right], \end{aligned} \tag{3.7}$$

where $S_i \equiv \left(\frac{\partial R}{\partial \alpha_i} \right)_{\alpha^0}$ are the sensitivity coefficients of the response function to system parameters α_i. Also, Eq. 3.7 can be written in matrix form, resulting in Eq. 3.8, which is colloquially known as the "sandwich rule":

$$var\left(R\right) = S V_\alpha S^T. \tag{3.8}$$

In Eq. 3.8, S is a column vector that contains $S = (S_1, \ldots, S_k)$, and V_α denotes the covariance matrix for the system parameters.

With the described method above, nuclear data uncertainties can be propagated to response functions. However, the main issue is to calculate the sensitivity coefficients to each parameter of the problem. Different methodologies can be used to obtain such sensitivity coefficients, such as the Forward Sensitivity Analysis Procedure (FSAP) [Cacuci, 2003] or the Adjoint Sensitivity Analysis Procedure (ASAP) [Cacuci, 2003]. Further descriptions are not provided because their are not in the scope of this work.

This approach has some drawbacks, especially the first order – linear – approximation applied. If variations of the parameters are too big, equivalent to high uncertainties, or response functions are non-linear, then, the perturbed system response obtained with a sensitivity methodology differs from the real value obtained by applying the perturbed parameters. This issue is illustrated in Fig. 3.2. To overcome such a limitation, it is necessary to use higher order approximations. When they are used, deviations between the mean value and reference value are found, so the propagation of uncertainties becomes more complex.

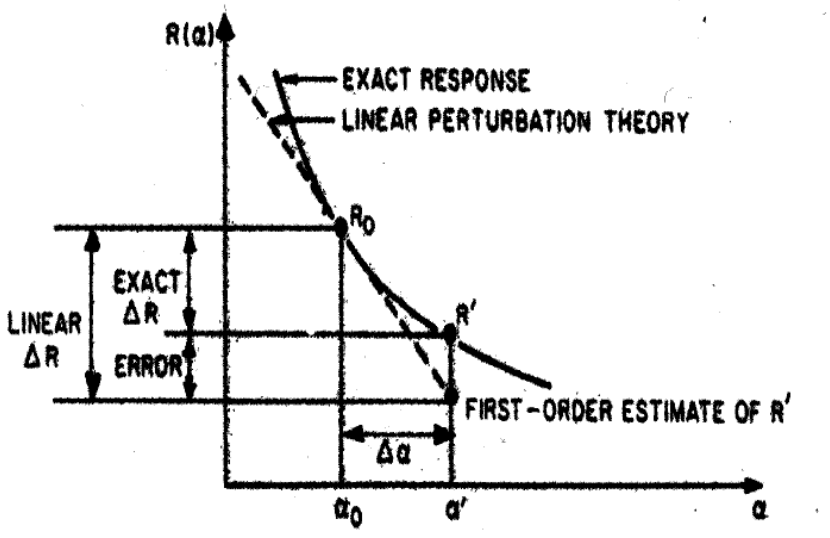

FIGURE 3.2: Differences between actual uncertainty and calculated uncertainty using a First-order approximation.

3.2.2 Monte Carlo sampling

Monte Carlo sampling is an stochastic methodology where mathematical expressions are evaluated using random numbers [Gentle, 2003]. These mathematical expressions can be definite integrals, systems of equations, or more complicated mathematical models. In this case, system parameters are treated as random variables, and the objective is to evaluate their impact on response functions.

Variables with uncertainties, which will be propagated, are considered as random variables. They are sampled using mean values and covariance matrices with an associated PDF. Then, the random draws are fed into the mathematical model or code that will provide the response functions to study. In this way, the uncertainties are propagated to response functions due to the variation of system parameters.

Each sampling of the system parameters provides new values, with which response functions are calculated. Each time this step is performed, a new result – history – is obtained. So when an large enough number of histories is reached, a statistical study can be done on the histories obtained. The effect of the uncertainties on response functions can thus be analysed. Fig. 3.3 represents the scheme of Monte Carlo sampling.

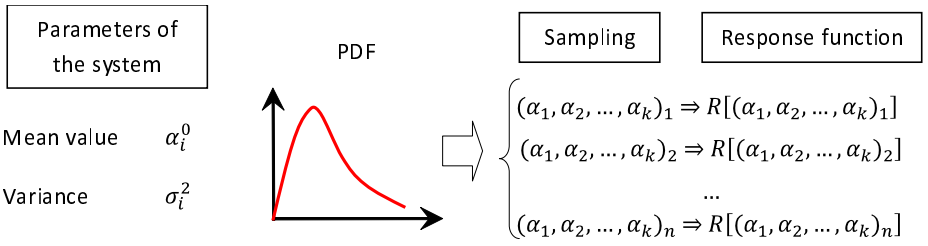

FIGURE 3.3: Scheme of Monte Carlo sampling

In order to know if it is necessary to increase the number of histories, a study of the different statistical moments of the response function is performed, observing the convergence of these values. Here, the convergence of the relative standard deviation (second moment) is followed. Also, statistics of such variables can be evaluated in order to know their confidence intervals, but here the convergence is addressed only by following the statistical moment mentioned before.

This technique also allows to study partially the individual effect of each system parameter, their relevance and contributions the total uncertainty on response functions, and the possible

correlations between parameters due to system equations and response functions. This is achieved by sampling one-by-one the parameters to study, and then, a statistical analysis is performed on the response function. This is equivalent to a First Order approach, where sensitivity coefficients are calculated in such a way. However, the limitation of the linear approximation is avoided.

There are other approaches that try to use the results from sampling all the system parameters to assess their individual relevance, such as Sobol's variance decomposition [Sobol, 2001, Arwade et al., 2010].

3.3 Methodologies/codes/tools for nuclear data uncertainty propagation

Nowadays, there are several codes/tools that can carry out UQ studies of nuclear data for nuclear applications. However, there also exist other tools, more general, that can perform UQ studies independently of the source of uncertainty. Depending on the methodology/code/tool, either transport or depletion of both (burn-up) problems can be addressed.

As stated before, there are two main trends for UQ codes/tools which propagate nuclear data uncertainties: the ones that use First Order Perturbation Theory, and the others which use Monte Carlo sampling. Grouping in these two methods, the most relevant codes/tools are presented:

Based on First Order Perturbation Theory:

- SCALE6.0 [ORNL, 2009], thanks to its TSUNAMI sequence, UQ studies on criticality calculations (transport calculations) can be carried out. It implements the First Order Perturbation Theory with the Adjoint-Weighted Technique (described in [ORNL, 2009, Sect.F22]). That means adjoint solutions of the transport problem are evaluated, obtaining sensitivity coefficients of response functions to cross section data. Only uncertainties from cross sections, fission neutron emission and fission neutron spectra are propagated. Uncertainties are taken from the SCALE6.0 uncertainty library (already presented in Chapter 2, Sec. 2.6.3).

- MCNPX-2.7e [Pelowitz, 2008] and MCNP5 [X-5 Monte Carlo Team, 2003] can calculate sensitivity coefficients to cross sections for criticality calculations (transport calculations), once an energy-group structure is defined for them. It makes use of the Differential Operator Technique, which applies the First Order Perturbation Theory. It performs perturbations on the cross section values for which their sensitivity coefficients are required. To obtain uncertainty values, the sandwich formula and data handling should be implemented by the user, as done e.g. in [Díez et al., 2013b].

- SUSD3D [Kodeli, 2008] calculates sensitivity coefficients and standard deviation in the calculated detector responses or design parameters of interest due to input cross sections and their uncertainties. That means only criticality calculations (transport calculations) can be addressed. Several types of uncertainties can be considered, i.e. those due to: neutron/gamma multigroup cross sections, energy-dependent response functions, secondary angular distribution or secondary energy distribution (SED) uncertainties. Direct and adjoint solutions for the neutron flux should be provided, in conjunction with nuclear data covariances processed with NJOY, to estimate uncertainties.

- ERANOS [Rimpault et al., 2002] stands for European Reactor ANalysis Optimized calculation System. It consists of data libraries, deterministic codes and calculation procedures capable of solving transport, depletion and burn-up calculations. Sensitivity analysis based on First Order Perturbation Theory has been implemented, performing adjoint calculations. In combination with the RIB tool [Venard et al., 2009], uncertainties on transport calculations can be estimated for neutron multiplication factor k_{eff}, ratios of linear or bilinear integrals and reactivity effects.

TSUNAMI-SCALE6.0 and MCNPX-2.7e/MCNP5 techniques have been compared for criticality calculations [Díez et al., 2013b], giving a better understanding of how to apply the First Order Perturbation Theory. All the previous tools are limited to criticality (transport) calculations. Although, as shown in [Cabellos, 2013], results from such codes/tools can be used also for burn-up calculations if estimations of the depletion part are provided. So, depletion effect on transport are assessed with sensitivity coefficients to isotopic concentrations. It is summed up with the transport effect in order to provide an estimation of both sources. However, also in [Cabellos, 2013], joint effects are observed as important, therefore, it is necessary for burn-up problems to overcome the uncertainty propagation in both parts at the

same time. Up to now, there is no implementation of the First Order Perturbation theory that tackles uncertainty propagation in burn-up problems as one unique entity.

Based on Monte Carlo sampling:

- Hybrid Method [García-Herranz et al., 2008], which performs UQ studies only in depletion calculations, decoupling the depletion part from transport when burn-up calculations are addressed. It is described later in Chapter 4.
- Kiwi [Mattoon et al., 2012], is a LLNL's application designed to be an interface between nuclear data covariances and UQ studies. It can be used to produce random draws of nuclear data, varying them accordingly to their covariances. The sampling is performed by obtaining the Single Value Decomposition (SVD) of the covariance matrix, and it keeps the total cross section values as being an energy conservation constraint. Up to now, it has been only applied to criticality calculations. However, if random draws of nuclear data are also applied in depletion calculations, it is possible to carry out UQ studies also on burn-up problems.
- NUDUNA [Buss et al., 2011] carries out UQ studies on transport, depletion and burn-up calculations based on variations of nuclear data according to their uncertainty information, given in ENDF-6 format files. Further description is given in Sec. 3.5.
- Total Monte Carlo (TMC) [Koning and Rochman, 2008c], as NUDUNA, can perform UQ studies on transport, depletion and burn-up problems, thanks to the generation of random nuclear data through nuclear model codes. It is based on experimental and evaluated data. A complete description is provided in Sec. 3.4.
- XSUSA [Zwermann et al., 2009] can propagate nuclear data uncertainties by means, again, of sampling the nuclear data based on their uncertainties. Up to now, it can be only used with SCALE, providing random realisations of cross section, decay data and fission yields. So not only transport and depletion calculations can be tackled, but also burn-up problems. For cross sections, it is limited to multi-group cross section data.

Apart from above mentioned codes, which are specifically developed for propagating nuclear data uncertainties, there are tools such as DAKOTA [Adams et al., 2009], which provides general-purpose uncertainty quantification modules. In this case, DAKOTA can apply Monte Carlo sampling (with different sampling schemes e.g. Latin Hypercube Sampling – LHS),

reliability methods like mapping method, or stochastic expansion methods like PCE. The only requirement for users is to create the interface between DAKOTA and the simulation code/s to transmit the inputs/outputs between them. DAKOTA also performs the analysis of outcomes.

3.4 Total Monte Carlo – TMC

The main aim of the TMC approach is to simulate consequences of uncertainties in microscopic nuclear physics on nuclear designs without any limitation in between. Then, nuclear data uncertainties can be propagated in any kind of calculation without any approximation. This approach is based on the TALYS software package [Koning et al., 2009, Koning et al., 2013a], but TMC makes use of other different codes. A flowchart of the codes used by TMC is presented in Fig.3.4. It shows that by looping over the entire process of basic nuclear physics, data file production, data file processing and applied calculations, a natural statistical approach towards uncertainty propagation can be obtained. The codes are briefly explained as followed:

- TALYS is the nuclear reaction code that simulates reactions that involve neutrons, gamma-rays from thermal to 200 MeV energy range. With a single run, cross-sections, energy spectra, angular distributions for all open channels over the whole incident energy range are predicted. These nuclear models are driven by a restricted set of parameters that can be varied in each TALYS input file.

- TARES is the code that generates the resonance information in the ENDF-6 format, including covariance information. It uses the resonance parameter databases such as EXFOR database [Otuka et al., 2011], resonance parameters from other libraries or compilations.

- TEFAL is the computer code for the translation of the nuclear reaction results from TALYS, and data from other sources if TALYS is not adequate, into ENDF-6 formatted nuclear data libraries.Then, the results of TALYS can be used directly on processing codes and application codes.

- TANES is a simple program to calculate fission neutron spectrum based on the Los Alamos model [Talou, 2007]. The original Madland-Nix [Madland and Nix, 1982] for

the calculation of prompt fission neutrons characteristics (spectra and multiplicity) has been implemented in a stand-alone module. The TANES code uses this stand-alone module, combined with parameter uncertainties (on the total kinetic energy, released energy and multi-chance fission probabilities) to repeat and randomise the fission neutron spectrum. The output of this program are central values for the fission neutron spectra at different incident energies and random fission neutron spectra.

- TAFIS is used to calculate both fission yields, prompt neutron emission from fission and necessary fission quantities (kinetic energy of the fission products, kinetic energy of the prompt and delayed fission neutrons, total energy released by prompt and delayed gamma rays and beta). It calculates the independent and cumulative fission yields at any incident energy up to 200 MeV and for different incident particles (spontaneous, neutrons, protons, deuterons...). The output of this program is a fission yield file with uncertainties, prompt neutron emission files for central and random values and a list of central and random fission quantities.

- TASMAN is a computer code for the production of random nuclear data files and the production of covariance data using results of the nuclear model code TALYS and TARES, and for automatic optimization of the TALYS/TARES results with respect to experimental data. The essential idea is to assume that each nuclear model parameter has its own uncertainty. Then, this parameter should follow a PDF that is assumed to be a Gaussian. Running TALYS many times, whereby each time all parameters are randomly sampled from a Normal PDF, provides all needed statistical information to produce a full covariance matrix.

TASMAN uses central value parameters obtained from a best fit to experimental cross-sections and angular distributions. The uncertainties on these parameters are obtained after randomly sampling the parameters and checking which ones are inside the experimental data uncertainties (i.e. retrieved from EXFOR database). This approach tends to reproduce the experimental uncertainties. Then, the process of assigning uncertainties to the nuclear data parameters consists in two steps. First, suggested parameter uncertainties are used to start the sampling of cross-sections. Using these results, it is checked which ones are inside the experimental data. Second, this information is fed back to reduce or increase the parameter uncertainty, producing uncertainties that properly reproduce the experimental data and their

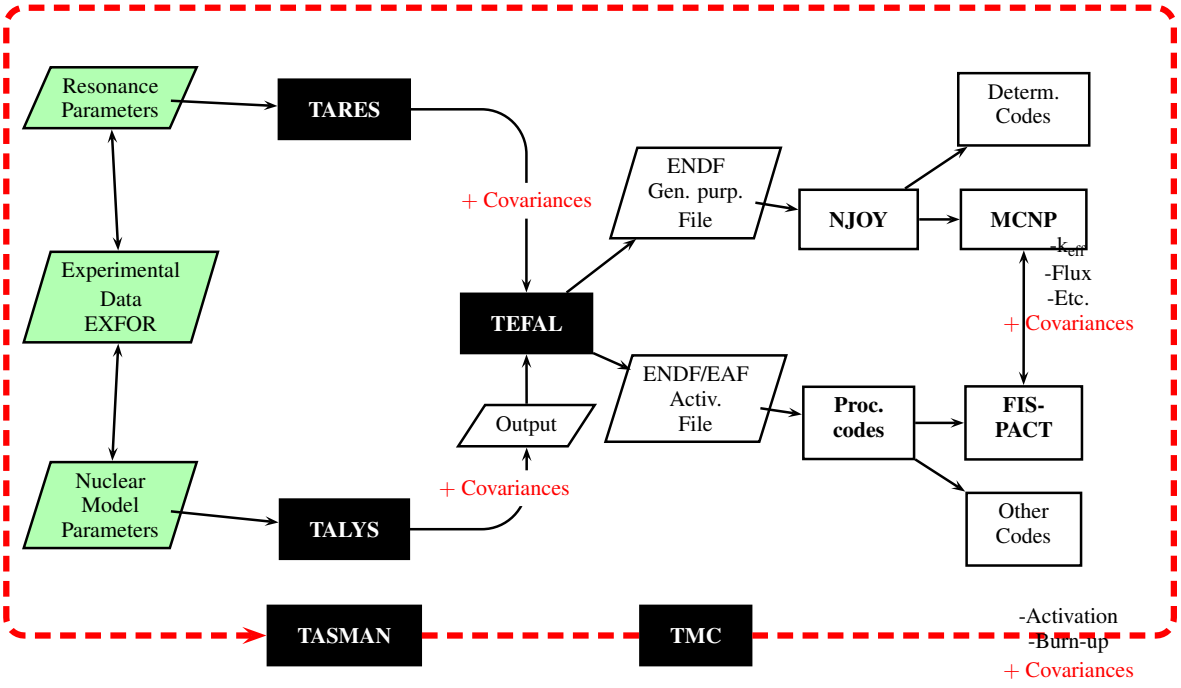

FIGURE 3.4: Flowchart of Total Monte Carlo (TMC) calculations, involving the four codes from the TALYS code system, processing codes and transport/reactor codes. (From [Díez et al., 2013a])

dispersions. The PDF can be chosen among uniform, Normal or other. In principle, with the least information available, the uniform is chosen; otherwise, the Normal PDF is selected.

There are differences between how thermal, resonance and fast cross-sections are randomly generated. In the thermal region, there is no *a priori* randomising process. The thermal cross-section values come from integral measurements, which have uncertainties. Then, in the resonance region, using TARES, each resonance is randomised using all parameters except the energy positions (the energy, E_0, at which resonance takes place). After sampling all resonances, it is checked if the thermal tail of the resonance region is within the uncertainty range of the thermal cross-section. If not, uncertainties in resonance parameters should be reduced. Therefore, thermal cross-sections are randomised *a posteriori* through the randomising of resonances. In the fast region (TALYS), all differential data are randomised. That means, cross-sections which are the sum of other cross-sections are not randomised, and their uncertainties are mathematically calculated. So, there is no normalisation factors in the fast region.

As presented above, the cross-section generation is split into two regions, so the covariance generation is also split in these two regions. Because two different methods are used, no

correlations are assumed between the thermal and the fast region. Correlation discontinuities could appear in the resonance-fast connection point. But it does not mean that cross-sections have also a discontinuity between these two regions.

Note that nuclear model parameters are independently randomised. However, because there are several constraints on the variation between different cross-sections inside the nuclear models, different cross-sections are highly correlated. The main constraint is the total cross-section. This magnitude is calculated using one nuclear model, and then, it is fed to the other nuclear models that calculate differential cross-sections such as (n, γ), (n,2n) or (n,inel) reactions. That means the sum of all these differential cross-sections cannot exceed the total cross-section value. So, if one of them increases, the others will decrease. That provokes high correlation factors between cross-sections such as $(n, fission)$ and (n, γ). Also, there are high correlation factors between different energies (within the same energy region, thermal or fast) because of the nuclear model stiffness. That means the shapes of the cross-sections could be almost always the same whichever parameter or set of parameters are modified, depending on the reaction.

If these uncertainty results are compared with experimental uncertainties, it can be seen that they are different because experimental values have low correlation. In order to reduce the correlations between different energies and to reproduce better the experimental uncertainties, these experimental uncertainties could be introduced also in the nuclear model. However, such a development has not been implemented yet.

The amount of parameters for nuclear models used on TALYS is rather high (from 50 to 80) and TARES needs at least two parameters per resonance for each non-actinide isotopes while it needs three per resonance for each actinide isotopes. Then, different techniques to sample the phase-space of parameters could be used, but here the Sobol quasi-random number generator is used.

As presented for MC approaches, the convergence of the problem should be checked in order to get reliable results after the statistical analysis. For TMC calculations, the convergence is checked in two ways. The first one is the convergence of the cross section: its mean value and its relative standard deviation are followed as convergence indicators, but also the structure of the covariance matrix should not change even if the amount of histories increases after convergence is reached. The second one is the convergence of application calculations, which is checked using the mean and relative standard deviation values of the calculated variables.

3.5 The NUDUNA tool

The NUDUNA (NUclear Data UNcertainty Analysis) program package [Buss et al., 2011] has been developed by AREVA GmbH. Here, it will be used as the main code to assess different approximations for UQ studies on burn-up problems, in conjunction with SCALE6.0.

It aims to provide full Monte Carlo sampling of the nuclear data inputs of nuclear transport/depletion/burn-up code calculations. Given such a tool, one can sample a finite number of input files, and perform for each input file a separate calculation. Then, the scattering of the individual results due to the different inputs leads to uncertainty estimation for the response function/observable by means of an statistical analysis. The flowchart of the NUDUNA random sampling procedure is depicted in Fig. 3.5.

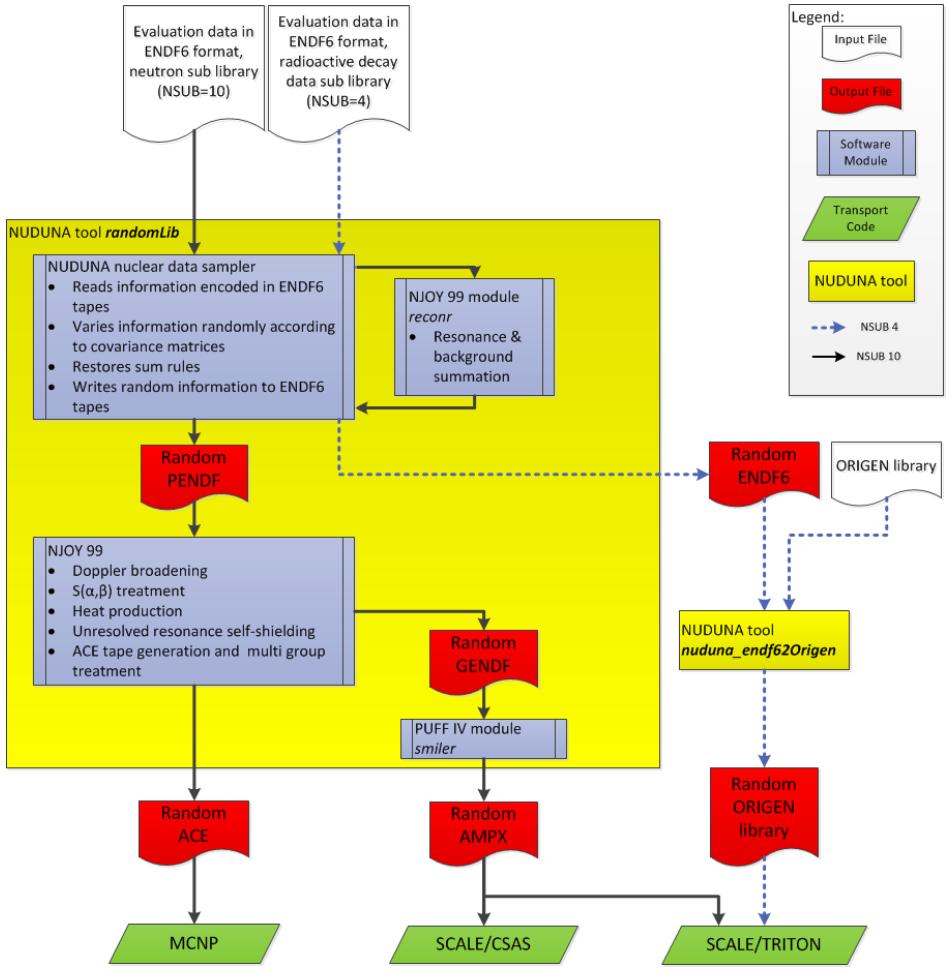

FIGURE 3.5: Flowchart of the NUDUNA procedure for sampling nuclear data input libraries.

NUDUNA retrieves the necessary nuclear data information from nuclear data evaluations which provide their results in the standardised ENDF-6 format and is capable of sampling

the data stored in the ENDF-6 formatted files based on the given covariance data.

Currently, NUDUNA is providing support for the MCNP5 code and the SCALE6.0 tool suite (for the TRITON depletion sequence).

3.5.1 Generation of random nuclear data

NUDUNA is capable of retrieving and handling nuclear data from ENDF-6 formatted files. At present, the following data are included in the random sampling process, generating random ENDF-6 formatted files:

- fission neutron emission $\overline{\nu}$ - MF1,
- resonance parameters - MF2,
- cross sections - MF3,
- angular distributions - MF4,
- decay data - MF8 MT457.

The next sections summarise how the nuclear data are randomised. The user can always choose between using normal or log-normal probability distributions.

3.5.1.1 Fission neutron emission $\overline{\nu}$ - MF1

Fission neutron emission $\overline{\nu}$ is the average number of neutrons emitted per fission. They are stored in MF1, accounting for total, prompt and delayed fission neutron emissions. They obey the sum rule

$$\overline{\nu}_{total}(E) = \overline{\nu}_{delayed}(E) + \overline{\nu}_{prompt}(E), \tag{3.9}$$

where $\overline{\nu}_{total}(E)$ is the total fission neutron emission, while $\overline{\nu}_{delayed}(E)$ the delayed and $\overline{\nu}_{prompt}(E)$ the prompt fission neutron emission.

The data are sampled according to their covariances, provided in MF31. Next, the sum rule given in Eq. 3.9 is checked and, if necessary, restored. If the ENDF-6 file provides no information on how this rule should be restored, by default total data will be discarded, and it is re-calculated by the sum of prompt and delayed.

3.5.1.2 Resonance Parameters - MF2

The resonance region is divided into the so-called Resolved Resonance Region (RRR) and Unresolved Resonance Region (URR). The parameters that describe the resonances in both sub-regions are given in MF2, whose uncertainties given in MF32.

Due to an ambiguity in the ENDF-6 format for the definition of the URR parameter covariances, they are at present not sampled. This does not create an issue for ENDF/B-VII.1, since it does not include URR covariance parameters for any isotope relevant to LWR analyses.

The RRR parameters are randomised, but only the most important formalisms have been considered: Reich-Moore, Single-level Breit-Wigner and Multi-level Breit-Wigner. For the Breit-Wigner formalisms, the identity

$$\Gamma_{total} = \Gamma_\gamma + \Gamma_n + \Gamma_f + \Gamma_X, \tag{3.10}$$

which relates the different reaction-channel widths of the resonances, should be fulfilled. However, Γ_X is not given explicitly in MF2, so it is reconstructed by the nuclear data processing codes.

3.5.1.3 Cross sections - MF3

Cross section data are stored in MF3, and their uncertainties in MF33. These data have to be added to the resonance cross sections defined by RRR and URR parameters.

As stated in the ENDF-6 format manual, the covariance information provided in the cross section covariance files (File 33) is related to the sum of non-resonant and resonant contribution. Thus first the resonance cross sections have to be reconstructed and added to MF3, and only then the random sampling can be performed.

The covariance data are given in energy ranges, and it is assumed that all points defined in the same energy range are completely correlated. Finally, sum rules have to be fulfilled and the following procedure is applied if the ENDF-6 file does not provide complete data on how to restore the sum rule:

- If a cross section is given by the sum of others, e.g. the total cross section, and has no uncertainty information, then this cross section is calculated using its sum rule.

- If there is covariance information for the sum and at least for one of the addends, then the sum is evaluated as sum of the random draws of all addends. So, the covariance information on the sum is neglected.
- If there is uncertainty information for the sum but for none of the addends, then the addends are re-scaled in order to fulfil the sum rule.

There are nuclear data evaluations that provide covariance information between different nuclides. However, such correlations are not yet implemented in NUDUNA.

3.5.1.4 Angular distributions - MF4

Angular distributions of the final state particles are stored in MF4, while their uncertainties are in MF34. Usually, they are expressed as normalised probability distributions given in Legendre representation. All, except the 0^{th} term of the expansion, are randomised accordingly to their covariances (the 0^{th} term remains unchanged because it defines the normalisation factor). The distribution must be always positive. If the random draws lead to negative distributions, then they are rejected and additional random draws are performed.

3.5.1.5 Decay data - MF8 MT457

The decay data in ENDF-6 format are stored in the radioactive decay data sub-library 4 (NSUB=4), File (MF8), Section 457 (MT457). Randomise decay data is a new feature implemented in NUDUNA, where random draws of half-life and branching ratio values can be generated. They are sampled from uncertainty data stored in ENDF-6 formatted files.

Generating random decay data is very simple for half-life values: because there is no existing correlation with any other magnitude, it is just enough to choose a PDF to sample from. Meanwhile, the sampling of the branching ratios is not straightforward, and the following scheme is applied, for two or more decay modes. For two decay modes:

- Whose both standard deviations of the branching ratios are identical: it is assumed that the uncertainty values have been evaluated by taking into account that the sum over all the branching ratios is constrained to one. Therefore, both variables are fully correlated, so the sampling is performed only for one of the variables and the other is calculated according to the constraint.

- Whose both standard deviation values are given, but are not identical: it is assumed that the constraint on the sum of the branching ratios was not yet taken into account. Here the constraint is enforced by updating the covariance matrix according to a Generalised Least Square (GLS) update. The result yields identical standard deviation values for both decay modes and the sampling is again performed only for one of the variables, calculating the other according to the constraint.

- If only one uncertainty value is given (so for the other, the ENDF-6 file just provides 0.0 as value), then it is assumed that both branching ratios have the non-zero uncertainty value. So that, the case of identical standard deviation values is again applied.

- No uncertainty values are given: No sampling is performed.

For more than two decay modes:

- At least uncertainty for one branching ratio is provided: the branching ratios, for which uncertainties are given, are sampled independently. For the other branching ratios without uncertainty information, a normalisation factor f is applied to the nominal values which is calculated according to

$$f = \frac{1 - \sum_{i \in \mathcal{A}} \beta_i}{\sum_{i \in \mathcal{B}} \beta_i}, \tag{3.11}$$

  where β are the branching ratios, $\mathcal{A}$ is the group of branching ratios with uncertainties, and $\mathcal{B}$ is the group without uncertainties. So the non-randomised part is re-adjusted in order to fulfil the constraint.

- All branching ratios have uncertainties: again, it is assumed that the constraint of the branching ratios was not yet taken into account. The constraint is enforced by updating the covariance matrix with a GLS procedure, and the branching ratios are sampled from the updated covariance matrix.

- No uncertainty values are given: no sampling is performed.

The sampled decay data are checked for validity: branching ratios and half-lives have to be positive, and the formers cannot get larger than one (1).

By default, NUDUNA assigns 100% uncertainty to every decay data that has no uncertainty information. This assumption is implemented before the the sampling procedure. That means, by default, the case where all the branching ratios have uncertainties will occur.

3.5.2 Converting ENDF-6 files into code-dependent format

NUDUNA provides also the capability of generating cross section libraries for MCNP and SCALE, and decay data libraries for ORIGEN-SCALE6.0.

The AMPX format is the input format for the SCALE transport codes KENO and NEWT [ORNL, 2009]. This format can contain so-called multi-group cross sections, where the original data have been collapsed to an energy group-wise structure representative for the application. Continuous-energy (CE) libraries can be read also by KENO, but NUDUNA does not provide the option to generate such CE libraries yet.

The multi-group cross section AMPX libraries are compiled with the help of the NJOY [MacFarlane and Kahler, 2010] and PUFF [Wiarda and Dunn, 2008] codes, as presented in Fig. 3.5. NJOY converts ENDF-6 files to group-wise ENDF-6 formatted tapes (called GENDF tapes), and then PUFF converts them into AMPX files.

As stated in Sec. 3.5.1, the cross section uncertainties have to be applied to the sum of resonance contributions (MF2) and background cross sections (MF3). So NJOY is eventually called twice in the process of generating random ENDF-6 files, first after sampling MF1, MF2 and MF4 in order to perform the resonance reconstruction, and then after sampling MF3.

The GENDF tapes are created based on the 238-groups structure and collapsing spectra of SCALE [ORNL, 2009] (which is suitable for typical PWR reactors). Once the GENDF file is created, PUFF is applied and the AMPX file is obtained. With the usage of the AJAX module of SCALE, these random libraries can be used in calculations.

Since ORIGEN is responsible of carrying out the depletion part of a burn-up problem, it has to be fed with the previous random cross section data. Thanks to the updating scheme of the cross section data in the TRITON sequence (which solves burn-up problems), the cross sections used by ORIGEN are updated automatically with the ones used in the transport part. However, this updating is not performed for all isotopes, just only for those ones specified by different input options. Furthermore, random cross sections cannot be used for all isotopes

treated by ORIGEN (in the depletion part), just for those relevant for transport calculations (which are the ones that can be selected through input parameters).

In order to generate random/nominal decay data libraries for SCALE6.0, the scheme presented in Fig. 3.5 is followed. It is necessary to translate ENDF-6 files into the ORIGEN format, so several considerations have to be taken into account when performing such translation:

- The ENDF-6 format can handle multiple particle emission decay modes, while the ORIGEN format can store only β^-+n. Therefore, branching ratios of any multiple particle emission decay mode that involves at least a β^-+n, are added to the β^-+n decay mode.
- The ENDF-6 format can provide branching ratios to daughters in excited levels higher than the first, while the ORIGEN format can only handle decay modes to the first excited (metastable) state. So, branching ratios to higher excited states than the first excited (metastable) state are added to the branching ratio to the first excited (metastable) state.
- The ENDF-6 format provides neutron emission decay modes (not related to β^-+n), while the ORIGEN format cannot handle. This decay mode is omitted in the translation.

After the conversion between formats, checks on the sum of branching ratios are performed. Finally, with the COUPLE module of SCALE6.0, random decay libraries can be used in depletion calculations with ORIGEN.

PART II

DEVELOPMENTS

Chapter 4

Developments with Hybrid Method

Abstract - This Chapter describes the Hybrid Method, aimed at propagating nuclear data uncertainties on isotopic evolution calculations, performing UQ studies of nuclear data uncertainties on depletion calculations. Two different approaches for its application are presented, depending on which cross section group-structure is used. Surrounding tools/sequences for nuclear data processing, routines for sampling, the ACAB depletion code and statistical analysis procedures are explained here together with how to use.

This chapter shows, partially or completely, works already presented in the following references:

- International Conference Proceeding [Díez et al., 2011].
- ANDES Deliverable D2.1 [Cabellos et al., 2011a].
- ANDES Deliverable D2.5 [Mills et al., 2013].
- ANDES Deliverable D2.6 [Cabellos et al., 2013].
- International Journal Article [Díez et al., 2013a].
- International Journal Article [Díez et al., 2014b].
- International Journal Article [Díez et al., 2014c].

Motivation

The impact of nuclear data uncertainties in depletion calculations is investigated in this thesis. A methodology denominated as "Hybrid Monte Carlo method" or Hybrid Method (HM) is developed by UPM. In [García-Herranz et al., 2008], its first implementation and application were presented, and this reference is selected as the starting point for further developments.

Then, the main tasks are, first, to review the initial implementation of HM and the methodology applied. That means not only going through theoretical research, but also reading hundreds of Fortran 77 code lines. No comparisons were made against other Monte Carlo sampling methodologies, only with First Order Perturbation approaches, so further investigations are required. HM has to be fed with nuclear data and uncertainties, requiring to perform a set of tasks such as processing data or collapsing data. Such tasks are carried out with sequences of codes/tools. These tools/codes are reviewed and updated in order to e.g. make HM capable of using new covariance data provided in different storing formats not already implemented. Additionally, the sampling stage needs to be reviewed for implementing the multi-covariate normal variables sampling. Finally, the different tools/sequences developed to read and analyse different response functions are merged, so only one sequence/tool is used.

All statements mentioned above motivates the realisation of a PhD Thesis, in addition to the state-of-the-art study performed previously. It departs from the first implementation of HM, reviewing its methodologies and others similar, comparing with different methodologies, implementing new sequences for handling new formats, improving the sampling state, translating code from Fortran 77 to Fortran 90 with a more modular implementation, etc.

The main achievements, described also later, are:

- Improvement of UQ studies with HM when using one-group cross sections in depletion problems with different depletion steps by implementing correlated sampling.
- Implementation of the multi-group cross section approach for addressing depletion problems with different depletion steps.
- Review and enhancement of tools/sequences to use ENDF-6 format data.
- Implementation of tools/sequence to read and use COVERX format data.

- Improvement of the sampling stage, with proper multi-covariate normal sampling.
- Translation from Fortran 77 code to Fortran 90, with a modular implementation to make easier their reuse, application and further developments.
- Unification of tools/sequence for the statistical analysis of response functions.
- Implementation of analysis of most important contributor.

4.1 Description of the Hybrid Method

This method proposes to perform the uncertainty propagation of nuclear data based on Monte Carlo sampling, decoupling the depletion part from the transport calculation. That means uncertainties are only propagated to response functions that come from the depletion problem, i.e. from solving the Bateman equation for the temporal evolution of isotopic concentrations presented in Eq. 3.1. Then, the response functions derived from isotopic concentrations can be addressed, such as decay heat and radiotoxicity.

With this method, neither uncertainties on the neutron spectrum nor the feedback of uncertainties in isotopic composition to neutron spectrum are taken into account. That means possible effects of coupling with transport calculations are assumed to be smaller compared with the explicit effect of nuclear data uncertainties on isotopic compositions. Indeed, the effect of statistical uncertainties in neutron spectrum due to usage of Monte Carlo transport solvers has been addressed already in [García-Herranz et al., 2008], showing that its impact is negligible when large enough amount of transport histories are run.

The main advantage of decoupling depletion from transport is that transport calculations are not required to be performed between two different burn-up points. A real improvement can be obtained since the transport part is usually the bottleneck of burn-up calculations regarding CPU-time performance, even more if a Monte Carlo sampling scheme is selected for transport. Although, new developments are currently reducing such a CPU-time demand [Zwermann et al., 2012, Rochman et al., 2014].

4.2 Working flowcharts/schemes

There are two approaches about how to apply the Hybrid Method to depletion calculations. One was initially proposed in [García-Herranz et al., 2008], based on the usage of one-group effective cross sections. However, an approach using multi-group cross sections can be used too, which is more general.

4.2.1 Using one-group cross sections

For depletion calculations, only collapsed one-group cross sections are required as input. So, uncertainties collapsed in one-group can be used instead of the multi-group, reducing the amount of variables to sample.

In the same way as the multi-group cross sections (σ_i, where i refers to the energy group) are collapsed to one-group value (σ_{1g}) with Eq. 4.1 using the multi-group neutron spectrum (ϕ_i), their uncertainties can be collapsed as well with Eq. 4.2. It is derived from the Taylor series and propagation of moments, where V is the covariance matrix in which the uncertainties of multi-group cross section data are represented. Then, the one-group cross sections can be treated as random variables, and can be sampled using these means and covariance matrices.

$$\sigma_{1g} = \left(\frac{\phi_1}{\phi_T}, \cdots, \frac{\phi_n}{\phi_T}\right)(\sigma_1, \cdots, \sigma_n)^T = \omega^T \sigma, \tag{4.1}$$

$$var(\sigma_{1g}) = \omega^T V \omega \quad ; \quad \omega_i = \frac{\phi_i}{\phi_T}. \tag{4.2}$$

Under the assumption of keeping the neutron spectrum invariant in every burn-up step, and considering that only depletion equations are being solved, Eq. 4.2 conserves reaction rate uncertainties independently whether one-group or multi-group cross sections are used.

As shown before, for depletion calculations, reaction rates (R) only depend on one-group cross sections and neutron flux level (ϕ_T):

$$R = \phi_T \cdot \sigma_{1g}. \tag{4.3}$$

Therefore, if the neutron spectrum and flux are assumed to be constant during the burn-up time analysed, cross sections are the unique source of uncertainty. No uncertainty can come

through the spectrum or flux after under this assumption. Then, the uncertainty on such reaction rates can be calculated through the propagation of moments method (see Chapter 3, Sec. 3.2.1):

$$var(R) = \phi_T^2 \cdot var(\sigma_{1g}), \tag{4.4}$$

$$var(\sigma_{1g}) = \left(\frac{d\sigma_{1g}}{d\sigma_i}\right)^T V \left(\frac{d\sigma_{1g}}{d\sigma_i}\right), \tag{4.5}$$

$$\left(\frac{d\sigma_{1g}}{d\sigma_i}\right) = \left(\frac{\phi_i}{\phi_T}\right) = \omega_i, \tag{4.6}$$

where the sensitivity coefficients of σ_{1g} have been already defined as the ω vector in Eq. 4.1. From these equations, one can observe that it is completely equivalent to use one- or multi-group cross section uncertainties under such assumptions.

Finally, the scheme to follow when using one-group cross section uncertainties is presented in Fig. 4.1, and explained below:

1. A single complete coupled transport-depletion problem is performed, from which the spectrum in every depletion step is retrieved. No uncertainties are propagated.
2. Collapse the multi-group cross section library and their uncertainties to one-group for every burn-up step, using the neutron spectrum obtained in the best-estimated calculation.
3. Sample the one-group cross sections accordingly to their collapsed covariance matrix.
4. After a large enough set of histories are carried out, the uncertainties on the cross section data are propagated, and their effects are assessed with a statistical analysis of the response functions.

4.2.1.1 The need of correlated sampling

Burn-up calculations are split into several burn-up steps in order to update the neutron flux and spectrum used in the depletion part. So variations in the spectrum modify the cross-section mean values, σ_{1g}, and their variance-covariances. That means PDF parameters (mean values and covariance matrices), different from the previous burn-up steps, will be used in the burn-up step being calculated. However, the original random variables were the multi-group cross sections, σ_i, and they do not change between burn-up steps. If the multi-group

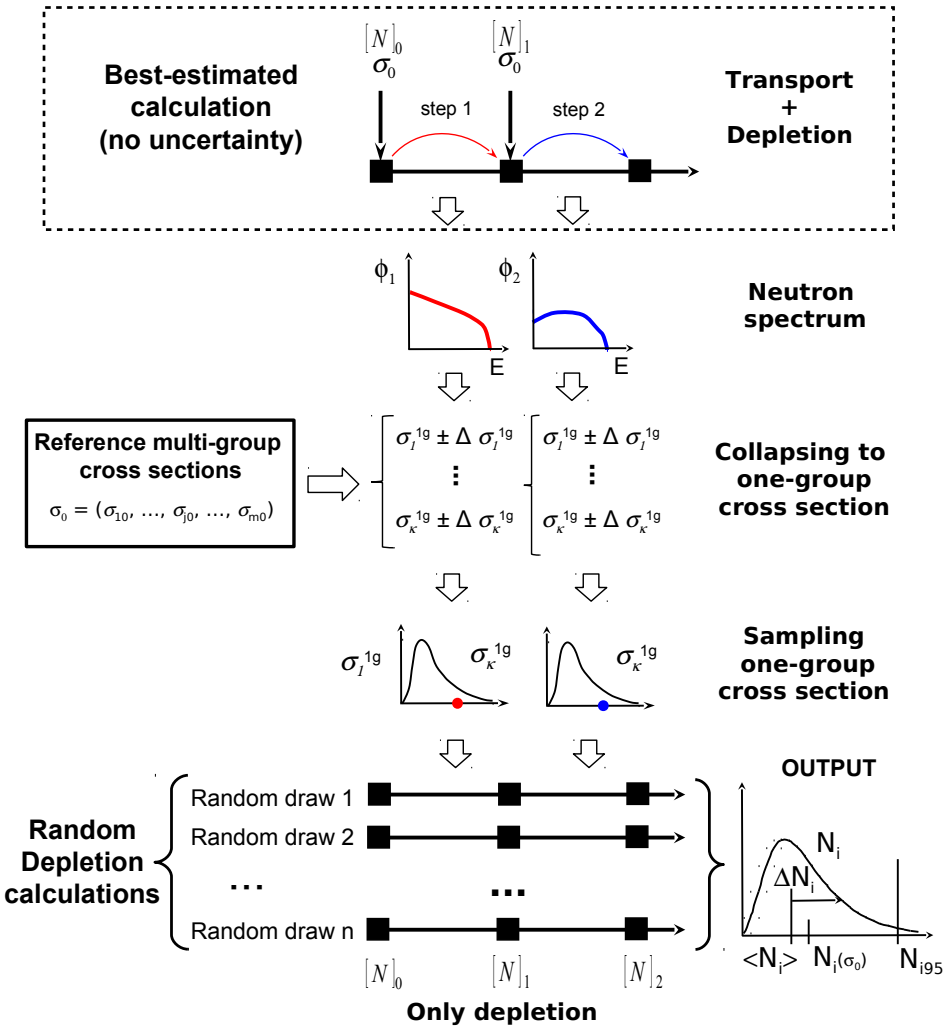

FIGURE 4.1: Scheme of the Hybrid Method using one-group cross section uncertainties.

cross-sections were sampled instead, the random cross section would be determined from the very beginning because in each step the random one-group cross-section would be calculated collapsing the random multi-group cross section with the neutron spectrum corresponding to its burn-up step. Hence, if one-group random cross-sections are used, that implies a relationship between one-group random cross section values of each burn-up step for a given history.

Therefore, sampling one-group cross sections of different burn-up steps cannot be done independently. Statistically, the random one-group cross section of two different burn-up steps (e.g j and k) are correlated, as given in Eq. 4.7:

$$Var(\sigma_{1g,j}, \sigma_{1g,k}) = Var(\omega_j^T \sigma, \omega_k^T \sigma) = \omega_j^T V \omega_k. \tag{4.7}$$

If spectrum variations between burn-up steps are small, correlations between the same reaction cross section of two different burn-up steps are close to one. Also, if relevant group cross sections of different burn-up steps (because of the high values of their spectrum group) are highly correlated through V, correlations close to one will be obtained.

In such cases, when variations of the spectrum take place between burn-up steps or depletion steps, correlated sampling is implemented in order to keep a Monte Carlo scheme and to avoid the introduction of spectrum variation terms into Eq. 4.2. As represented in Fig. 4.2, correlated sampling uses the same random vector drawn from the selected PDF, e.g. Gaussian PDF N(0,1), for calculating the random one-group cross sections in every burn-up steps (for the same history). In this way, all the one-group cross sections in every burn-up step are determined with such a vector for this draw/history, and the correlation between cross sections of different burn-up steps is kept to one.

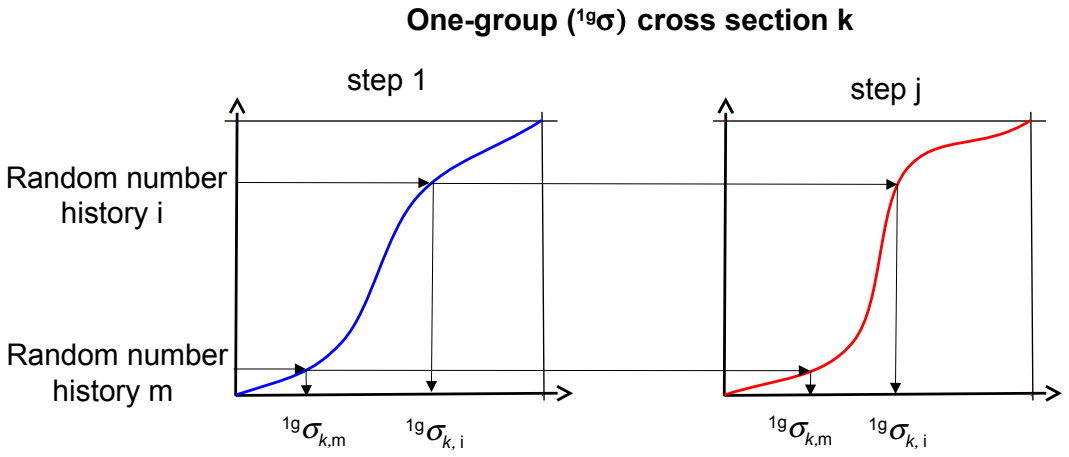

FIGURE 4.2: Relationship of one-group random cross sections between different burn-up steps when correlated sampling is performed.

4.2.2 Using multi-group cross sections

The scheme of work is presented in Fig. 4.3, and explained below, when multi-group cross section uncertainties are used:

1. (Idem as using one-group cross sections) A single complete coupled transport-depletion problem is performed, from which the spectrum in every depletion step is retrieved. No uncertainties are propagated.

2. Random multi-group cross section are drawn by sampling appropriate probability density functions (PDFs), – Normal or Lognormal – , accordingly to the covariance data used.

3. With one sample of the multi-group cross section, a complete depletion calculation is performed, obtaining one history. In every burn-up step, the random multi-group cross sections are collapsed with the neutron spectrum of the burn-up step to one-group, as required for depletion calculations.

4. (Idem as using one-group cross sections) After a large enough set of histories are carried out, the uncertainties on the cross section data are propagated, and their effects are assessed with a statistical analysis of the response functions.

As shown before, using multi-group cross sections avoids the problem of approximating the correlations of the same cross section between different burn-up steps because the multi-group cross sections are the origin of such correlations. So, if multi-group cross sections are used, the correlation issue does not appear. Indeed, burn-up/depletion problems with large spectrum/flux variations can be tackled properly, even if there are no correlations between relevant energy-groups for the application studied.

4.3 Application of the Hybrid Method – Implementation

In order to apply and carry out any of the two approaches described before, using one- or multi-group uncertainties, the next steps have to be completed:

- Processing and collapsing nuclear data and their uncertainties.
- Sampling nuclear data.
- Running the ACAB depletion code.
- Calculating response function uncertainties.

4.3.1 Processing and collapsing nuclear data and their uncertainties

Nuclear data information is not always stored using the same format, as shown in Chapter 2, and these formats do not correspond to the one used by the ACAB depletion code. In

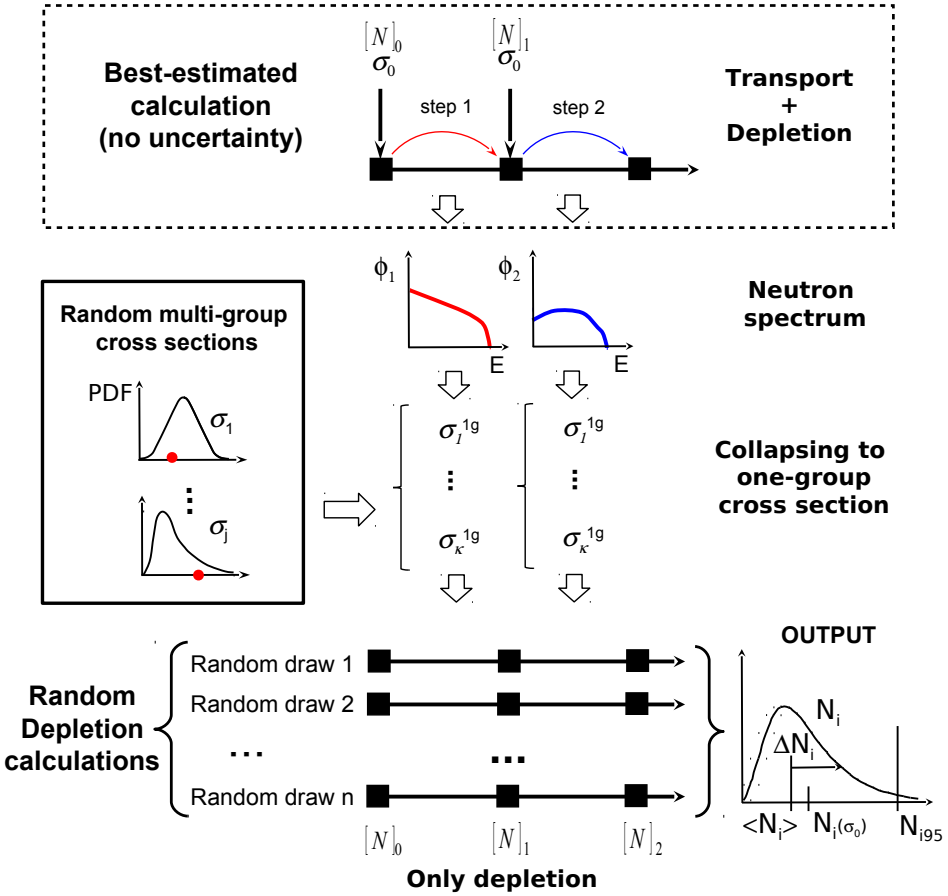

FIGURE 4.3: Scheme of the Hybrid Method using multi-group cross section uncertainties.

addition, most of the times such formats are not suitable for sampling, especially in the case of cross section data, where for example:

- In the ENDF-6 format, uncertainty data can only be applied to restored cross sections after combining resonance data and background cross sections.
- The amount of cross section points could be very large, so the amount of random variables to randomise is excessive and the size required to store those random files is unmanageable.

Thus, the nuclear data are processed to a format easy to read and to randomise, and then, they are fed to ACAB.

As presented in Chapter 2, the three types of nuclear data presented there are required for depletion calculations: decay, fission yield and cross section data. Each one has their own tools or sequences to process and collapse them:

- For decay data, the PROCDECAY tool is developed to translate ENDF-6 formatted data into the ACAB decay format.
- For fission yield data, the COLLAPS tool is used, which generates collapsed fission yield values using cross section data and spectrum information. Currently, fission yield data can only be provided in the ENDF-6 format, while cross section data should be provided in the EAF format if COLLAPS is used.
- For cross section data, different tools or sequences can be used, depending on the original data format. With COLLAPS, the EAF format have to be used. ENDF-6 formatted files are converted into the EAF format thanks to a sequence of codes which includes the NJOY processing code. Also, COVERX formatted files can be also used by converting them into the ENDF-6 format, or by feeding them into the sampling tool (explained later).

One-group approach can be used within all data format mentioned above: EAF, ENDF-6 and COVERX, while multi-group approach can only be applied within COVERX.

4.3.1.1 PROCDECAY

It reads decay data libraries in the ENDF-6 format and processes them into the ACAB decay format. Two input files are necessary:

- `DBL.dat`, which is the decay data library in the ENDF-6 format.
- `Natural.dat`, in which the natural abundances are stored. By default, this provides the tool with information from Nuclear Wallet Cards (July 1995) [Tuli, 1995].

With just these two input files, PROCDECAY can be run and the following output files are obtained:

- `DECAY.dat`, which is the decay data library after processing, converted into the ACAB decay format.
- `UNDECAY.dat`, which stores the uncertainty decay data. It has the same format as `DECAY.dat`, however instead of mean values, here standard deviation values are stored. Here, information regarding stable isotopes is not recorded.

An example of `DECAY.dat` and `UNDECAY.dat`are showed in Fig. 4.4 in order to explain which information is included in these files. There, ^{101}Nb, identified with the ZZAAAM code (where M refers to the isomeric state, being the ground state equal to 0), has a half-life of 7.1 s with a rel.std.dev. of 4.225%, and the total sum of its decay energies (α+β+γ) is 2.236 MeV with a rel.std.dev. of 63.13%.

```
Decay.dat

 1  411010  1     7.100E+00 0.000E+00 0.000E+00 0.000E+00 0.000E+00 0.000E+00
 1      1.000E+00 0.000E+00 0.000E+00 2.236E+00   0.000000 1.000E+00 1.000E+00

Undecay.dat

 1  411010  1     4.225E-02 0.000E+00 0.000E+00 0.000E+00 0.000E+00 0.000E+00
 1      0.000E+00 0.000E+00 0.000E+00 6.313E-01
```

FIGURE 4.4: Example of `DECAY.dat` and `UNDECAY.dat` files for ^{101}Nb after running PROCDECAY.

4.3.1.2 COLLAPS

The COLLAPS tool is used to read the cross section data in the EAF format and the fission yield data in ENDF-6 format, and process them. In conjunction with the neutron spectrum data, one-group cross section and fission yield data are generated.

The main features of this module are:

- To collapse cross section data libraries and their uncertainties, in the EAF format, into one-energy group.
- To collapse fission yield data libraries and their uncertainties, in the ENDF-6 format, into one-energy group. Fission yield data are weighted with fission cross sections.
- To choose between different neutron spectrum to collapse the above data, or to collapse with a user-given spectrum.

Fig. 4.5 presents the input/output files required/provided by COLLAPS, described below.

Input files:

- `COLL.inp`, where input parameters for COLLAPS are provided. Also, the neutron spectrum used to collapse the cross section library and fission yield library is defined in this file.

- `XSBL.dat` is the cross section data library in the EAF format.
- `UNCBL.dat` is the uncertainty cross section data library in the EAF format, which is provided in a different file from where mean values are stored.
- `FYBL.dat` is the fission yield data library in the ENDF-6 format.
- `eaf_asscfy.dat` is the file in which information of fissile isotopes are. In case fission yield data are not provided for fissionable isotopes for which fission cross sections are provided, this file gives the information of which isotope fission yields will be used.

Output files:

- `XSECTION.dat` is the file which contains the cross section data in one-energy group. It has a different format from EAF, and it is ready to be read with ACAB.
- `FLUX.inf`, where neutron flux information and and the spectrum in one-energy group can be found. Also, it stores some information about how COLLAPS performed the processing and collapsing, as a log file.
- `REACTIONS.dat` contains the information about the nuclear reactions that take place using the above cross section library. It is used by ACAB to identify the different reaction chains to take into account.
- `XSUNC_1G.dat` provides collapsed one-group cross section uncertainties. The values stored are given as squared relative standard deviations.
- `FY.dat` contains collapsed one-group fission yield data. To create this file, `eaf_asscfy.dat` was used for providing fission yield data to those isotopes which have no fission yield data provided in `FYBL.dat`.
- `UNFY.dat` stores collapsed one-group uncertainty data for fission yields.

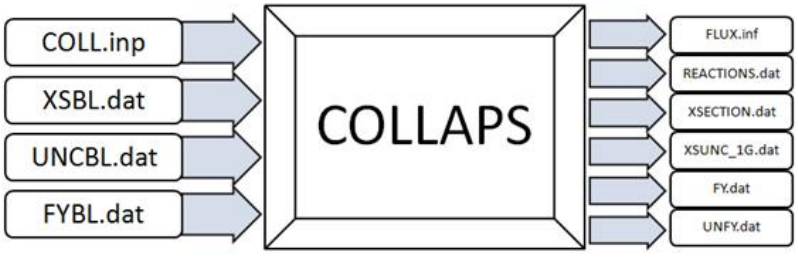

FIGURE 4.5: Flowchart input/output files for COLLAPS.

How to collapse cross section data and their uncertainties to one-group has been already presented with Eq. 4.1 and 4.2, respectively. Usually, spectrum and cross section data are not provided with the same energy structure, so a common energy grid is generated.

For fission yield data, as stated in the COLLAPS manual, two possible values can be provided, but only the one obtained through Eq. 4.8 is used for UQ studies. There, $\sigma_{f,i}$ refers to the fission cross section of the energy-group i, while ϕ_i energy-group i spectrum. Its collapsed one-group uncertainty is calculated by means of Eq. 4.9, where V_γ is the fission yield covariance matrix:

$$\gamma_{1g} = \frac{\sum_i \gamma_i \sigma_{f,i} \phi_i}{\sum_i \sigma_{f,i} \phi_i}, \tag{4.8}$$

$$var(\gamma_{1g}) = \omega^T V_\gamma \omega \qquad , \omega = \left(\frac{\sigma_{f,1}\phi_1}{\sum_i \sigma_{f,i}\phi_i}, \cdots, \frac{\sigma_{f,n}\phi_n}{\sum_i \sigma_{f,i}\phi_i} \right)^T. \tag{4.9}$$

In such a collapsing process, the contribution of fission cross section uncertainties is not taken into account because the fission cross section uncertainties will be included later due to the subsequent multiplication of the one-energy group fission yield γ_{1g} value by the one-group fission cross section $\sigma_{1g,f}$.

4.3.1.3 Using ENDF-6 formatted files

Cross section data provided within ENDF-6 formatted files can be processed for their use with ACAB, and their uncertainties can thus be included in UQ studies.

This task is carried out with the module *gen-lib-xs*, which makes use of different codes in order to generate an equivalent file to `XSUNC_1G.dat`. If covariance data between different reactions are also given in the ENDF-6 files, an equivalent file to `covariance.dat` (described in Sec. 4.3.2) could be generated, but this feature is not already implemented and should be added manually by the user.

The processing sequence is provided in Fig. 4.6, where the main tasks are:

- Read the information stored in the ENDF-6 file and prepared it to be processed. This is carried out with the MERGER [Cullen, 2012] and LISTEF [Dunford, 2008] codes.
- Generate input files for NJOY, setting the output group structure (one-group) and the neutron spectrum used in the collapsing stage. Once these inputs are ready, NJOY is run.

- Convert the NJOY output into ACAB readable cross section files, equivalent to `XSUNC_1G.dat`.

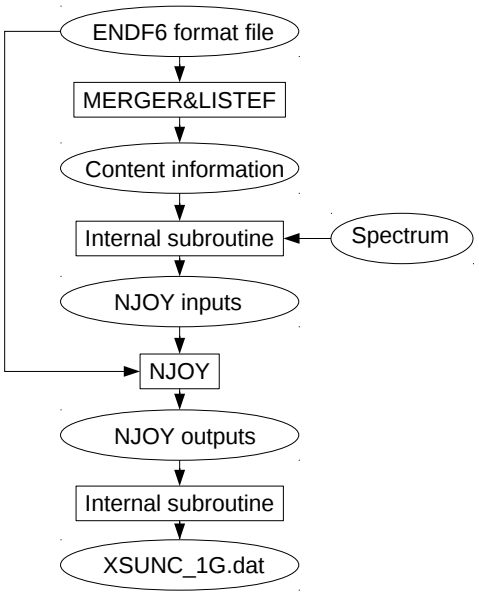

FIGURE 4.6: Flowchart of the processing sequence for using ENDF-6 formatted files within the Hybrid Method.

4.3.1.4 Using COVERX formatted files

As described in Chapter 2, the COVERX format is aimed to be used within SCALE6.0. Being able to use such data stored in those files opens the door to analyse the impact of covariance data between different reactions, even between different isotopes.

Two tools/codes are capable of reading such a format and converting it into user readable files: ANGELO [Kodeli, 2010] and VIEWCVX (provided as a module of the ERRORJ code [Chiba, 2007]). The former was initially used, however it was discarded due to a bug found [Ceresio et al., 2011]. Thus, the latter is used instead for reading COVERX files.

One specific tool has been developed in order to process such a format and to get an equivalent file to `XSUNC_1G.dat`, where one-group cross section values and uncertainties are stored. Additionally, another file is produced where covariance data in one-group are stored. This latter file is analogue to `covariance.dat` (described in Sec. 4.3.2). Because one-group cross section and uncertainty values are the outputs, the neutron spectrum to collapse with has to be provided. This tool has to change also the identifier numbers of isotopes in COVERX to their identifiers in the ACAB nomenclature. Cross section data not required by ACAB are not included in the output, such are the cases of total, elastic and inelastic reactions, and average fission neutron emission and spectra.

So, the input files are the COVERX files to be processed, and the neutron spectrum in the 44-group SCALE structure. As outputs, a file containing cross section values in one-group with the same format as `XSUNC_1G.dat` is provided, with another file which contains the covariance data information between reactions and isotopes (with the same format as the `covariance.dat` file).

4.3.2 Sampling

Once the libraries are processed, and collapsed for cross sections and fission yields, the input files for ACAB are ready. But in order to propagate the uncertainties by means of Monte Carlo sampling, it is necessary to sample the nuclear data before launching ACAB.

The sampling sequence makes use of the following subroutines:

- *genera_decay*, which generates random decay data using Normal or Log-normal PDFs with the information of decay uncertainties. Both files generated with PROCDECAY, `DECAY.dat` and `UNDECAY.dat` are required, and the outcome are random `DECAY.dat` files. Half-life, branching ratio and decay energy values are randomised according to their uncertainty data.

- *genera_xs* generates random cross section files, `XSECTION.dat`, using Normal or Log-normal PDFs, with the information of cross section uncertainties. Two files are required as input: `XSECTION.dat` and `XSUNC_1G.dat`, both generated with COLLAPS. This module can only handle correlations between reactions, if they are included manually by the user in the covariance matrix used to sample.

- *cholesky*, this subroutine is analogue to *genera_xs*, but it can handle covariances between different reactions, even isotopes, and take them into account in the sampling. Only one additional file is required: `covariance.dat` (that can be named in a different way), apart from the ones necessary for *genera_xs*. The format of this new file is presented in Fig.4.7, and is equivalent to the format of `XSUNC_1G.dat` with the following differences: the first line defines the reaction cross sections for which covariance data are provided, while in the fourth line, one-group cross section values are given (in the same order as the reactions are given) followed by the covariance value, given as squared covariance, between the reaction cross section stated in the first line.

- *genera_yields* produces random fission yield files, `FY.dat`, using data provided within `FY.dat` and `UNFY.dat` ,generated with COLLAPS. Normal PDFs are used for sampling.

```
 922330  180 922330 1020    1
cvx.mat92233 v7rec ornl-10/2008
COVARIANCE - Processed with PROCESA_SCALE-6.0
 2.66640E+00 3.23315E-01 1.55001E-04
```

FIGURE 4.7: Example of the `covariance.dat` file format for providing covariance data between different reaction cross sections.

With these three modules, a flowchart of work for propagating uncertainties is given in Fig. 4.8. There, *genera_xs* can be substituted with *cholesky*, with their corresponding input files.

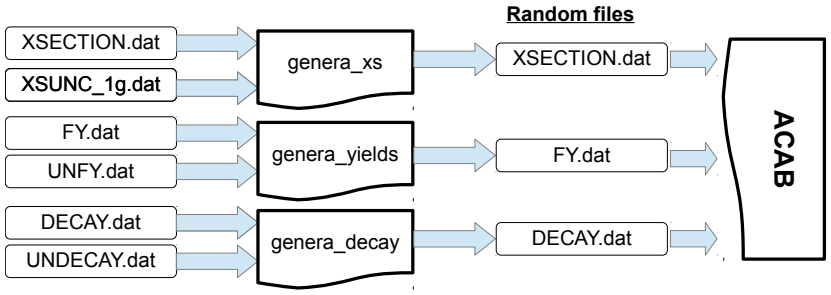

FIGURE 4.8: Flowchart of sampling modules.

Random cross sections can be generated from COVERX files using multi-group uncertainties, but other tool has to be used: *random-44g-cvx*. This tool can retrieve data already in the COVERX format by wrapping VIEWCVX. As inputs are: a file with the list of the COVERX files to process, and a file with the neutron spectrum already collapsed to the 44-energy groups defined for COVERX files. Random cross sections in 44-groups are generated, and then, collapsed to one-group using the given neutron spectrum. Random `XSECTION.dat` files are obtained as output.

The sampling process itself is the same for all modules. Non-correlated variables are sampled, one-by-one, using Eq. 4.10:

$$x = \mu(1+\alpha); \quad \alpha \sim N(0, \frac{\sigma^2}{\mu^2}), \tag{4.10}$$

where x is the non-correlated variable (e.g. half-life), μ is its mean value, σ is its std.dev. and α is the multiplication factor which is randomised using e.g. a Gaussian PDF with the relative standard deviation value as the PDF standard deviation parameter.

For correlated variables, the full relative covariance matrix is created, including all random variables. Sampling correlated variables with multivariate normal distributions can be performed using Cholesky decomposition and Single Value Decomposition (SVD) [Gentle, 2003].

Here, Cholesky decomposition on the relative covariance matrix V is performed, saving the lower triangular part L. The symmetry and positive-definite properties of V are checked, because they are requirements for the Cholesky decomposition. If V is not found as positive definite, diagonal terms are increased by 0.01% (up to a max of 10%) for making the matrix positive. If neither symmetry is proved nor positive-definite is achieved, the sampling process is stopped (that happened rarely with the SCALE6.0 covariance data, when full complete matrices, including total reaction, are used). Next, n values (equal to the amount of correlated variables) are sampled from Gaussian N(0,1) PDFs independently, and stored in the column vector z. With Eq. 4.11, n random variables designated as the x column vector are obtained. These follows a multivariate normal distributions, with the corresponding mean values μ (as a column vector) and the covariance matrix V. Remember that in Eq. 4.11, "$\cdot$" is the dot multiplication, and 1 refers to a column vector of ones.

$$x = \mu \cdot (1 + Lz). \tag{4.11}$$

All the final variables, x as a vector or scalar value, have to be positive by definition of the represented physical magnitudes. So any negative random draw found in x is set to zero. Such approximation, leads to small bias for the mean value and relative standard deviation to be reproduced. Different techniques/truncations can be carried out to avoid negative values instead of setting it to zero. However, the selected truncation introduces the smallest bias in the relative standard deviation (but not in mean). Such a bias can be of importance when large uncertainty values are treated, because the sampled PDF is largely truncated.

For generating random numbers from Gaussian PDFs N(0,1), two different routines can be used: KISS (Keep It Simple Stupid) [Marsaglia and Tsang, 2004] and an adaptation of the proposed one in [Dagpunar, 1988] by Alan Miller. Thanks to the KISS random number generator, correlated sampling is possible and easy to implement. It provides subroutines to save and load random seeds, which determine the random numbers generated.

As presented in Sec. 4.2.1.1, correlated sampling is achieved by using the same random draw from N(0,1) for generating random variables in different burn-up steps which have to be correlated. Such a task is achieved by using the same random seed for every burn-up step. That means if cross sections are randomised, the same random seed used to generated one-group cross section values in the first burn-up step is used for the rest of burn-up steps. Caution should be taken for `XSUNC_1G` and `covariance.dat` files from different burn-up steps, because they can have different amount of reactions, since different spectra have been used to collapse and COLLAPS can ignore reactions with negligible cross section values. Such files have to have the same order for the cross section descriptions, and the same amount of cross sections and correlations.

4.3.3 Depletion code ACAB

The ACAB code [Sanz et al., 2008] is a computer program designed to perform activation and transmutation calculations for nuclear applications. It solves the Bateman equation with the ORIGEN algorithm [Gauld et al., 2010, Isotalo and Aarnio, 2011], which uses a truncated Taylor series expansion of the exponential matrix, from which all the short-lived nuclides are removed and handled separately with Gauss–Seidel iterative method under the assumption of secular equilibrium.

ACAB is able to perform space-dependent inventory calculations allowing for a very flexible geometry and neutron flux description. The code solves the general nuclear transmutation chains for multidimensional neutron flux distributions. 1-D and 2-D multi-group neutron fluxes generated by discrete ordinates transport codes can be used. Also, a 3-D neutron fluxes generated by Monte Carlo neutron transport codes can be used, allowing inventory calculations to be performed for complex geometries. The multi-group neutron fluxes may be given in an arbitrary group structure, thanks to its collapsing tool COLLAPS.

This code considers decay transitions that proceed from the ground, first and second isomeric states. All the neutron reactions that may occur in the different components of a nuclear facility are treated in the code. The energies range from thermal region up to 20 MeV, and it is updated to predict transmutation calculations with neutron energies above 20 MeV.

One capability of ACAB is to deal with all nuclides (including actinides), all nuclear processes (including fission) and all the products of the nuclear reactions (including fission products).

The main result obtained by ACAB is the isotopic composition in each time step by a defined geometry of the system. With this result, other derived response functions can be calculated such as isotopic activity, decay heat, decay gamma spectrum, contact dose, radiotoxicity, neutron emission source, etc.

The major part of its input files have been described already: `DECAY.dat`, `REACTION.dat`, `XSECTION.dat`, `FY.dat`. Only `inp.5` is still not described. It contains the input data regarding cells/material composition to be depleted, the neutron flux and the burn-up/depletion steps. All the output information is given with `fort.6` file.

Running ACAB with random input files like `XSECTION.dat`, generates random outputs, that are saved in the form of `fort.6.ih`, where `ih` denotes the history number (corresponding to the random file `XSECTION.dat.ih`). Different types of random input files can be included at the same time in order to see joint effects, e.g. random fission yield and cross section data.

4.3.4 Statistical analysis of response functions

Once all random output files are generated, a statistical analysis of the response functions can be performed.

The first response function calculated is the nuclide composition in each time step. Then, other derived response functions are calculated, such as decay heat and radiotoxicity.

One tool performs the statistical analysis for the following response functions:

- Concentration given in (atoms), (atoms·gr) or (gr)
- Activity (Bq).
- Decay Heat (W).
- Inhalation and Ingestion dose.

They can be followed throughout burn-up/depletion time and cooling time. For all isotopes (and their individual contribution to previous response functions), the following statistical values are provided as function of number history for every studied burn-up steps: mean value, variance and relative standard deviation. These files are named as `variable.xmed.ih.it.step`, `variable.desv.ih.it.step`, `variable.erro.ih.it.step`, correspondingly. A summary

of the mean, covariance and relative standard deviation after running the total amount of histories is provided as a function of time (burn-up/depletion time or cooling time). This information is saved in the next files: `variable.xmed.out`, `variable.desv.out` and `variable.erro.out`.

It is possible to follow the convergence of variables on the fly, following Eq. 4.12 for the mean, and Eq. 4.13 for the variance:

$$\overline{x}_n = \frac{(n-1)\cdot \overline{x}_{n-1} + x_i}{n}, \tag{4.12}$$

$$\sigma_n^2 = \frac{\sum_{i=1}^{n}\left(x_i^2\right) - n\cdot \overline{x}_n}{n-1} = \frac{S_{n-1} + x_n^2 - n\cdot \overline{x}_n}{n-1}, \tag{4.13}$$

where n refers to the current history calculated and S_{n-1} is equal to $\sum_{i=1}^{n-1}\left(x_i^2\right)$. Therefore, only tracking the mean value $\overline{x}$ and the sum of the squared values S_n is enough to calculate the standard deviation after a new history is run.

4.3.4.1 Analysis for determining the maximum contributor to variance

Analysis of contributors for any response function which is a linear function of individual contributions, like decay heat, can be performed easily because every single contribution is recorded and analysed statistically for each time step. In these cases, the relative contribution can be calculated, and also the relative contribution to the response function variance. Hence, the maximum contributors to mean and to variance can be detected. However, this analysis can not identify generation/depletion pathways or main cross-section reactions that causes such contributions, just only the isotopes involved.

To perform this analysis, the next mathematical development is followed. Eq. 4.14 presents the variance of a response function x as a sum of two term: sum of individual contributions y_i and sum of covariances between individual contributions:

$$var(x) = var\left(\sum_{i=1}^{N} y_i\right) = \sum_{i=1}^{N} var\left(y_i\right) + \sum_{\substack{i,j=1 \\ i\neq j}}^{N} cov\left(y_i, y_j\right). \tag{4.14}$$

Then, if the covariance contribution term is negligible compared to the sum of variances, the response function variance can be approximated by the latter, as shown in Eq. 4.15:

$$\sum_{i=1}^{N} var\left(y_i\right) >> \sum_{\substack{i,j=1 \\ i \neq j}}^{N} cov\left(y_i, y_j\right) \quad \Rightarrow \quad var(x) \approx \sum_{i=1}^{N} var\left(y_i\right) \Leftrightarrow \sigma_x^2 \approx \sum_{i=1}^{N} \sigma_{y_i}^2. \tag{4.15}$$

Now, if the variance of the response function is divided by its mean value, the squared relative standard deviation is obtained, as seen in Eq. 4.16:

$$\left[rel.std.dev.(x)\right]^2 = \frac{\sigma_x^2}{\overline{x}^2} = \sum_{i=1}^{N} \frac{\sigma_{y_i}^2}{\overline{x}^2}. \tag{4.16}$$

Multiplying and diving every individual variance σ_{y_i} by the mean value of the individual contribution $\overline{y_i}$, the response function variance becomes a sum of relative standard deviations of individual contributions multiplied by their relative contribution $\frac{\overline{y_i}}{\overline{x}}$, as presented in Eq. 4.17:

$$\left[rel.std.dev.(x)\right]^2 = \sum_{i=1}^{N} \frac{\sigma_{y_i}^2}{\overline{y_i}^2} \cdot \frac{\overline{y_i}^2}{\overline{x}^2} = \sum_{i=1}^{N} \left[rel.std.dev.(y_i)\right]^2 \cdot \frac{\overline{y_i}^2}{\overline{x}^2}. \tag{4.17}$$

Accordingly with Eq. 4.17, the individual contribution to the response function relative standard deviation can be analysed. Because two terms are involved in every contribution, whether the uncertainty in the contribution or the contribution itself is more important can be determined. With this information, contributors can be sorted by importance.

Since the covariance term in Eq. 4.14 has been neglected, such a hypothesis has to be checked. This check can be performed, because the variance of response function is also calculated. So comparing it with the sum of individual contributions enables the assessment of the importance of the covariance term.

Chapter 5

Generation of fission yield covariance data

Abstract - This Chapter summarises different methodologies proposed for generating covariance data for fission yield. They are briefly described and discussed in regard to their applicability. An small exercise shows the need of covariance data for fission yields, where inconsistencies are revealed between independent and cumulative fission yield covariance data. Finally, the Bayesian/GLS updating procedure is selected and implemented for generating covariance data for thermal neutron induced fission yields of ^{235}U and ^{239}Pu, which will be used later in UQ studies.

This chapter shows, partially or completely, works already presented in the following references:

- International Journal Article [Fiorito et al., 2014].

Motivation

Fission yield uncertainties have been often neglected or partially treated, because their effects were considered of second order compared to cross-sections [García-Herranz et al., 2010]. However, the Working Party on International Nuclear Data Evaluation Co-operation (WPEC) – group dedicated to assess the needs of nuclear data improvement – shows a new interest on fission yield data within its Subgroup 37 (SG37), with the goal to develop "Improved

Fission Product Yield evaluation methodologies" [Mills, 2013], not only in order to quantify the impact of such uncertainties, but also to provide a proper set of variances and correlation matrices. Great efforts are being committed to develop methodologies for generating such covariance data for FYs, and several methodologies were proposed at the kick-off meeting of WPEC-37, based mainly on:

- Using the Q-matrix approach for generating covariances for IFYs from CFYs, proposed in [Mills, 2013].
- Applying perturbation theory to the "Five Gaussians and Wahl's models", proposed in [Pigni et al., 2013].
- Performing Monte Carlo parameter perturbation using the GEF code, presented in [Schmidt, 2013].
- Updating data with the Bayesian/General Least-Squares (GLS) method, where the IFY covariance matrix is updated with information on the chain yields, as proposed in [Kawano and Chadwick, 2013] and previously applied in [Katakura, 2012]. A variation of this proposal is described and reported in this work, updating IFY covariance matrix with CFY data.

These proposed methodologies are reviewed and discussed. The last one is then selected and applied to generate covariance data for thermal fission yields of ^{235}U and ^{239}Pu, which will be used in Chapter 6. It is selected because it has been applied previously and is easy to implement. Not only are the updating schemes implemented, but also the capability of sampling fission yield data based on these new covariances. Thanks to the modular implementation carried out in the sampling stage (Chapter 4, Sec. 4.3.2), the same procedure can be used. Only new small subroutines to handle fission yield data are required.

5.1 Methodologies for generating fission yield covariances

5.1.1 Using Q-matrix approach

This approach is proposed in [Mills, 2013] and intends to generate covariances between IFYs using CFY uncertainties by means of the Q-matrix.

The Q-matrix relates the Independent Fission Yields (IFYs) to the Cumulative Fission Yields (CFYs) by means of the decay paths, as seen in Chapter 2, Sec.2.5. Recalling Eq. 2.2, the complete definition of the $Q_{i,j}$ terms is provided:

$$Q_{i,j} \;=\; \sum_{allpaths} \left(\prod_{j \to i} \beta_{j,j+1} \beta_{j+1,j+2} \cdots \beta_{i-1,i} \right), \tag{5.1}$$

where $\beta_{j,j+1}$ is the fraction of isotope j that decays to isotope $j+1$, both being in the decay path from isotope j to i. When $j = i$, $Q_{i,i} = 1$, and $Q_{k,i} = 0$ when isotope k does not decay into isotope i. If the variance of the CFYs is calculated with Eq. 2.2, a relationship appears between variance/covariances of IFYs and variances of CFYs:

$$var(C_i) \;=\; var(\sum_j Q_{j,i} y_i). \tag{5.2}$$

Departing from the assumption that $Q_{j,i}$ values have no uncertainty (which is not true, because the branching ratios are involved in the decay paths and have uncertainty), the previous equation can be converted into

$$var(C_i) \;=\; \sum_j Q_{j,i}^2 var(y_j) \;+\; \sum_j \sum_{k \neq j} Q_{j,i} covar(y_j, y_k) Q_{k,i}, \tag{5.3}$$

where the covariance terms $covar(y_j, y_k)$ among IFYs show up, which are the ones unknown and to be determined.

In that system, the amount of unknown variables are $(n-1)n/2$, while the number of equations is n, then the number of degrees of freedom is $(n-3)n/2$. In order to make the system determined, it is necessary to establish a set of constrains or hypothesis to deal with such a non-determined system.

As presented in [Cabellos et al., 2013, Appendix E], O. Cabellos proposed a way to determine the covariance terms of Eq. 5.3. A minimisation problem of the following error function,

$$F(i) \;=\; var(C_i) \;-\; \left[\sum_j Q_{j,i}^2 var(y_j) \;+\; \sum_j \sum_{k \neq j} Q_{j,i} covar(y_j, y_k) Q_{k,i}) \right], \tag{5.4}$$

should be overcome. But the system still remains non-determined, so only one possible solution after one iteration of the minimisation problem is provided.

In conclusion, this approach tries to relate uncertainties in CFYs to uncertainties in IFYs. However, this approach is incomplete because constrains should be established on the previous systems to make it determined in order to establish IFYs uncertainties.

5.1.2 Perturbation theory applied to "Five Gaussians and Wahl's models"

Using the Five Gaussians model [Musgrove et al., 1973] for the total mass yields $Y(A;\vec{\mu})$, Wahl's model [Wahl, 1985, Wahl, 1988] for the fractional yields $f(A,Z;\vec{\lambda})$ and Madland and England functions [Madland and England, 1976] for the isomeric yield ratio $r(A,Z,M)$, the IFYs can be calculated by recalling Eq. 2.1:

$$y(A,Z,M) \;=\; Y(A;\vec{\mu})f(A,Z;\vec{\lambda})r(A,Z,M), \tag{5.5}$$

where $\vec{\mu}$ and $\vec{\lambda}$ group the independent parameters of the five gaussians model (means, standard deviations,etc) and the Wahl's model, respectively. In order to generate a covariance matrix for IFYs, Eq. 5.5 is linearised with a first order Taylor series expansion for the model parameters $\vec{\mu}$ and $\vec{\lambda}$. Such parameters are then taken as random variables with given uncertainties, so that variance/covariance matrices for IFYs can be calculated with the moment propagation equation (sandwich formula), which takes the form of Eq. 5.6:

$$cov(y_i,y_j) \;=\; \sum_{k,l} \frac{\partial y_i(A,Z)}{\partial x_k} \langle \delta x_k \delta x_l \rangle \frac{\partial y_j(A,Z)}{\partial x_l}, \tag{5.6}$$

where $\frac{\partial y_i(A,Z)}{\partial x_k}$ are the sensitivity coefficients of IFYs to the model parameters $\vec{\mu}$ and $\vec{\lambda}$, and $\langle \delta x_k \delta x_l \rangle$ are the covariance terms between parameters (x_k and x_l represents any parameter). In [Pigni et al., 2013], no correlations amongst the parameters of different models are assumed.

5.1.3 Monte Carlo sampling on parameters of the GEF code

The GEF code [Schmidt and Jurado, 2010, Schmidt and Jurado, 2012] implements a semi-empirical model of the fission process, which covers most of the properties of the fission fragments and the emitted neutrons and photons in a global and consistent way. The model is based on fragment shells that are deduced from measured fission-fragment mass distributions, assuming that the macroscopic contribution of the compound nucleus and the microscopic

contributions of the nascent fragments in the potential-energy surface are separable. It reproduces all measured fission yields and neutron data rather well with a unique set and a relatively small number of free parameters. These free parameters are mainly 13, related to the fission channels (constant position of the fission valleys in Z, depth and curvature), the dissipated energy fraction in intrinsic and normal modes, the neck distance, the additional shift of the charge polarisation and the parameters of the even-odd effect.

Then, for the generation of random fission yield data with GEF, these free parameters are perturbed: those related to the fission channels and charge polarisation, the width in N/Z of the fission fragment distribution, and the weakening due to the distance from the value of ^{132}Sn (for further information about the range of variation, check the GEF code source). They are taken as random variables, and are sampled using Gaussian distributions independently from each other. The range of fluctuation has been established from a fitting procedure to the experimental data. Therefore, complete sets of perturbed FYs are generated through Monte Carlo sampling of the model parameters. Covariance calculations with perturbed model parameters reveal correlations between any two yield values. So, the analysis of all the correlations between all the fission yields produces the desired covariance matrix. Indeed, this capability is already available in GEF.

5.1.4 Bayesian/General Least-Squares Method

The Bayesian/General Least-Squares (GLS) method is an adjustment technique which states that the information on some prior system parameters can be improved with the addition of new knowledge – new data e.g. experimental or evaluated response values η, for which relationships between data and parameters are established (see Eq. 5.7). These relationships or constraints must be linearised in the form of:

$$y - y_a = S(\theta - \theta_a), \tag{5.7}$$

where θ are the parameters of the system, θ_a the prior estimates of θ, y the responses of the constraining equation, y_a the responses of the constraining equation to the prior estimates θ_a, and S are the sensitivity coefficients of the response $y - y_a$ to the parameters $\theta - \theta_a$.

Then, further information η could be introduced in order to derive refined values for the parameters θ, with all the available uncertainty information properly incorporated into the

formalism. The least-squares condition can be written in a general form, namely

$$\chi^2 = \begin{bmatrix} \theta - \theta_a \\ \eta - y_a \end{bmatrix}^T \begin{bmatrix} V_a & H \\ H^+ & V \end{bmatrix}^{-1} \begin{bmatrix} \theta - \theta_a \\ \eta - y_a \end{bmatrix} = minimum, \tag{5.8}$$

where H represents the correlation that exists between the prior and new information. For the purpose of this work H is assumed to be a zero matrix. The updating process is represented by Eq. 5.9 and 5.10:

$$\theta \; - \; \theta_a \; = \; V_a S^T (S V_a S^T + V)^{-1} (\eta - y_a), \tag{5.9}$$

$$V_s \; = \; V_a - V_a S^T (S V_a S^T + V)^{-1} S V_a, \tag{5.10}$$

where V_a is the variance matrix of prior estimates of the parameters (θ_a), V is the variance matrix of the introduced data fitting the constraining system (η), and V_s is the updated covariance matrix of the system parameters (θ). Superscript T refers to the transpose of a matrix.

In [Kawano and Chadwick, 2013], updating IFYs and CFYs is proposed by using information on experimental MFY data which constraints $\sum_{M,Z} y(A,Z,M) = Y(A)$ for all A, followed by the application of normalisation $\left(\sum_{A,Z,M} \; y(A,Z,M) \; = 2\right)$, charge and mass conservation equations. In such case, S becomes the array of sensitivity coefficients of MFYs to IFYs, η the evaluated MFYs introduced into the system and y_a the MFYs calculated with the prior IFYs (θ_a) in Eq. 5.7, that is, summing up all the yields belonging to the same chain. V_a is the variance matrix of θ_a and V is the variance matrix of the experimental MFYs. Evaluated ChFY are used as MFYs in the updating process, because chain yields and total mass yields differ only slightly from each other [James et al., 1991].

A similar procedure with a single constraint on the chain yields is applied in [Katakura, 2012], where V and V_a are diagonal matrices as no correlation is initially provided for either IFYs or MFYs. Simple equations to generate the updated covariance matrix for IFYs can be derived from Eq. 5.10, resulting in Eq. 5.11 and 5.12, which represent the diagonal and off-diagonal terms, respectively:

$$\mu_{ii} \; = \; \sigma_i^2 \left(1 - \frac{\sigma_i^2}{\sigma^2 + \sum_j \sigma_j^2}\right), \tag{5.11}$$

$$\mu_{ij} \; = \; -\frac{\sigma_i^2 \sigma_j^2}{\sigma^2 + \sum_j \sigma_j^2}, \tag{5.12}$$

where σ_i is the standard deviation of the *i-th* IFY and σ is the standard deviation of evaluated MFY. Sum $\sum_j \sigma_j^2$ includes all the isotopes in the same mass chain as it relates MFYs to IFYs.

A new proposal introduced in this current work is to use the CFY evaluated data to update the variance matrix of the IFYs. Then, η becomes the evaluated CFYs with variance matrix V, y_a is the array of CFYs calculated with Eq. 5.7, where θ_a is the vector of prior IFYs and V_a its variance matrix. Here, the Q-matrix equation (Eq. 2.2) is the linear constraining system and S are the sensitivity coefficients of IFYs to CFYs.

5.2 Justification of FY covariance generation methodologies

FY covariance generation may have a strong impact on several aspects of standard nuclear operations and design, like burn-up calculations. A way to measure the level of burn-up in a nuclear system is a direct quantification of the Neodymium generated by fission, as it is a stable FP with a very low capture cross-section and a very low migration in the UO_2 matrix of the fuel: its concentration is therefore an accurate indicator of the local or averaged burn-up [Suyama and Mochizuki, 2005]. In particular, ^{148}Nd is very sensitive to burn-up variations, so accurate calculations of its concentration are often a critical target for depletion problems. The nuclear density of ^{148}Nd can be retrieved analytically along irradiation time from the equation system in Eq. 5.13:

$$\begin{aligned} \frac{dN_7(t)}{dt} &= (-\lambda_7 + \sigma_c^7\phi)N_7 + \Sigma_f\phi C_7 \\ \frac{dN_8(t)}{dt} &= -\sigma_c^8\phi N_8 + \sigma_c^7\phi N_7 + \Sigma_f\phi C_8, \end{aligned} \tag{5.13}$$

where N are the isotopic concentrations, Σ_f the macroscopic fission cross section, ϕ the neutron flux, σ_c the microscopic capture cross section and C_i the CFY. Subscripts and superscripts 7 and 8 refer respectively to ^{147}Nd and ^{148}Nd. Evaluated burn-up values and the density of ^{148}Nd are also affected by the neutron capture reaction of ^{147}Nd, although this effect is small for low fluence values [Suyama and Mochizuki, 2005]. Neglecting this contribution, Eq. 5.14 gives the concentration of ^{148}Nd as a function of irradiation time t:

$$N_8(t) \approx \frac{\Sigma_f\phi C_8}{\sigma_c^8\phi}\left(1 - e^{-\sigma_c^8\phi t}\right). \tag{5.14}$$

CFYs are inherently related to IFY through the Q-matrix equation (Eq. 2.2),therefore any correlation between IFYs can substantially affect the uncertainty and safety margins on burn-up evaluations. The Q-matrix equation guarantees full consistency between IFYs and CFYs, but it does not work the same for their uncertainties. IFY uncertainties are propagated through Eq. 2.2 as described in Eq. 5.3.

Information about the contributors to the cumulative yield of ^{148}Nd, using Eq. 5.3, is reported in Table 5.1 for JEFF-3.1.2, and in Table 5.2 for ENDF/B-VII.1. The comparison between calculated and evaluated uncertainties for the ^{235}U thermal fission is reported in Table 5.3.

TABLE 5.1: Information on the IFY contributors to the ^{148}Nd CFY and (C_8) its uncertainty according to JEFF-3.1.2 data for the ^{235}U thermal fission. (From [Fiorito et al., 2014])

Isotope	Q_{ij}	y_i	Δy_i	$\Delta y_i/y_i$ (%)	contrib. to C_8 (%)	contrib. to C_8 unc. (%)
^{148}Cs	0.75	1.6E-7	5.9E-8	37.5	0.0	0.0
^{149}Cs	0.02	3.5E-9	1.3E-9	36.8	0.0	0.0
^{148}Ba	1	2.1E-4	8.0E-5	37.2	1.3	0.2
^{149}Ba	0.02	1.3E-5	4.8E-6	36.7	0.0	0.0
^{148}La	**1**	**3.3E-3**	**1.0E-3**	**31.8**	**19.9**	**42.8**
^{149}La	0.01	9.4E-4	3.3E-4	34.7	0.1	0.0
^{148}Ce	**1**	**1.2E-2**	**1.2E-3**	**9.7**	**73.7**	**54.7**
^{148}Pr	1	1.6E-4	5.7E-5	35.3	1.0	0.1
^{148m}Pr	1	6.8E-4	2.4E-4	35.3	4.1	2.2
^{148}Nd	1	1.1E-5	4.1E-6	37.5	0.1	0.0

TABLE 5.2: Information on the IFY contributors to the ^{148}Nd CFY (C_8) and its uncertainty according to ENDF/B-VII.1 data for the ^{235}U thermal fission. (From [Fiorito et al., 2014])

Isotope	Q_{ij}	y_i	Δy_i	$y_i/\Delta y_i$ (%)	contrib. to C_8 (%)	contrib. to C_8 unc. (%)
^{148}Cs	0.75	1.3E-7	8.4E-8	64.0	0.0	0.0
^{149}Cs	0.02	3.6E-9	2.3E-9	64.0	0.0	0.0
^{148}Ba	1	2.2E-4	1.4E-4	64.0	1.3	0.2
^{149}Ba	0.02	1.0E-5	6.6E-6	64.0	0.0	0.0
^{148}La	**1**	**3.4E-3**	**2.2E-3**	**64.0**	**20.1**	**36.0**
^{149}La	0.01	8.0E-4	5.1E-4	64.0	0.0	0.0
^{148}Ce	**1**	**1.2E-2**	**2.8E-3**	**23.0**	**73.8**	**62.8**
^{148}Pr	1	3.9E-4	2.5E-4	64.0	2.3	0.5
^{148m}Pr	1	3.9E-4	2.5E-4	64.0	2.3	0.5
^{148}Nd	1	9.9E-6	6.4E-6	64.0	0.1	0.0

The total variance calculated for ^{148}Nd CFY is relatively large, as IFY uncertainties are directly propagated without any correlation term, and disagrees in at least one order of magnitude with the evaluated CFY uncertainty stored in the libraries. Then, a smaller version of the IFY covariance matrix, which includes only the chains of cumulative ^{148}Nd yield, is created by means of the Bayesian/GLS technique extensively described in Sec. 5.1.4. The purpose is to assess the influence of correlation terms and justify the covariance generation

methodology. Then, the new covariance information is propagated with Eq. 5.3 and results are reported in Table 5.3.

CFY evaluated uncertainties show a good agreement with those obtained propagating correlated IFYs, due to negative correlations generated through Bayesian technique. The inconsistency assessed when no correlation is taken into account influences the uncertainty of ^{148}Nd density and burn-up, that could lead to a overestimation of the uncertainties.

The need of optimal agreement between evaluated data as well as uncertainties justifies the efforts spent on covariance generation for fission product yields. Within this practical application, the requirement of accurate ranges of uncertainties for practical applications is highlighted.

5.3 FY covariance data generated

IFY covariance matrices are generated using the Bayesian/GLS method (Sec. 5.1.4). The approach described in [Katakura, 2012] is used to create a covariance matrix with experimental chain yield data updating the prior IFY variance.

Uncertainties of IFYs, reported in Eq. 5.11 and 5.12, are provided by ENDF/B-VII.1 and JEFF-3.1.2. Evaluated chain yield uncertainties are taken from [England and Rider, 1994] for ENDF/B-VII.1 and from [IAEA, 1974] for JEFF-3.1.2.

TABLE 5.3: Comparison between the ^{148}Nd CFY uncertainty value in the libraries (evaluated), uncertainties calculated without correlations between IFYs (no corr.) and uncertainties calculated with correlations between IFYs, generated with Bayesian/GLS technique using introducing evaluated CFY data (corr. CFY) or evaluated MFY data (corr. MFY) for the ^{235}U thermal fission. (From [Fiorito et al., 2014])

JEFF-3.1.2	Uncertainty (%)
Evaluated ΔC_{Nd148}	0.70
Calculated ΔC_{Nd148} (no corr.)	9.67
Calculated ΔC_{Nd148} (corr. CFY)	1.01
Calculated ΔC_{Nd148} (corr. MFY)	1.76
ENDF/B-VII.1	**Uncertainty (%)**
Evaluated ΔC_{Nd148}	0.35
Calculated ΔC_{Nd148} (no corr.)	21.42
Calculated ΔC_{Nd148} (corr. MFY)	0.35

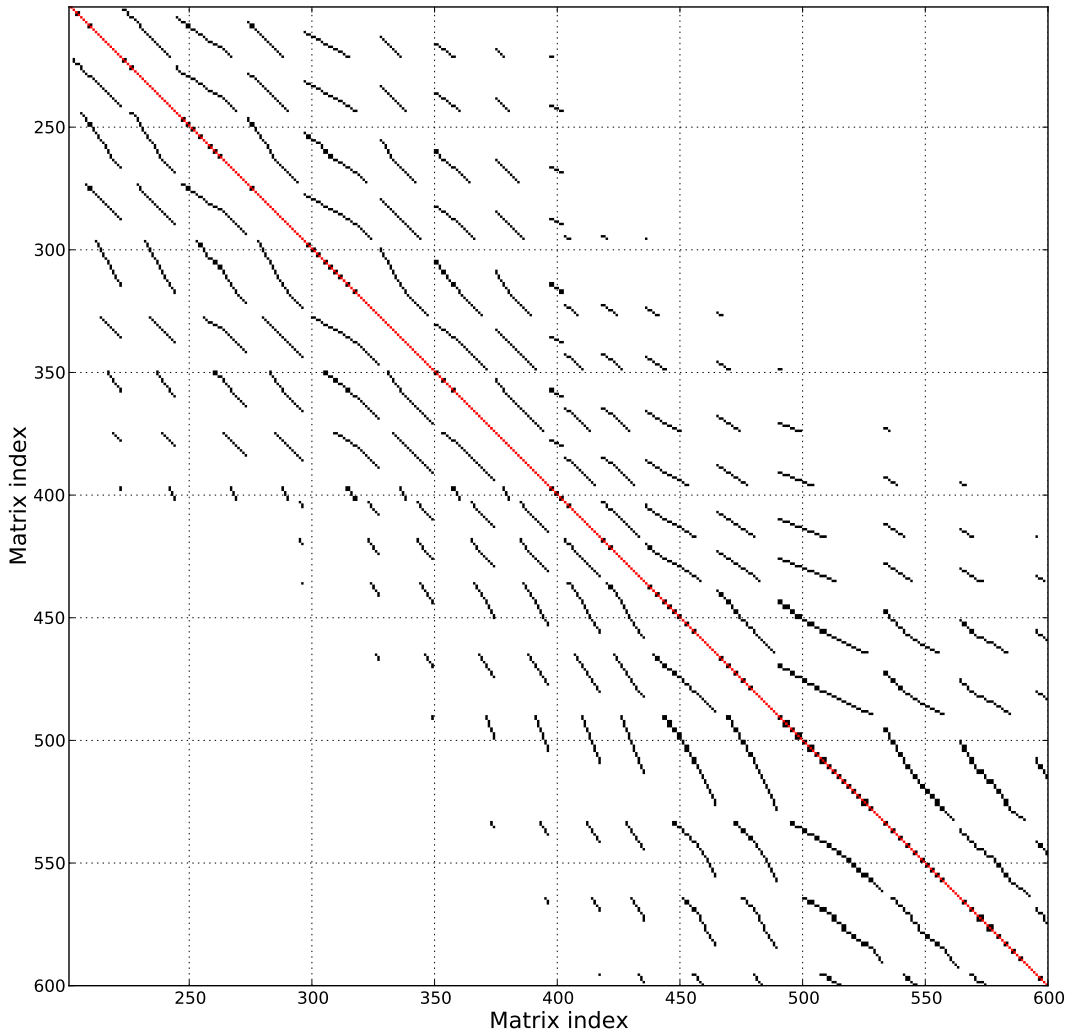

FIGURE 5.1: Section of the IFY correlation matrix for the ^{235}U thermal fission obtained by updating ENDF/B-VII.1 data with MFY uncertainties. Each matrix index refers to one fission product (FP), once the FPs are sorted by ZZZAAAM (Z, charge; A, mass; M, isomeric state) in increasing order. (From [Fiorito et al., 2014])

Fig. 5.1 presents a zoom-in of the correlation matrix obtained with the approach described above, where red dots are positive correlations and black dots are negative correlations, otherwise no correlation exists. Each matrix index refers to one fission product (FP), once the FPs are sorted by ZZZAAAM (Z, charge; A, mass; M, isomeric state) in increasing order. (e.g. index 1 refers to the lowest ZZZAAAM value). FY data are taken from the ENDF/B-VII.1 library, although one could obtain a similar plot using JEFF-3.1.2. The nature of the covariance generation technique and the imposed constraint make the matrix very sparse, with only negative correlations. Off-diagonal terms lay very close to the main diagonal as correlations appear only between FPs belonging to the same mass chain. Correlations range from -0.99 to -0.1, and those whose absolute values are below 0.1 are neglected.

Another correlation matrix is generated for JEFF-3.1.2 IFY data based on Eq. 5.10, shown in Fig. 5.2. The updating process resorts to the relationship between IFYs and CFYs, thus the Q-matrix needs to be calculated. Then, the IFY covariance matrix is updated with the CFY uncertainties stored in JEFF-3.1.2. As the previous matrix, this one is also sparse with non-zero negative values close to the diagonal. Again, correlations whose absolute values are below 0.1 are neglected.

When the same update is applied to ENDF/B-VII.1, an inconsistency halts the process because inconsistencies between the decay library and the fission yield library are found: isotopes defined in one are not found in the other and vice versa. That makes the Q-matrix impossible to calculate without a deep study of both libraries and restoring the consistency between libraries.

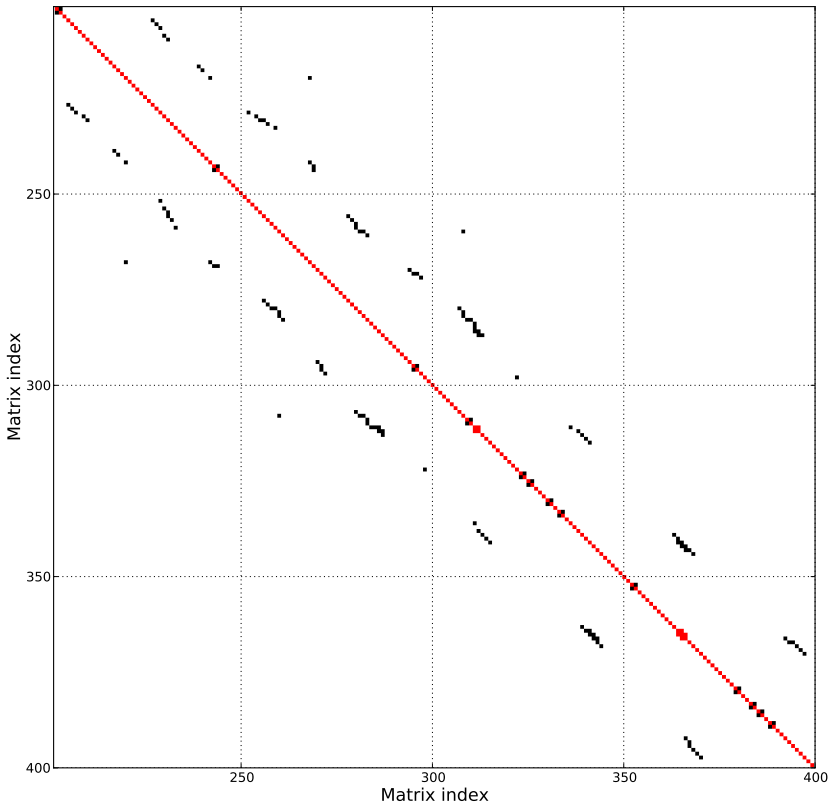

FIGURE 5.2: Section of the IFY correlation matrix for the ^{235}U thermal fission obtained by updating JEFF-3.1.2 data with CFY uncertainties in JEFF-3.1.2. Each matrix index refers to one fission product (FP), once the FPs are sorted by ZZZAAAM (Z, charge; A, mass; M, isomeric state) in increasing order. (From [Fiorito et al., 2014])

Introducing fission yield information, such as mass or cumulative fission yields, has a great impact on the prior covariance data. Strong variance reductions occur when the uncertainty of a single parameter (IFY) has a very high sensitivity to the constrained system in Eq. 5.7.

Most of the uncertainty is removed from the variance (diagonal values of the covariance matrix) to be reintroduced as negative correlations between IFYs. Fig. 5.3 shows the ratio of the adjusted to prior variance data for all the IFYs in the system. A glance at Eq. 5.11 and Eq. 5.12 immediately explains this behaviour. Evaluated chain yield uncertainties in the right-hand term of the equation cut down the diagonal terms of the FY covariance matrix. This effect is more significant when the new data introduced in the system carry uncertainties smaller than the prior parameters.

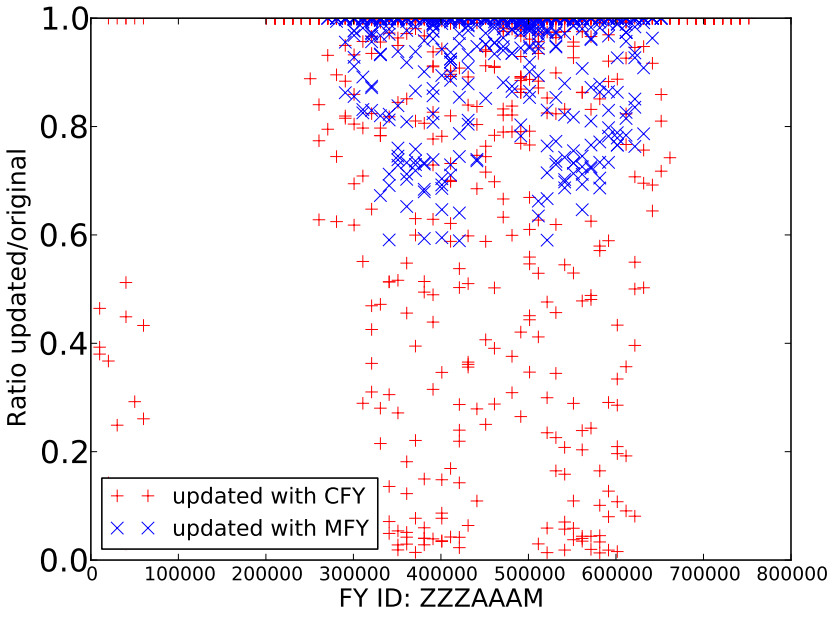

FIGURE 5.3: Ratio of updated to original variance terms of JEFF-3.1.2 when using Mass Fission Yields (MFY) or Cumulative Fission Yields (CFY) for the ^{235}U thermal fission yields. (From [Fiorito et al., 2014])

Updated data have sharply-reduced variances in correspondence of the two peaks of MFYs, due to the likeness of a greater database of measurements and the consequently more precise values, as seen in Fig. 2.4. Bayesian/GLS technique introduces more information (in the sense that new data have a higher influence on the system) by updating with CFYs than with MFYs, as the ratios obtained from the former are smaller than the latter.

PART III

APPLICATIONS

Chapter 6

Uncertainty Quantification studies

Abstract - All the UQ studies performed with the Hybrid Method during this thesis are compiled here. The first application studied is the Fission Pulse Decay Heat (FPDH) for ^{235}U and ^{239}Pu thermal fission, where the impact of fission yield covariance data generated in Chapter 5 is also assessed. Next, the European Facility for Industrial Transmutation (EFIT) fuel cycle is analysed, focusing on isotopic composition, decay heat and radiotoxicity uncertainties due to decay, fission yield and cross section uncertainties. Finally, the European Sodium Fast Reactor (ESFR) fuel cycle is investigated. Only isotopic composition uncertainties are addressed, because different approaches of the Hybrid Method are used and compared: one-group with and without correlated sampling, and multi-group. Target uncertainties suggested in [Salvatores et al., 2008] are checked, assessing the uncertainty levels obtained with each library used.

This chapter shows, partially or completely, works already presented in the following references:

- International Conference Proceeding [Díez et al., 2011].
- ANDES Deliverable D2.1 [Cabellos et al., 2011a].
- ANDES Deliverable D2.5 [Mills et al., 2013].
- ANDES Deliverable D2.6 [Cabellos et al., 2013].
- International Journal Article [Fiorito et al., 2014].
- International Journal Article [Díez et al., 2014b].

- International Journal Article [Cabellos et al., 2014].
- International Journal Article [Díez et al., 2014c].

6.1 UQ study on Fission Pulse Decay Heat calculations

6.1.1 Description of calculations

The Fission Pulse Decay Heat (FPDH) is the heat generated by radioactive decay after that a single atom of a specific material undergoes fission. Accurate calculations of such values assume a crucial importance in reactor operation strategies as the residual heat, which inevitably follows the reactor shutdown, is one of the most important parameters for reactor safety.

In FPDH calculations, radioactive decay and fission yield data are taken from the libraries, whereas cross sections do no take part in this kind of calculation. The time evolution of radioactive material subject to pure decay is described by the system of Ordinary Differential Equations (ODEs) in Eq. 6.1, which is a simplification of the Bateman equation (see Eq. 3.1) where only decay sources are considered:

$$\frac{dN_i}{dt} = -\lambda_i N_i + \sum_j \lambda_j \beta_{ji} N_j \qquad i = 1, ..., M \; ; \tag{6.1}$$

where λ are the decay constants, N are the concentrations of isotopes involved in the calculation, β_{ji} is the branching ratio which indicates the decay mode and the fraction of decays that converts isotope j into i, and M is a finite integer, that is, the size of the system. The initial composition, $N(t = 0)$, is the same as the FY distribution given in the library for the fissioning system studied, in this case ^{235}U and ^{239}Pu thermal fission.

The decay heat is calculated with Eq. 6.2, after calculating the isotopic inventory throughout the whole cooling time:

$$DH = \sum_i DH_i = \sum_i \lambda_i N_i \left(\sum_j \beta_{ij} E_j \right), \tag{6.2}$$

where, E_j is the average released energy for the corresponding decay mode given by the β_{ij} branching ratio.

6.1.2 The UQ study

As observed in Eq. 6.2, the nuclear data involved are decay constants (or half-life values), branching ratios, decay energy release and fission yield data. Thus, it is a perfect framework to show the impact and the importance of decay and fission yield data. Additionally, since it is only a depletion calculation, there are no uncertainties from transport calculations as in burn-up problems. So that, no approximation is assumed in that sense. Finally, the application of the Hybrid Method is straight forward thanks to the absence of irradiation and cross sections, so only decay and fission yield data have to be processed.

Here, UQ studies are performed for FPDH of two different isotopes: ^{239}Pu and ^{235}U, due to thermal incident neutrons. For the former, different sources of uncertainties are taken into account: decay data – decay constants, branching ratios and decay energies – and fission yield data; retrieved from evaluated libraries. Whereas for the latter, fission yield data uncertainties are propagated: not only the uncertainties stored in the nuclear data libraries, but also the covariance data generated in Chap. 5.

Two different nuclear data libraries are in use: JEFF-3.1.1 and ENDF/B-VII.1, from which decay and fission yield data are retrieved. The main method applied for these UQ studies is Monte Carlo sampling, by means of the Hybrid Method. However, for ^{235}U case, the propagation of moments – perturbation theory – is applied as well. For all these calculations, as part of the Hybrid Method, the depletion code ACAB is used.

6.1.3 Setting up the problem

Only one fission event is desired to happen, then the ACAB input file should contain the right information to achieve it. But also the cross section library and decay library should be modified.

The decay library is modified because no decay event of either ^{239}Pu or ^{235}U are desired, so their decay constants have to become zero. The way to implement that in ACAB is to modify the decay data library by changing `DECAY.dat` file. There, ^{239}Pu and ^{235}U are set as stable isotopes. The change for ^{239}Pu is shown in Fig. 6.1.

unmodified DECAY.dat

```
1  942390  1     7.606E+11 0.000E+00 0.000E+00 0.000E+00 1.000E+00 0.000E+00
1      0.000E+00 0.000E+00 0.000E+00 5.244E+00   0.000000 1.000E+00 1.000E+00
```

modified DECAY.dat

```
1  942390  6     0.000E+00 0.000E+00 0.000E+00 0.000E+00 1.000E+00 0.000E+00
1      0.000E+00 0.000E+00 0.000E+00 5.246E+00   0.000000 1.000E+00 1.000E+00
```

FIGURE 6.1: Changes in the `DECAY.dat` file for ^{239}Pu thermal FPDH calculations in order to avoid ^{239}Pu decay.

Only one fission event is desired for obtaining only a single fission pulse, so it is necessary to establish the right values of the fission cross section, neutron flux and isotopic concentration. With Eq. 6.3, parameters can be fixed:

$$R_{fission} = N\,\sigma_{fission}\,\phi\,t, \tag{6.3}$$

where $R_{fission}$ $(fissions/cm^3)$ is the amount of fission events that occur throughout the burn-up time, t (s); N is the density of ^{239}Pu or ^{235}U in $atoms/(barn \cdot cm^2)$, $\sigma_{fission}$ is the fission cross section of ^{239}Pu or ^{235}U in one energy group given in $barn$, and ϕ is the total neutron flux in $n/(cm^2 \cdot s)$. These parameters are set to the values given in Table 6.1 to obtain only one fission event.

TABLE 6.1: Parameters for Fission Pulse Decay Heat calculation.

Parameter	Value
N	$10^{-4}\ atoms/(barn \cdot cm)$
$\sigma_{fission}$	$1\ barn$
ϕ	$10^{14}\ neutrons/(cm^2 \cdot s)$
t	$10^{-10}\ s$

All the other neutron cross sections are removed from `XSECTION.dat`, so any other neutron reaction different from the fission of ^{239}Pu or ^{235}U is avoided. The rest of the parameters presented before are included in the ACAB input file (Fig. 6.3).

Since only FPDH due to thermal incident neutrons is calculated, fission yield data should be collapsed using only thermal neutron spectrum. Then, a simplified input for COLLAPS is used as presented in Fig 6.2. There, five energy groups are defined within the neutron flux: irrelevant groups are set to 10^{-20}, while the thermal group (from 10^{-11} MeV to 10^{-7} MeV)

is set to 10^{10}. Then, after running COLLAPS, `FY.dat` and `UNFY.dat` store fission yield data and their uncertainties only for thermal incident neutrons.

```
 12   5
        16
  1   0   1   1
  5.000E+06   2.000E+05
    5   0
1.00000E-11 1.00000E-07 1.00190E-01 2.00000E-01 5.00000E+00 6.00000E+01
1.00000E+10 1.00000E-20 1.00000E-20 1.00000E-20 1.00000E-20
          0
          0
```

FIGURE 6.2: COLLAPS input for thermal incident neutron FPDH calculations.

```
Caso EFIT
<Block #1, card #2
 0 IUNC
   3849  900000  0  1  1  0  2  2  0 24  1  0  4  1  1  0  1  0  0  1  0
   1.000000E+00    1.0E+00
  1
        1
  2.00E+01  1.40E+01  1.20E+01  1.00E+01  8.00E+00  6.50E+00  5.00E+00
4.00E+00
  3.00E+00  2.50E+00  2.00E+00  1.70E+00  1.40E+00  1.20E+00  1.00E+00
8.00E-01
  6.00E-01  4.00E-01  3.00E-01  2.00E-01  1.00E-01  5.00E-02  2.00E-02
1.00E-02
  0.00E+00
  0.00E+00  0.00E+00  0.00E+00  0.00E+00  0.00E+00  0.00E+00
  1  0  0  1  0  0  1  0  0  1  0  0  0  0  0  0  0  0
 1.E+14
< No hay Restart
          0
< Isotopia
942390
1.0E-04
< 1 otro bloque
  1 1   1 0   1 0   0 0
  1.000E-10
< Bloque. DECAY
    0  10   1  1  1 0   0 0
    1.00E-01  1.00E+00 2.00E+00 4.00E+00 6.00E+00
    8.00E+00  1.00E+01 2.00E+01 4.00E+01 6.00E+01
< Bloque. DECAY
    0  10   1  10  1 0   0 0
    8.00E+01  1.00E+02 2.00E+02 4.00E+02 6.00E+02
    8.00E+02  1.00E+03 2.00E+03 4.00E+03 6.00E+03
< Bloque. DECAY
    0  10   0  10  1 0   0 0
    8.00E+03  1.00E+04 2.00E+04 4.00E+04 6.00E+04
    8.00E+04  1.00E+05 2.00E+05 6.00E+05 1.00E+06
  1.0000000E-25   1.000000
<Block #10 Fission product inventory
 1 1 0              IGFP IWFYD IFORT96
 1 0 0 0 0 1 0 1 0 0   IWP(1) IMTX(2) IWDR(3) IDOSE(4) IPHCUT(5) IDHEAT(6)
IOFFSD(7) IDCEDE(8) INEMISS(9) IDAMGE(10)
 0 0 4 0   NOPUL  NTSEQ  NOTTS   NVFL
          0 NMULT
          0          1 NCYO IFSO
          1  1  1   1 (ITSO(I),I=1,NOTTS)
```

FIGURE 6.3: ACAB input file for performing ^{239}Pu thermal FPDH calculations. For the ^{235}U case, only the concentration changes from ^{239}Pu to ^{235}U.

6.1.4 ^{239}Pu thermal FPDH

An extensive study is carried out here, using the JEFF-3.1.1 library for decay and fission yield data. The different sources of decay heat: beta and gamma, are analysed separately, and also its total sum. The contributions of the isotopes which have or not uncertainty in their decay energy are assessed. These isotopes have been identified already in Chapter 2,

Sec. 2.4. Finally, all these results are compared with the experimental data provided by Tobias [Tobias, 1980, Tobias, 1989].

Table 6.2 shows the uncertainties given to those isotopes which have no uncertainty for their decay energy. Other source [Katakura, 2013] proposes to add 100% uncertainty instead, however such an assumption seems to be very conservative. In spite of that, a comparison between both assumptions can show their impact.

Therefore, UQ studies are performed on six different calculations for the FPDH of ^{239}Pu thermal fission:

- Total, beta and gamma decay heat produced by all isotopes when all of them have uncertainty in their decay energies provided either with JEFF-3.1.1 or in Table 6.2.
- Total, beta and gamma decay heat produced by all isotopes, using only the uncertainties given in JEFF-3.1.1.

Regarding the uncertainties propagated in these calculations for ^{239}Pu, only the ones of fission yields and decay data (energy, half-life and branching ratios) are considered. Random variables are sampled using a log-normal distribution.

TABLE 6.2: Decay energy uncertainties given to those isotopes for which JEFF-3.1.1 provides no uncertainty in their decay energy. These values are only used for ^{239}Pu FPDH calculations.

Decay Mode	Uncertainty
α	10%
β	15%
γ	15%

6.1.4.1 Convergence study

In order to assure the convergence of the results, due to the usage of a Monte Carlo sampling scheme, two estimators are followed as a function of the number of histories: the mean and the relative standard deviation (rel.std.dev.). Fig 6.4 shows the evolution of rel.std.dev. for different time steps of cooling time for FPDH, when all uncertainties are propagated together. Convergence is achieved with only 300 histories. This analysis has been performed for all the calculations stated in the previous section, obtaining the same convergence results.

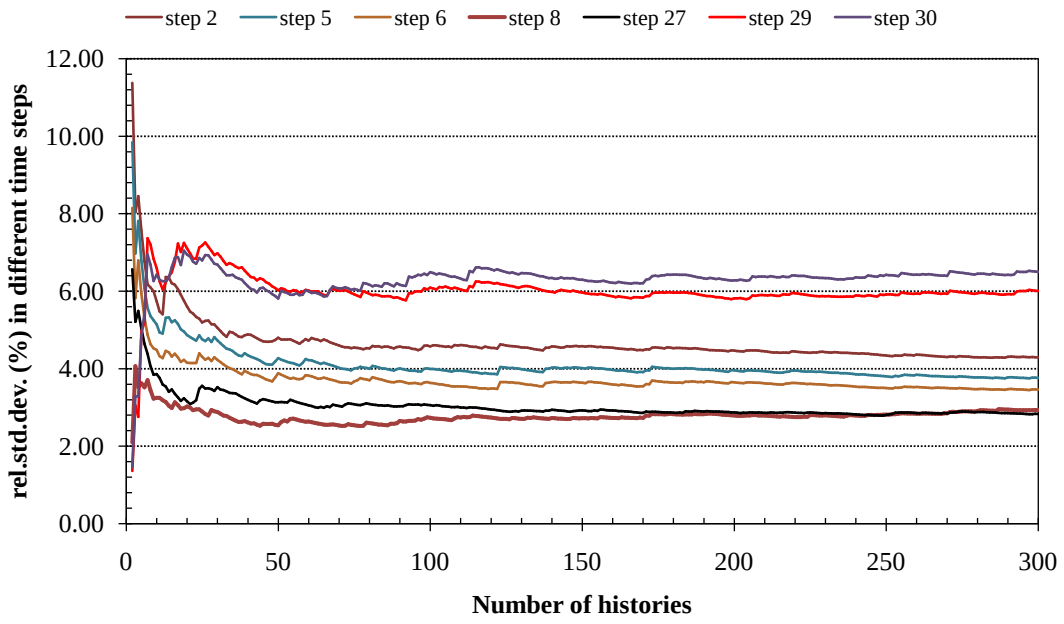

FIGURE 6.4: Relative standard deviation versus number of histories run for total FPDH of the ^{239}Pu thermal fission in a selected set of time steps during cooling time.

6.1.4.2 Reference calculations

The so-called reference calculations are obtained with the reference (best-estimated) values stored in the nuclear data libraries. They are calculated for being compared later with the mean values obtained from uncertainty propagation calculations.

Fig 6.5 presents FPDH reference calculations. The calculations presented are: considering only the isotopes with decay energy uncertainty data in JEFF-3.1.1 (dashed-lines empty markers) and when all isotopes carry uncertainties (solid-line filled markers). Also, the different contributions, gamma decay heat (black lines) and beta decay heat (red lines), to the total decay heat (blue line) are shown.

Contributions of those isotopes that have no uncertainties is only relevant for the first time interval, up to 2×10^3 seconds. Without their contributions, up to a 15% of the FPDH could be missed during the considered cooling time.

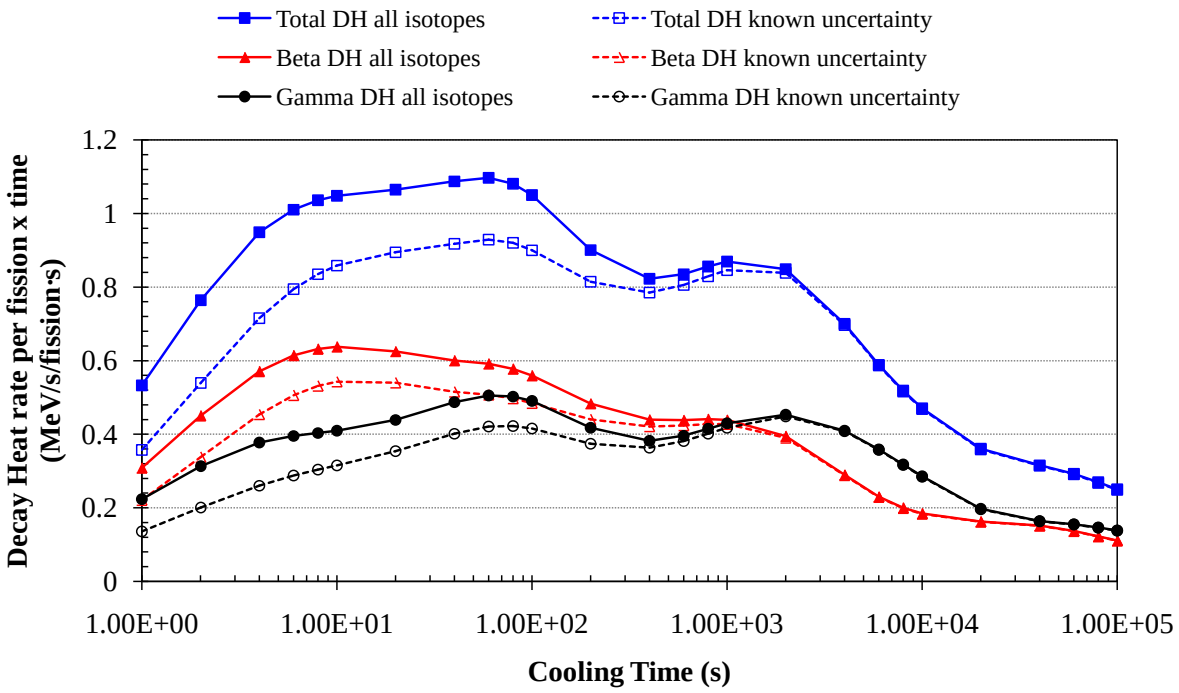

FIGURE 6.5: Reference calculation for FPDH of the ^{239}Pu thermal fission using JEFF-3.1.1, differencing between gamma and beta contribution, and between the contribution of isotopes which have decay energy uncertainties stored in JEFF-3.1.1 and when all carry uncertainties.

6.1.4.3 Total FPDH

Here, the results of propagating uncertainties on the Total FPDH of ^{239}Pu thermal fission are described. Fig 6.6 shows the reference value (green), the mean value with its uncertainty band (as one std.dev.) when all isotopes have decay energy uncertainties (blue), and the mean value with its uncertainty band (as one std.dev.) when only the isotopes with decay energy uncertainty stored in JEFF-3.1.1 are taken into account (red). Also, the results of Tobias experimental data are plotted (black square markers).

Several results can be extracted from this figure:

- A positive bias appears between the mean value obtained from the uncertainty propagation calculation and the reference value.
- The contribution of the isotopes with no uncertainty on their decay energies is of relevance up to 2×10^3 seconds.
- The uncertainty on FPDH obtained from all isotopes and only from the ones that have decay energy uncertainties are similar.

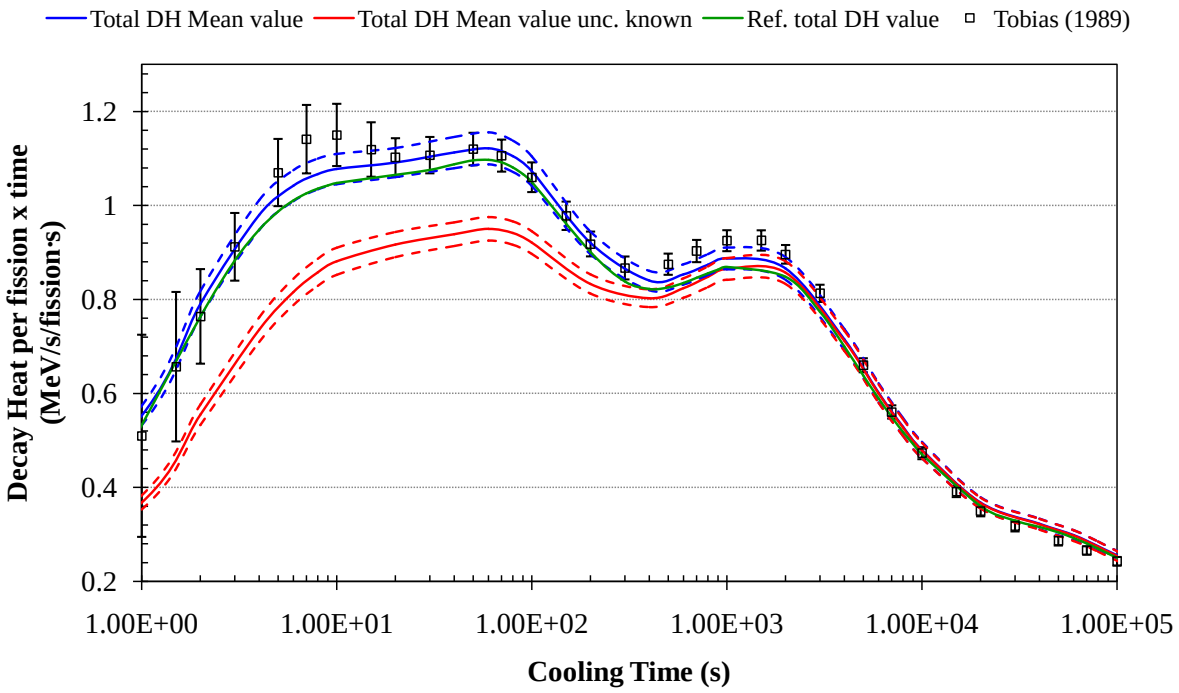

FIGURE 6.6: Total FPDH for the ^{239}Pu thermal fission as a function of cooling time for the reference calculation, mean values from UQ calculations and experimental data. Uncertainty bands (dashed lines) represents one standard deviation, obtained from UQ calculations. Used data are retrieved from JEFF-3.1.1.

The comparison between reference results and mean values of the uncertainty propagation calculations is presented in Fig. 6.7. Both values are divided by the Tobias's experimental data, showing whether calculated values are within the experimental uncertainty (blue line). The positive bias seen before, from the reference value to the mean values obtained from the uncertainty propagation, is again observed. The origin of this bias comes from the usage of log-normal distribution for sampling, because log-normal distributions induces a positive bias in the sampled mean value which lead to higher values of decay energy.

Each source of uncertainty is propagated individually, showing their results in Fig. 6.8. Here, the uncertainty due to fission yield is presented in red, due to half-lives in green and due to decay energy in pink. The result when all of them are propagated together is also shown, in blue. Experimental uncertainty is plotted in grey. The most important contributors are the fission yield uncertainties, followed by the decay energy uncertainties and, finally, the half-life uncertainties. The total uncertainty never exceeds 4%.

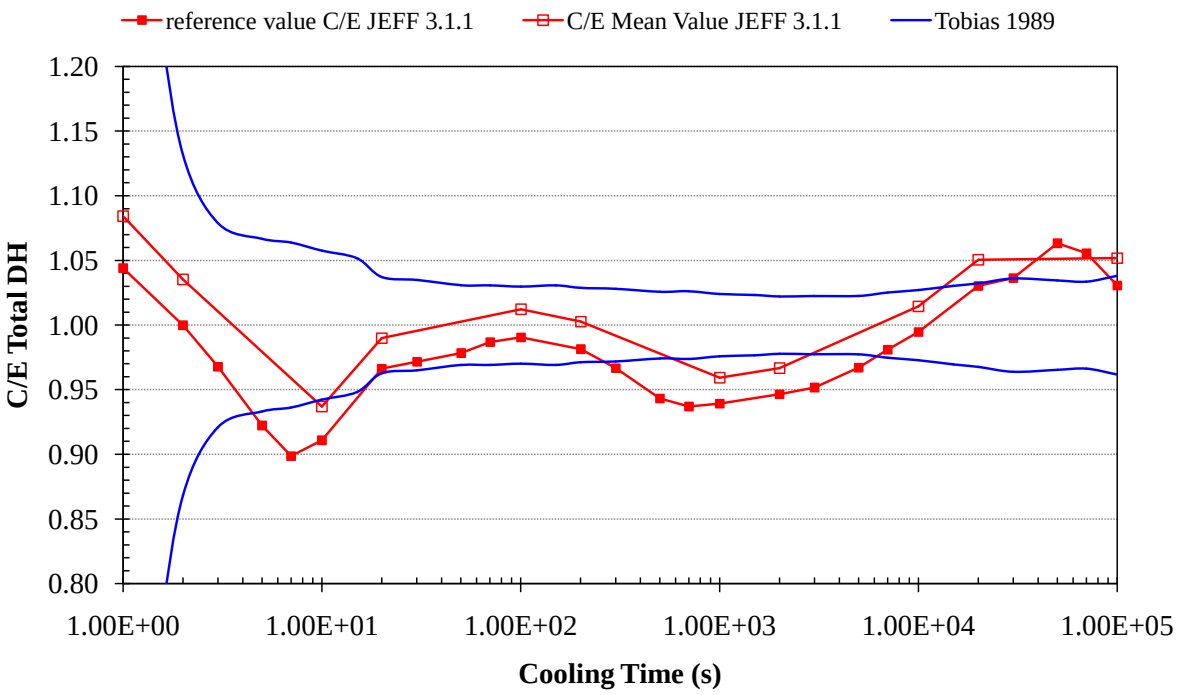

FIGURE 6.7: Calculated values (reference and mean values) divided by Tobias' experimental data, and the experimental uncertainty band, for the Total FPDH of ^{239}Pu thermal fission using JEFF-3.1.1.

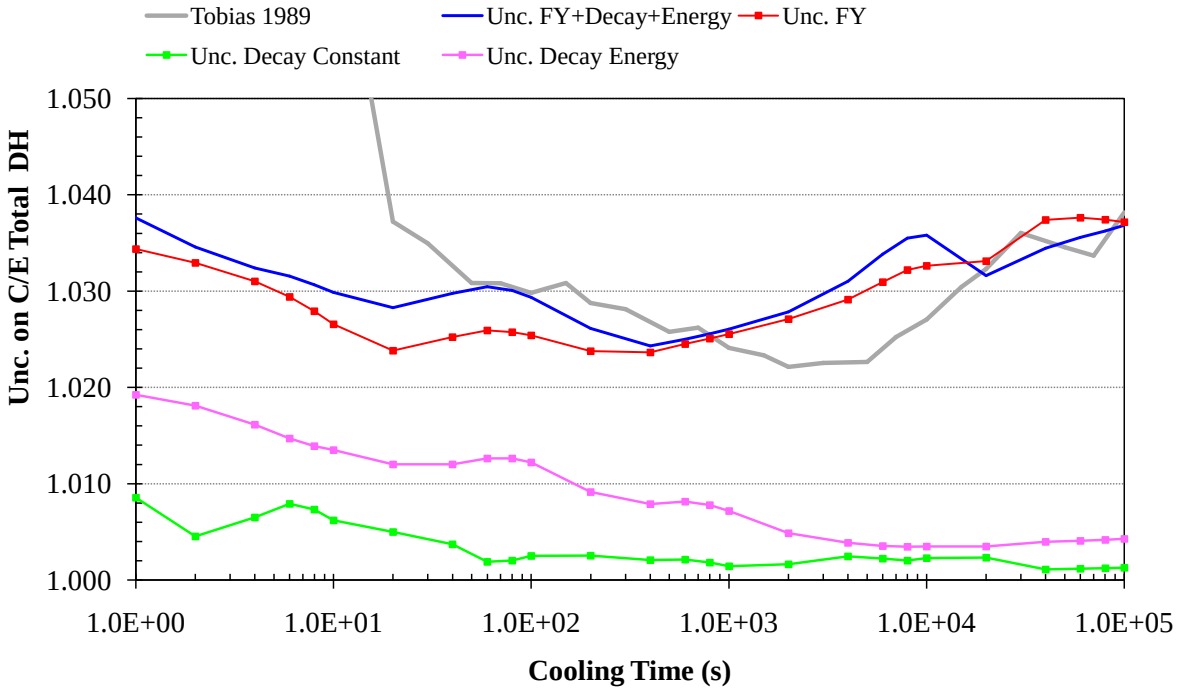

FIGURE 6.8: Relative uncertainty on the Total FPDH of ^{239}Pu thermal fission, calculated with JEFF-3.1.1, given its upper limit as a factor of the C/E value, due to fission yield, decay energy and half-life uncertainties, propagated individually and all together.

6.1.4.4 Beta FPDH

The same study done for Total FPDH is repeated for Beta FPDH. In Figs. 6.9, 6.10 and 6.11 the results for beta FPDH are presented.

In these figures, the same results as in Total FPDH are observed: the positive bias from the reference value to the mean value obtained from uncertainty propagation calculations, the importance of the isotopes without decay energy uncertainties goes up to 2×10^3 seconds, and the main contribution to the total uncertainty is due to fission yield uncertainties. The uncertainty obtained is always smaller than the experimental. Only at very short cooling times, its goes slightly above 4%. An important results to highlight is that Beta FPDH is overestimated compared with the experimental data.

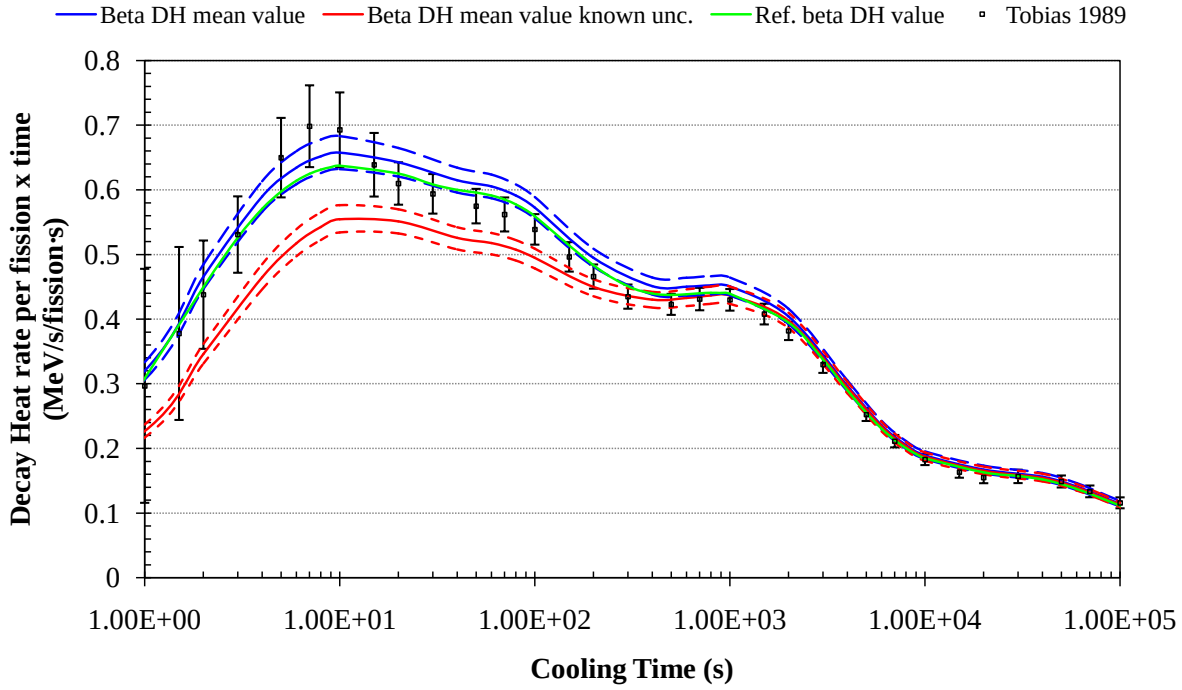

FIGURE 6.9: Beta FPDH values for ^{239}Pu thermal fission, calculated with JEFF-3.1.1, as a function of cooling time for the reference calculation, mean values from UQ calculations and experimental data. Uncertainty bands (dashed lines) represents one standard deviation, obtained from UQ calculations.

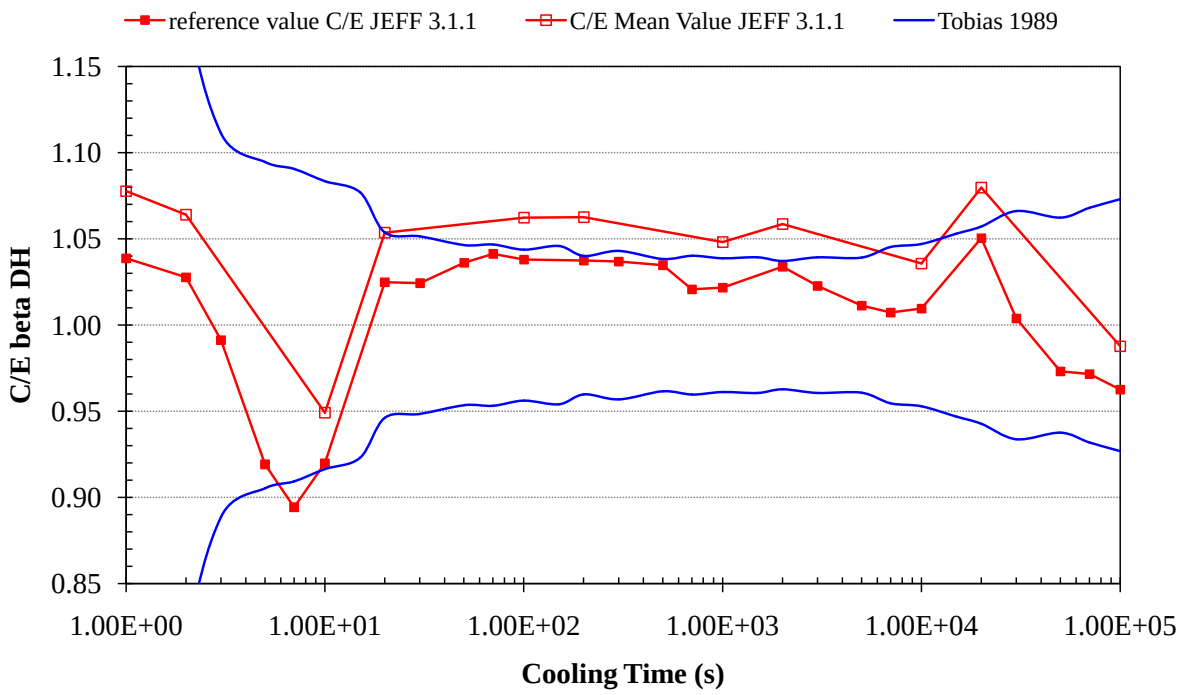

FIGURE 6.10: Calculated values (reference and mean values) divided by experimental data, and the experimental uncertainty band for the Beta FPDH of ^{239}Pu thermal fission, calculated with JEFF-3.1.1.

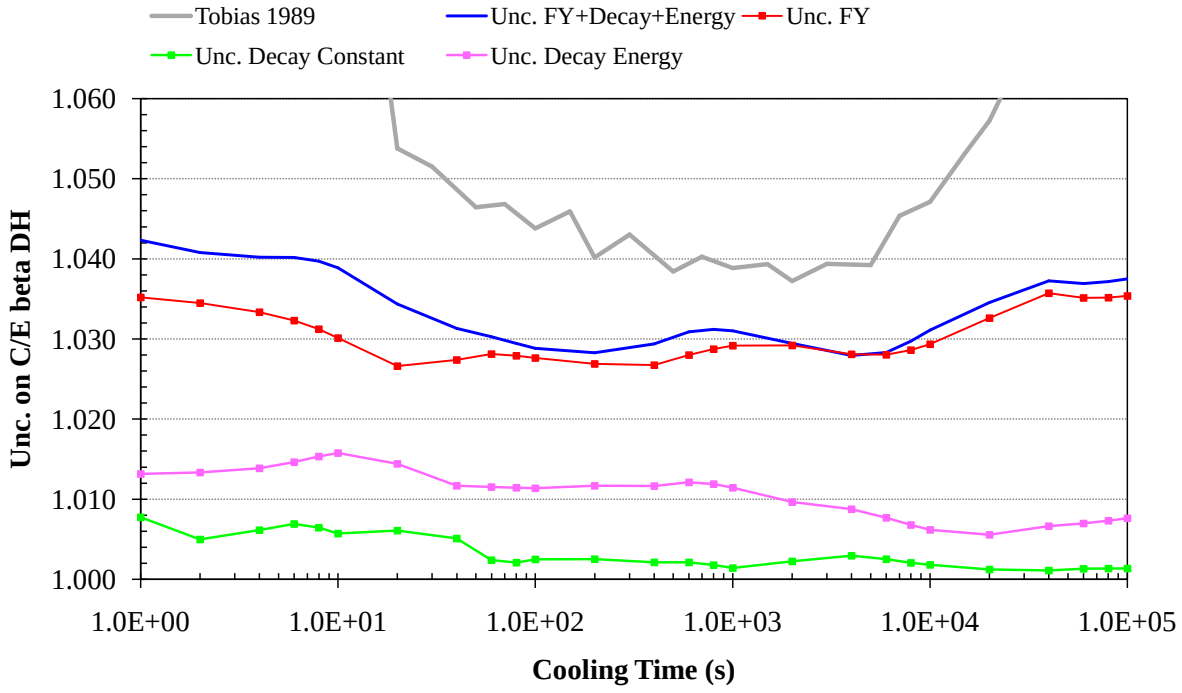

FIGURE 6.11: Relative uncertainty on the Beta FPDH of ^{239}Pu thermal fission, calculated with JEFF-3.1.1, given its upper limit as a factor of the C/E value, due to fission yield, decay energy and half-life uncertainties, propagated individually and all together.

6.1.4.5 Gamma FPDH

An analysis for Gamma FPDH is carried out, following the study done for Total FPDH and Beta FPDH for the ^{239}Pu thermal fission. The results are given in Figs. 6.12, 6.13, 6.14.

Again, the results obtained are similar to the previous ones: the positive bias from the reference value to the mean value obtained from the uncertainty propagation, and the importance of the isotopes without decay energy uncertainties goes up to 2×10^3 seconds. The main source of uncertainty is the fission yields, but in this case, the calculated uncertainty is larger than the experimental for the time interval between 2×10^3 s and 8×10^4 s. Also, during such time, the uncertainty surpasses 4%. When the C/E value is observed, both reference and mean value are always outside the experimental uncertainty band. In contrast to Beta FPDH, Gamma FPDH is underestimated compared with the experimental data.

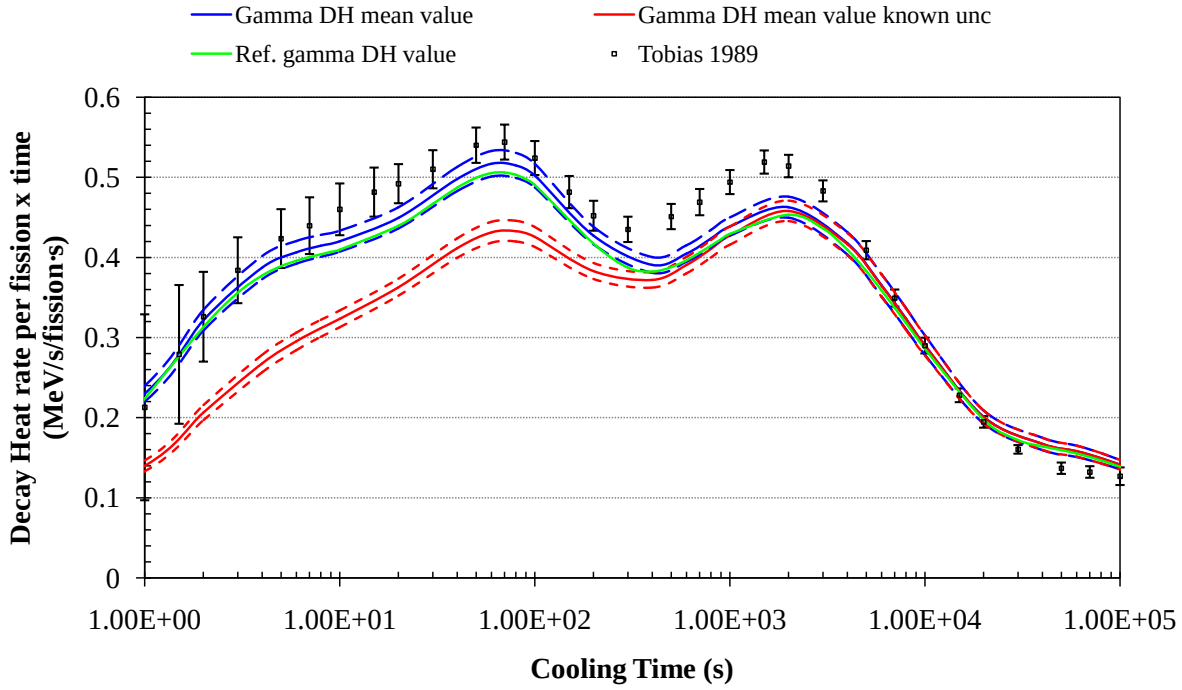

FIGURE 6.12: Gamma FPDH values for ^{239}Pu thermal fission, calculated with JEFF-3.1.1, as a function of cooling time for the reference calculation, mean values from UQ calculations and experimental data. Uncertainty bands (dashed lines) represents one standard deviation, obtained from UQ calculations.

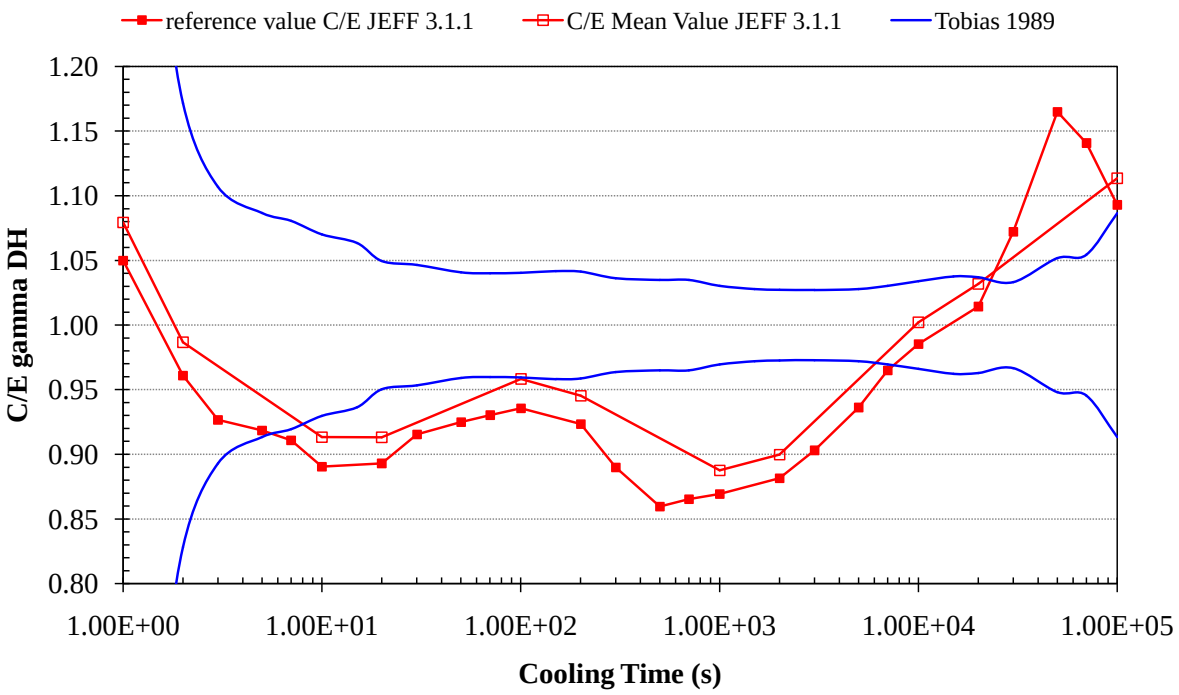

FIGURE 6.13: Calculated values (reference and mean values) divided by experimental data, and the experimental uncertainty band for the Gamma FPDH of ^{239}Pu thermal fission, calculated with JEFF-3.1.1.

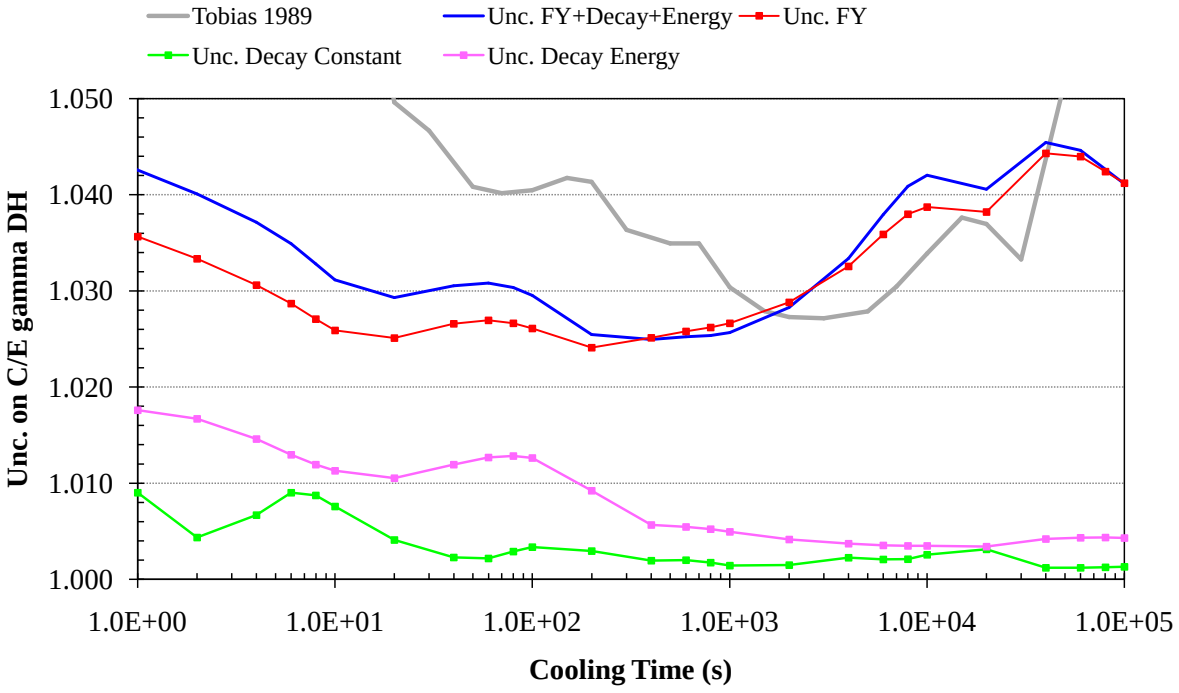

FIGURE 6.14: Relative uncertainty on the Gamma FPDH of ^{239}Pu thermal fission, calculated with JEFF-3.1.1, given its upper limit as a factor of the C/E value, due to fission yield, decay energy and half-life uncertainties, propagated individually and all together.

6.1.4.6 Contributor analysis

The decay heat contributions of every isotope involved in FPDH are calculated, performing also statistical analyses on them. Because the total, beta and gamma decay heats are sum of individual contributions, the development presented in Chapter 4, Sec. 4.3.4.1 is applied.

The maximum contributors to FPDH and their uncertainties are calculated for all the cases presented before: total, beta and gamma; distinguishing also between when only the uncertainties of decay energies provided within JEFF-3.1.1 are propagated, and when all decay energies have uncertainties. In all these cases, all the uncertainty sources: half-lives, branching ratios and fission yields; are propagated together.

Only main results are provided here. The complete study can be found in [Cabellos et al., 2013].

Total FPDH

The analysis of the main contributors for total FPDH, when only the isotopes with decay energy uncertainties provided in JEFF-3.1.1 are taken into account, is shown in Fig. 6.15. Whereas, the results when all isotopes have uncertainties in their decay energies are presented in Fig. 6.16. In both plots, the most important contributors to the total FPDH uncertainty throughout cooling time are drawn with the total decay heat uncertainty.

Many contributors with similar contributions are observed. For short cooling times (from 0.1 s to 20 s): Nb, Zr and Y isotopes are the main contributors. Then, Tc and Cs isotopes become the main contributors until 2000 s of cooling time. Above 2000 s, Y, La, Xe and I isotopes are the main contributors up to the end of the studied cooling time. More than 20 contributors should be taken into account in order to obtain at least a contribution, by summing the squared individual contributions, larger than the actual total uncertainty at the beginning of cooling time. While at the end of the cooling time studied, ^{134,135}I contributions provide at least the half of the total uncertainty. When decay energy uncertainties are suggested to isotopes without uncertainty, ^{102,103}Nb, ^{136m}I and ^{139}Xe become the most important contributors during their period of relevance.

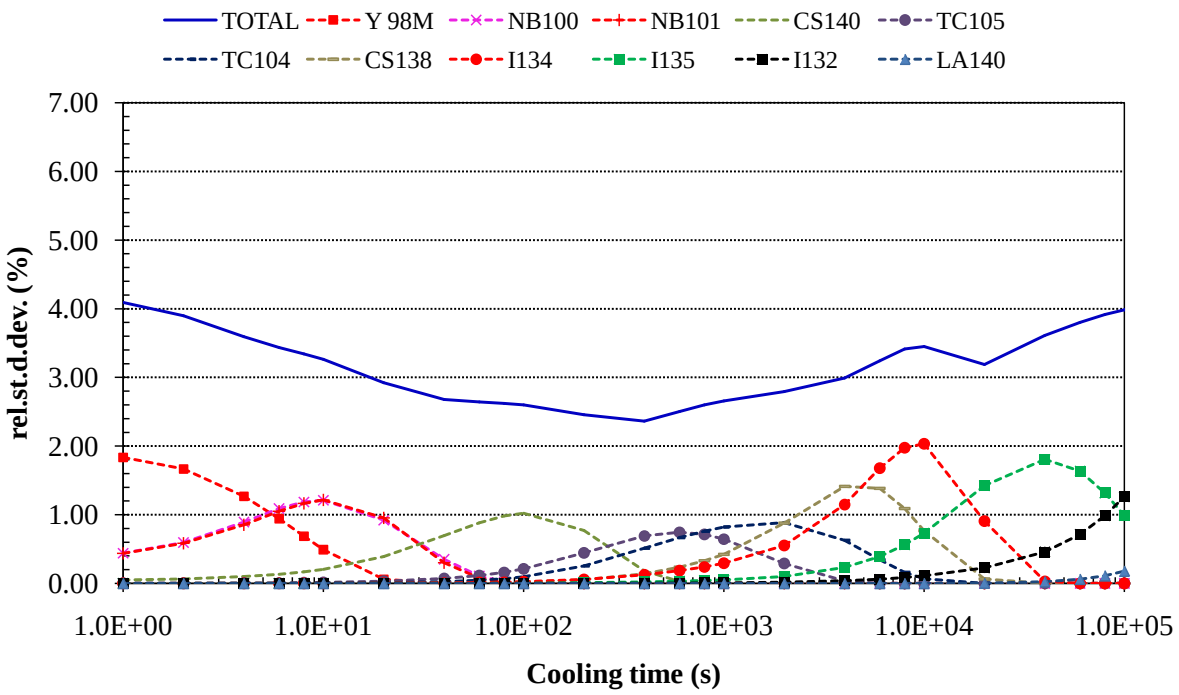

FIGURE 6.15: Main uncertainty contributors to the total FPDH of ^{239}Pu thermal fission when only isotopes with decay energy uncertainties provided in JEFF-3.1.1 are considered.

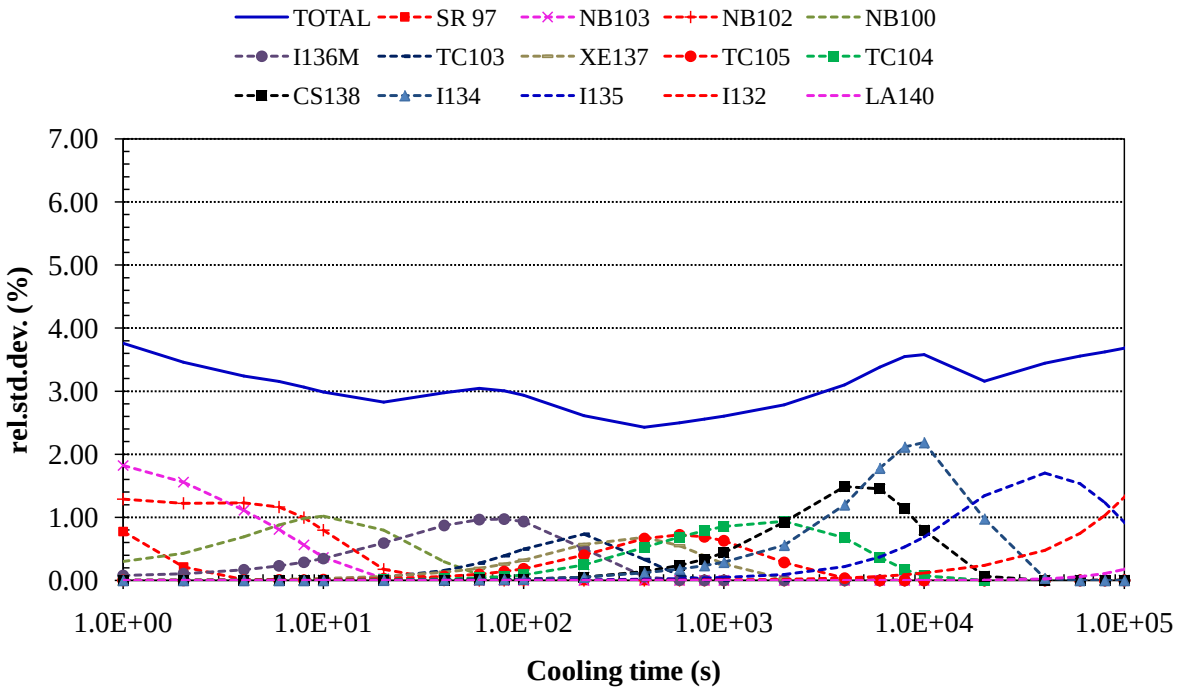

FIGURE 6.16: Main uncertainty contributors to the total FPDH of ^{239}Pu thermal fission when all isotopes have decay energy uncertainties. JEFF-3.1.1 is used in these calculations.

Beta FPDH

The same analysis is performed for beta contribution, showing in Fig. 6.17 the results when only the decay energy uncertainties provided in JEFF-3.1.1 are propagated, and in Fig. 6.18 when all decay energies have uncertainty.

Again, it is observed that there are many contributors with similar contributions. More than 20 contributors should be taken into account in order to obtain at least a total contribution larger than the actual total uncertainty. Both cases, when all decay energies have uncertainties and when only the ones in JEFF-3.1.1 are propagated, present the same tendency as in Total FPDH, with some minor differences in the order of main contributors, except for $^{102,103}Nb$ and ^{97}Sr that appear as main contributors when decay energy uncertainties are suggested for them. That means the isotopes with unknown uncertainties are of importance for beta FPDH calculations, and for its uncertainty, throughout short cooling time periods ($t < 2 \times 10^3$ s).

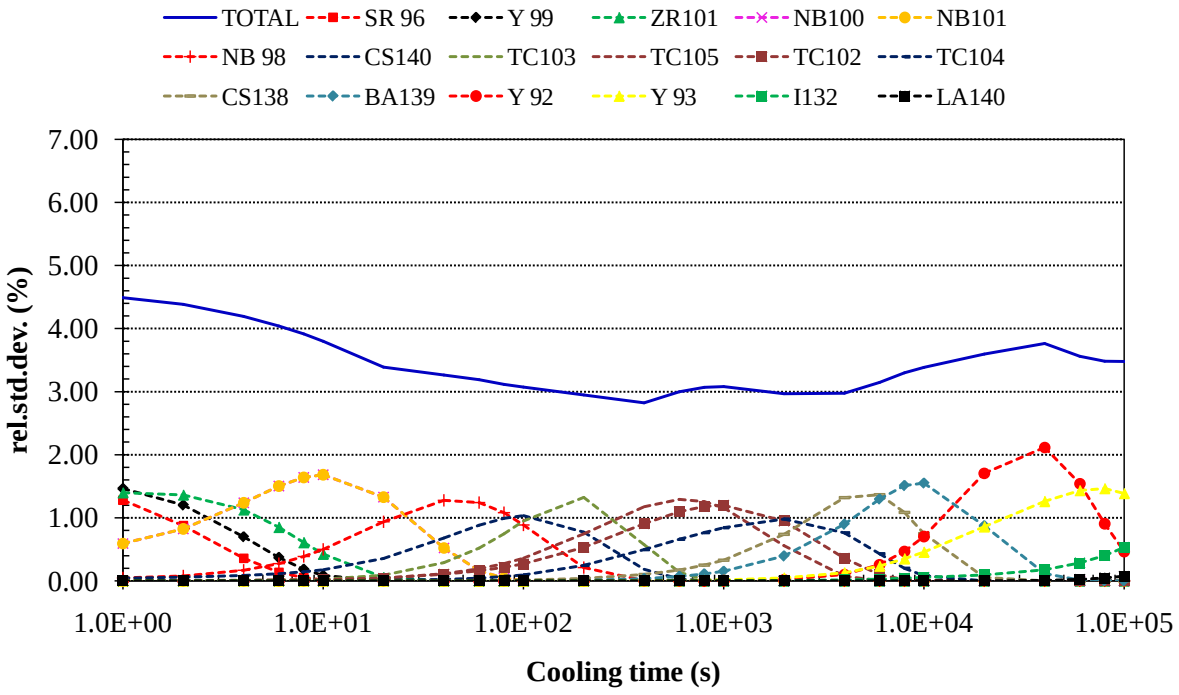

FIGURE 6.17: Main uncertainty contributors to the beta FPDH of ^{239}Pu thermal fission when only isotopes with decay energy uncertainties provided in JEFF-3.1.1 are considered.

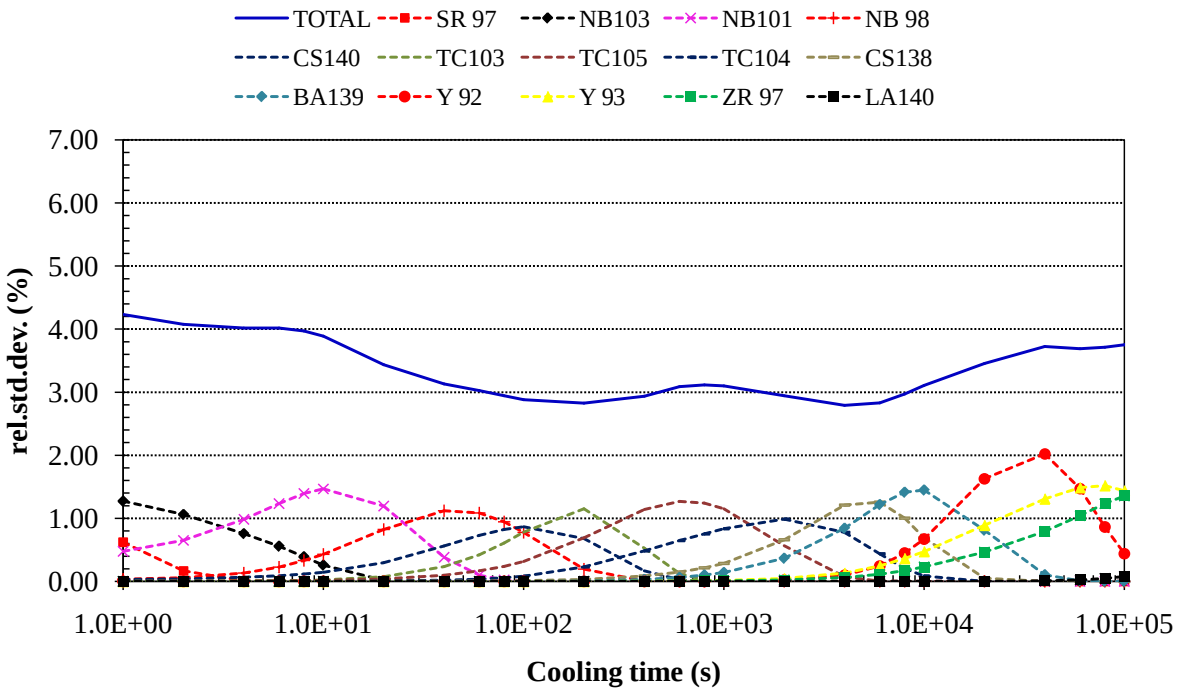

FIGURE 6.18: Main uncertainty contributors to the beta FPDH of ^{239}Pu thermal fission when all isotopes have decay energy uncertainties. JEFF-3.1.1 is used in these calculations.

Gamma FPDH

Finally, gamma FPDH is addressed, showing its contributors when only the isotopes with decay energy uncertainties provided in JEFF-3.1.1 are taken into account in Fig. 6.19, and when all decay energies have uncertainties in Fig. 6.20.

The results for both cases show again that there are a lot of main contributors for short cooling times, up to 20 seconds, e.g. Nb, Rb and Y isotopes. After that time, La and Cs isotopes become the main contributors until 1000 seconds. The most important contributors above 1000 seconds are I, La, Te and Sb. Indeed, ^{134,135}I appear as the most important contributors, supplying at least 50% of the total uncertainty.

When all isotopes have decay energy uncertainties, $^{102,103}Nb$, ^{97}Sr and ^{136m}I appear as main contributors. That means the isotopes with unknown uncertainties do play an important role in gamma FPDH calculations and its uncertainty for short cooling time periods ($t < 2\times10^3$ s), as they do in beta FPDH.

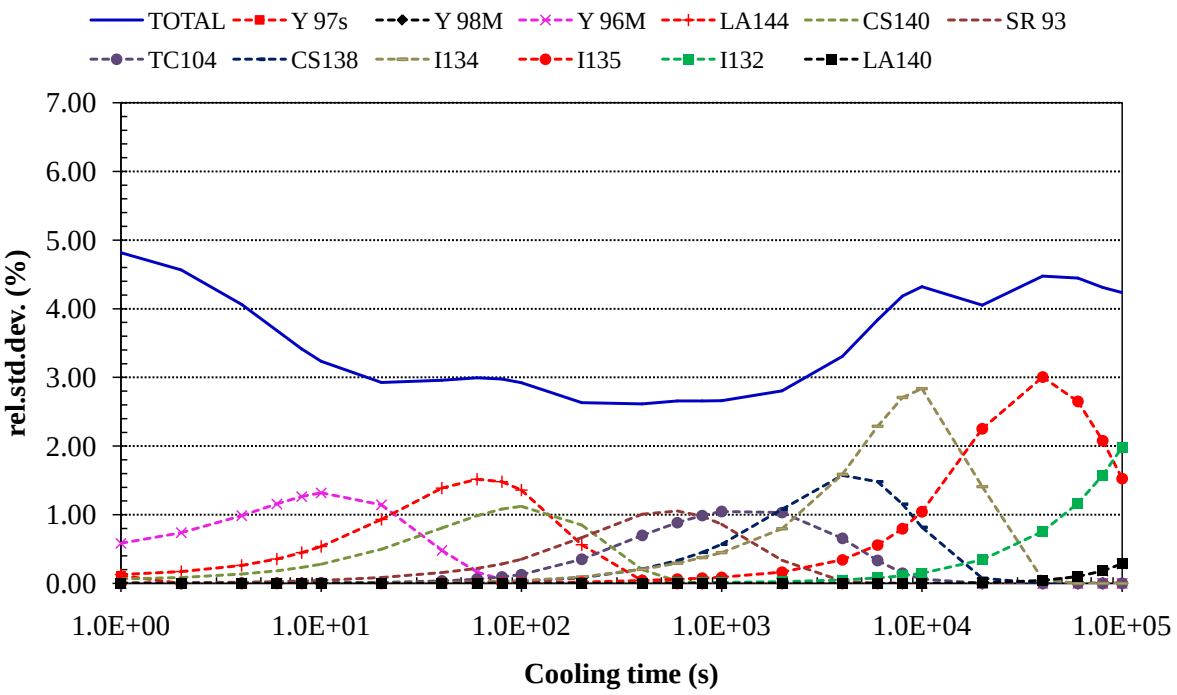

FIGURE 6.19: Main uncertainty contributors to the gamma FPDH of ^{239}Pu thermal fission when only isotopes with decay energy uncertainties provided in JEFF-3.1.1 are considered.

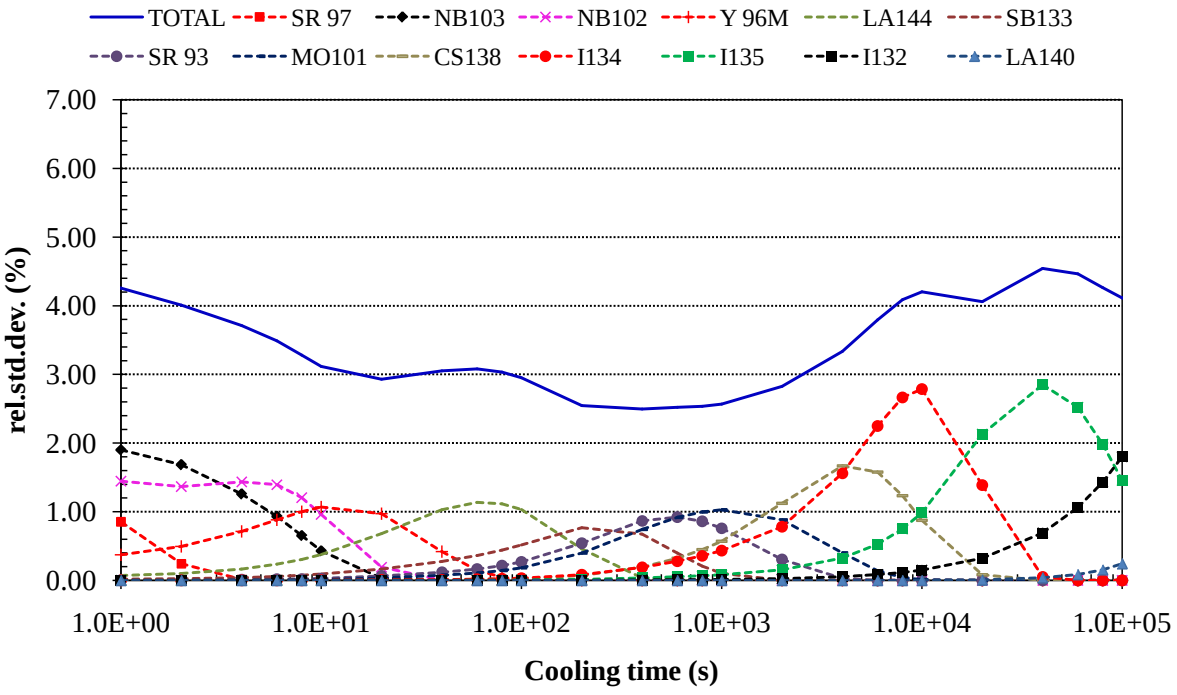

FIGURE 6.20: Main uncertainty contributors to the gamma FPDH of ^{239}Pu thermal fission when all isotopes have decay energy uncertainties. JEFF-3.1.1 is used in these calculations.

6.1.4.7 Including latest TAGS experimental values in JEFF-3.1.1

As already mentioned in Chapter 2, decay energy coming from gamma rays is underestimated, while decay energy from beta decay particles is overestimated, this is know as "Pandemonium effect" [Hardy et al., 1977]. New experiments are aimed to overcome this issue by means of the use of TAGS (Total Absorption Gamma Spectrometer) experiments. As explained in [Algora et al., 2010], new values for decay energies are proposed for various isotopes, which are presented in Table 6.3. An increase of gamma decay energies and a decrease of beta decay energies are observed. Large changes are proposed for one isotope: ^{101}Nb, whose uncertainty for the gamma decay energy has increased from 9% to 62.7%, while its uncertainty for the beta decay energy has decreased from 16.5% to 7.4%.

TABLE 6.3: Comparison between mean values and uncertainties for beta and gamma decay energies included in the JEFF-3.1.1 library and new TAGS experimental data [Algora et al., 2010].

		Decay energy (keV)			
Nuclide	$T_{1/2}$ (s)	$\overline{E}_{\gamma,JEFF}$	$\overline{E}_{\gamma,TAGS}$	$\overline{E}_{\beta,JEFF}$	$\overline{E}_{\beta,TAGS}$
^{101}Nb	7.1 ± 0.3	244.46 ± 22	445 ± 279	1863 ± 307	1797 ± 133
^{105}Mo	35.6 ± 1.6	551.5 ± 24	2407 ± 93	1922 ± 122.5	1049 ± 44
^{102}Tc	5.28 ± 0.15	80.8 ± 4.6	106 ± 23	1945 ± 15.5	1935 ± 11
^{104}Tc	1098 ± 18	1890 ± 30.7	3229 ± 24	15956 ± 75	931 ± 10
^{105}Tc	456 ± 6	668.4 ± 19	1825 ± 174	1310 ± 173.2	764 ± 81
^{106}Tc	36 ± 1	2191 ± 51.2	3132 ± 70	1943 ± 68.7	1457 ± 30
^{107}Tc	21.2 ± 0.2	514.8 ± 10.9	1822 ± 450	2056 ± 254.1	1263 ± 212

Analysis of the impact of these new decay energy values is performed for reference calculations, showing these results in Figs. 6.21, 6.22 and 6.23. The usage of new TAGS data improves the agreement between simulations and experimental data. For total FPDH, there are some cooling times where simulations still underestimate the total FPDH. For beta FPDH, there is still an underestimation between 2 s and 20 s, while after 20 s it is always overestimated. And for gamma FPDH, almost at any cooling time FPDH is still underestimated, excepts between 20 s and 100 s when it is overestimated. In general, the new TAGS data improve the agreement between experimental data and calculations, but there is still discrepancies to be resolved.

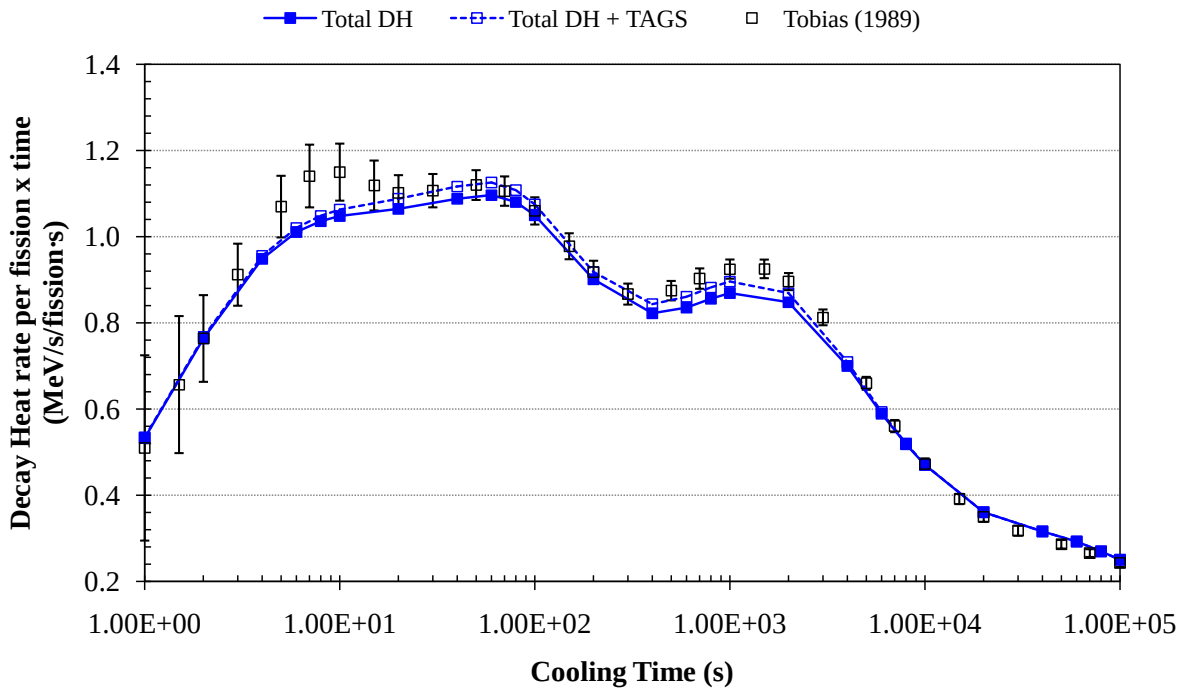

FIGURE 6.21: Total FPDH for the ^{239}Pu thermal fission using JEFF-3.1.1 compared with the inclusion of new TAGS data into JEFF-3.1.1.

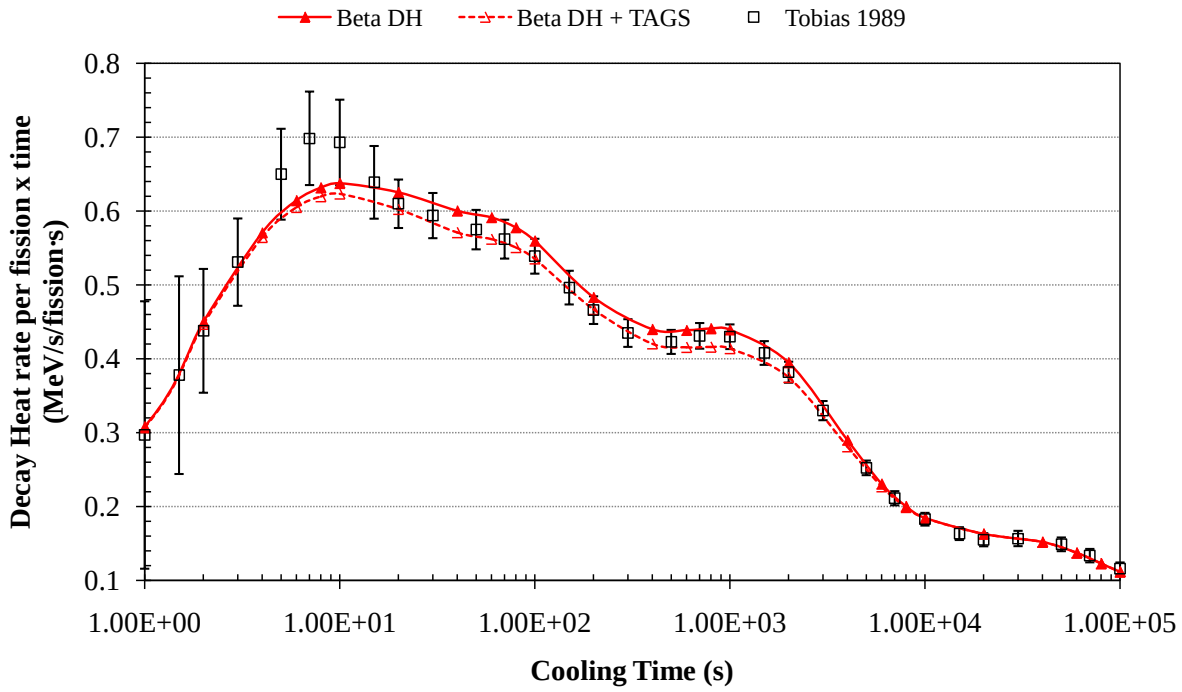

FIGURE 6.22: Beta FPDH for the ^{239}Pu thermal fission using JEFF-3.1.1 compared with the inclusion of new TAGS data into JEFF-3.1.1.

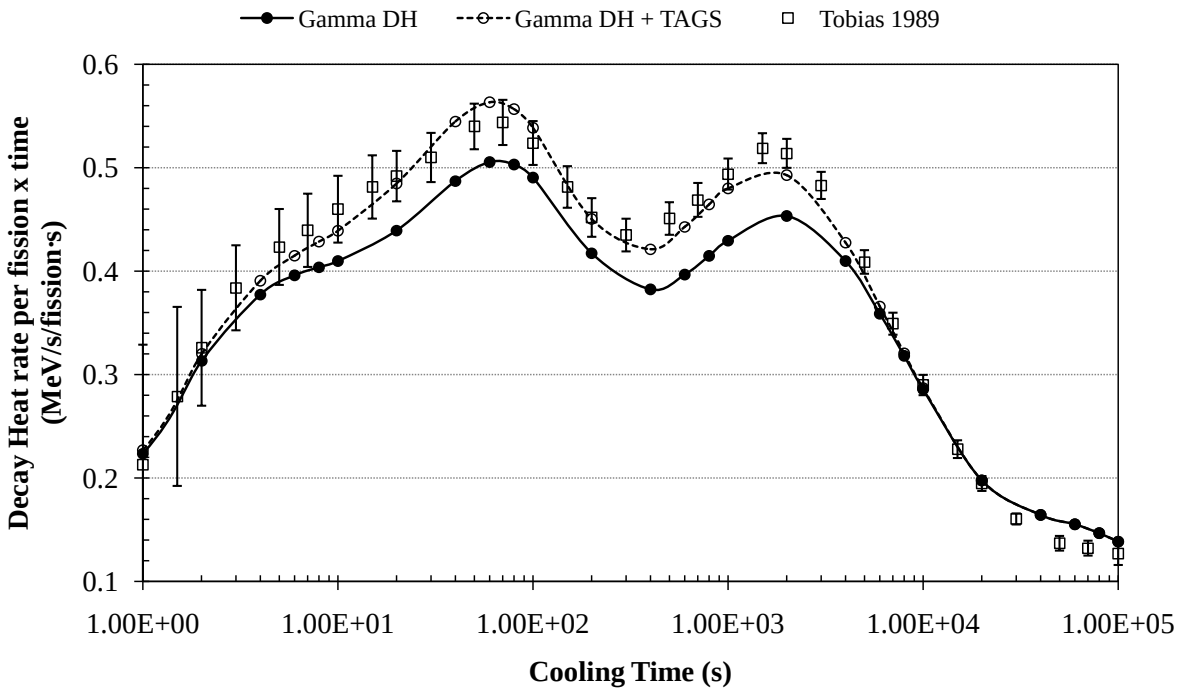

FIGURE 6.23: Gamma FPDH for the ^{239}Pu thermal fission using JEFF-3.1.1 compared with the inclusion of new TAGS data into JEFF-3.1.1.

The impact of these new values on previous UQ studies are only addressed for the case in which all isotopes have decay energy uncertainties. Results for Beta and Gamma FPDH of the ^{239}Pu thermal fission are shown in Fig. 6.24 and Fig. 6.25, respectively.

For Beta FPDH, negligible differences arise between using or not new TAGS data. In contrast, for Gamma FPDH, an increase of the uncertainty appears from 2 s to 60 s, and from 400 s to 2000 s. The effect on Total FPDH is the same as on Beta FPDH, the usage of new TAGS data has no impact.

Analysis of the contributors has been performed, revealing that the main contributors to Total FPDH are $^{98,99,100,101,103}Nb$, $^{96,97m}Y$, $^{99,100}Zr$, ^{140}Cs and ^{103}Mo. If they are compared with previous results without using new TAGS data, same main contributors, only ^{135}Te and ^{137}I become slightly more relevant.

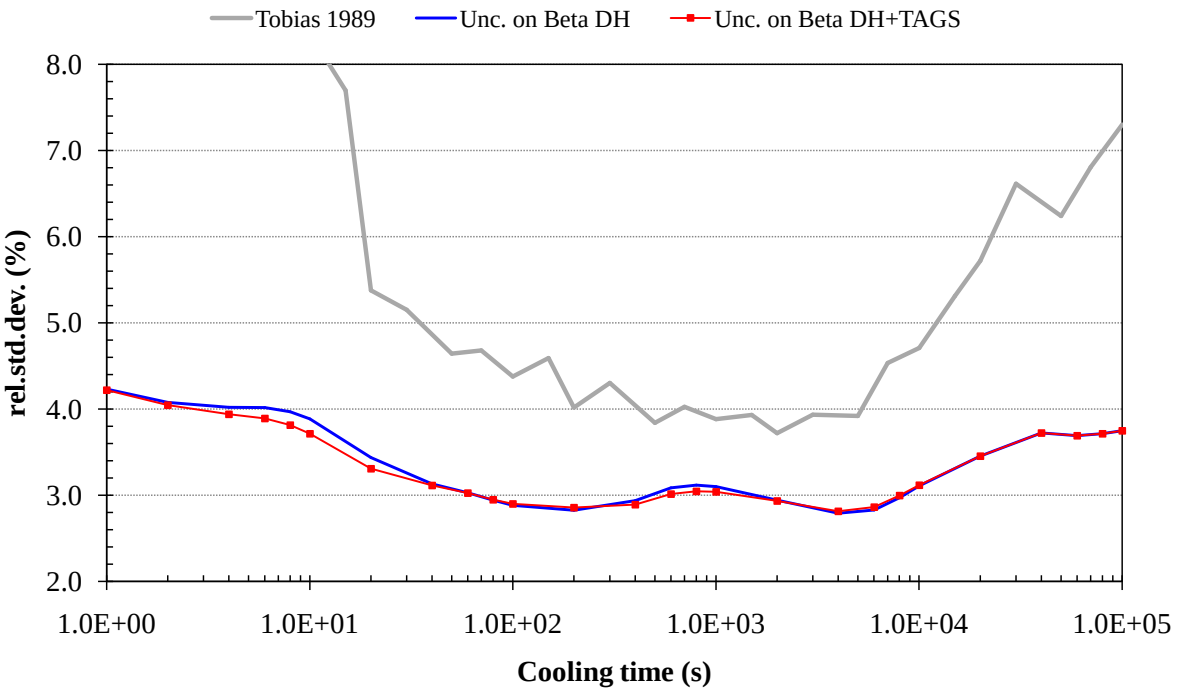

FIGURE 6.24: Beta FPDH uncertainty for the ^{239}Pu thermal fission, obtained with JEFF-3.1.1 by adding or not the new TAGS data, compared with Tobias' experimental uncertainty data.

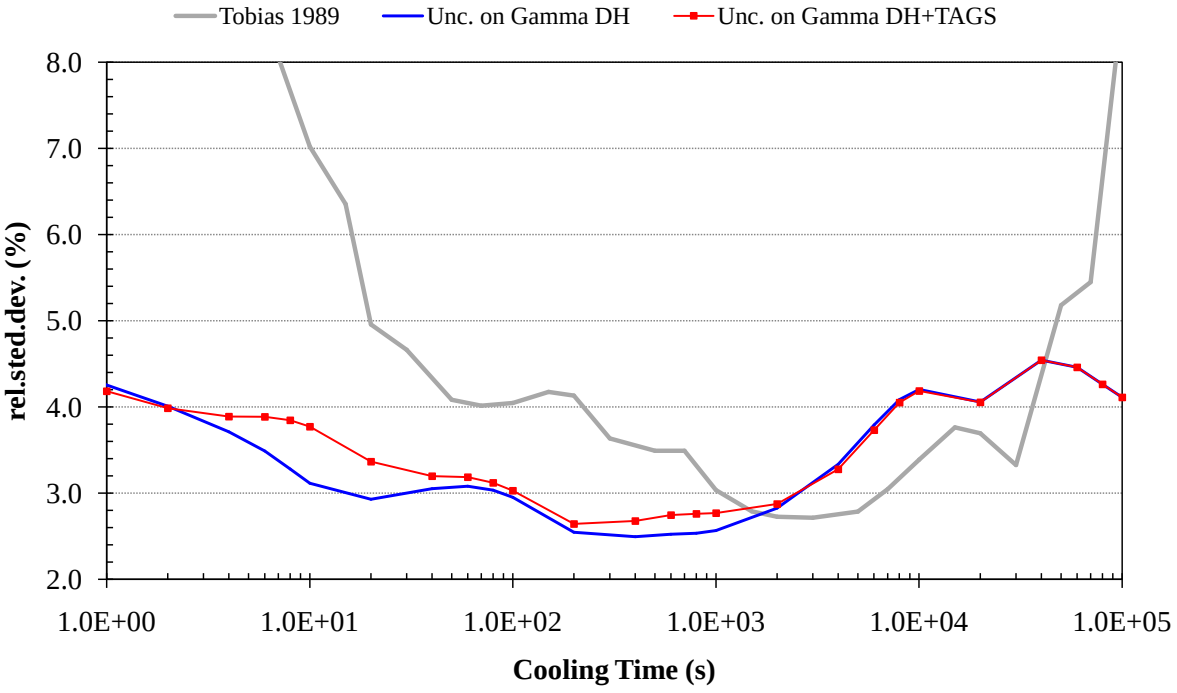

FIGURE 6.25: Gamma FPDH uncertainty for the ^{239}Pu thermal fission, obtained with JEFF-3.1.1 by adding or not the new TAGS data, compared with Tobias' experimental uncertainty data.

6.1.4.8 Comparison with ENDF/B-VII.1 results

Calculations for the ^{239}Pu thermal FPDH with the ENDF/B-VII.1 library are carried out in order to compare with the JEFF-3.1.1 results. Then, the uncertainty propagation on total FPDH is repeated with ENDF/B-VII.1. The uncertainty sources, decay data (half-life and decay energy values) and fission yield data, are propagated, first all at the same time, and after, individually, as done before with JEFF-3.1.1. The results are presented in Figs. 6.26 and 6.27.

Fig. 6.26 shows the total FPDH resulting from both libraries, ENDF/B-VII.1 and JEFF-3.1.1, and the experimental data from Tobias [Tobias, 1980, Tobias, 1989] and other measurements [Dickens et al., 1981, Akiyama et al., 1982b, Akiyama et al., 1982a] [Schier and Couchell, 1997] used in ENDF/B-VII.1 evaluations. ENDF/B-VII.1 results are in good agreement with all the experimental data mentioned above, except for Lowell's data [Schier and Couchell, 1997]. JEFF-3.1.1 results fail to simulate such data as well. However, these experimental data have large discrepancies with the rest, so they seem not to be reliable. For short cooling times (below 20 s), simulations with JEFF-3.1.1 and ENDF/B-VII.1 reproduce better other experimental data than Tobias' ones.In addition, calculations performed with the ORIGEN-S depletion code [Gauld et al., 2010] by ORNL are also shown, observing a good agreement between ACAB and ORIGEN-S calculations.

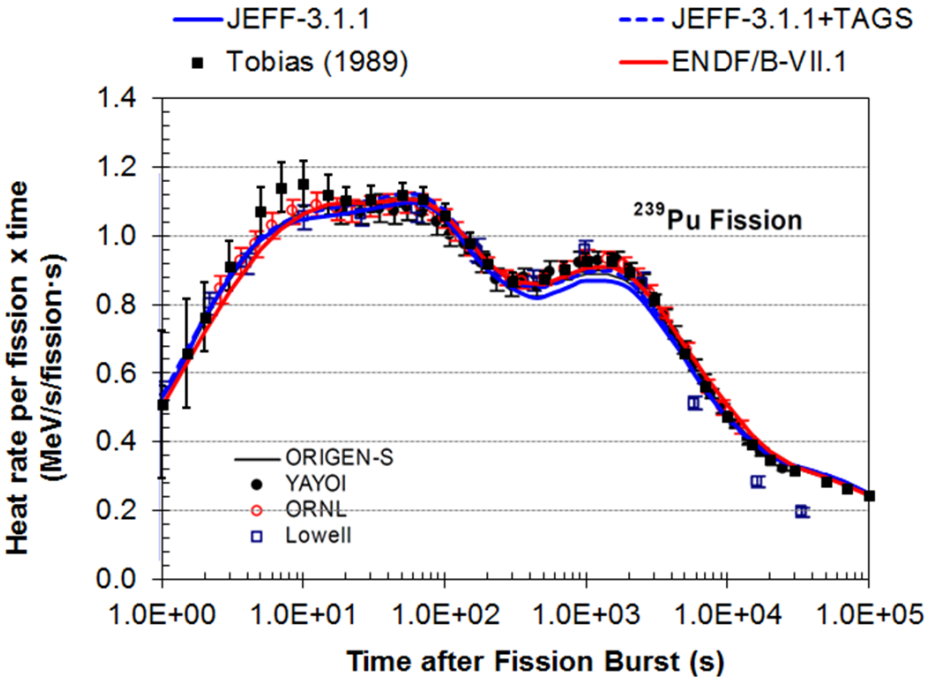

FIGURE 6.26: Comparison of simulated total FPDH for the ^{239}Pu thermal fission with different experimental data, Simulations performed with ACAB using JEFF-3.1.1 (with/without new TAGS data [Algora et al., 2010]) and ENDF/B-VII.1. Results from ORIGEN-S with ENDF/B-VII.1 are also presented. (From [Cabellos et al., 2013])

When decay energy uncertainties are propagated, the same assumption is taken into account as done before for the previous calculations: decay energies without uncertainty values, or zero values, are assumed to have an uncertainty as provided in Table 6.2. As shown before in Fig. 6.6, the contribution of those nuclides can account up to 15% of total FPDH for cooling times smaller than 2000 s.

The uncertainty propagation results are presented in Fig. 6.27. The ENDF/B-VII.1 calculations have been carried out with the Hybrid Method, as done before for JEFF-3.1.1. The performances of both libraries are plotted there, showing the uncertainty due to every source when treated individually and when all are propagated together at the same time. Similar results are obtained with both libraries for decay energy and decay constant uncertainties. However, large differences are found for fission yield uncertainties. ENDF/B-VII.1 provokes a final uncertainty larger than with JEFF-3.1.1 throughout the whole cooling time. In spite of that fact, both libraries present that fission yield uncertainties are the most relevant contributors.

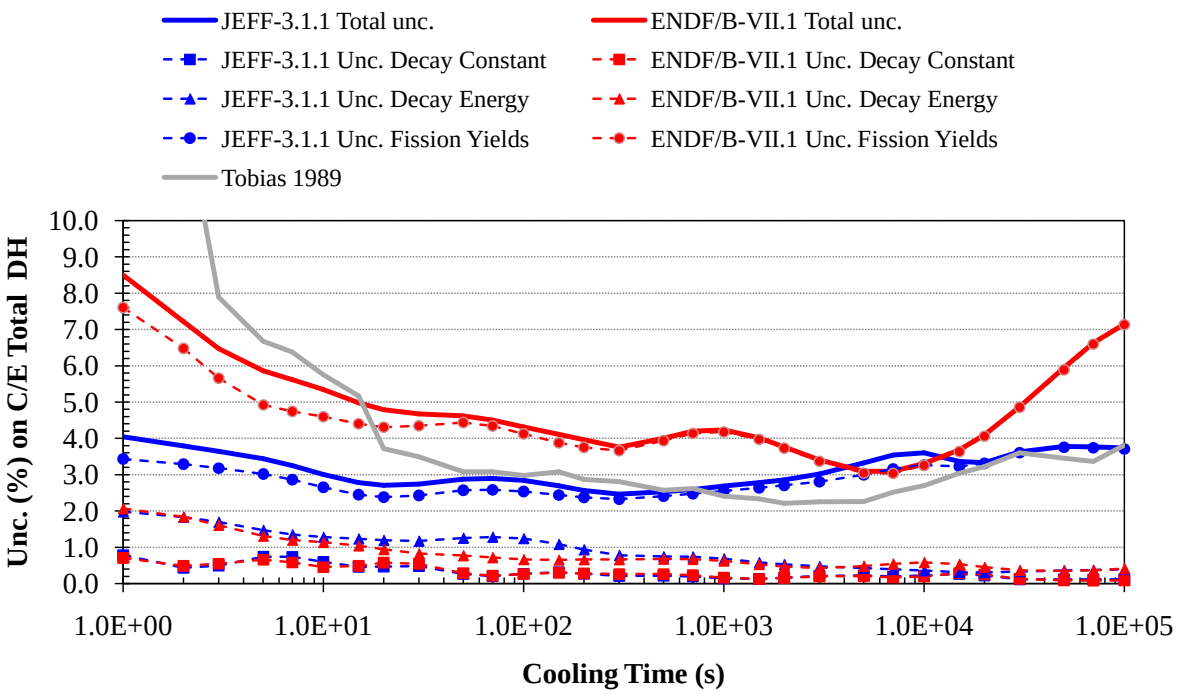

FIGURE 6.27: Uncertainties in the ^{239}Pu total FPDH due to all nuclear data uncertainty sources, propagated together and individually, using the ENDF/B-VII.1 and JEFF-3.1.1. They are compared with experimental uncertainties [Tobias, 1980, Tobias, 1989].

In Table 6.4, a list of the most important contributors at 1000 s after the fission burst is shown. Nuclides measured in [Algora et al., 2010] are marked with ^{a}. Same contributors are observed with ENDF/B-VII.1 and JEFF-3.1.1, although the order differs. The use of new TAGS data in ENDF/B-VII.1, and not in JEFF-3.1.1 is the origin of such a difference.

TABLE 6.4: List of the major contributors to Total FPDH for ^{239}Pu thermal fission after 1000 s from the fission burst. Nuclides measured in [Algora et al., 2010] are marked with *a*.

JEFF-3.1.1	(%)	ENDF/B-VII.1	(%)
Total: 0.87 MeV/fission		Total: 0.91 MeV/fission	
^{104}Tc^{a}	8.6	^{104}Tc^{a}	9.9
^{95}Y	5.3	^{105}Tc^{a}	5.7
^{102}Tc^{a}	5.2	^{95}Y	5.1
^{101}Mo	5.1	^{102}Tc^{a}	5.1
^{139}Cs	4.9	^{101}Mo	4.7
^{105}Tc^{a}	4.6	^{139}Cs	4.4

6.1.5 ^{235}U thermal FPDH

After addressing the ^{239}Pu FPDH, here a UQ study on the ^{235}U FPDH calculation induced by thermal neutrons is performed using ENDF/B-VII.1 and JEFF-3.1.2. that the fission yield and decay data in JEFF-3.1.2 is identical to that in JEFF-3.1.1. In spite of the propagation of all possible nuclear data uncertainty sources as done for the ^{239}Pu FPDH, only Fission Yield (FY) uncertainties are propagated here. Same methodology for propagating uncertainties is used as in the ^{239}Pu FPDH study. More over, the Monte Carlo sampling methodology is also compared with the First Order Perturbation Theory – Propagation of moments, and the impact of the covariance matrices generated for IFYs in Chapter 5 is analysed.

The list of performed calculations is presented in the following. All the simulated values have been compared again with Tobias' compiled data [Tobias, 1980, Tobias, 1989].

Calculations using the ENDF/B-VII.1 library:

I Total FPDH calculation using only best-estimated values (ENDF/B-VII.1).

II Total FPDH calculation with variance matrix without correlations (ENDF/B-VII.1 + no corr.).

III Total FPDH calculation with the correlation matrix generated with Bayesian/GLS method and mass chain yield information (ENDF/B-VII.1 + COV(MFY)).

Calculations using the JEFF-3.1.2 library:

V Total FPDH calculation using only best-estimated values (JEFF-3.1.2).

VI Total FPDH calculation with variance matrix without correlations (JEFF-3.1.2 + no corr.).

VII Total FPDH calculation with correlation matrix generated with Bayesian/GLS method and mass chain yield information (JEFF-3.1.2 + COV(MFY)).

VIII Total FPDH calculation with correlation matrix generated with Bayesian/GLS method and cumulative yield information (JEFF-3.1.2 + COV(CFY)).

Reference FPDH results obtained with calculations I (blue lines) and V (red lines) in Fig. 6.28 (top) approach Tobias' compiled data (black) along the whole decay process. Fig. 6.28 (bottom) shows the ratio of calculated to experimental values (C/E), with Tobias' experimental

uncertainty bars reported in black. Both libraries, JEFF-3.1.2 and ENDF/B-VII.1, underestimate the decay heat for times shorter than 2000 seconds. The ENDF/B-VII.1 decay library has been extended including new TAGS experimental data [Algora et al., 2010], improving the accuracy of the calculations for ^{235}U and ^{239}Pu FPDH thermal fission [Chadwick et al., 2011], as seen here and previously for the ^{239}Pu thermal FPDH when such data are included. However, here JEFF-3.1.2 does not included such new TAGS data.

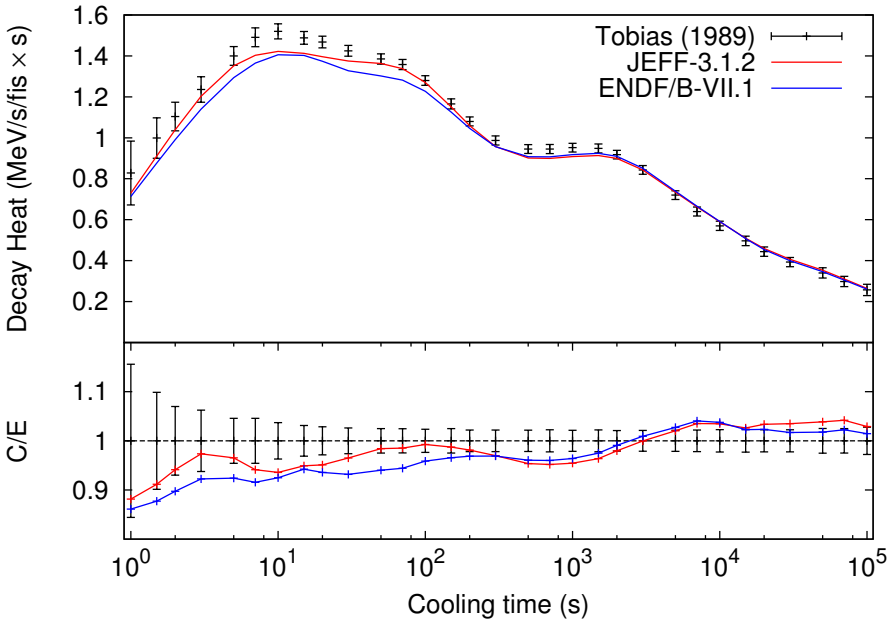

FIGURE 6.28: Thermal neutron induced FPDH calculations with ENDF/B-VII.1 and JEFF-3.1.2 for ^{235}U (top) and C/E ratio with experimental uncertainty bars (bottom).

6.1.5.1 Results with ENDF/B-VII.1 uncertainties

Uncertainties in the thermal FPDH of ^{235}U, measured as relative standard deviations (%), due to ENDF/B-VII.1 uncertainties are presented in Fig. 6.29 as a function of cooling time. The uncertainties presented are the ones from the calculations II and III. Again, they are compared with the experimental uncertainty coming from Tobias' work.

For calculation II, the IFY uncertainties stored in the library have been taken as the diagonal coefficients of the IFY covariance matrix. While for calculation III, the covariance matrix generated with the introduction of the evaluated chain yield information from [England and Rider, 1994] is used, shown such a matrix in Fig. 5.1. The full covariance matrix for IFYs contributes to strongly reduce the uncertainty on decay heat. The small updated uncertainties of IFYs, as seen in Chapter 5, inevitably contribute to reduce the uncertainty on decay heat. However, reduced IFY variances are not the only contributors to this effect.

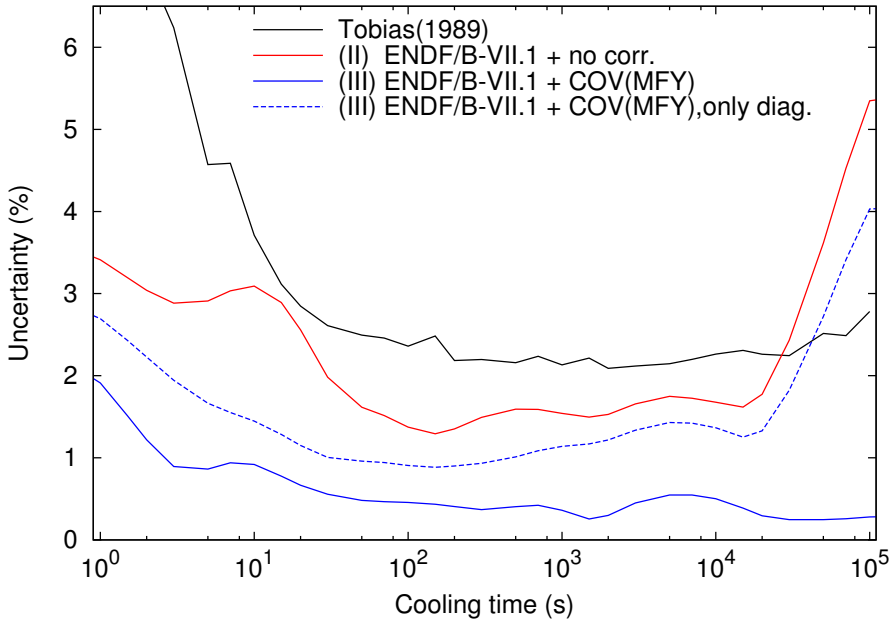

FIGURE 6.29: Uncertainty (%) of thermal FPDH for ^{235}U calculated with ENDF/B-VII.1

An additional calculation is presented in Fig. 6.29. It has been obtained using only the diagonal terms of the covariance matrix generated for calculation III. Its objective is to present the effect of neglecting off-diagonal terms that have appeared after including chain yield information. As a result, a larger final uncertainty is reached if compared with when the full covariance matrix is used. However, less uncertainty is obtained than in calculation II as a results of reducing the values of the diagonal terms. Then, the importance of correlations between IFYs is highlighted, and they should be always considered.

6.1.5.2 Results with JEFF-3.1.2 uncertainties

Results obtained with the JEFF-3.1.2 data library are reported in Fig. 6.30. Uncertainties, in the form of relative standard deviations, are plotted as a function of the decay/cooling time and compared with Tobias' experimental uncertainties (black line).

The red curve is calculated using non-correlated fission yields (VI). The green curve corresponds to calculation VII, where information on evaluated mass fission yields [IAEA, 1974] is introduced. The blue solid line shows the results for calculation VIII in which the IFY covariance matrix has been updated with the CFY covariance data.

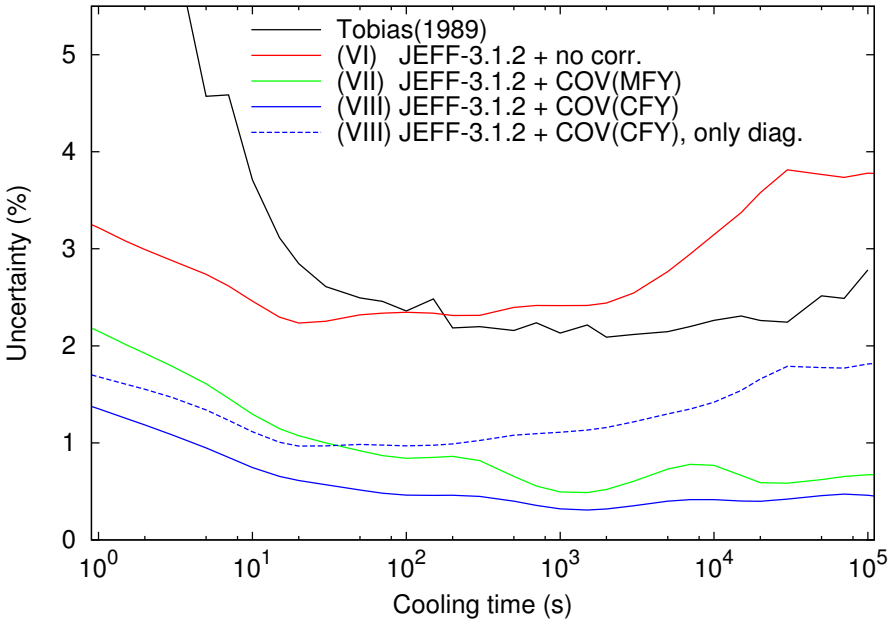

FIGURE 6.30: Uncertainty (%) of thermal FPDH for ^{235}U calculated with JEFF-3.1.2.

For calculation VIII, lower FPDH uncertainty values than those for calculation VII are observed. For the same reasons already explained in Chapter 5, the calculated covariance matrices introduce high negative correlations that affect the outcomes significantly as the variance on decay heat is strongly reduced. Part of this effect is lost when computing FPDH uncertainty by keeping only the variance (diagonal) data, as shown when the extra calculation (only diag., blue dashed line) in Fig. 6.30 is compared with the outcome uncertainty for calculation VII. Therefore, it is important to include such IFY correlations in UQ studies for FPDH problems.

6.1.5.3 Comparison between Monte Carlo sampling and First Order Perturbation

To complete the study, a further perturbation analysis is performed. All the calculations done with Monte Carlo sampling using the JEFF-3.1.2 library are recalculated again, but this time using a linear perturbation technique. For every IFY involved in the problem, a FPDH simulation is performed introducing a perturbation on the same yield. With perturbed calculations, sensitivity coefficients are calculated. Then, they are used in conjunction with the same covariance data used before in the moment propagation equation, Eq. 3.8, to get the variance on the decay heat response. That leads to a comparison of methodologies: Monte Carlo sampling and First Order Perturbation.

Results for JEFF-3.1.2, plotted in Fig. 6.31, show that linear perturbation (PERT) and Monte Carlo sampling (MC) account for the same effects on the decay heat uncertainty. The linearity of the problem and the small perturbations allow the perturbation technique to perform as well as Monte Carlo sampling, even though it is presumable that the introduction of higher perturbations in the same system, combined with non-linear effects, will highlight the superiority of the latter for uncertainty propagation problems.

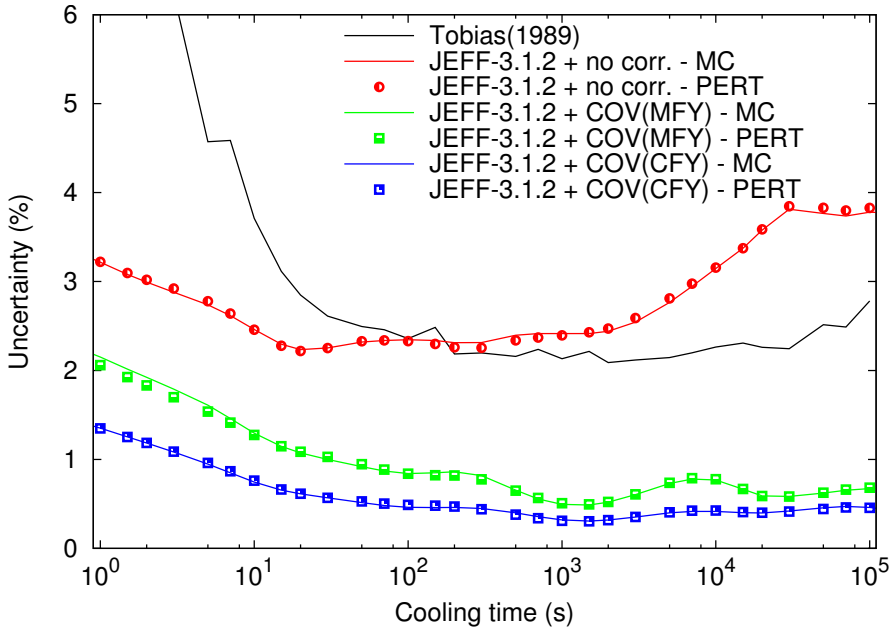

FIGURE 6.31: Comparison of thermal FPDH uncertainties for ^{235}U obtained using Monte Carlo sampling (MC) and linear perturbation (PERT) with JEFF-3.1.2.

6.1.5.4 Comparison between libraries

Fig. 6.32 plots the uncertainties of total FPDH for non-correlated IFY uncertainties (red) from JEFF-3.1.2 (dashed) and ENDF/B-VII.1 (solid). Blue solid and dashed lines are the results obtained for calculations III and VII, respectively. Results obtained with ENDF/B-VII.1 data have lower uncertainties than those calculated with JEFF-3.1.2. This can be inferred from the low uncertainties provided by ENDF/B-VII.1 to those nuclides with high IFY (Fig. 2.4), as stated in Chapter 2, Sec. 2.5.3.

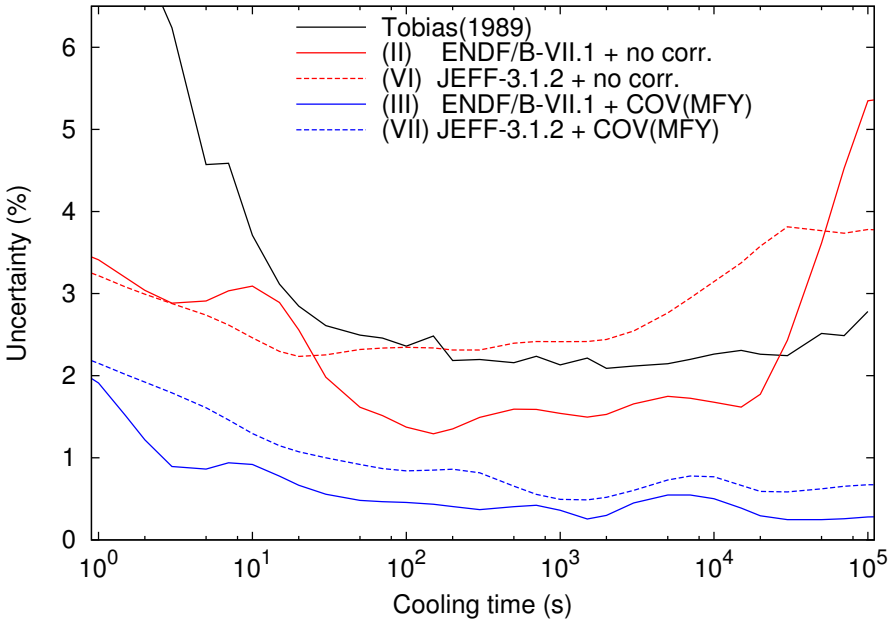

FIGURE 6.32: Comparison of uncertainties in thermal FPDH for ^{235}U calculated with both JEFF-3.1.2 and ENDF/B-VII.1.

A sorted list of 39 nuclides, with their sensitivity coefficients (%/%) calculated with JEFF-3.1.2, is presented in Table 6.5 for whose IFYs contribute the most to thermal FPDH calculations of ^{235}U at any decay time. If these results are compared with the ones in [Katakura, 2013], a perfect agreement is observed. As expected, most of the nuclides with the largest sensitivities to FPDH in terms of IFYs belong to the peaks of the thermal fission yield distribution (see Fig. 2.4). The temporal evolution of the effect of each FY to FPDH can be followed in this table.

TABLE 6.5: List of the 39 most important nuclides, with their sensitivity coefficients as (%/%), to the total FPDH of ^{235}U thermal fission. Sensitivity coefficients values below 10^{-2} are not presented, while the rest are multiplied by 10^2.

	Decay time (s)					
Nuclide	10^0	10^1	10^2	10^3	10^4	10^5
^{88}Br	-	1.58	-	-	4.43	-
^{88}Kr	-	-	-	-	5.16	-
^{89}Kr	-	-	2.20	5.66	-	-
^{90}Kr	-	1.71	6.82	1.94	-	-
^{91}Kr	1.30	3.76	4.49	-	1.52	5.85
^{92}Kr	2.88	3.55	-	-	2.95	1.08
^{92}Rb	2.41	3.08	-	-	4.35	1.60
^{93}Rb	2.09	3.73	1.02	3.59	1.09	4.18
Sensitivity coefficients multiplied by 10^2						

Continued on next page

Table 6.5 – continued from previous page

	Decay time (s)					
Nuclide	10^0	10^1	10^2	10^3	10^4	10^5
^{95}Rb	1.51	-	-	-	-	-
^{94}Sr	-	-	3.41	4.78	-	-
^{95}Sr	-	2.65	3.07	4.94	-	-
^{96}Sr	6.21	3.99	-	-	-	-
^{97}Sr	5.15	1.33	-	-	-	6.42
^{97m}Y	4.20	-	-	-	-	8.09
^{97n}Y	1.33	-	-	-	-	2.17
^{98m}Y	4.06	1.62	1.30	-	-	-
^{99}Y	3.34	1.61	-	-	-	-
^{99}Zr	3.07	1.94	-	-	-	2.21
^{100}Zr	1.66	6.97	-	-	-	-
^{101}Zr	2.84	3.11	-	3.27	-	-
^{102}Zr	2.03	2.86	-	1.73	-	-
^{132}Sb	-	-	-	-	-	2.86
^{132m}Sb	-	-	-	-	-	2.11
^{133}Sb	-	-	1.58	2.24	-	3.42
^{132}Te	-	-	-	-	-	3.77
^{133m}Te	-	-	-	1.26	3.57	4.29
^{134}Te	-	-	-	2.51	18.44	-
^{135}Te	-	1.85	-	-	2.94	8.45
^{136}Te	-	1.39	3.38	-	-	-
^{135}I	-	-	-	-	2.04	5.84
^{138}I	-	1.46	-	1.77	1.50	-
^{138}Xe	-	-	-	6.62	5.68	-
^{139}Xe	-	1.60	4.37	4.25	2.85	-
^{140}Xe	-	2.61	5.24	-	-	1.36
^{140}Cs	-	-	2.21	-	-	-
^{142}Cs	3.21	-	-	2.04	5.08	-
^{142}Ba	-	-	-	2.42	6.02	-
^{143}Ba	-	2.12	-	2.70	-	3.62
^{144}Ba	-	2.52	5.84	-	-	-

Sensitivity coefficients multiplied by 10^2

6.1.6 Conclusions of FPDH calculations

The results of ^{239}Pu FPDH shows that the contribution to the decay heat of the isotopes without decay energy uncertainties could go up to a 15% of the contribution. However, they

are only of relevance for cooling time periods smaller than 2×10^3 s. When difference sources of uncertainties are compared, FY uncertainties are the most relevant, followed first by the decay energy uncertainties, and then by decay constants and branching ratios. This could change if a different assumption is made for the uncertainty values suggested for those isotopes which has no uncertainty for their decay energies, as seen if compared with [Katakura, 2013] where decay energy uncertainties become the most important contributor. When the gamma and beta contributions of the FPDH are analysed, same results are extracted concerning the relevance of the uncertainty sources. The analysis of isotope contributors reveals that their results can be affected by the uncertainty suggested for such isotopes without a given uncertainty in JEFF-3.1.2. The comparison against experimental data shows that beta contribution is overestimated, while gamma one is underestimated. However, this could be improved with the inclusion of new TAGS experimental data, as provided in [Algora et al., 2010], in JEFF-3.1.2. The JEFF-3.1.2 results are compared with the ENDF/B-VII.1 ones, showing that a better agreement with experimental data is obtained for decay times above 10 s with ENDF/B-VII.1. However, the final uncertainty obtained with ENDF/B-VII.1 is always larger than the obtained with JEFF-3.1.2. Although, the importance of the uncertainty sources for ENDF/B-VII.1 is the same as for JEFF-3.1.2.

The UQ study on the ^{235}U FPDH reveals the importance of providing full covariance matrix for FY data. If no correlations among FY are assumed, large uncertainty values are obtained if compared with the cases where full covariance matrix are used. In any of the studied cases, the uncertainties on IFY are reduced when uncertainty data from CFY or Mass FY (MFY) are taken into account with a Bayesian/GLS updating scheme. However, the amount of uncertainty that is subtracted from the diagonal terms is converted into correlations. The effect of using solely the new diagonal values is compared against the usage of the full covariance, showing that the effect of the generated correlations (negative always) is to reduce even further the final uncertainty. In addition, the comparison of Monte Carlo sampling and linear perturbation shows that both approaches provide the same results. Then, it is proved that the latter can be also applied without any drawback when only one source of uncertainty is applied for this kind of problem, and the uncertainties considered are rather small. Moreover, thanks to the sensitivity analysis, the most important contributors to the final uncertainty at any decay time of interest can be studied. The performance comparison between JEFF-3.1.2 and ENDF/B-VII.1 shows that ENDF/B-VII.1 induces smaller uncertainties than JEFF-3.1.2, even after updating IFY with Mass FYs.

6.2 UQ study on the European Facility for Industrial Transmutation fuel cycle

UQ studies are performed on the European Facility for Industrial Transmutation (EFIT) fuel cycle, analysing uncertainties on the isotopic composition and two derived magnitudes: decay heat and radiotoxicity. Also, this calculation serves as a framework for comparing two different UQ methods performed later: Total Monte Carlo and the Hybrid Method, applying both only to depletion calculations.

6.2.1 Description of EFIT fuel cycle depletion calculations

The basic characteristics of the industrial-scale transmutation facility EFIT [Artioli, 2006, Álvarez-Velarde et al., 2009] are:

- core cooled by pure lead,
- 400 MW of thermal power,
- initial total mass of actinides 2.074 tones (21.7%MA).

Two burn-up discharges are studied here, 150 GWd/THM (equivalent to 778 days of irradiation) and 500 GWd/THM (3250 days of irradiation).

The composition of actinides in the EFIT fuel is given in Table 6.6, being the main transuranic isotopes loaded in fuel ^{238}Pu, ^{239}Pu, ^{240}Pu, ^{241}Pu, ^{242}Pu, ^{241}Am, ^{243}Am and ^{244}Cm.

The EFIT fuel cycle is studied through a depletion calculation of a representative pin-cell of the core in one burn-up step. That means, a constant neutron environment representative of the equilibrium cycle is assumed for all the irradiation period, with an average energy spectrum of 0.375 MeV and a flux intensity of 3.12×10^{15} n/cm^2s for the 150 GWd/THM burn-up case. The assumed neutron flux and spectrum, presented in Fig. 6.33, have been taken from fully detailed 3D burn-up calculations performed with the EVOLCODE2 code [Álvarez-Velarde et al., 2007], and correspond to a representative cell in the inner part of the core at mid-burn-up after 400 days. For 500 GWd/THM, the same neutron flux and spectrum are taken, because of the study of fuel multi-recycling in the same reactor. Such a process is characterised for having the same neutron flux since the initial isotopic fuel composition

is the same for each equilibrium cycle. Then, the thermal power will decrease and the fissile isotope inventory will be also largely reduced.

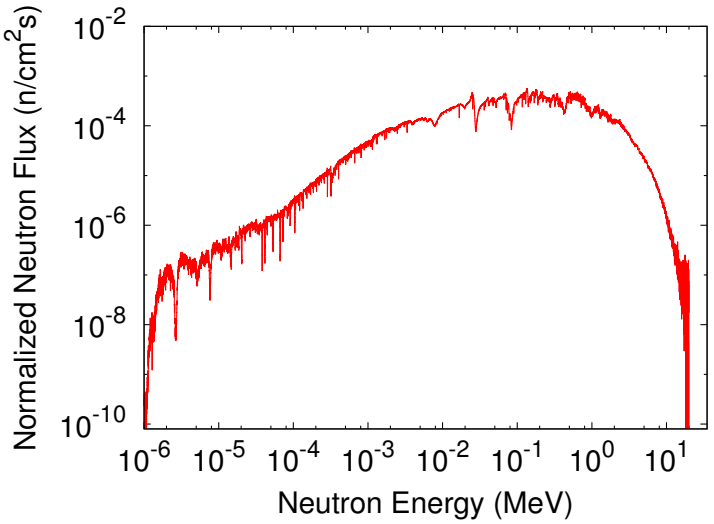

FIGURE 6.33: The EFIT neutron spectrum corresponding to a representative cell in the inner part of the core at mid-burn-up, i.e. after 400 days of irradiation.

Both depletion calculations, 150 GWd/THM and 500 GWd/THM, are addressed with ACAB, with the following details:

- For 150 GWd/THM: There are 30 time steps for depletion and 30 time steps for cooling. The depletion period starts at 1 second and ends after 778 days (6.721920×10^7 s), and the cooling period starts 10^{-3} seconds after shutdown and ends after 10^6 years.
- For 500 GWd/THM: There are 40 time steps for depletion and 30 time steps for cooling. The depletion period starts at 1 second and ends after 3250 days, and for the cooling is the same as for 150 GWd/THM.

With this information, the ACAB input files can be written, showing the one for 150 GWd/THM in Fig. 6.34 and for 500 GWd/THM in Fig. 6.35. In these inputs, the isotope composition is omitted, because they have been already presented. For preparing cross section and fission yield files and their uncertainties, the neutron spectrum given in Fig. 6.33 is used for collapsing.

```
Caso EFIT
<Block #1, card #2
 0 IUNC
   3849  900000  0  1  1  0  2  2  0 24  1  0  4  1  1  0  1  0  0  1  0
   1.000000E+00    1.0E+00
  1
       104
  2.00E+01  1.40E+01  1.20E+01  1.00E+01  8.00E+00  6.50E+00  5.00E+00  4.00E+00
  3.00E+00  2.50E+00  2.00E+00  1.70E+00  1.40E+00  1.20E+00  1.00E+00  8.00E-01
  6.00E-01  4.00E-01  3.00E-01  2.00E-01  1.00E-01  5.00E-02  2.00E-02  1.00E-02
  0.00E+00
  0.00E+00  0.00E+00  0.00E+00  0.00E+00  0.00E+00  0.00E+00
  1  0  0  1  0  0  1  0  0  1  0  0  0  0  0  0  0  0
 3.11972E+15
< No hay Restart
          0
< Isotopia
80160
120240
120250
120260
370850

......

2.6707E+02
7.8158E+01
5.1960E+01
1.1172E+01
8.3339E+00
< 1 otro bloque
  10 10   1 0   1 0   0 0
  1.000E+00 2.000E+00 4.000E+00 8.000E+00 1.600E+01
  3.200E+01 6.400E+01 1.280E+02 2.560E+02 5.120E+02
< 2 otro bloque
   10 10   1 10  1 0  0 0
  1.024E+03 2.048E+03 4.096E+03 8.192E+03 1.638E+04
  3.277E+04 6.554E+04 1.311E+05 2.621E+05 5.243E+05
< 3 otro bloque
   10 10   1 10  1 0  0 0
  1.0490E+06 2.097E+06 4.194E+06 8.389E+06 1.678E+07
  3.1536E+07 3.456E+07 4.32E+07  5.0E+07   6.721920E+07
< Bloque. DECAY
    0  10   1  10  1 0   0 0
    1.00E-03     1.00E+00    6.00E+01    3.60E+03    8.64E+04
    6.04800E+05  2.592000E+06 7.776000E+06 1.555200E+07 2.332800E+07
< Bloque. DECAY
    0  10   1  10  5 0   0 0
    1.00E+00     2.00E+00    5.00E+00    1.00E+01    2.00E+01
    4.00E+01     6.00E+01    8.00E+01    1.00E+02    1.20E+02
< Bloque. DECAY
    0  10   0  10  5 0   0 0
    2.00E+02     3.00E+02    5.00E+02    1.00E+03    5.00E+03
    1.00E+04     5.00E+04    1.00E+05    5.00E+05    1.00E+06
  1.0000000E-25   1.000000
<Block #10 Fission product inventory
 1 1 0               IGFP IWFYD IFORT96
 1 0 0 0 0 1 0 0 0 0   IWP(1) IMTX(2) IWDR(3) IDOSE(4) IPHCUT(5) IDHEAT(6)
IOFFSD(7) IDCEDE(8) INEMISS(9) IDAMGE(10)
 0 0 6 0   NOPUL  NTSEQ  NOTTS   NVFL
           0 NMULT
           0          1 NCYO IFSO
           1  1  1  1  1  1 (ITSO(I),I=1,NOTTS)
```

FIGURE 6.34: ACAB input file for the EFIT calculation with a burn-up of 150 GWd/THM.

```
Caso EFIT 500 GWd/tHM
<Block #1, card #2
 0 IUNC
   3849  900000  0  1  1  0  2  2  0 24  1  0  4  1  1  0  1  0  0  1  0
   1.000000E+00    1.0E+00
  1
        104
  2.00E+01  1.40E+01  1.20E+01  1.00E+01  8.00E+00  6.50E+00  5.00E+00
4.00E+00
  3.00E+00  2.50E+00  2.00E+00  1.70E+00  1.40E+00  1.20E+00  1.00E+00
8.00E-01
  6.00E-01  4.00E-01  3.00E-01  2.00E-01  1.00E-01  5.00E-02  2.00E-02
1.00E-02
  0.00E+00
  0.00E+00  0.00E+00  0.00E+00  0.00E+00  0.00E+00  0.00E+00
  1  0  0  1  0  0  1  0  0  1  0  0  0  0  0  0  0  0
 3.11972E+15
< No hay Restart
          0
< Isotopia
80160
120240

...

2.9024E+00
9.9412E-01
< 1 otro bloque
  10 10   1 0   1 0   0 0
  1.000E+00 2.000E+00 4.000E+00 8.000E+00 1.600E+01
  3.200E+01 6.400E+01 1.280E+02 2.560E+02 5.120E+02
< 2 otro bloque
   10 10   1 10  1 0  0 0
  1.024E+03 2.048E+03 4.096E+03 8.192E+03 1.638E+04
  3.277E+04 6.554E+04 1.311E+05 2.621E+05 5.243E+05
< 3 otro bloque
   10 10   1 10  1 0  0 0
  1.0490E+06 2.097E+06 4.194E+06 8.389E+06 1.678E+07
  3.1536E+07 3.456E+07 4.32E+07  5.0E+07   6.721920E+07
< 4 otro bloque.
   10 10   1  10  4 0   0 0
  1.0E+03 1.25E+03 1.50E+03 1.750E+03  2.0E+03
  2.25E+03 2.50E+3  2.75E+03 3.0E+03  3.250E+03
< 5 Bloque. DECAY
   0  10   1  10  1 0   0 0
    1.00E-03     1.00E+00    6.00E+01    3.60E+03    8.64E+04
    6.04800E+05  2.592000E+06 7.776000E+06 1.555200E+07 2.332800E+07
< 6 Bloque. DECAY
    0  10   1  10  5 0   0 0
    1.00E+00     2.00E+00    5.00E+00    1.00E+01    2.00E+01
    4.00E+01     6.00E+01    8.00E+01    1.00E+02    1.20E+02
< 7 Bloque. DECAY
    0  10   0  10  5 0   0 0
    2.00E+02     3.00E+02    5.00E+02    1.00E+03    5.00E+03
    1.00E+04     5.00E+04    1.00E+05    5.00E+05    1.00E+06
  1.0000000E-25   1.000000
<Block #10 Fission product inventory
 1 1 0              IGFP IWFYD IFORT96
 1 0 0 0 0 1 0 0 0 0   IWP(1) IMTX(2) IWDR(3) IDOSE(4) IPHCUT(5) IDHEAT(6)
IOFFSD(7) IDCEDE(8) INEMISS(9) IDAMGE(10)
 0 0 7 0   NOPUL  NTSEQ  NOTTS   NVFL
           0 NMULT
           0          1 NCYO IFSO
           1  1  1  1  1  1  1 (ITSO(I),I=1,NOTTS)
```

FIGURE 6.35: ACAB input file for the EFIT calculation with a burn-up of 500 GWd/THM.

6.2.2 UQ study on isotopic composition

Uncertainties on isotopic composition due to cross section, fission yield and decay data were calculated in [Cabellos et al., 2011b], using the Hybrid Method. The sources of uncertainties were: EAF-2007 for cross section data, and JEFF-3.1.1 for fission yield and decay data. Only the burn-up case of 150 GWd/THM was studied, addressing uncertainties on concentrations of light isotopes, actinides and fission products designated as the most relevant either due to transmutation or due to their importance on the response functions (e.g. decay heat, neutron emission, public dose), or both. The results of such a UQ study are presented in Table 6.6 for uranic and transuranic isotopes, and in Table 6.7 for fission products. Initial composition and nominal variation (without uncertainties) of actinide concentrations at the end of irradiation are shown, while for fission product concentrations only the final concentration. Uncertainty values always refer to concentrations at the end of burn-up.

Decay data uncertainties (λ) have a negligible effect on the isotopic prediction for both actinides and fission products, except for ^{126}Sb and ^{151}Eu. For ^{151}Eu, its uncertainty comes from the 6.67% uncertainty on the ^{151}Sm decay constant, because the decay of ^{151}Sm is the main production source of ^{151}Eu. However, the removal of ^{151}Sm is governed by cross sections not by decay, so that, its decay uncertainty has no effect on its concentration uncertainty. The uncertainty in ^{126}Sb is due to the uncertainty of 28.6% for ^{126m}Sb branching ratio which leads to ^{126}Sb, and because ^{126m}Sb has a slightly higher fission yield value than ^{126}Sb.

Uncertainties of the rest of fission products due to fission yields (γ) remain below 10%, while larger uncertainties were found due to cross section uncertainties.

Regarding uncertainty data for cross sections, EAF-2007 (σ_{EAF}) seems to be very conservative, because very large uncertainty values are obtained if compared with SCALE6.0 (σ_{SCALE}). In some cases, uncertainties obtained with EAF-2007 can go up to 10 times the uncertainties obtaiend with SCALE6.0.

Results are updated using EAF-2010 uncertainties [Díez et al., 2014b]. Table 6.8 shows those isotopes whose uncertainties have changed because of using EAF-2010 instead of EAF-2007. There, the uncertainties on concentrations at the end of burn-up are shown for each source of uncertainty. In general, the uncertainties on almost every isotope concentration decrease, while those for ^{240}Pu and ^{242}Cm increase.

TABLE 6.6: Uranic and transuranic initial compositions (N_i), nominal variations ($N_f - N_i$) and their uncertainties at the end of burn-up for 150 GWd/THM due to different nuclear sources: decay data (λ), cross sections from EAF-2010 (σ_{EAF}) and cross sections from SCALE6.0 (σ_{SCALE}).

Nuclide	N_i (atoms/cm^3)	$N_f - N_i$ (atoms/cm^3)	Uncertainty (%) due to		
			Decay	Cross sections	
			JEFF-3.1.1	EAF-2007	SCALE6.0
^{232}U	-	4.37E+20	5.2	9.8	1.0
^{233}U	-	1.57E+21	0.1	12.6	14.9
^{234}U	7.67E+25	6.79E+25	0.0	4.6	1.9
^{235}U	1.84E+25	1.83E+25	0.0	13.2	3.0
^{236}U	2.54E+25	2.46E+25	0.0	1.8	2.3
^{237}U	2.33E+18	4.07E+22	0.1	7.9	3.5
^{238}U	1.30E+23	1.27E+23	0.0	1.3	2.2
^{237}Np	2.25E+26	1.39E+26	0.0	6.1	1.4
^{238}Np	6.07E+18	2.40E+23	0.1	7.8	1.8
^{239}Np	2.75E+20	5.67E+20	0.2	16.3	15.9
^{238}Pu	4.26E+26	3.99E+26	0.0	4.3	2.5
^{239}Pu	5.21E+26	3.50E+26	0.0	4.8	1.3
^{240}Pu	1.73E+27	1.44E+27	0.0	1.9	0.3
^{241}Pu	3.13E+26	3.01E+26	0.0	8.3	0.9
^{242}Pu	7.50E+26	6.77E+26	0.0	2.2	0.7
^{244}Pu	1.55E+23	1.83E+23	0.0	4.0	2.2
^{241}Am	3.50E+26	2.25E+26	0.0	7.0	2.0
^{242}Am	3.81E+20	1.31E+23	0.2	8.6	2.6
^{242m}Am	2.96E+25	1.81E+25	0.0	12.8	6.4
^{243}Am	3.14E+26	2.78E+26	0.0	6.1	1.4
^{242}Cm	3.17E+23	2.64E+25	0.1	10.4	3.4
^{243}Cm	3.10E+24	3.64E+24	0.2	23.4	11.7
^{244}Cm	2.67E+26	2.92E+26	0.0	6.2	3.1
^{245}Cm	7.82E+25	7.57E+25	0.0	13.2	9.7
^{246}Cm	5.20E+25	5.19E+25	0.0	7.3	3.5
^{247}Cm	1.12E+25	1.11E+25	0.0	15.7	11.0
^{248}Cm	8.33E+24	8.79E+24	0.0	6.6	4.3
^{249}Bk	-	3.28E+23	1.0	20.2	17.3
^{249}Cf	-	2.72E+23	1.1	20.4	17.9
^{250}Cf	-	8.42E+22	0.4	30.6	24.2
^{251}Cf	-	5.03E+21	0.3	44.0	30.3
^{252}Cf	-	1.03E+20	0.3	56.4	35.6

TABLE 6.7: Fission product concentrations at the end of burn-up for 150 GWd/THM (N_f) with their uncertainties due to different nuclear data sources.

Nuclide	N_f	Uncertainty (%) due to			
		Decay	FYs	Cross sections	
	(atoms/cm^3)	JEFF-3.1.1		EAF-2007	SCALE6.0
^{79}Se	2.25E+23	0.00	5.9	4.3	1.6
^{93m}Nb	1.81E+19	6.19	2.9	3.5	1.3
^{94}Nb	1.39E+20	0.03	5.9	17.6	4.6
^{93}Mo	1.45E+18	0.01	2.7	82.6	1.2
^{103}Rh	5.52E+25	0.00	3.7	5.2	1.7
^{107}Pd	3.52E+25	0.01	4.0	4.9	2.3
^{109}Ag	2.09E+25	0.02	3.9	5.4	2.7
^{126}Sn	2.02E+24	0.00	7.2	4.8	2.1
^{126}Sb	2.90E+21	5.21	9.2	9.0	3.3
^{126m}Sb	4.43E+18	1.05	7.5	16.4	1.9
^{129}I	1.06E+25	0.07	4.1	4.7	2.1
^{149}Sm	9.68E+24	0.00	3.6	6. 8	4.5
^{150}Sm	4.57E+24	0.01	3.0	11.0	7.7
^{151}Sm	5.11E+24	0.05	4.2	10.9	6.7
^{152}Sm	8.94E+24	0.01	3.1	6.6	4.0
^{151}Eu	3.74E+22	6.66	3.8	9.8	6.5
^{153}Eu	3.65E+24	0.01	4.4	14.6	5.2
^{155}Gd	2.87E+23	0.26	7.1	7.8	3.8

TABLE 6.8: Uncertainties on concentrations for those isotopes whose concentration uncertainties have changed because of using EAF-2010 instead of EAF-2007 at the discharge burn-up of 150 GWd/THM for EFIT.

Nuclide	Uncertainty (%) due to				
	Decay	FYs	Cross sections		
	JEFF-3.1.1		EAF-2007	SCALE	EAF-2010
^{235}U	0	-	13.2	3.0	3.6
^{237}Np	0	-	6.1	1.4	3.0
^{240}Pu	0	-	1.9	0.3	3.2
^{241}Pu	0	-	8.3	0.9	2.9
^{241}Am	0	-	7.0	2.0	3.5
^{243}Am	0	-	6.1	1.4	2.7
^{242}Cm	0.1	-	10.4	3.4	14.0
^{243}Cm	0.2	-	23.4	11.7	3.7
^{245}Cm	0	-	13.2	9.7	3.4
^{247}Cm	0	-	15.7	11.0	6.3
^{249}Bk	1	-	20.2	17.3	7.4
^{252}Cf	0.3	-	56.4	35.6	15.4
^{94}Nb	0.03	5.9	17.6	4.6	4.3
^{93}Mo	0.01	2.7	82.6	1.2	35.7
^{126}Sb	5.21	9.2	9.0	3.3	2.9
^{126M}Sb	1.05	7.5	16.4	1.9	6.6
^{150}Sm	0.01	3.0	11.0	7.7	5.2
^{151}Sm	0.05	4.2	10.9	6.7	3.1

6.2.3 UQ study on EFIT decay heat

Once uncertainties on isotopic concentrations are calculated, it is straight forward to assess uncertainties on derived response functions. In this case, the decay heat during cooling time is followed. Then, uncertainties on decay energies are included in the calculations. The sources of uncertainties are JEFF-3.1.1 for fission yield and decay data, and EAF-2007 for cross section data.

Individual uncertainty propagation of the uncertainty sources are performed, as well as the joint calculation with all of them propagated at the same time. In addition, the most important contributors to final uncertainties are studied.

Results for 150 GWd/THM are presented in Fig. 6.36, while for 500 GWd/THM in Fig. 6.37. In these plots, the reference calculation (black solid line) and the mean value (red line with

cross marks) obtained with the Hybrid Method are completely the same. The uncertainties due to all nuclear data uncertainties propagated together (solid blue line), and due to the individual propagation of cross sections (red dashed line), fission yields (pink dashed line) and decay data (green dashed line) are provided.

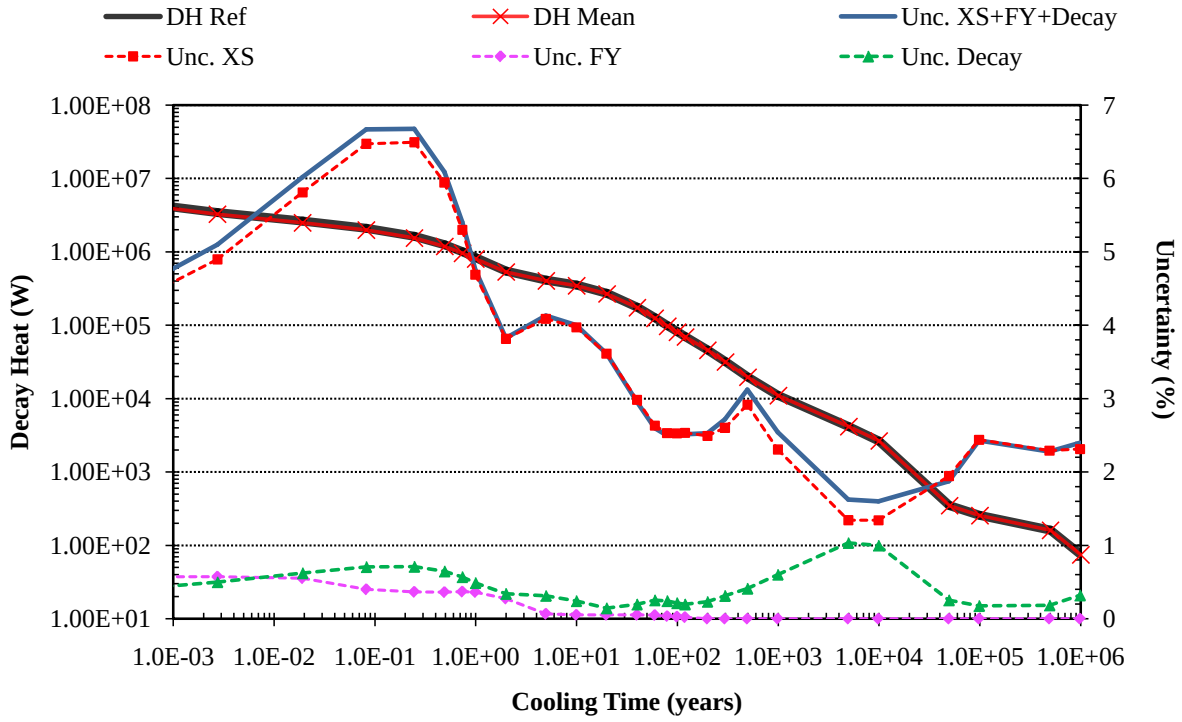

FIGURE 6.36: Decay heat and its uncertainty as a function of cooling time for a EFIT fuel pin-cell burned up to 150 GWd/THM, comparing the reference calculation (DH ref) and the mean value (DH Mean) obtained with the Hybrid Method, and showing the total and individual uncertainty contributions of different nuclear data sources: cross sections (XS), fission yields (FY) and decay data (decay).

For 150 GWd/THM, when all uncertainties are propagated, decay heat uncertainty never exceeds 10%. After 90 days (0.245 years) of cooling time, the decay heat uncertainty reaches its maximum of 6.67%, when the fission products have started to disappear. For 500 GWd/THM, similar trend is observed, reaching the decay heat uncertainty its maximum of 9.83% after 10 years of cooling time. In both cases, the main source of uncertainty is cross section uncertainties. The other two sources, fission yield and decay data uncertainties, are not relevant throughout the cooling time period studied except for the 150 GWd/THM case between 10^3 and 3×10^4 years, when decay data uncertainties become relevant with a similar impact as for cross section uncertainties.

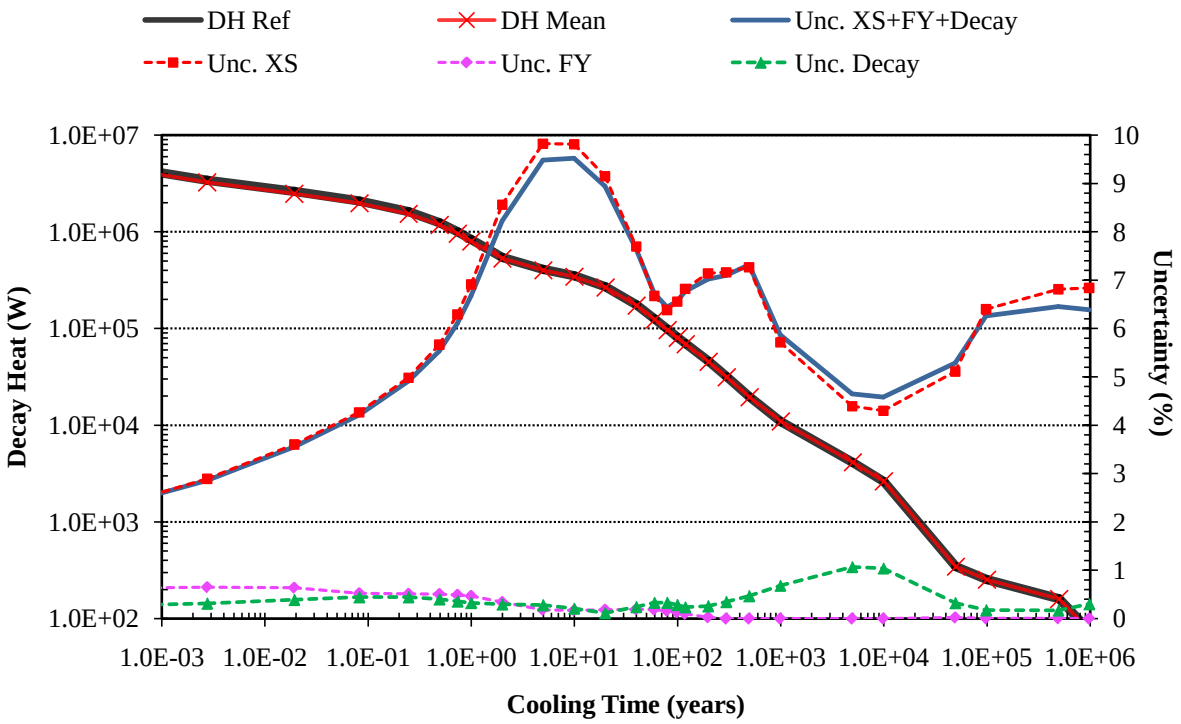

FIGURE 6.37: Decay heat and its uncertainty as a function of cooling time for a EFIT fuel pin-cell burned up to 500 GWd/THM, comparing the reference calculation (DH ref) and the mean value (DH Mean) obtained with the Hybrid Method, and showing the total and individual uncertainty contributions of different nuclear data sources: cross sections (XS), fission yields (FY) and decay data (decay).

Analysis of the main contributors to decay heat uncertainty is carried out, using again the development in Chapter 4, Sec. 4.3.4.1. Presented in Fig. 6.38 for 150 GWd/THM, the most important contributors are in order of appearance: ^{242}Cm, ^{244}Cm, ^{238}Pu, ^{241}Am, ^{240}Pu, ^{239}Pu, ^{214}Po and ^{213}Po. The importance of Po isotopes is really small if compared with the others, because there are a lot of contributors after 10^5 years, and most of them provide small contributions as Po ones.

If the variance of total decay heat is compared against the sum of variances of all the individual contributions ($\sum var(i)/var(\sum)$), the contributors analysis can be checked for validity. Such a check is presented with Fig. 6.39, where the ratios of previous values are presented (also the complementary, $\sum cov(i,j)/var(\sum)$). Between 10^{-2} and 10^5 years, almost all the total uncertainty comes from few individual contributions. But outside such a period, it cannot be stated which are the most relevant uncertainty contributors. That is the case at the beginning of cooling time and at the end of the studied cooling time period, when there are a lot of radionuclides with small contributions.

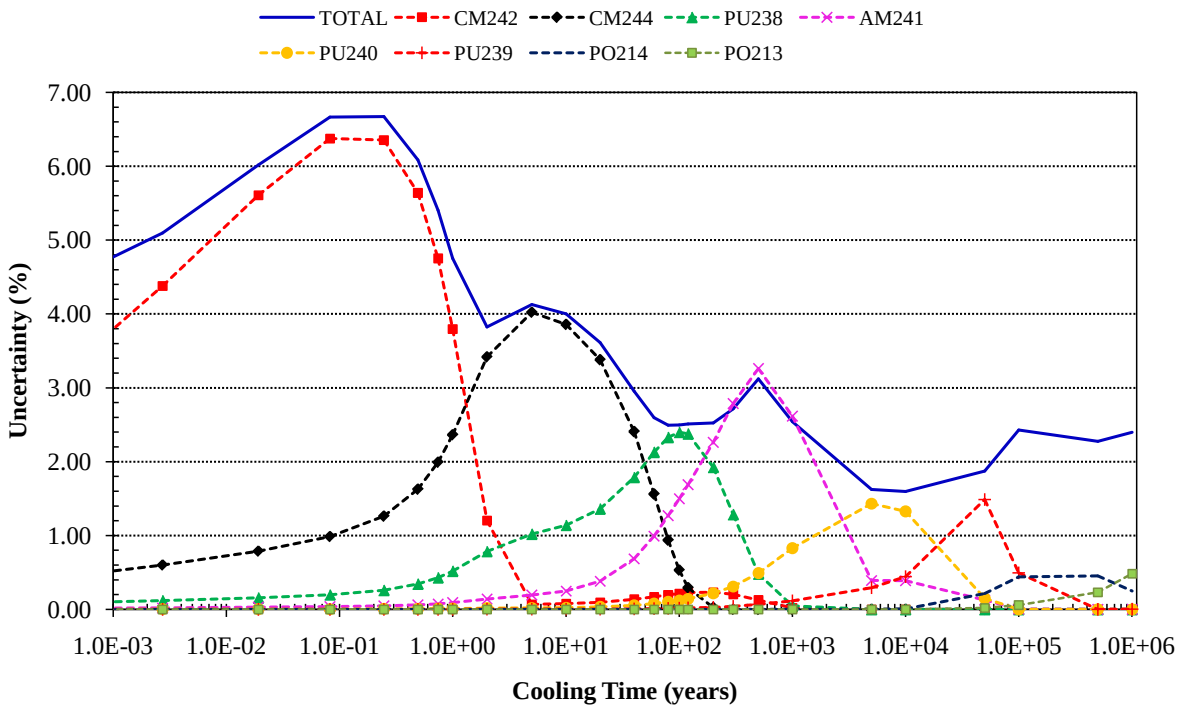

FIGURE 6.38: Total uncertainty and main uncertainty contributors to decay heat as a function of cooling time, when all nuclear data sources are propagated throughout burn-up and cooling time for a EFIT fuel pin-cell burned up to 150 GWd/THM.

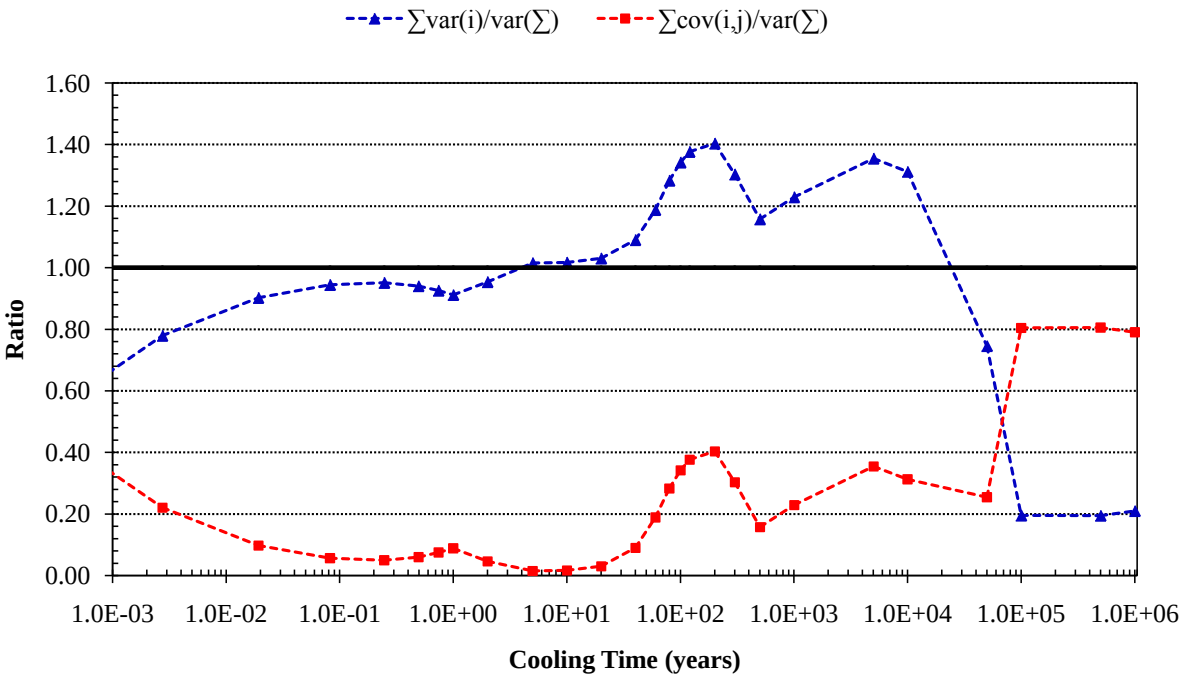

FIGURE 6.39: Ratio of the sum of individual contribution variances to the total variance of decay heat as a function of cooling time, when all nuclear data sources are propagated throughout burn-up and cooling time for a EFIT fuel pin-cell burned up to 150 GWd/THM.

The analysis of most important contributors for the 500 GWd/THM burn-up case is presented in Fig. 6.40. They are in order of appearance: ^{244}Cm, ^{238}Pu, ^{241}Am, ^{240}Pu, ^{239}Pu, ^{214}Po and ^{213}Po. Again Po isotopes are of low importance compared with others. Only ^{242}Cm are missed from the 150 GWd/THM case. In addition, the same result as 150 GWd/THM is obtained when comparing variances of the individual contributions with the total variance: only up to 10^5 years the contributor analysis is valid.

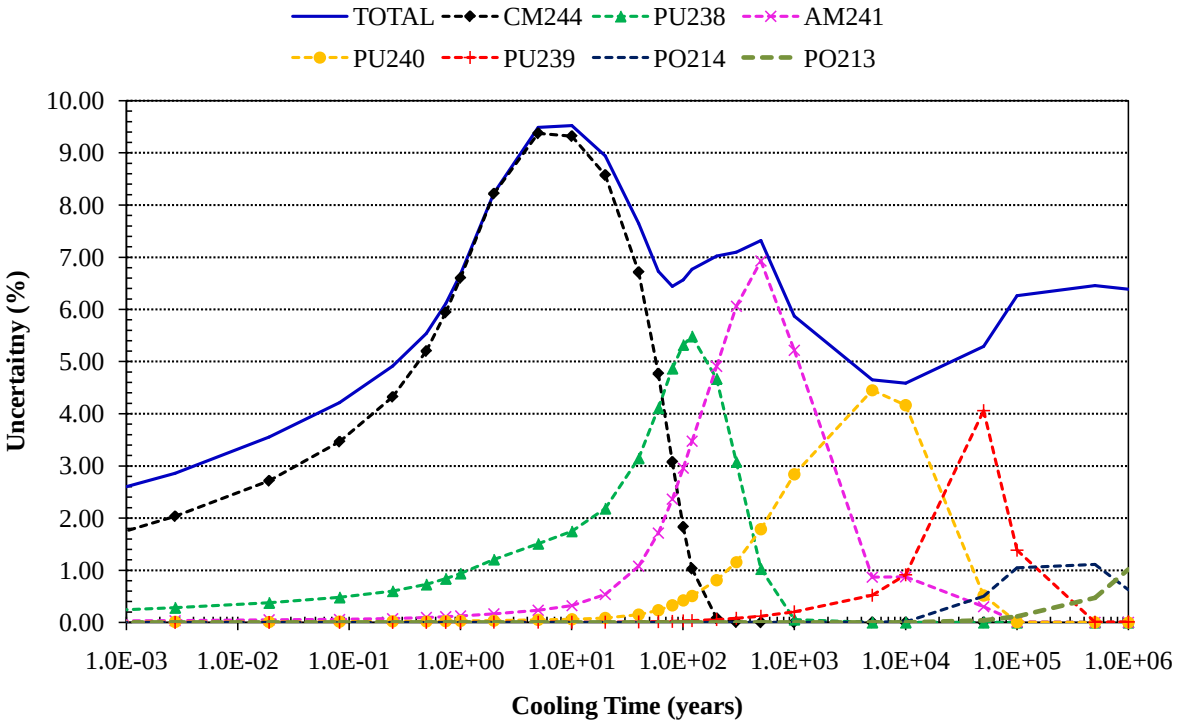

FIGURE 6.40: Total uncertainty and main uncertainty contributors to decay heat as a function of cooling time, when all nuclear data sources are propagated throughout burn-up and cooling time for a EFIT fuel pin-cell burned up to 500 GWd/THM.

Note that in both cases, 150 GWd/THM and 500 GWd/THM, the main uncertainty contributors are almost the same as the main contributors to decay heat. So, the way that they contribute to the uncertainty is by means of their large relative contribution to decay heat. Thus, there is not any nuclide with large uncertainty but with low contribution that has a relevant impact.

6.2.4 UQ study on EFIT Radiotoxicity: Inhalation and Ingestion doses

The same UQ study as on for the EFIT decay heat is performed for radiotoxicity (Inhalation and Ingestion doses), analysing both burn-ups (150 GWd/THM and 500 GWd/THM), the different nuclear data uncertainty sources and most important contributors. The sources of uncertainties are JEFF-3.1.1 for fission yield and decay data, and EAF-2007 for cross section data.

These doses are referred as the dose received by a man over his lifetime (50 years) following the ingestion or inhalation of 1 Bq of activity of a particular radionuclide. They are calculated with dose coefficients, so-called Committed Effective Dose Equivalent (or CEDE), provided within the activation nuclear data libraries. Here, EAF-2007 has been selected to supply these coefficients. These coefficients are treated without uncertainties, even if their uncertainties are likely to surpass the ones obtained due to nuclear data uncertainties.

Results for 150 GWd/THM are presented in Fig. 6.41, while for 500 GWd/THM in Fig. 6.42. In both cases, inhalation (blue) and ingestion (red) dose reference values and their uncertainties are given. For both burn-ups, 150 GWd/THM and 500 GWd/THM, the inhalation dose is larger than ingestion, and for the former burn-up higher values are obtained for both doses. But the behaviour of their uncertainties is different: higher uncertainty values for both doses are obtained for 500 GWd/THM whose uncertainties do not surpass 9%, while uncertainties scarcely goes beyond 4% for 150 GWd/THM. For 150 GWd/THM, uncertainties values for inhalation and ingestion are quite similar throughout the whole cooling time period studied. Only at few points, the ingestion uncertainty is higher than the inhalation one. Meanwhile for 500 GWd/THM, inhalation dose uncertainties are higher until after 500 years of cooling time, above such time the trend switches.

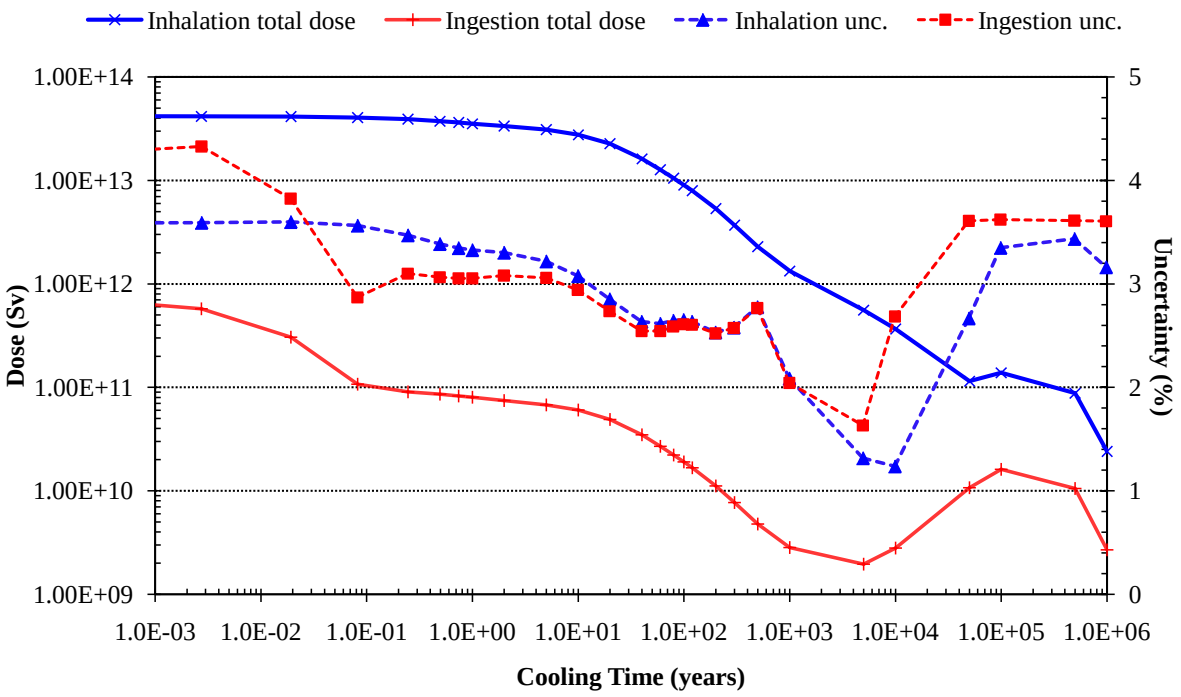

FIGURE 6.41: Radiotoxicity due to inhalation and ingestion doses and their uncertainties as a function of cooling time, when all nuclear data sources are propagated throughout burn-up and cooling time for a EFIT fuel pin-cell burned up to 150 GWd/THM.

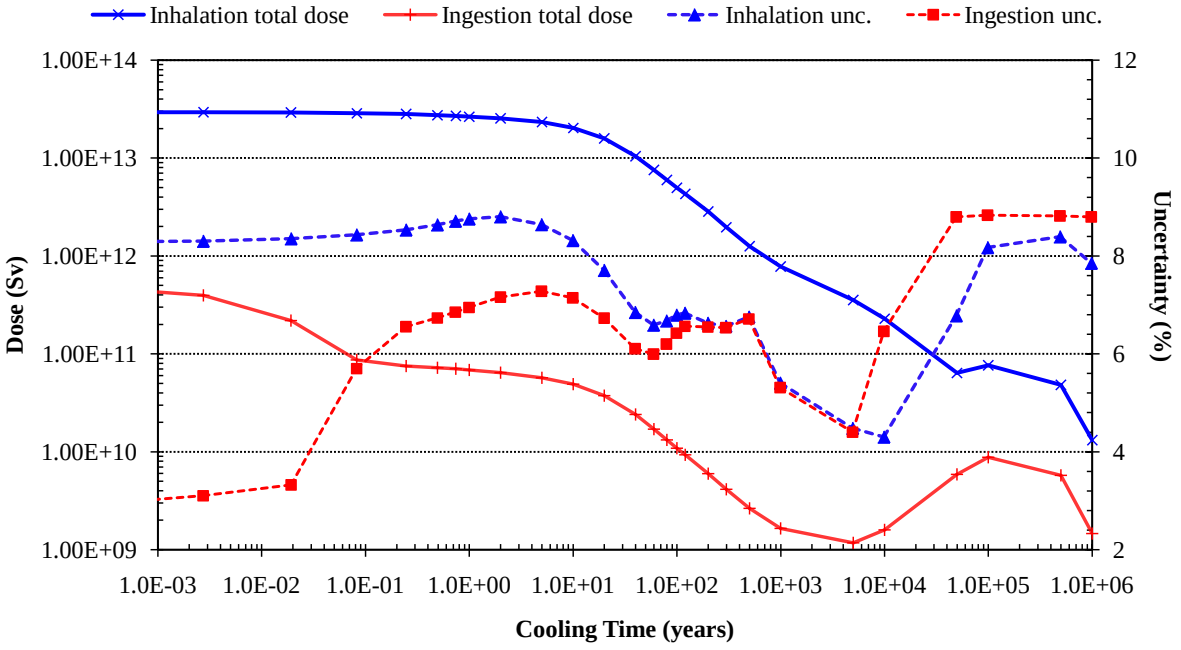

FIGURE 6.42: Radiotoxicity due to inhalation and ingestion doses and their uncertainties as a function of cooling time, when all nuclear data sources are propagated throughout burn-up and cooling time for a EFIT fuel pin-cell burned up to 500 GWd/THM.

Nuclear data uncertainty sources are propagated individually, presenting the results in Figs. 6.43 (inhalation) and 6.44 (ingestion) for 150 GWd/THM, and in Figs. 6.45 (inhalation) and 6.46

(ingestion) for 500 GWd/THM. For both burn-up cases, the inhalation dose uncertainty comes from cross section uncertainties. However, for the ingestion uncertainty, cross sections are the main source of uncertainty, with an important contribution from fission yield uncertainties up to 2×10^{-2} years after shutdown.

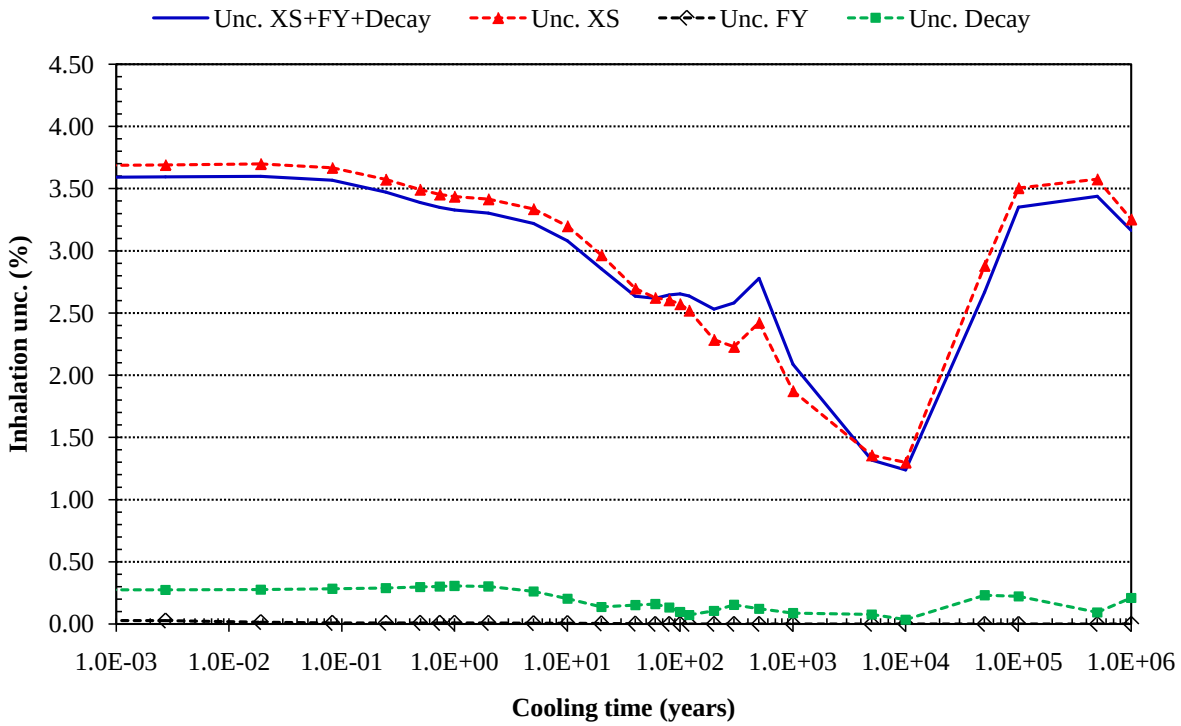

FIGURE 6.43: Inhalation dose uncertainty as a function of cooling time due to different nuclear data uncertainties: cross sections (XS), fission yields (FY) and decay data (Decay), which are propagated throughout burn-up and cooling time for a EFIT fuel pin-cell burned up to 150 GWd/THM.

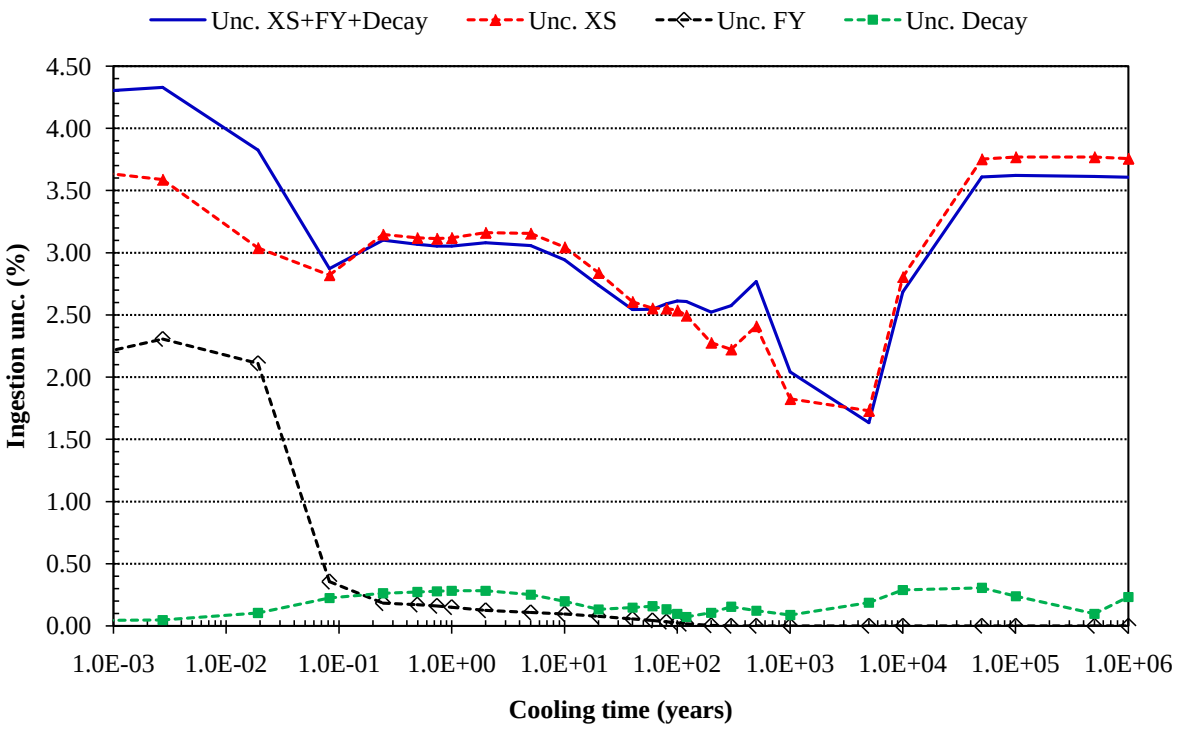

FIGURE 6.44: Ingestion dose uncertainty as a function of cooling time due to different nuclear data uncertainties: cross sections (XS), fission yields (FY) and decay data (Decay), which are propagated throughout burn-up and cooling time for a EFIT fuel pin-cell burned up to 150 GWd/THM.

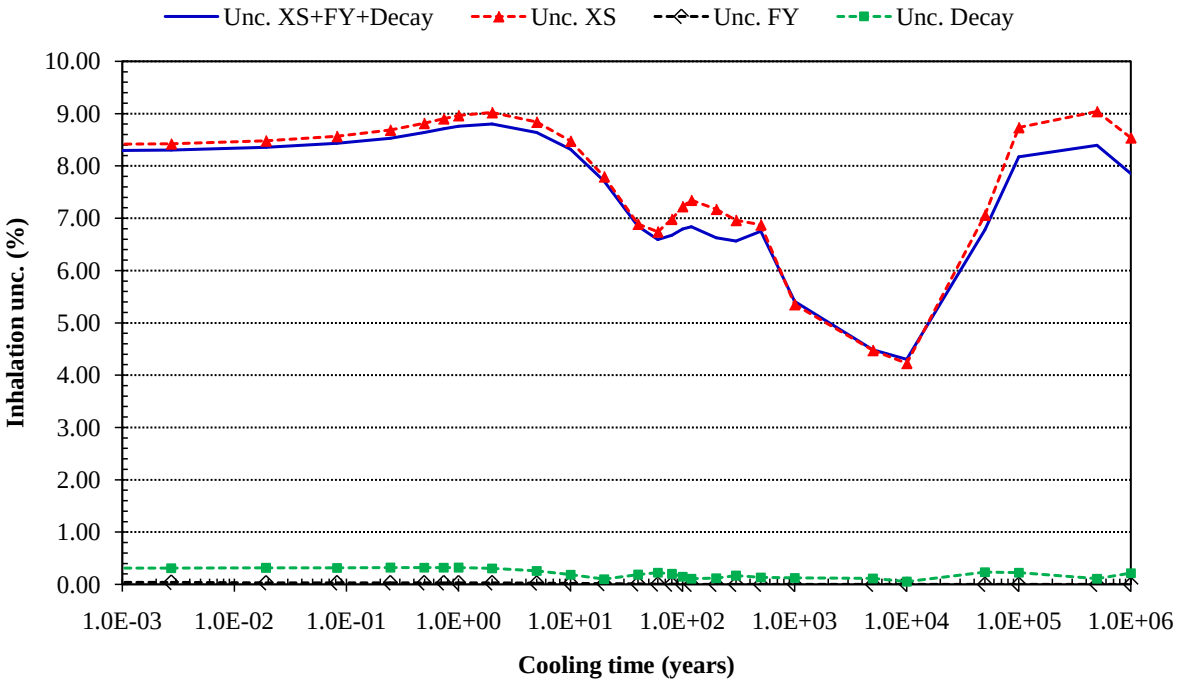

FIGURE 6.45: Inhalation dose uncertainty as a function of cooling time due to different nuclear data uncertainties: cross sections (XS), fission yields (FY) and decay data (Decay), which are propagated throughout burn-up and cooling time for a EFIT fuel pin-cell burned up to 500 GWd/THM.

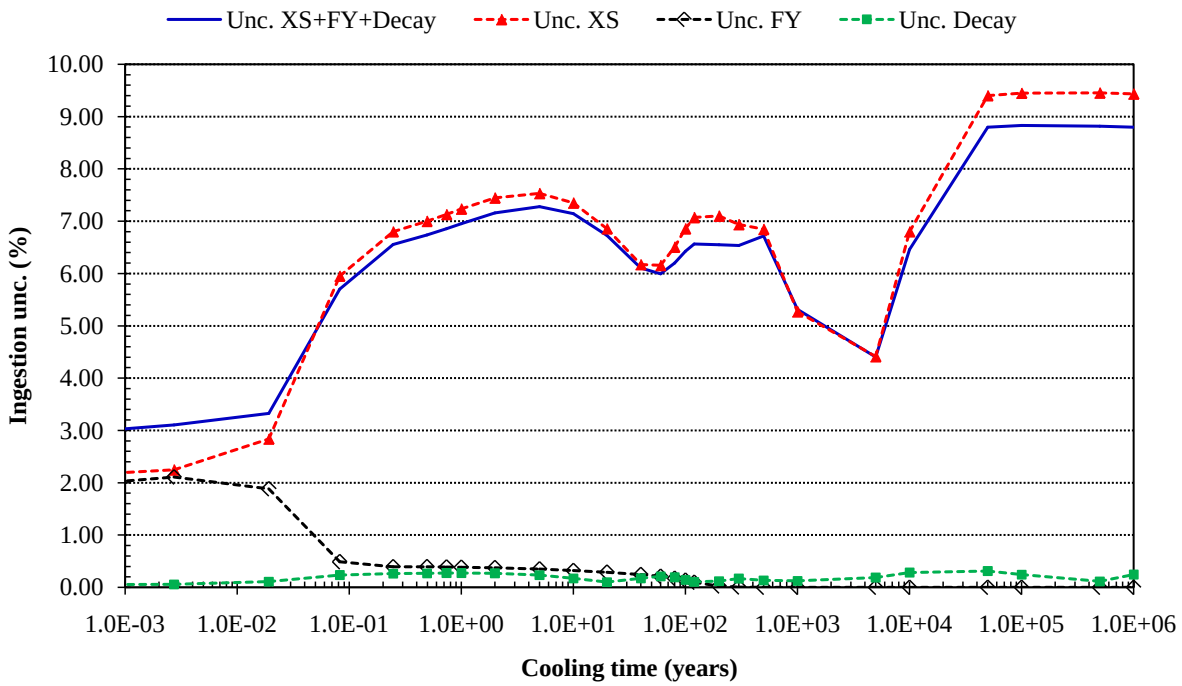

FIGURE 6.46: Ingestion dose uncertainty as a function of cooling time due to different nuclear data uncertainties: cross sections (XS), fission yields (FY) and decay data (Decay), which are propagated throughout burn-up and cooling time for a EFIT fuel pin-cell burned up to 500 GWd/THM.

Most important contributors for each type of dose are assessed, for the two discharge burn-ups studied. For 150 GWd/THM, Fig. 6.47 presents the contributors for inhalation, and Fig. 6.48 for ingestion. Meanwhile, for 500 GWd/THM, Figs. 6.49 and 6.50 show the contributors for inhalation and ingestion, respectively.

For both burn-ups, the main contributors to inhalation uncertainties are ^{244}Cm, ^{238}Pu, ^{241}Am, ^{240}Pu and ^{222}Rn, whereas for ingestion uncertainties are ^{133}Xe, ^{244}Cm, ^{238}Pu, ^{241}Am and ^{222}Rn. ^{240}Pu does not appear as a main contributor to ingestion because its contribution could have been covered by ^{241}Am and ^{222}Rn between 10^3 and 10^4 years. Highlight that there is only one fission product marked as main contributor for ingestion uncertainty: ^{133}Xe. This is the reason why fission yield uncertainties play an important role, as seen in Figs. 6.44 and 6.46, for short cooling time periods: uncertainty on the ^{133}Xe concentration comes mainly from fission cross sections and fission yields.

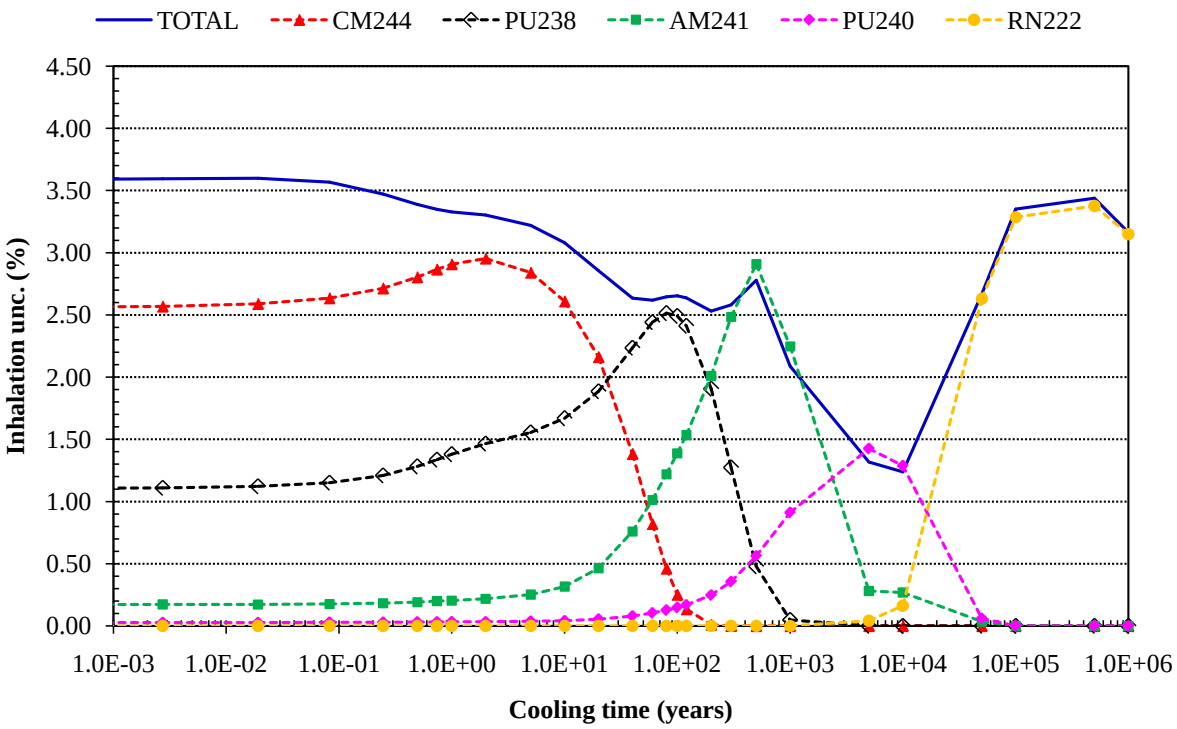

FIGURE 6.47: Total inhalation dose uncertainty and its main uncertainty contributors as a function of cooling time when all nuclear data sources are propagated throughout burn-up and cooling time for a EFIT fuel pin-cell burned up to 150 GWd/THM.

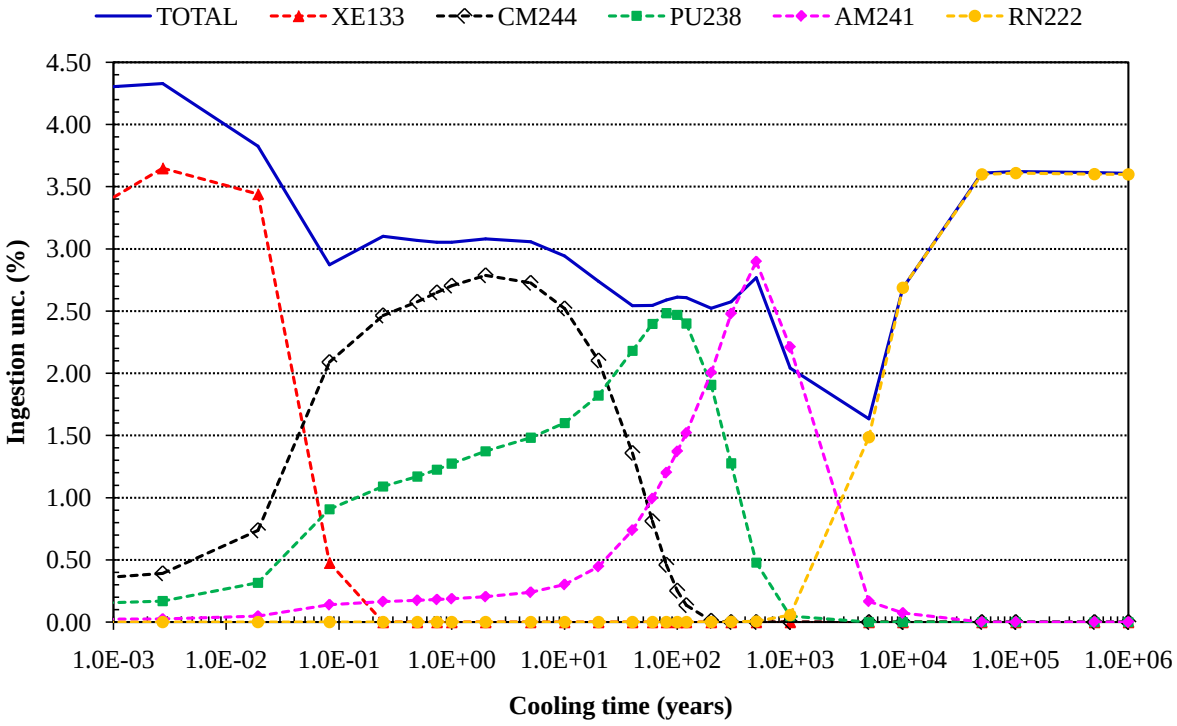

FIGURE 6.48: Total ingestion dose uncertainty and its main uncertainty contributors as a function of cooling time when all nuclear data sources are propagated throughout burn-up and cooling time for a EFIT fuel pin-cell burned up to 150 GWd/THM.

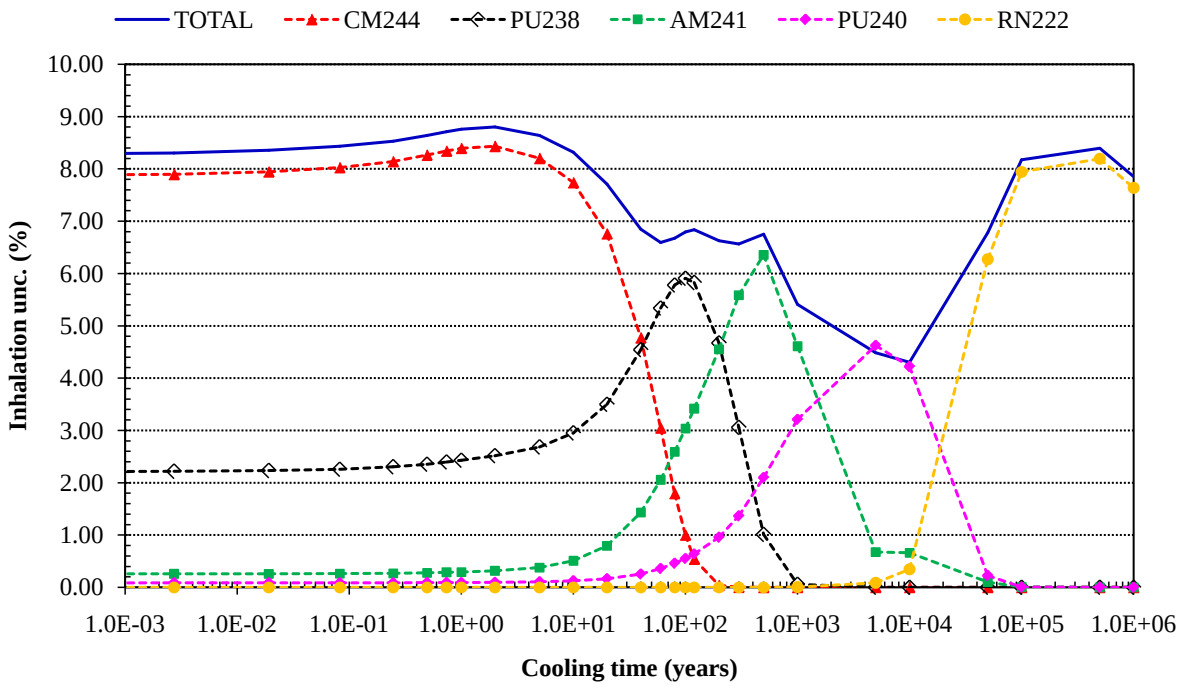

FIGURE 6.49: Total inhalation dose uncertainty and its main uncertainty contributors as a function of cooling time when all nuclear data sources are propagated throughout burn-up and cooling time for a EFIT fuel pin-cell burned up to 500 GWd/THM.

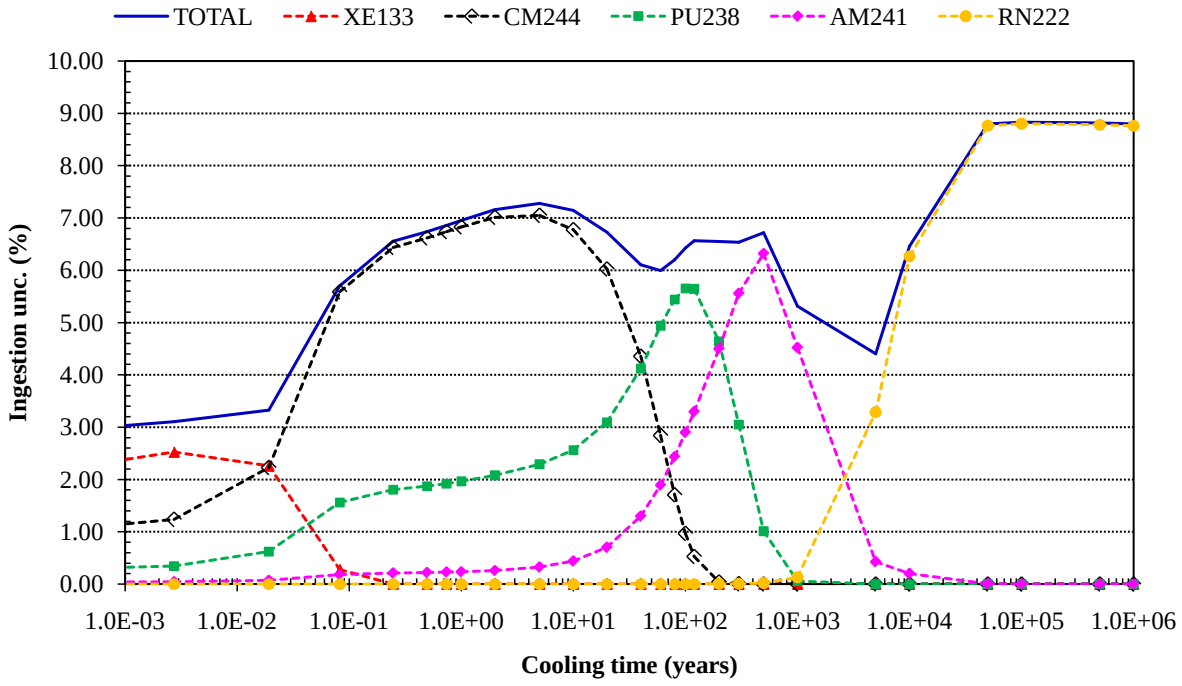

FIGURE 6.50: Total ingestion dose uncertainty and its main uncertainty contributors as a function of cooling time when all nuclear data sources are propagated throughout burn-up and cooling time for a EFIT fuel pin-cell burned up to 500 GWd/THM.

Again, the ratio of the sum of individual contribution variances to the total variance is analysed in order to assess the validity of the contributor analyses. Figs. 6.51 and 6.52

present the evolution of the ratio (and its complementary) as a function of cooling time for 150 GWd/THM. The sum of variances is observed to be quite similar to the total variance for the whole cooling time period studied, proving that the total uncertainty comes mainly from few contributors, or even just one. For 500 GWd/THM, the same results are obtained, with a ratio even closer to one.

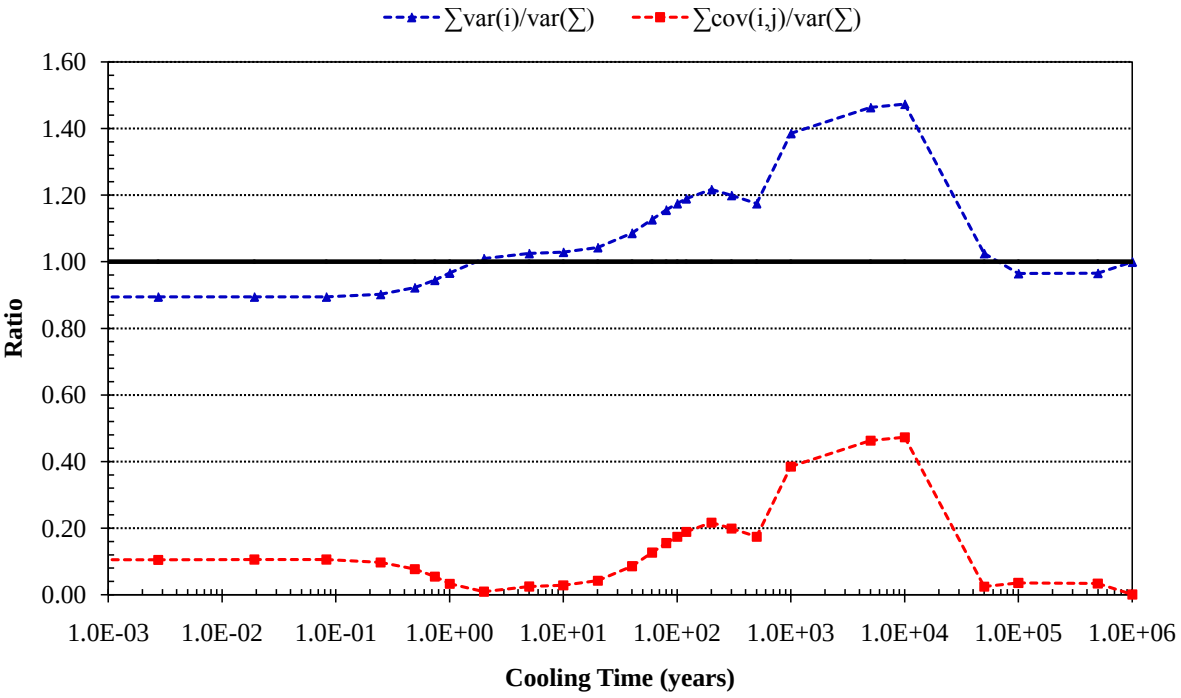

FIGURE 6.51: Ratio of the sum of individual contribution variances to the total variance of inhalation dose as a function of cooling time when all nuclear data sources are propagated throughout burn-up and cooling time for a EFIT fuel pin-cell burned up to 150 GWd/THM.

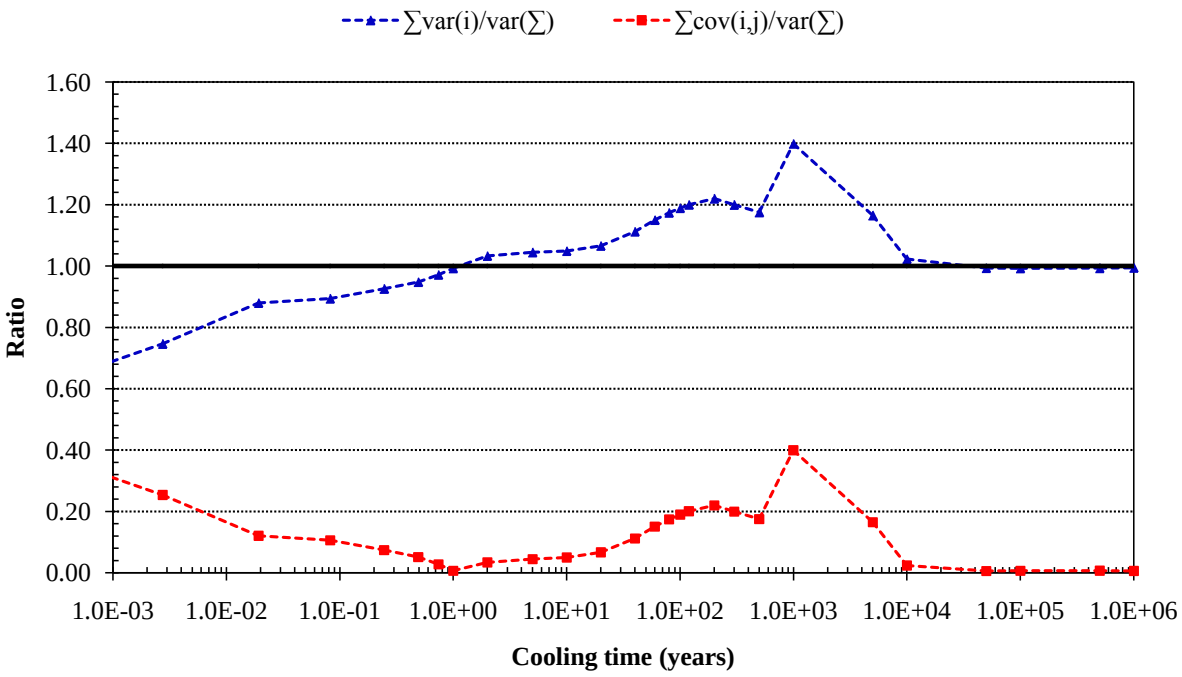

FIGURE 6.52: Ratio of the sum of individual contribution variances to the total variance of ingestion dose as a function of cooling time when all nuclear data sources are propagated throughout burn-up and cooling time for a EFIT fuel pin-cell burned up to 150 GWd/THM.

6.2.5 Conclusions of the UQ studies

Three UQ studies have been performed for the EFIT fuel cycle, in which the Hybrid Method has been used to propagate uncertainties in: decay, fission yield and cross section data. The first one is aimed to assess uncertainties on isotopic composition for a discharge burn-up of 150 GWd/THM, and compares the performance of different cross section data libraries: EAF-2007, EAF-2010 and SCALE6.0. For decay and fission yield data, JEFF-3.1.1 is used. The two others focus on response functions: decay heat and radiotoxicity (inhalation and ingestion doses), for two different burn-ups: 150 GWd/THM and 500 GWd/THM. For these latter studies, the propagated uncertainties come from EAF-2007 for cross sections, and from JEFF-3.1.1 for decay and fission yield data. Main contributor analyses have been carried out only for uncertainties in response functions, meanwhile analyses of the impact of the different nuclear data uncertainties have been performed for the three studies.

The UQ study that quantifies uncertainties on the EFIT fuel isotopic concentrations shows that uncertainties in decay data are negligible. So, the most relevant source of uncertainty comes from cross section data. EAF-2007 provokes the largest uncertainties, followed by EAF-2010, and then by SCALE6.0. However, with EAF-2010 lower uncertainties are reached

than with SCALE6.0 for a group of minor actinides (MA): ^{243,244,245,247}Cm, ^{249}Bk and ^{252}Cf. The results are in agreement with the comparisons done in Chapter 2, especially through Table 2.6, where one-group cross section uncertainties were compared. Such a comparison shows that SCALE6.0 provides higher uncertainties for the mentioned isotope cross sections than EAF-2010, and EAF-2007 gives the highest uncertainty values. The uncertainty levels reached by uranic and transuranic isotopes does not surpass 5%, except for isotopes heavier than ^{242m}Am whose uncertainties can go up to 35% if SCALE6.0 is used (15% with EAF-2010). Fission product concentrations, uncertainties from cross section and fission yield data have to be propagated together in order to account for possible joint effects. Although, from the obtained results it can be stated that their uncertainties will barely exceed 10%.

From the results on EFIT response function uncertainties (decay heat and radiotoxicity), the impact of decay and fission yield data uncertainties is very small, even negligible. There are only two exceptions: one for the decay heat after 10^4 years from shutdown for 150 GWd/THM, in which decay uncertainties provoke a contribution as important as cross section uncertainties; the second for the ingestion dose during cooling time obtained with both burn-ups. This latter exception is explained through ^{133}Xe, which is an important contributor to ingestion dose uncertainty due to uncertainties in fission yield and cross section data. The maximum uncertainty values reached throughout the whole cooling time for each response function are presented in Table 6.9. Note that maximum values increase as discharge burn-up does, however, the cooling time at which these maximums are reached is completely different.

The main contributors to decay heat and radiotoxicity uncertainties are shown in Table 6.10. The main contributors are the same for both discharge burn-ups, with only one exception: ^{242}Cm, which is the most important contributor for decay heat at the beginning of cooling time only for 150 GWd/THM. Contributor analysis assumptions are valid: for the whole cooling period studied for radiotoxicity, and between 10^{-2} to 10^5 years for decay heat.

TABLE 6.9: Maximum uncertainty values reached by response functions during cooling time for different discharge burn-ups of a EFIT fuel pin-cell, 150 GWd/THM and 500 GWd/THM, when all nuclear data sources are propagated throughout burn-up and cooling time.

	Decay Heat	Inhalation Dose	Ingestion Dose
150 GWd/THM	6.67 %	3.70 %	4.33 %
500 GWd/THM	9.83 %	9.04 %	9.45 %

TABLE 6.10: Most relevant contributors to EFIT response functions for different discharge burn-ups of a EFIT fuel pin-cell, 150 GWd/THM and 500 GWd/THM, when all nuclear data sources are propagated throughout burn-up and cooling time.

	Relevance	
Isotope	150 GWd/THM	500 GWd/THM
^{133}Xe	Ing	Ing
^{222}Rn	Inh, Ing	Inh, Ing
^{238}Pu	DH, Inh, Ing	DH, Inh, Ing
^{239}Pu	DH	DH
^{240}Pu	DH, Inh	DH, Inh
^{241}Am	DH, Inh, Ing	DH, Inh, Ing
^{242}Cm	DH	–
^{244}Cm	DH, Inh, Ing	DH, Inh, Ing

DH: Decay Heat Inh: Inhalation dose Ing: Ingestion dose

For ADS systems, like EFIT, there are target accuracies proposed in [Salvatores et al., 2008, Álvarez-Velarde et al., 2009, García-Herranz et al., 2010] for different response functions or system variables:

- Major nuclide isotope concentrations at the end of burn-up: 2% [Salvatores et al., 2008] - 5% [Álvarez-Velarde et al., 2009, García-Herranz et al., 2010].
- Other nuclide isotope concentrations at the end of burn-up: 5% [Álvarez-Velarde et al., 2009] - 10% [Salvatores et al., 2008, García-Herranz et al., 2010].
- Response functions, such as decay heat and radiotoxicity: 10% [Álvarez-Velarde et al., 2009, García-Herranz et al., 2010]

For isotopic concentrations, the 2% requirement is still very tough to achieve, even selecting SCALE6.0 as source of cross section uncertainties. However, with the 5% target, EAF-2010 and SCALE6.0 can fulfil it, if fission products are not considered. Only isotopes heavier than ^{242m}Am do not fulfil such target. Looking at decay heat and radiotoxicity, such responses satisfy they targets, although for 500 GWd/THM they are close to the maximum allowed.

6.3 UQ study on the European Sodium Fast Reactor fuel cycle

Impact of nuclear data uncertainties on the European Sodium Fast Reactor (ESFR) fuel cycle are analysed in this section. Uncertainties on isotopic composition will be addressed and followed throughout the whole cycle. This exercise will also serve as a framework for comparing different approaches of the Hybrid Method: using one-group cross section uncertainties with/without correlated sampling and multi-group cross section uncertainties.

6.3.1 Description of ESFR calculations

The European Sodium Fast Reactor is a 3600 MWth Sodium-cooled Fast Reactor, which includes two separated driver fuel regions, as shown in Fig. 6.53, of 225 inner Fuel Assemblies (FAs) (full blue hexagons) and 228 outer fuel assemblies (full orange hexagons) respectively, with 271 fuel pins/FA. The FAs are loaded with MOX fuel. The inner and outer regions have different Pu contents (14.76 wt% and 17.15 wt%, respectively) in order to reduce local power peaks. The core is completed radially with some reflector assemblies made of steel. The specifications of the analysed core here have been taken from the EU Project CP-ESFR [Rineiski, 2011, Fiorini and Vasile, 2011].

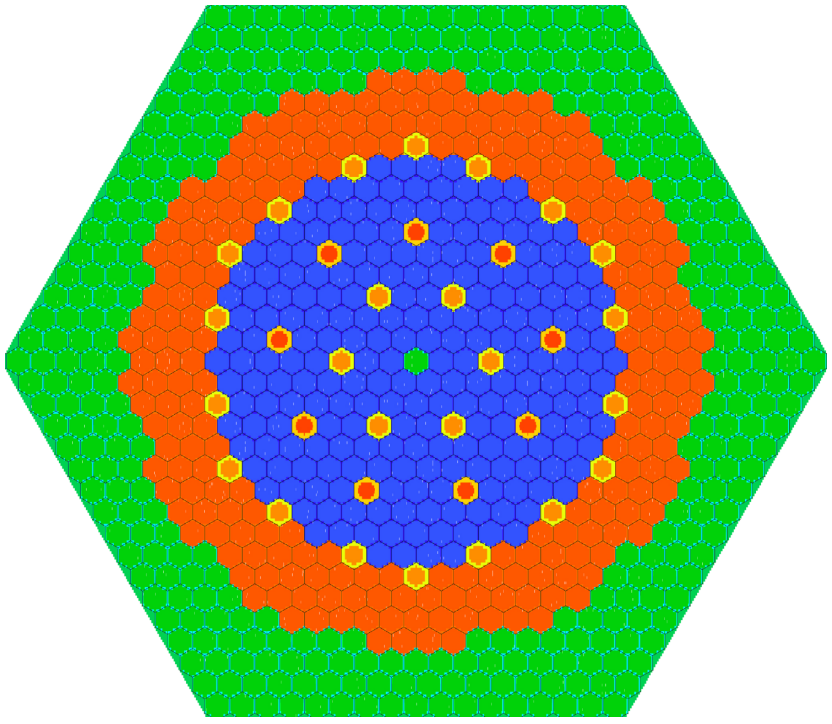

FIGURE 6.53: Radial view of the ESFR core including inner core (blue assemblies), outer core (orange) and reflector (green). The control and shutdown systems are also shown as 9 red-orange assemblies and 24 yellow-orange assemblies, respectively.

The axial layout of the optimised core includes a large sodium plenum above the active region. Further above in the axial direction, there is a layer of boron carbide and then another layer of steel reflector. Below the active region, a fertile layer of depleted uranium and then a lower gas plenum are included.

The core definition also includes the Control Rod System and the Control and Shutdown Device. The first system is formed by 9 assemblies (^{10}B, 90 wt%) and is located in the second control ring as shown in Fig 6.53 in red-orange. The second system is formed by 24 assemblies and it is shown in the same figure as yellow-orange assemblies. Other characteristics of the ESFR reactor are provided in Table 6.11.

TABLE 6.11: Main characteristics of the ESFR reactor, extracted from [Rineiski, 2011, Fiorini and Vasile, 2011].

Parameter	Value
Burn-up	99 GWd/THM
Fuel Residence Time	2050 days
Cycle Length	410 days
Average Plant Lifetime	60 yr
Net thermodynamic yield	42%
Sub-assemblies pitch	210.8 mm
Outer clad diameter	10.73 mm
Fuel pellet diameter	9.43 mm
Inner clad diameter	9.73 mm
Cladding material	ODS steel

One configuration of the core is studied: a MA-enriched configuration so-called HOM4, where the MOX fuel has 4% of MA homogeneously distributed. The isotopic composition is shown in Table 6.12, averaging every reactor fuel zone.

TABLE 6.12: Initial composition of the ESFR characteristic fuel pin-cell for the HOM4 configuration.

Nuclide	Mass (g)	Nuclide	Mass (g)	Nuclide	Mass (g)
^{235}U	2.04×10^{5}	^{241}Pu	9.83×10^{5}	^{243}Cm	2.70×10^{3}
^{238}U	8.05×10^{7}	^{242}Pu	1.24×10^{6}	^{244}Cm	1.98×10^{5}
^{237}Np	6.50×10^{5}	^{241}Am	2.34×10^{6}	^{245}Cm	4.86×10^{4}
^{238}Pu	4.27×10^{5}	^{241m}Am	9.25×10^{3}	^{246}Cm	3.47×10^{3}
^{239}Pu	5.66×10^{6}	^{243}Am	6.05×10^{5}	**Total (g)**	
^{240}Pu	3.54×10^{5}	^{242}Cm	7.71×10^{2}	**9.64×10^{7}**	

Based on the above description, the depletion of an equivalent fuel pin-cell is calculated for the HOM4 configuration, taking the initial composition from Table 6.12. The parameters needed

for the burn-up calculation are retrieved from Table 6.11. Then, a burn-up of 99 GWd/THM is achieved within 2050 days, divided in 5 cycles of 410 days. For this purpose, the EVOLCODE2 system [Álvarez-Velarde et al., 2007], which integrates the ACAB code [Sanz et al., 2008] as the depletion solver, has been used for simulating the isotopic composition, neutron spectrum and neutron flux intensity throughout the burn-up.

Only five (5) burn steps are considered for the depletion calculations because there are only small variations of the neutron spectrum during the burn-up. That means the neutron spectrum and neutron flux intensity are kept as constants along these burn-up steps. Indeed, the burn-up steps are the same as the burn-up cycles, so the "burn-up step" and "burn-up cycle" terms will be treated indistinguishably. Table 6.13 provides the neutron flux intensity values in each burn-up step, whereas Fig. 6.54 presents the neutron spectra at the Beginning of Life (BOL) and at the End of Life (EOL). Small, even negligible, differences are found between BOL and EOL spectra.

TABLE 6.13: ESFR neutron flux intensity in each burn-up cycle (given in time).

Time (days)	Flux intensity (n/cm^{2}s)
410	3.1637×10^{15}
820	2.9798×10^{15}
1230	2.8168×10^{15}
1640	2.5980×10^{15}
2050	2.4464×10^{15}

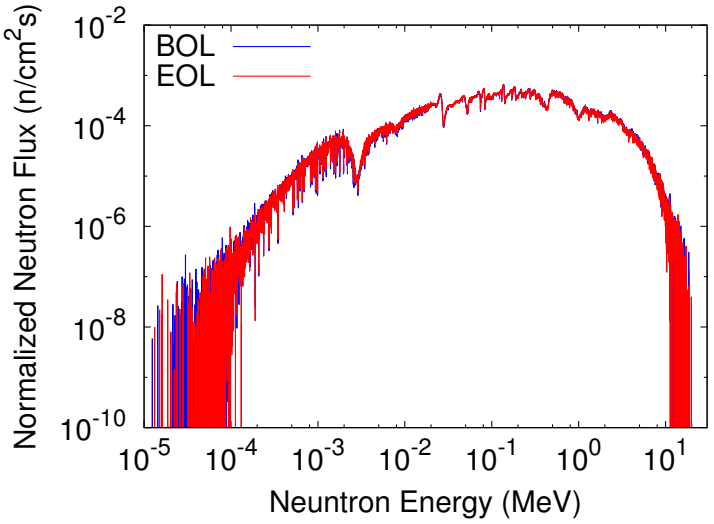

FIGURE 6.54: ESFR neutron spectra at Beginning of Life (BOL) and End of Life (EOL).

6.3.2 UQ study on isotopic composition for the HOM4 configuration

A UQ study is carried out on the depletion calculations described before using different Hybrid Method approaches. First, a comparison for the one-group cross section approach between using or not correlated sampling and assuming constant neutron spectrum is performed. Then after, a comparison between the one-group approach with correlated sampling and multi-group approach is carried out to validate previous results. In these two comparisons, the uncertainty on isotopic composition of the equivalent fuel pin-cell described previously for the HOM4 configuration is assessed, and the performance of different cross section uncertainty libraries are studied.

6.3.2.1 Comparison between different one-group approaches

Because the burn-up is split into five burn-up steps, one can selected between different approaches of Hybrid Method:

- Use correlated sampling for random cross sections between burn-up steps (Case A).
- Not correlate random cross section between burn-up steps for a given history (Case B).
- Using the random cross sections sampled in the first step for every step (Case C).

Case A and Case C are expected to provide very similar values because the neutron spectrum almost does not change from BOL to EOL. Meanwhile, Case B approximation is not fully consistent since the isotopic composition should be sampled after every burn-up step if random cross sections are not correlated between steps. These approaches are applied only when propagating cross section uncertainties.

Additionally to cross sections, fission yields and decay data uncertainties are also propagated. Decay nuclear data and fission yield data are retrieved from the JEFF-3.1.1 library [Kellet et al., 2009], while the EAF-2010 library is used for the cross section reference values. For the cross section data uncertainties, three different sources are used: EAF-2010 [Sublet et al., 2010], SCALE6.0 [ORNL, 2009] and COMMARA-2.0 [Herman et al., 2011]. That means, if SCALE6.0 or COMMARA-2.0 provide cross sections or uncertainty data, they are merged with the EAF-2010 data, and thus used in the calculations.

Results are compiled in Table 6.14 and 6.15, where the initial composition, its variation from BOL to EOL, and uncertainties on the number of atoms at EOL due to cross sections, decay data and fission yields (FYs) are shown. As expected, a good agreement between Case A and Case C is observed, because the differences between the neutron spectra in each burn-up steps/cycles are really small, even negligible, to produce large differences on the isotopic composition. Meanwhile, Case B provides a completely random behaviour that provokes an underestimation of the uncertainties except for ^{242}Cm, ^{126}Sb and ^{126m}Sb.

TABLE 6.14: Uncertainties on the number of atoms of heavy isotopes for a ESFR characteristic fuel cell after 99 GWd/THM burn-up, using different approaches of the Hybrid Method: one-group cross section uncertainties with correlated sampling (Case A) and without correlate sampling (Case B), and using the random one-group cross section in the first step for every other burn-up step (Case C). The performance of different cross section libraries are compared.

Nuclide	N_i (atoms)	N_f - N_i (atoms)	Uncertainty (%)										
			Decay	FYs	EAF-2010			SCALE			COMMARA-2.0		
			JEFF-3.1.1		Case A	Case B	Case C	Case A	Case B	Case C	Case A	Case B	Case C
^{232}U	-	2.20×10^{22}	2.73	-	9.41	4.81	9.60	8.08	4.05	7.97	9.45	4.60	9.20
^{233}U	-	4.63×10^{21}	0.64	-	8.44	4.90	8.79	12.04	7.18	11.87	17.32	9.51	16.66
^{234}U	-	7.45×10^{25}	0.16	-	6.92	3.76	6.80	3.90	1.99	4.13	3.13	1.61	3.24
^{235}U	5.24×10^{26}	-3.52×10^{26}	0.01	-	6.56	2.86	6.41	6.19	2.85	6.29	4.02	1.69	3.82
^{236}U	-	7.31×10^{25}	0.00	-	3.90	1.97	3.90	20.31	9.45	20.48	13.60	5.93	13.05
^{237}U	-	6.96×10^{23}	0.15	-	3.14	3.08	3.07	12.51	11.62	12.96	10.00	10.13	10.34
^{238}U	2.04×10^{29}	-3.28×10^{28}	0.00	-	0.64	0.29	0.63	0.23	0.11	0.24	0.22	0.10	0.21
^{237}Np	1.65×10^{27}	-8.29×10^{26}	0.00	-	6.32	2.86	6.19	3.19	1.39	3.19	3.25	1.47	3.21
^{238}Np	-	7.72×10^{23}	0.09	-	4.07	8.21	4.08	2.50	3.12	2.55	2.27	4.16	2.27
^{239}Np	-	3.75×10^{25}	0.16	-	2.89	3.24	2.90	1.16	1.31	1.22	1.26	1.36	1.18
^{238}Pu	1.08×10^{27}	1.35×10^{27}	0.04	-	7.62	3.60	7.57	4.32	2.10	4.41	3.32	1.56	3.53
^{239}Pu	1.43×10^{28}	7.65×10^{27}	0.00	-	5.29	2.48	5.17	1.28	0.59	1.29	1.30	0.61	1.21
^{240}Pu	8.89×10^{27}	6.52×10^{26}	0.00	-	3.22	1.47	3.21	2.15	1.01	2.12	2.39	1.06	2.30
^{241}Pu	2.46×10^{27}	-7.78×10^{26}	0.02	-	5.75	2.78	6.11	1.70	0.83	1.67	3.69	1.83	3.58
^{242}Pu	3.09×10^{27}	-3.75×10^{26}	0.05	-	2.84	1.32	2.79	1.29	0.53	1.32	3.87	1.73	3.92
^{244}Pu	-	3.24×10^{23}	0.01	-	3.58	1.68	3.61	4.47	2.02	4.34	5.09	2.49	5.32
^{241}Am	5.84×10^{27}	-3.38×10^{27}	0.02	-	12.39	5.92	12.47	3.86	1.72	3.83	1.79	0.86	1.85
^{242}Am	-	8.07×10^{23}	0.19	-	5.50	15.86	5.53	1.62	4.49	1.57	1.14	1.87	1.17
^{242m}Am	2.30×10^{25}	7.60×10^{25}	0.01	-	18.69	8.99	18.50	18.95	8.43	17.91	18.37	8.77	19.60
^{243}Am	1.50×10^{27}	-4.04×10^{26}	0.02	-	3.19	1.45	3.37	4.11	1.88	4.02	6.98	3.10	7.02
^{242}Cm	1.92×10^{24}	1.67×10^{26}	0.12	-	6.42	13.43	6.48	1.91	3.79	1.84	3.39	3.07	3.48
^{243}Cm	6.69×10^{24}	2.05×10^{25}	0.22	-	16.00	7.89	16.08	19.41	8.95	18.45	54.79	25.07	52.79
^{244}Cm	4.89×10^{26}	3.98×10^{26}	0.04	-	3.09	1.53	3.13	5.76	2.60	5.81	9.12	4.43	9.15
^{245}Cm	1.19×10^{26}	3.80×10^{25}	0.02	-	6.99	3.49	7.12	16.21	7.91	16.31	35.08	17.96	34.27
^{246}Cm	8.49×10^{24}	2.49×10^{25}	0.01	-	5.99	2.61	5.89	13.09	6.08	13.46	21.84	10.12	21.42
^{247}Cm	-	3.11×10^{24}	0.00	-	8.55	4.52	8.30	24.10	13.24	25.12	26.11	14.94	27.63
^{248}Cm	-	3.46×10^{23}	0.00	-	10.07	5.02	10.20	33.59	17.26	34.41	25.05	13.04	26.57
^{249}Bk	-	5.27×10^{21}	0.91	-	10.72	6.28	10.82	42.35	23.75	41.78	25.12	14.08	26.38
^{249}Cf	-	5.54×10^{21}	0.79	-	10.58	5.88	10.66	42.77	21.76	42.52	24.72	14.77	26.07
^{250}Cf	-	1.04×10^{21}	0.25	-	12.28	7.31	12.51	47.30	26.14	47.78	25.50	15.92	26.98
^{251}Cf	-	5.23×10^{19}	0.22	-	14.88	9.30	15.28	53.11	29.15	52.36	27.39	17.77	28.67
^{252}Cf	-	1.00×10^{18}	0.21	-	15.65	9.66	15.68	58.97	33.56	55.04	27.83	18.98	29.09

TABLE 6.15: Uncertainties on the number of atoms of fission products for a ESFR characteristic fuel cell after 99 GWd/THM burn-up, using different approaches of the Hybrid Method: one-group cross section uncertainties with correlated sampling (Case A) and without correlate sampling (Case B), and using the random one-group cross section in the first step for every other burn-up step (Case C). The performance of different cross section libraries are compared.

Nuclide	N_i (atoms)	N_f - N_i (atoms)	Uncertainty (as rel.std.dev. %)									
			Decay	FYs	EAF-2010			SCALE			COMMARA-2.0	
			JEFF-3.1.1		Case A	Case B	Case C	Case A	Case B	Case C	Case A	Case B	Case C
^{93m}Nb	-	1.27×10^{21}	0.09	13.12	5.66	2.79	5.66	1.09	0.63	1.13	1.02	0.63	1.08
^{94}Nb	-	7.34×10^{21}	0.00	9.38	12.58	5.53	12.84	7.72	3.49	7.57	7.87	3.45	7.71
^{93}Mo	-	8.91×10^{18}	0.01	14.63	30.22	18.17	31.21	27.05	16.08	27.86	29.81	17.82	31.20
^{103}Rh	-	1.64×10^{27}	0.00	2.53	5.08	2.22	5.10	1.08	0.57	1.11	1.02	0.51	0.99
^{107}Pd	-	7.80×10^{26}	0.00	2.43	4.58	2.08	4.60	2.20	1.23	2.29	2.32	1.18	2.25
^{109}Ag	-	4.08×10^{26}	0.00	2.65	5.51	2.55	5.72	2.17	1.07	2.14	2.20	1.08	2.18
^{126}Sn	-	6.24×10^{25}	0.00	4.01	4.80	2.15	4.87	0.81	0.38	0.81	0.74	0.36	0.70
^{126}Sb	-	3.51×10^{22}	5.89	19.81	4.80	6.73	4.82	6.98	7.18	6.59	1.39	1.12	1.29
^{126m}Sb	-	6.13×10^{19}	0.99	13.43	6.17	7.02	6.05	3.92	3.92	3.91	4.22	4.09	3.98
^{129}I	-	3.36×10^{26}	0.03	2.36	4.79	2.16	4.86	1.34	0.69	1.46	0.82	0.41	0.79
^{149}Sm	-	2.68×10^{26}	0.00	2.85	5.47	2.56	5.67	5.36	2.79	5.18	5.59	2.74	5.19
^{150}Sm	-	1.31×10^{26}	0.00	3.03	7.06	3.55	6.90	10.53	5.62	10.39	10.68	5.31	9.91
^{151}Sm	-	1.46×10^{26}	0.06	2.74	5.08	2.43	5.09	9.49	4.97	9.20	7.93	4.31	7.37
^{152}Sm	-	2.46×10^{26}	0.01	1.97	4.97	2.22	5.05	5.00	2.66	4.91	4.51	2.49	4.27
^{151}Eu	-	2.19×10^{24}	3.85	2.76	6.70	3.62	6.65	10.69	5.87	10.27	7.76	3.94	7.31
^{153}Eu	-	8.48×10^{25}	0.01	2.54	12.08	6.17	12.05	6.75	3.61	6.62	6.79	3.60	6.65
^{155}Gd	-	1.30×10^{25}	0.13	3.04	6.53	3.10	6.40	4.27	2.23	4.23	4.31	2.23	4.33

A thorough comparison of the three cases of using Hybrid Method is done in Fig. 6.55, where the evolutions of the number of atoms of ^{239}Pu and its uncertainty are followed. For the three cases, the number of atoms are equivalent. However, when the uncertainties are observed, Case B presents an odd behaviour, definitely different from Case A and C, because in every burn-up step/cycle the cross sections are sampled without taking any correlation with the samples of previous burn-up steps. Thus, an oscillatory behaviour appears, and each burn-up steps/cycle can be distinguished among the others. Again, Case A and C are in a very good agreement along the whole burn-up, since only small/negligible changes in the spectra occur during burn-up.

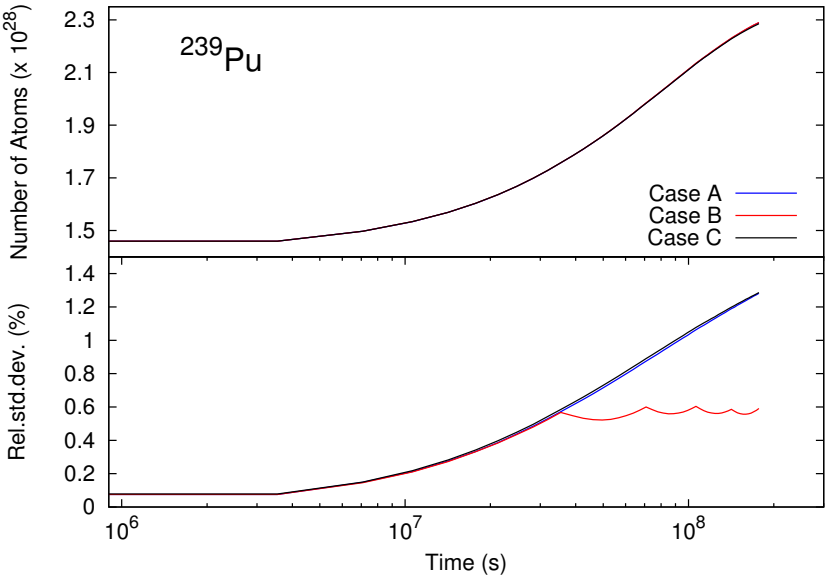

FIGURE 6.55: Number of atoms of ^{239}Pu and its uncertainty as a function of burn-up time of a ESFR characteristic fuel cell up to 99 GWd/THM, using different approaches of the Hybrid Method: one-group cross section uncertainties with correlated sampling (Case A) and without correlate sampling (Case B), and using the random one-group cross section in the first step for every other burn-up step (Case C). SCALE6.0 uncertainties are applied.

Conclusions regarding uncertainty sources and library performance can be drawn from Table 6.14 and 6.15. Decay data uncertainties are only of relevance for two fission products:^{126}Sb and ^{151}Eu. Both cases haven been identified already in Sec. 6.2, and their origins are the same. Large differences are found between using different cross section libraries. EAF-2010 produces higher uncertainties than SCALE and COMMARA-2.0 except for isotopes heavier than ^{242}Cm. The fission yield uncertainties are of importance for Fission Products (FPs) like ^{93m,94}Nb, ^{126}Sn and ^{126,126m}Sb, since their impact is similar or even higher than the impact of any cross section library used. Only for ^{93}Mo, its uncertainty due to FYs is still small compared with the estimation from cross section data.

Examples of the evolution of the uncertainty on the number of atoms throughout burn-up due to each cross section library are presented in Fig. 6.56 for ^{233}U, in Fig. 6.57 for ^{237}Np and in Fig. 6.56 for ^{235}U. For all nuclides presented in Table 6.14 and 6.15, the evolution of their uncertainties due to each library can be found in [Mills et al., 2013, Appendix B].

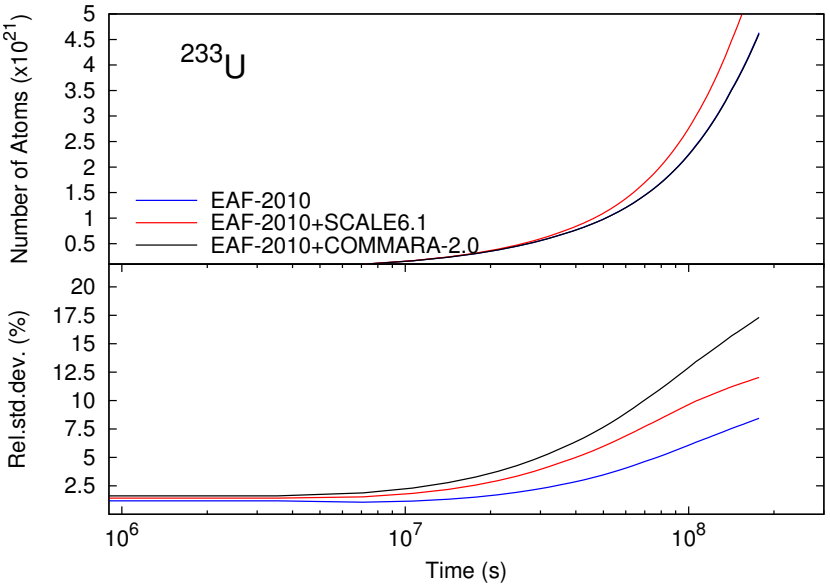

FIGURE 6.56: Number of atoms of ^{233}U and its uncertainty as a function of burn-up time for a ESFR characteristic fuel cell up to 99 GWd/THM, using the Hybrid Method with one-group cross section uncertainties with correlated sampling and comparing the performance of different cross section libraries.

For ^{233}U, COMMARA-2.0 and EAF-2010 provide the same evolution for the number of atoms, while SCALE gives a slightly larger value due to differences with the EAF cross section values. This difference between SCALE and COMMARA-2.0/EAF-2010 increases as the burn-up increases. For uncertainties, COMMARA-2.0 induces the highest uncertainty, followed by SCALE and finally by EAF-2010. Although, their trends during the whole burn-up are similar.

For ^{237}Np, a difference between the number of atoms arises after long irradiation times, when SCALE result starts to depart from the others, reducing the amount of ^{237}Np faster. The evolution of the uncertainties shows that SCALE and COMMARA-2.0 provide very similar results, while EAF-2010 induces larger uncertainties. Again, the same trend is observed for the three libraries.

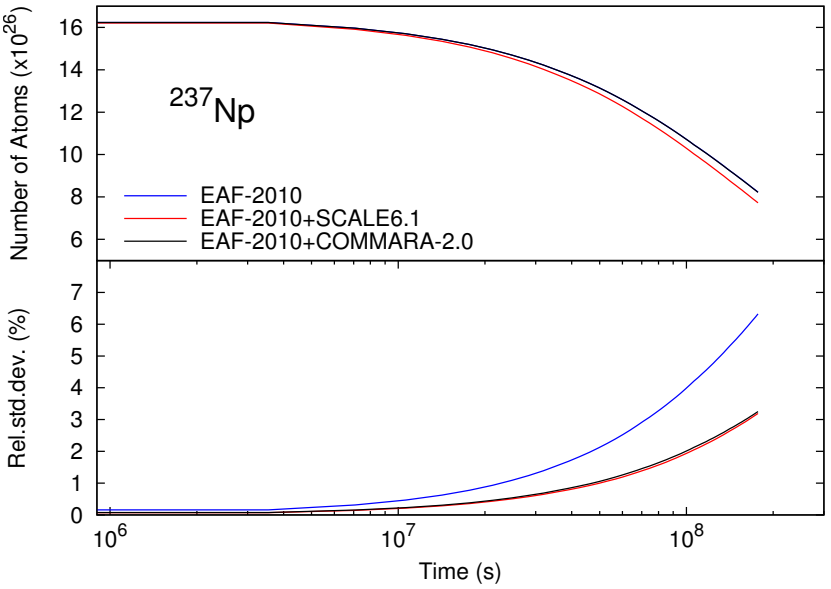

FIGURE 6.57: Number of atoms of ^{237}Np and its uncertainty as a function of burn-up time for a ESFR characteristic fuel cell up to 99 GWd/THM, using the Hybrid Method with one-group cross section uncertainties with correlated sampling and comparing the performance of different cross section libraries.

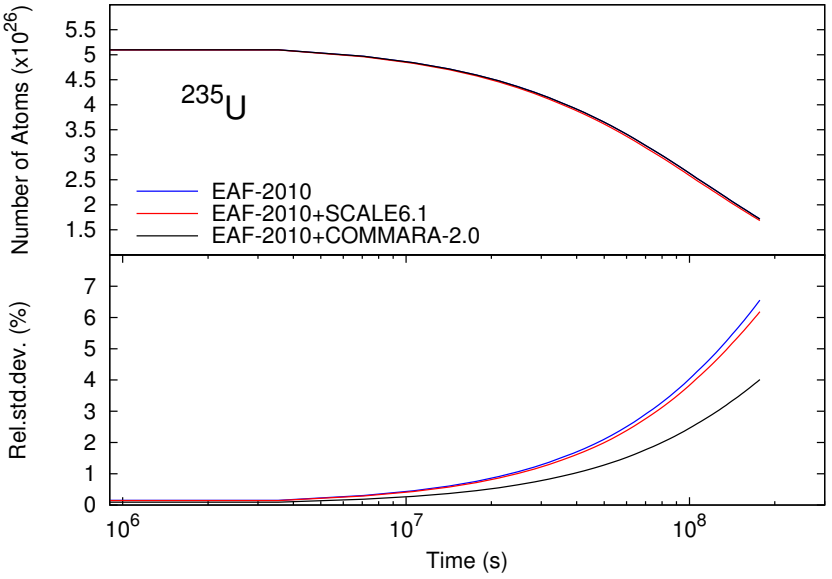

FIGURE 6.58: Number of atoms of ^{235}U and its uncertainty as a function of burn-up time for a ESFR characteristic fuel cell up to 99 GWd/THM, using the Hybrid Method with one-group cross section uncertainties with correlated sampling and comparing the performance of different cross section libraries.

For ^{235}U, no difference between the number of atoms is appreciable among the cross section libraries. However, larger uncertainties are reached with EAF-2010 and SCALE-6.0 than with COMMARA-2.0. Comparing SCALE and EAF-2010, the former provokes a slightly

smaller uncertainty than the latter. Their trend are completely similar, with the increase of the uncertainty as the burn-up increases.

6.3.2.2 Comparison between Hybrid Method approaches: one-group with correlated sampling and multi-group

Two approaches of the Hybrid Method, depending on how uncertainties on cross section data are treated and sampled, are compared:

- Sampling the cross sections in multi-group structure, and then, collapsing the random sample to one-group.
- Sampling the cross sections in one-group with correlated sampling, relating the random cross section samples in each burn-up step by using the same random number.

Two different cross section libraries are used in these calculations:

- EAF-2010, which provides cross section data in a 211-group structure, while their uncertainties are given only in 3-4 groups. In addition, no correlation between energies, nor reactions, are given. 100% correlation is assumed for the cross section groups that lay in the same uncertainty group.
- SCALE6.0, which supplies cross section data in a 44-group structure, using the same energy structure for their uncertainties. It provides correlations between different reaction channels of the same nuclide, even between different nuclides.

Once the random cross sections in one-group are obtained, the nominal EAF-2010 cross section values are replaced by the random ones.

The results are compiled in Table 6.16 and 6.17, where the initial composition and its variation between the beginning and the end of burn-up, and the uncertainties on the number of atoms obtained from the different approaches are shown. Very similar uncertainties are reached at the EOC using both approaches: one-group (1g) or multi-group (211g for EAF-2010, 44g for SCALE6.0). Meanwhile for nominal values of concentrations, negligible differences are found. The cells of those nuclides, which have differences between using one-group or multi-group cross sections, are coloured in grey. When EAF-2010 is used, with multi-group uncertainties,

fission products reach higher uncertainties than using one-group, such are the cases of ^{107}Pd and ^{109}Ag. Truncating the sampled PDF to avoid negative values, by setting them to zero, seems to be the issue. While using SCALE6.0, only a relevant difference appears for ^{236}U, but the source of such a difference is explained later.

TABLE 6.16: Uncertainties due to different cross section libraries on the atomic composition of heavy isotopes for a ESFR characteristic fuel cell after 99 GWd/THM burn-up, comparing two Hybrid Method approaches: using one-group cross section uncertainties with correlated sampling (1g) and using multi-group cross section uncertainties (211g/44g).

		EAF-2010			SCALE6.0		
Nuclide	N_i	N_f - N_i	Uncertainty (%)		N_f - N_i	Uncertainty (%)	
	(atoms)	(atoms)	1g	211g	(atoms)	1g	44g
^{232}U	-	2.20×10^{22}	9.41	9.70	2.08×10^{22}	4.38	4.63
^{233}U	-	4.63×10^{21}	8.44	8.46	5.91×10^{21}	12.16	11.45
^{234}U	-	7.45×10^{25}	6.92	6.98	7.13×10^{25}	3.63	3.84
^{235}U	5.24×10^{26}	-3.52×10^{26}	6.56	6.18	-3.55×10^{26}	6.44	6.08
^{236}U	-	7.31×10^{25}	3.90	3.84	7.43×10^{25}	21.29	19.67
^{237}U	-	6.96×10^{23}	3.14	3.09	7.32×10^{23}	12.13	12.18
^{238}U	2.04×10^{29}	-3.28×10^{28}	0.64	0.65	-3.51×10^{28}	0.24	0.22
^{237}Np	1.65×10^{27}	-8.29×10^{26}	6.32	6.25	-8.80×10^{26}	3.07	3.10
^{238}Np	-	7.72×10^{23}	4.07	4.01	7.90×10^{23}	2.41	2.38
^{239}Np	-	3.75×10^{25}	2.89	3.03	4.03×10^{25}	1.20	1.13
^{238}Pu	1.08×10^{27}	1.35×10^{27}	7.62	7.71	1.34×10^{27}	4.22	4.29
^{239}Pu	1.43×10^{28}	7.65×10^{27}	5.29	5.27	8.63×10^{27}	1.31	1.25
^{240}Pu	8.89×10^{27}	6.52×10^{26}	3.22	3.14	9.23×10^{26}	2.23	2.18
^{241}Pu	2.46×10^{27}	-7.78×10^{26}	5.75	5.88	-7.55×10^{26}	1.45	1.39
^{242}Pu	3.09×10^{27}	-3.75×10^{26}	2.84	2.90	-3.56×10^{26}	1.29	1.24
^{244}Pu	-	3.24×10^{23}	3.58	3.58	2.61×10^{23}	2.93	2.99
^{241}Am	5.84×10^{27}	-3.38×10^{27}	12.39	12.68	-3.46×10^{27}	3.63	3.61
^{242}Am	-	8.07×10^{23}	5.50	5.84	8.13×10^{23}	1.25	1.21
^{242m}Am	2.30×10^{25}	7.60×10^{25}	18.69	18.86	8.28×10^{25}	7.86	8.03
^{243}Am	1.50×10^{27}	-4.04×10^{26}	3.19	3.36	-8.50×10^{26}	3.32	3.35
^{242}Cm	1.92×10^{24}	1.67×10^{26}	6.42	6.82	1.76×10^{26}	1.63	1.60
^{243}Cm	6.69×10^{24}	2.05×10^{25}	16.00	15.49	1.37×10^{25}	18.91	19.36
^{244}Cm	4.89×10^{26}	3.98×10^{26}	3.09	3.14	6.50×10^{26}	5.68	5.62
^{245}Cm	1.19×10^{26}	3.80×10^{25}	6.99	7.26	7.93×10^{25}	16.20	16.24
^{246}Cm	8.49×10^{24}	2.49×10^{25}	5.99	5.97	2.99×10^{25}	13.24	12.96
^{247}Cm	-	3.11×10^{24}	8.55	8.26	3.37×10^{24}	24.57	25.13
^{248}Cm	-	3.46×10^{23}	10.07	9.76	3.69×10^{23}	34.02	33.01
^{249}Bk	-	5.27×10^{21}	10.72	10.35	5.28×10^{21}	42.41	42.24
^{249}Cf	-	5.54×10^{21}	10.58	10.25	5.44×10^{21}	42.89	42.48
^{250}Cf	-	1.04×10^{21}	12.28	12.07	1.10×10^{21}	48.44	48.05
^{251}Cf	-	5.23×10^{19}	14.88	14.67	3.87×10^{19}	53.23	52.40
^{252}Cf	-	1.00×10^{18}	15.65	15.56	7.95×10^{17}	57.86	57.94

TABLE 6.17: Uncertainties due to different cross section libraries on the atomic composition of fission products for a ESFR characteristic fuel cell after 99 GWd/THM burn-up, comparing two Hybrid Method approaches: using one-group cross section uncertainties with correlated sampling (1g) and using multi-group cross section uncertainties (211g/44g).

		EAF-2010			SCALE6.0		
Nuclide	N_i	N_f - N_i	Uncertainty (%)		N_f - N_i	Uncertainty (%)	
	(atoms)	(atoms)	1g	211g	(atoms)	1g	44g
^{93m}Nb	-	1.27×10^{21}	5.66	5.96	1.31×10^{21}	0.64	0.63
^{94}Nb	-	7.34×10^{21}	12.58	12.87	8.86×10^{21}	4.93	4.97
^{93}Mo	-	8.91×10^{18}	30.22	31.28	9.67×10^{18}	2.35	2.26
^{103}Rh	-	1.64×10^{27}	5.08	5.31	1.69×10^{27}	1.13	1.07
^{107}Pd	-	7.80×10^{26}	4.58	6.75	8.09×10^{26}	2.31	2.26
^{109}Ag	-	4.08×10^{26}	5.51	8.14	4.23×10^{26}	2.18	2.16
^{126}Sn	-	6.24×10^{25}	4.80	4.95	6.47×10^{25}	0.79	0.80
^{126}Sb	-	3.51×10^{22}	4.80	5.92	6.17×10^{22}	6.98	7.00
^{126m}Sb	-	6.13×10^{19}	6.17	6.85	6.40×10^{19}	1.08	1.06
^{129}I	-	3.36×10^{26}	4.79	5.29	3.32×10^{26}	1.41	1.38
^{149}Sm	-	2.68×10^{26}	5.47	6.63	2.82×10^{26}	5.20	5.22
^{150}Sm	-	1.31×10^{26}	7.06	7.70	1.32×10^{26}	10.38	10.24
^{151}Sm	-	1.46×10^{26}	5.08	7.19	1.43×10^{26}	8.81	8.95
^{152}Sm	-	2.46×10^{26}	4.97	7.54	2.61×10^{26}	4.64	4.72
^{151}Eu	-	2.19×10^{24}	6.70	8.27	1.97×10^{24}	10.02	10.36
^{153}Eu	-	8.48×10^{25}	12.08	13.00	8.65×10^{25}	6.37	6.77
^{155}Gd	-	1.30×10^{25}	6.53	8.78	1.39×10^{25}	4.37	4.36

The evolution of the number of atoms and its uncertainty as a function of burn-up is presented for ^{235}U, ^{236}U, ^{239}Pu, ^{240}Pu, ^{242m}Am and ^{243}Cm in Fig. 6.59, while for ^{107}Pd, ^{109}Ag, ^{151}Sm, ^{152}Sm, ^{151}Eu and ^{155}Gd in Fig. 6.60. There, the outcomes of using EAF-2010 and SCALE6.0, with one-group uncertainties (1g) or multi-group uncertainties (211g/44g), are shown.

When using SCALE6.0, only ^{236}U presents a non-negligible difference between using 1g- or 44g- approaches. It comes from the fact that its uncertainty is mainly dominated by the capture reaction of ^{235}U, whose uncertainty reached with the 1g-approach has a positive bias of 3.66% from the reference value, while this bias with the 44g-approach is negative and of 4.29%. Therefore, the difference between uncertainties reached with each approach for the same cross section is large enough to drive the observed difference.

For EAF-2010, the differences arisen in FPs between the 1g-approach and the 211g-approach are due to differences between the cross section uncertainties for fission reactions reached with each approach, as already explained for the ^{236}U case. In addition, the effect of truncating the PDF is also involved. For the rest of the nuclides not presented, the same uncertainty

values are reached using one-group or multi-group. This was expected because the spectrum changes are almost negligible throughout the whole burn-up.

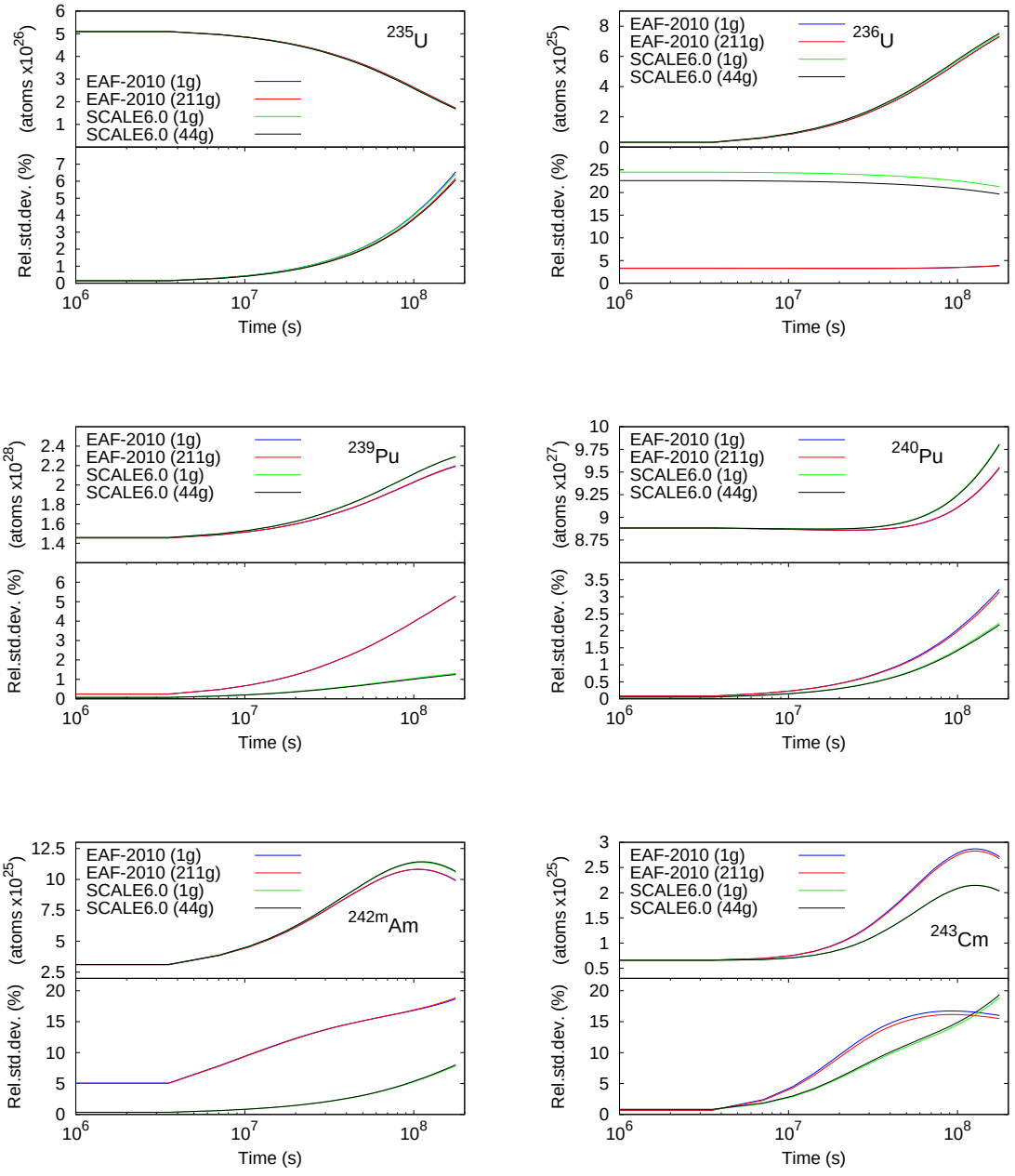

FIGURE 6.59: Evolution of the number of atoms and their uncertainties of the main transuranic nuclides as a function of burn-up time for a ESFR fuel cell up to 99 GWd/THM. Results with EAF-2010 and SCALE6.0 libraries, in one-group (1g) and in multi-group (211g/44g) are presented.

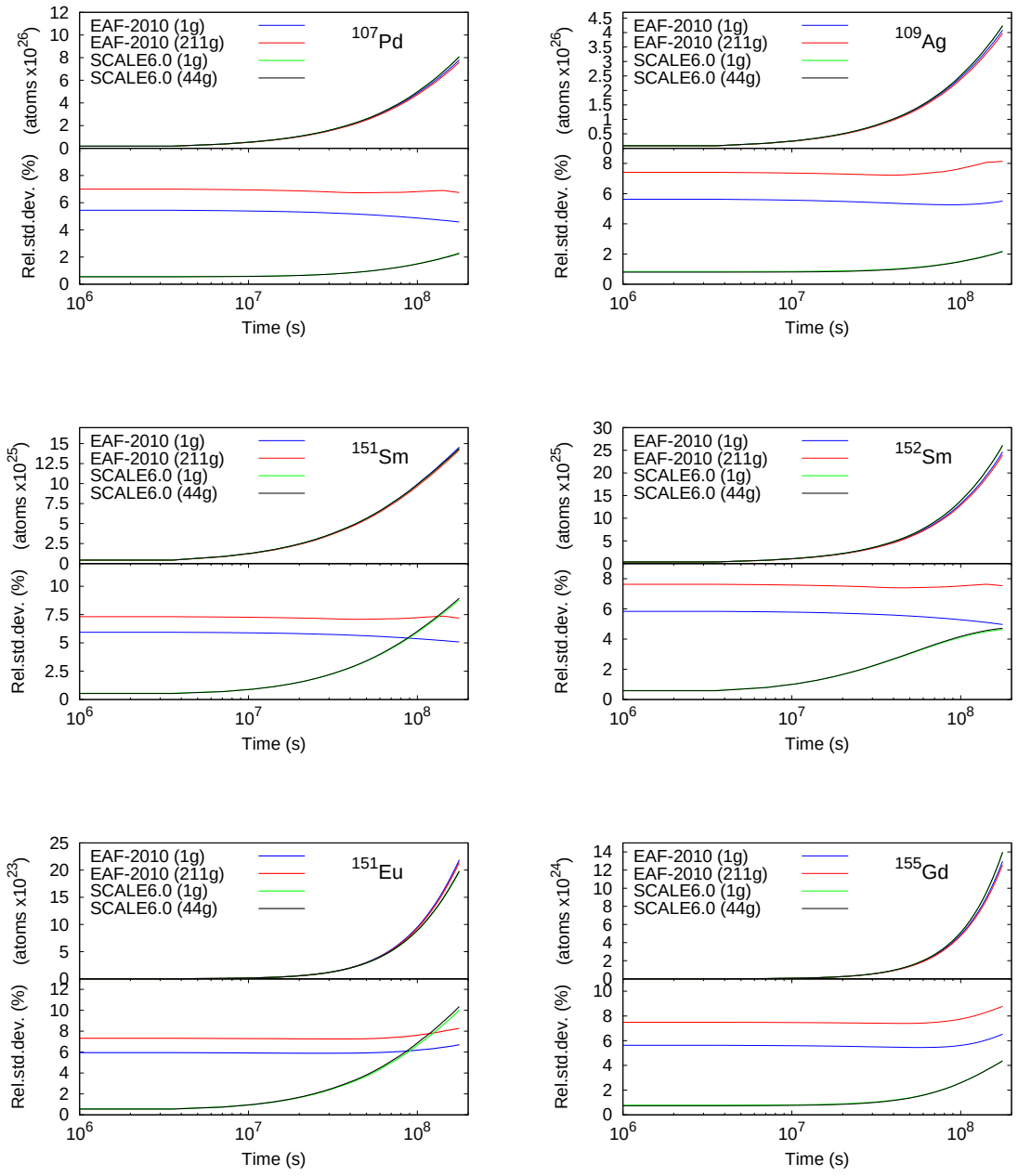

FIGURE 6.60: Evolution of the number of atoms and their uncertainties of a set of fission products (FP) as a function of burn-up time for a ESFR fuel cell up to 99 GWd/THM. Results with EAF-2010 and SCALE6.0 libraries, in one-group (1g) and in multi-group (211g/44g) are presented.

6.3.3 Conclusions from the UQ study on ESFR

A UQ study on the isotopic composition of a characteristic pin-cell of the ESFR fuel cycle has been carried out, making use of the Hybrid Method and propagating nuclear data uncertainties in decay data, fission yields and cross sections.

Because the depletion calculations consists in five (5) burn-up steps, different approaches of the Hybrid Method have be applied. First, the one-group cross section approach is used, showing the need of performing correlated sampling. Then, results from using correlated sampling are validated by comparing with the multi-group approach. Only differences between one-group with correlated sampling and multi-group approaches are found for fission product when EAF-2010 is used, such as the cases of ^{107}Pd and ^{109}Ag. The truncation of PDFs to avoid negative values (due to the usage of Gaussian PDFs), by setting them to zero, seems to be the issue, in addition to differences obtained between the sampled cross section uncertainties using one-group and multi-group approaches. Only for ^{236}U, differences between 1g- and 44g- approaches using SCALE6.0 have been found, whose origin is again the differences in the sampled cross section uncertainties between using one-group and multi-group approaches.

Regarding the uncertainty values obtained for the isotopic composition, cross sections are again the most importance source of uncertainty for uranic and transuranic isotopes. However, fission yields are of importance for several fission products: ^{93m}Nb, ^{94}Nb, ^{93}Mo, ^{126}Sb and ^{126m}Sb, whose induced uncertainty exceeds 10%, being even higher than the contribution due to cross sections. Decay data uncertainties are only of importance again for only two fission products: ^{126}Sb and ^{151}Eu. Both of them have been already identified also in the UQ study for EFIT (Sec. 6.2).

The performance of the different cross section libraries are studied, where COMMARA2.0 yields very similar results to SCALE6.0. There are exceptions for heavier isotopes than ^{248}Cm, where COMMARA2.0 provides smaller values than SCALE6.0. The same results as for EFIT are extracted here when SCALE6.0 and EAF-2010 are compared: the propagation of EAF-2010 uncertainties results into higher uncertainty values than when propagating SCALE6.0 uncertainties, except for isotopes heavier than ^{244}Cm.

Finally, the target accuracies given in [Salvatores et al., 2008] for advanced reactors are checked. The same uncertainty limits are for ESFR as for EFIT:

- Major nuclide isotope concentrations at the end of burn-up: 2%.

- Other nuclide isotope concentrations at the end of burn-up: 10%.

Neither 2% nor 5% limits are fulfilled for major isotopes. Only the following isotopic concentration uncertainties are within the target accuracies:

- When using SCALE6.0: ^{232}U, ^{234}U, ^{238}U, ^{237}Np, ^{238}Np, ^{239}Np, ^{238}Pu, ^{239}Pu, ^{240}Pu, ^{241}Pu, ^{242}Pu, ^{244}Pu, ^{241}Am, ^{242}Am, ^{243}Am, ^{242}Cm.
- When using EAF-2010: ^{236}U, ^{237}U, ^{238}U, ^{238}Np, ^{239}Np, ^{240}Pu, ^{242}Pu, ^{244}Pu, ^{243}Am, ^{244}Cm.

However, for uranic and transuranic isotopes, uncertainties are in almost every cases below 10%. Concerning fission product concentrations of those isotopes mentioned before, since the fission yield uncertainty contribution is equal or even larger than the cross section one, their final uncertainties will surpass such limits.

Chapter 7

Comparing methodologies with the Hybrid Method

Abstract - This Chapter collects the comparisons performed between other methodologies and the Hybrid Method. The aim is to show a comparison between approaches and to assess the limitations of the Hybrid Method due to its implementation and assumptions. Since comparisons with First Order Perturbation theory were already shown, only Monte Carlo sampling approaches are compared. Two methodologies are chosen: Total Monte Carlo (TMC) and NUDUNA, both already described in Chapter 3, Sec. 3.4 and Sec. 3.5, respectively. Equivalent working frameworks for the Hybrid Method and the compared methodology are used in order to analyse properly their differences/equivalences. An additional exercise is carried out for assessing the limitations of the one-group with correlated sampling approach.

This chapter shows, partially or completely, works already presented in the following references:

- ANDES Deliverable D2.5 [Mills et al., 2013].
- International Journal Article [Díez et al., 2013a].
- International Journal Article [Díez et al., 2014c].
- International Journal Article [Díez et al., 2014a].

7.1 Comparison of methodologies: TMC vs Hybrid Method

7.1.1 Differences between methodologies

Differences between TMC and HM are investigated based on their descriptions given in Chapter 3 and 4, respectively.

The first one is related to which variables are treated as random, and thus sampled. In TMC, the nuclear model parameters are sampled, meanwhile in HM, the cross-sections are directly sampled from the covariance information provided by nuclear data libraries after processing. Both of them have the same objective of producing random nuclear data libraries to perform uncertainty propagation calculations by means of Monte Carlo sampling.

The next difference is which uncertainty values are being propagated for each cross-section. The TMC approach can use different sources of information to calculate their random files, such as the EXFOR database (experimental data), nuclear data libraries or/and other compilations. These sources can be mixed or used individually. Meanwhile, HM only propagates the uncertainty information, given as covariance matrices, of the nuclear data library used.

The third difference is that TMC does not need the neutron spectrum of the application for generating random cross-section libraries, while HM needs first to process the nuclear data, and that means the neutron spectrum is needed before new random libraries are generated.

Covariance data used in HM and TMC can be completely equivalent if uncertainty data provided with TMC through random files are condensed into covariance matrices. This condensation is performed with an statistical analysis of the data provided within TMC random files. The output of the statistical analysis are the mean values and covariance matrices required for HM. In this way, uncertainties propagated with HM and TMC are expected to be the same. Fig.7.1 presents the flowchart of using TMC as a source of uncertainty information for HM.

More differences can be found between TMC and HM since there is at least one assumption in HM not found in TMC: the chosen PDF to sample cross-section information. Thus, HM can be partially/totally based on the TMC approach. However, the equivalence between approaches has to be checked, apart from the assessment of which information has been lost during the condensation process. These issues are addressed by applying both methodologies to the same problem under the basis proposed before, and represented in Fig. 7.1.

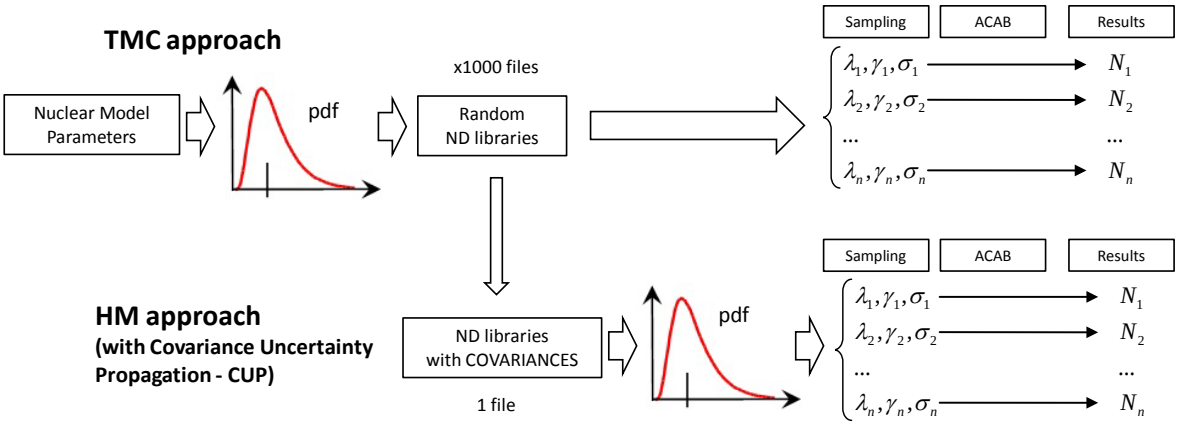

FIGURE 7.1: Flowchart of TMC, and HM based on TMC covariance data, applied to depletion calculations performed with the ACAB depletion code.

7.1.2 TMC and HM applied to a depletion calculation

The purpose of applying TMC and HM to a depletion calculation is to address the previous issues about differences between both approaches, and to check the equivalence of both approaches in uncertainty propagation calculations under the proposed framework: depletion calculations where HM uses the covariance data provided by TMC.

In order to take advantage of previous works, the EFIT fuel cycle depletion problem for 150 GWd/THM discharge burn-up is recalled (see Chapter 6, Sec. 6.2). The impact of using one or the other approach will be analysed with the propagation of cross section uncertainties, applying random libraries and covariance information retrieved from TENDL-2010. The one-group approach without correlated sampling will be used for HM as the depletion problem consists in only one depletion step. TMC can also generate one-group cross section random files, just the random files need to be collapsed to one-group cross section.

The depletion code used is ACAB, so only nuclear data processed for ACAB have to be prepared. Fission yield and decay data are taken from JEFF-3.1.1, while cross section data (from TENDL-2010) have be processed from ENDF-6 format into ACAB format. Such a task can be carried out thanks to the sequence described in Chapter 4. Random data obtained from sampling covariance information or from random ENDF-6 format files are merged with the complete library of EAF-2010, from which only reference cross section values are used, not uncertainties.

Uncertainties in concentrations of those isotopes, whose uncertainties are propagated, are analysed: four heavy isotopes – ^{235}U, ^{238}U, ^{239}Pu, ^{241}Pu; and one medium mass range isotope:

^{98}Mo. Only results for ^{239}Pu and ^{241}Pu are presented here, as done in [Díez et al., 2013a], whereas the rest can be found in [Mills et al., 2013, Appendix A].

Note that the equivalent working framework used here for HM and TMC is based on two assumptions:

1. The covariance information has to come from the random cross-sections files generated with TMC. For this reason, TENDL-2010 is chosen as the source of random libraries. It includes the covariance information obtained from the random files. The condensing stage is thus supposed to be checked and well done. The number of random files used for each isotope is enough to achieve the convergence of cross sections and depletion results.

2. The chosen PDF for sampling cross sections have to be the same for HM and TMC. As mentioned in Chapter 3, Sec. 3.4, TASMAN can use uniform or Normal PDFs to sample the nuclear data parameters. For TENDL-2010, the Normal PDF was used. Therefore assuming Normal PDFs for HM seems reasonable. Nevertheless, it should be checked whether TMC and HM one-group random cross sections follow the same PDF.

7.1.2.1 Application of TMC

The application of TMC to this problem can be split into four stages. The first one is the generation of random cross section libraries, where TASMAN is used. The second one is to process and collapse the random libraries using NJOY. The third stage is to translate from ENDF-6 format to ACAB format. The last stage is to feed ACAB with these random libraries and perform a statistical analysis on concentrations. These stages are represented in Fig. 7.2(a).

7.1.2.2 Application of HM

The scheme of application of HM, given in Fig. 7.2(b), is quite similar to the TMC one. The first stage is to process the nominal cross section data libraries with their uncertainty information and to collapse them into one-group. Then, the second stage is to convert the nominal libraries in one-group from ENDF-6 format to ACAB format. The third stage consists in the generation of random libraries in ACAB format. After sampling cross section

libraries, the final stage is to feed ACAB with the random libraries and perform a statistical analysis to calculate the uncertainty on concentrations.

The Hybrid Method is referred in [Díez et al., 2013a] as the Covariance Uncertainty Propagation (CUP), because with HM covariance uncertainty data generated with TMC are propagated. So any reference to CUP, from now onwards, means that the Hybrid Method is applied.

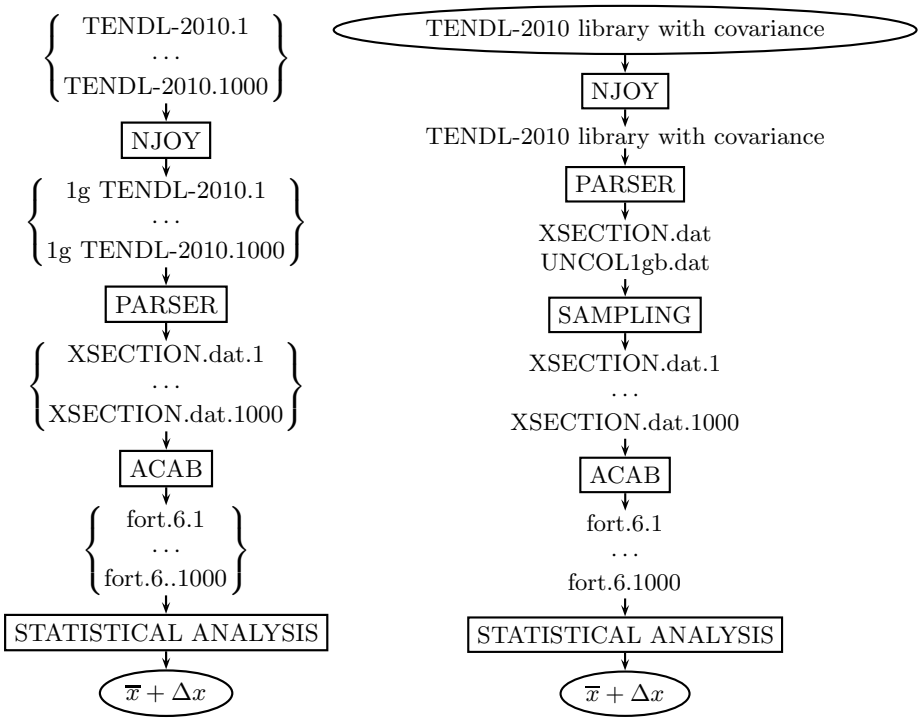

(a). TMC *(b).* HM

FIGURE 7.2: Flowcharts of both approaches applied to depletion calculations using the ACAB code, where the different modules/codes used with their corresponding input/output files are depicted.

7.1.3 Results and data analysis

The results for each studied isotope is presented by means of a consistent comparison between TMC and HM approaches. For all figures, blue colour refers to the TMC approach while red refers to HM, with the only exception of the ratios between TMC and HM that are presented in red.

7.1.3.1 ^{239}Pu

For ^{239}Pu, 700 random files (TMC) from TENDL-2010 are used, and then the same amount is generated with HM.

After processing all random files, the main reaction cross sections, (n,fission) and (n,γ), are compared and shown in Fig.7.3. There, the mean and relative standard deviation (rel.std.dev.) obtained from sampling with TMC and collapsed to one-group, and the mean and rel.std.dev. values of one-group cross sections sampled with HM, are compared with the one group cross section mean and rel.std.dev. values obtained from processing the TENDL-2010 nominal library with covariances. These nominal/reference values can be read in the labels of y-axes. Since HM uses Normal PDFs based on reference values and nominal values are based on TMC random values, the ratios of mean and rel.std.dev. values from the ones obtained with TMC and HM to reference values should be close to one. However, deviations could appear because of the statistics and truncation effects.

When the cross sections for TMC are analysed, one can observe:

- In Fig. 7.3(a), the largest ^{239}Pu cross section, (n,fission), is presented. Its cross section value is 1.912 barns with a rel.std.dev. of 1.0043%. Both TMC and HM mean values are close to the reference (less than 0.3% difference). The TMC rel.std.dev. is around 7.5% greater than the reference while the HM rel.std.dev. is close to the reference.
- In Fig. 7.3(b), the second largest cross section, (n,γ), is shown, and it is equal to 6.550×10^{-1} barns with an uncertainty of 3.269%. The HM mean value is close to the reference, while the TMC mean value is 1.2% smaller. In contrast, both sampled rel.std.dev. are close to each other, approx. 2% smaller than the reference.

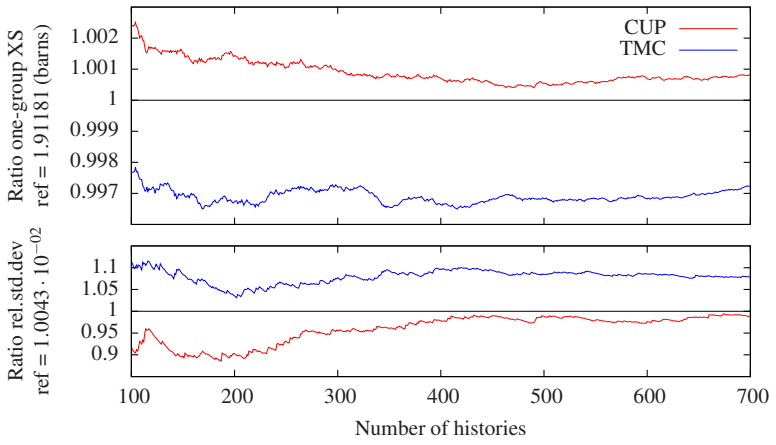

(a). (n,fission) cross section

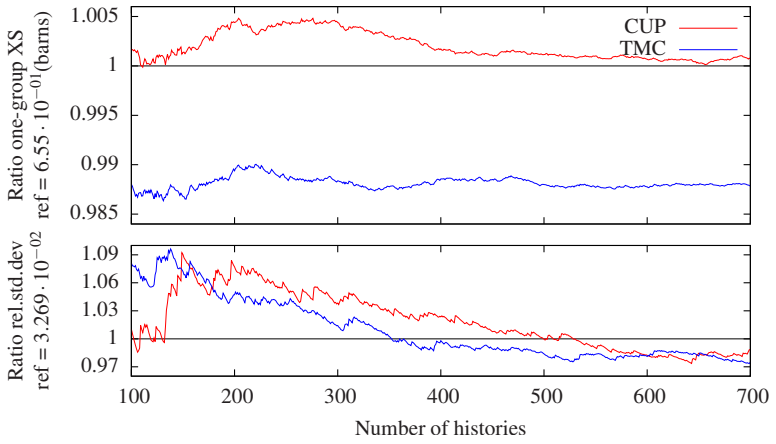

(b). (n,γ) cross section

FIGURE 7.3: Comparison of TMC and HM one-group cross section values and their relative standard deviation (rel.std.dev.) as a function of the number of random files for ^{239}Pu.

For both main reactions presented, (n,fission) and (n,γ), random files from TMC and HM are in close agreement with each other and with the reference values. All other reactions have a nominal mean value less than 10^{-3} barns, not being considered of relevance for the analysis.

To check that both approaches give the same PDFs, Fig.7.4 is presented. The black line is the Normal PDF which the random cross section values obtained with HM should follow. In Fig.7.4(a), a good agreement among PDFs (from TMC, HM and ideal Normal PDF) is observed for the (n,fission) reaction. Fig.7.4(b) shows the (n,γ) reaction, where the PDF of TMC differs from the Normal PDF. Consequently, it will lead to different results when the number of atoms' PDF is analysed.

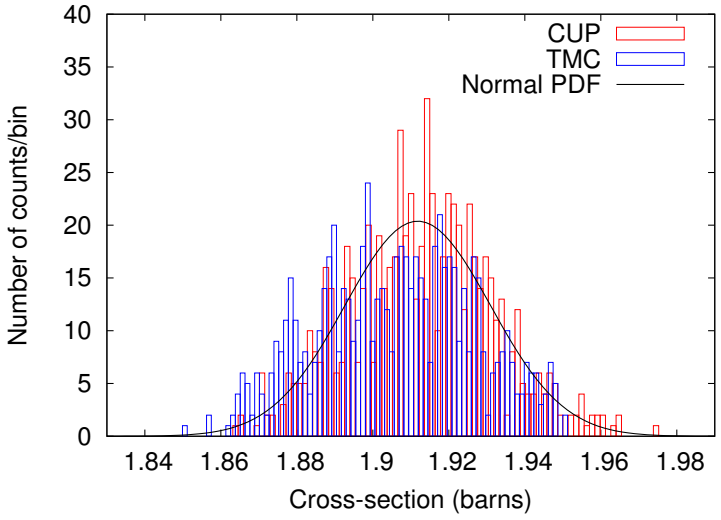

(a). (n,fission) cross section

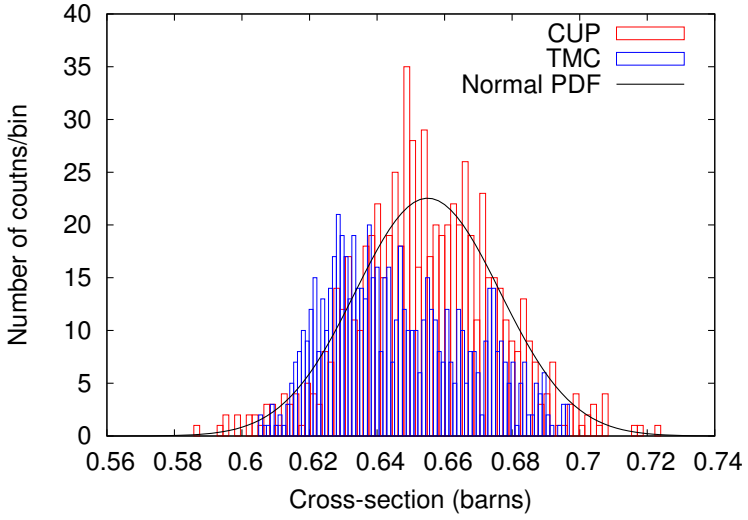

(b). (n,γ) cross section

FIGURE 7.4: One-group cross section histograms from HM and TMC random files for ^{239}Pu reactions, and the Normal PDF generated with the nominal covariance information.

Cross-correlations are not important is this calculation, because the covariance matrix between the main reactions (n,fission) and (n,γ), presented in Fig.7.5(b), shows that there are only small correlations. When this correlation is collapsed to one-group, a value of 3×10^{-3} is obtained. Thus its effect is negligible, as seen in Fig.7.5(a), where each point represents a pair of (n,fission) and (n,γ) cross sections of the same random library.

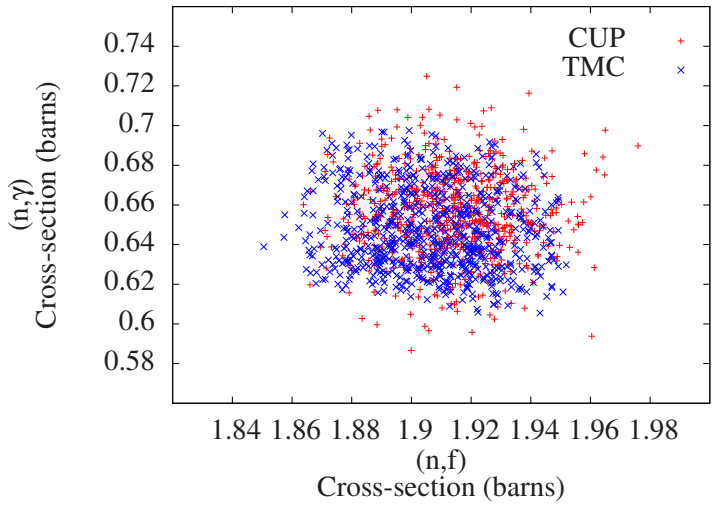

(a). TMC/HM (n,fission)-(n,γ) cross sections

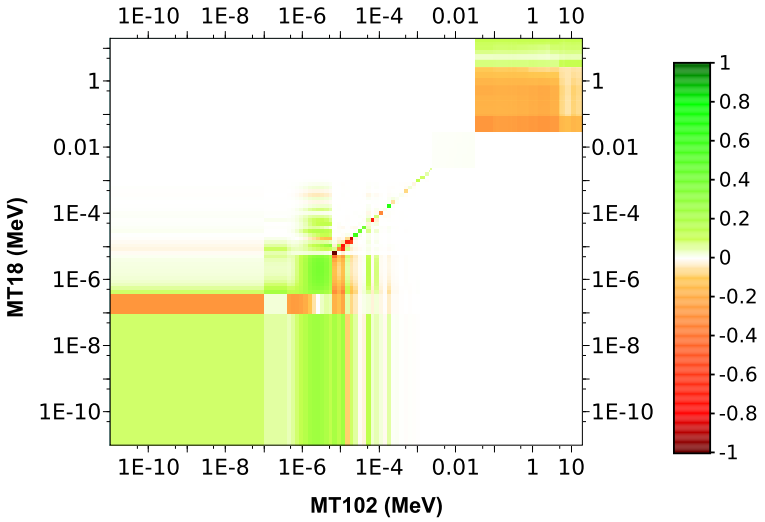

(b). Nominal (n,fission)-(n,γ) correlation matrix

FIGURE 7.5: Comparison of the pair (n,fission)-(n,γ) cross section values of TMC and HM, and the correlation matrix in multi-group provided with TENDL-2010 for ^{239}Pu.

All these random files generated with TMC and HM are used for the EFIT fuel cycle calculations with ACAB. Only the atomic concentrations throughout the burn-up are analysed and presented in Fig.7.6.

The ratio of mean values of HM/TMC shows that both values are close to each other and its difference is less than 0.3% at the end of burn-up. The rel.std.dev. is only appreciated above 10^7 s of burn-up for both approaches. The ratio HM/TMC shows that the HM rel.std.dev. is 4.8% higher than TMC. Below 10^6 s, results are meaningless because the precision used for storing numbers was not enough to appreciate variations on the rel.std.dev. The histogram of the number of atoms of ^{239}Pu at the end of burn-up is presented in Fig. 7.7. The percentile

95 for TMC is greater than for HM, so that the tail of TMC provides greater values than HM, even though HM provides a slightly higher rel.std.dev. than TMC.

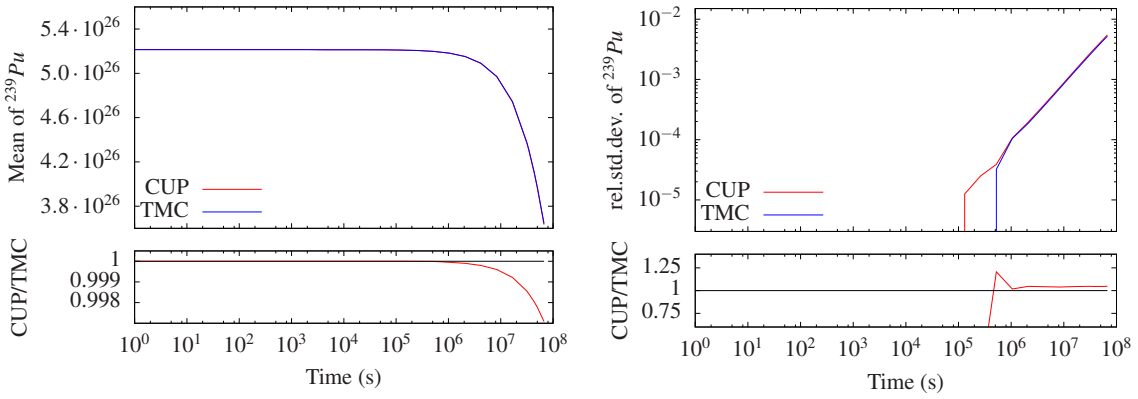

(a). mean value

(b). rel.std.dev.

FIGURE 7.6: TMC and HM statistics of the number of ^{239}Pu atoms during burn-up.

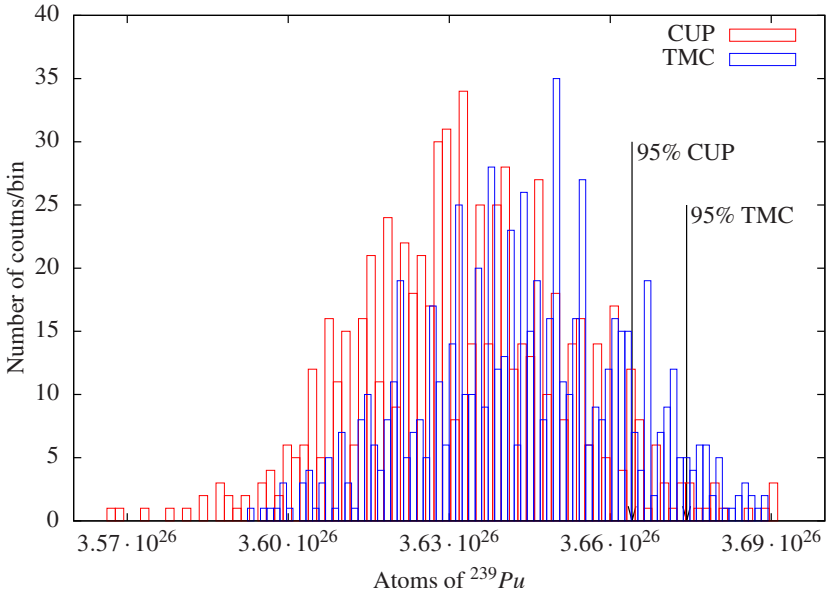

FIGURE 7.7: Histogram of the number of ^{239}Pu atoms at the end of burn-up for results from TMC and HM.

The convergence is checked for all time steps as done for the last burn-up step (at the end of burn-up) shown in Fig. 7.8. Increasing the number of histories above 500 changes neither mean values nor rel.std.dev.

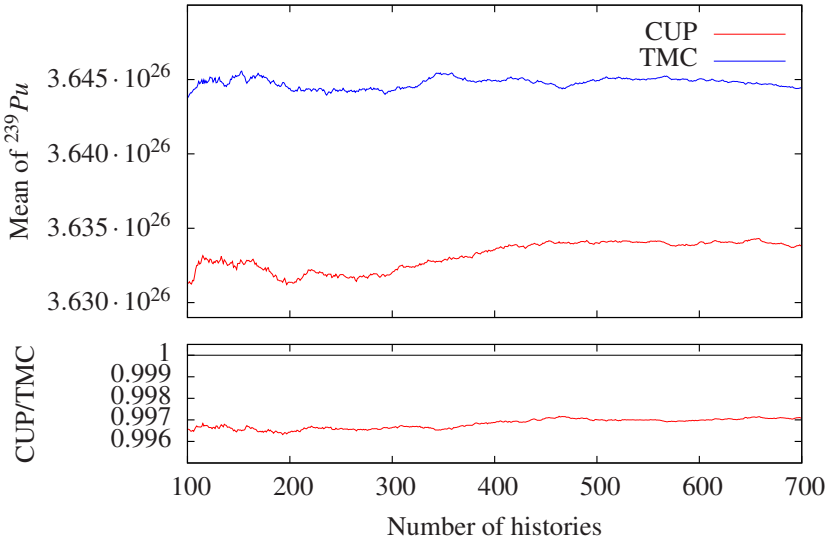

(a). mean value

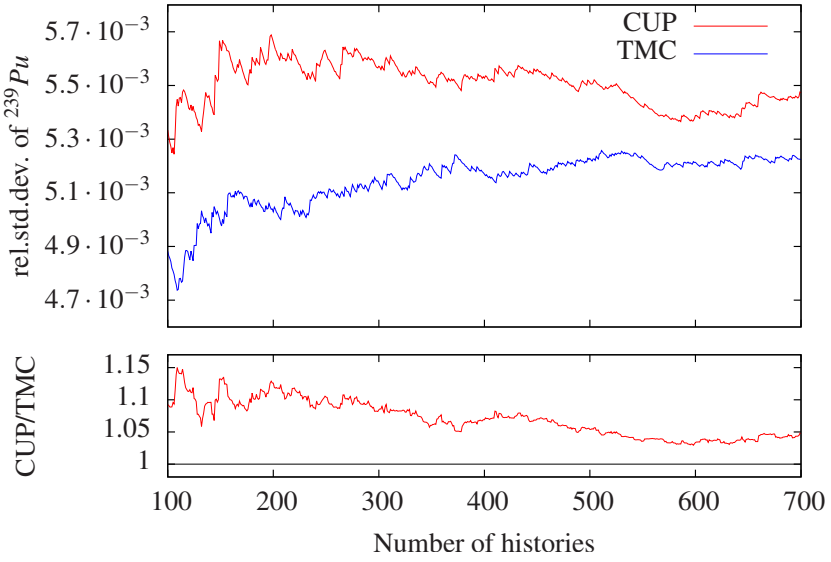

(b). rel.std.dev.

FIGURE 7.8: Mean value, its rel.std.dev. and the ratio HM/TMC for the number of ^{239}Pu atoms as a function of the number of histories at the end of burn-up.

The 4.8% difference between the rel.std.dev. of TMC and HM for the atomic density of ^{239}Pu comes from:

- The bias between mean and reference values obtained for each approach. However, the most important reactions are in close agreement between each other. Only for (n,γ) reaction, TMC provides a mean value 1.2% smaller than the one provided by HM.

- The bias between rel.std.dev. from samples and the reference one for each approach, especially for the (n,fission) reaction, where the TMC rel.std.dev. is about 8% higher than the HM one.
- The assumption of Normal PDF for the HM approach, because it does not yield a completely equivalent PDF for (n,γ) cross sections as given by TMC.
- The cross-correlations between reactions are not taken into account in the HM approach. However, as stated previously, the TMC approach does not exhibit cross-correlations among the most important reactions.
- Differences during the condensation process for covariance information generation from the random files of TMC. Instead of using the mean value (the mean value obtained from all random libraries) for calculating the covariance terms, the best-estimated value (which fits best the experimental data) is used instead. Therefore, a small bias between the HM mean value and the TMC mean value appears.

7.1.3.2 ^{241}Pu

For ^{241}Pu, the implementation of TMC and HM uses, as done for ^{239}Pu, an amount of 700 random libraries for each approach.

After processing all random files and generating 700 random files with the HM approach, the main reaction cross sections, (n,fission) and (n,γ), are compared and shown in Fig. 7.9 as a function of the number of random libraries. The statistical values presented are the ratios of the sampled mean and sampled rel.stad.dev. to the reference values provided with the nominal TENDL-2010 file, reading such reference values in the y-axis label.

In Fig. 7.9, differences are found between HM and TMC:

- In Fig. 7.9(a), the most important reaction of ^{241}Pu, (n,fission), with a cross section of 1.53 barns and a rel.std.dev. of 3.291×10^{-2}, is presented. For this reaction, TMC and HM provide mean values which are 1% smaller than the reference. Their rel.std.dev. values reach a good agreement with the reference, with TMC providing a rel.std.dev. value 4% smaller than reference and HM giving a rel.std.dev. 2% higher.
- In Fig. 7.9(b), the second largest cross section, (n,γ), is presented, with a cross section value of 3.648×10^{-1} barns and a rel.std.dev. of 1.393×10^{-1}. Here, TMC provides

a mean value 2.5% greater than reference while HM provides a mean value with a difference smaller than 0.5% to the reference. The rel.std.dev. provided by TMC is 4% greater than the reference, while the HM rel.std.dev. is less than 1% smaller than the reference.

Therefore, for these two reactions, the random files of TMC and HM do not present relevant differences between each other.

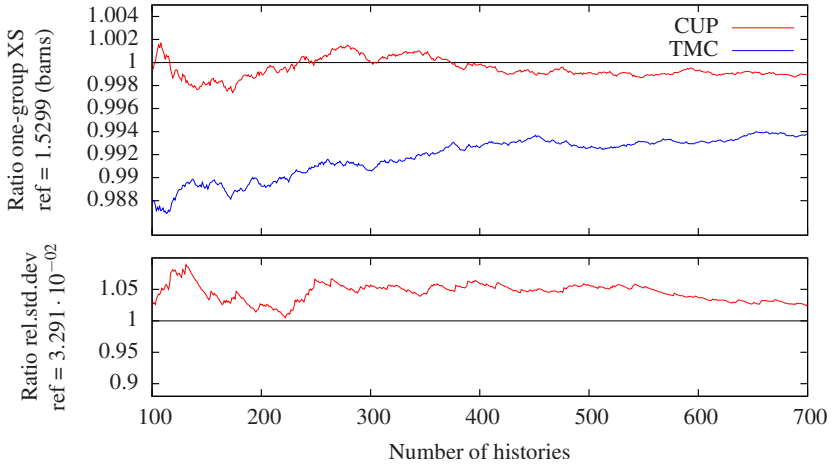

(a). (n,fission) cross section

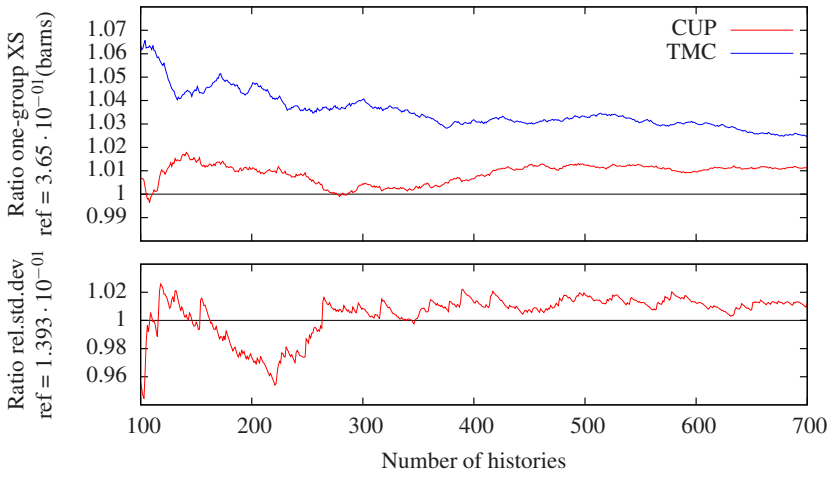

(b). (n,γ) cross section

FIGURE 7.9: Comparison of TMC and HM one-group cross-section values and their rel.std.dev. as a function of the number of random files for ^{241}Pu.

Histograms for (n,fission) and (n,γ) reactions from each approach are presented in Fig. 7.10. The black solid line represents the Normal PDF with the nominal cross section values that the HM should follow. For the (n,fission) reaction, PDFs are in close agreement with each other, with both shapes following the shape of a Normal PDF. Meanwhile, for the (n,γ) reaction,

the TMC PDF does not follow a Normal PDF, becoming a source for later differences in the results of depletion calculations.

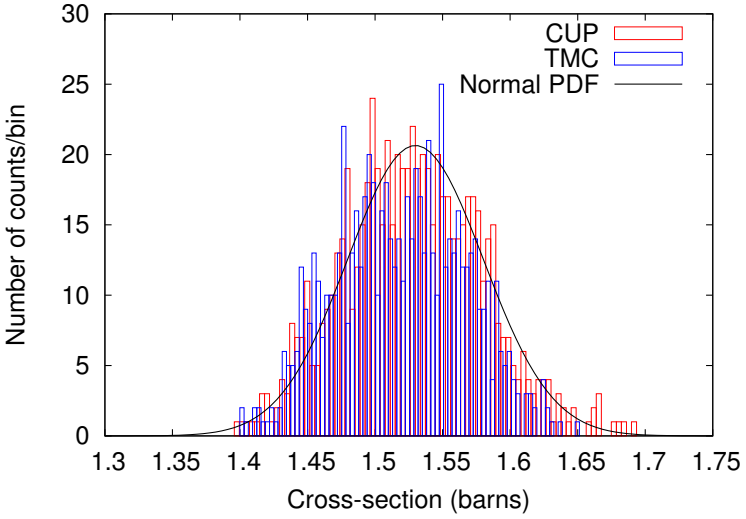

(a). (n,fission) cross section

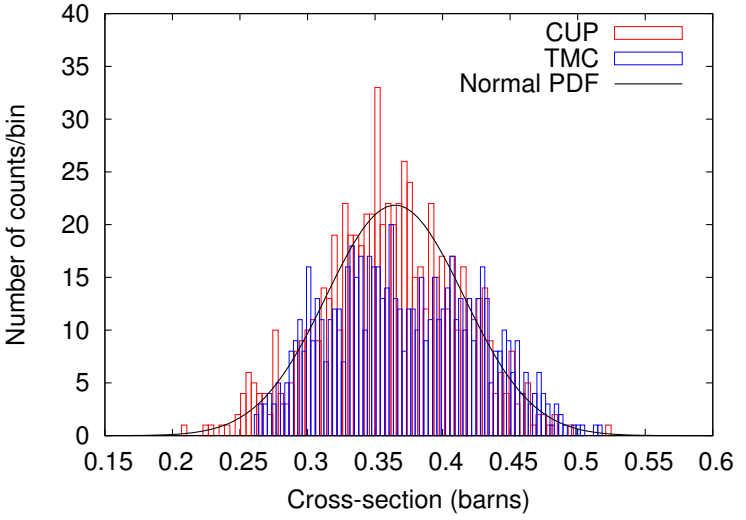

(b). (n,γ) cross section

FIGURE 7.10: One-group cross section histograms from HM and TMC random files for ^{241}Pu reactions, and the Normal PDF generated with the nominal covariance information.

For ^{241}Pu, the cross-correlation matrix for (n,fission)-(n,γ) cross sections provided with TENDL-2010, presented in Fig. 7.11(b), shows an anti-correlation between reactions. This correlation has to be taken into account if equivalent results from TMC and HM are desired. The correlation factor provided with the TENDL file for ^{241}Pu is -0.8370, while the correlation extracted from the TMC random one-group cross sections is -0.81792, so there is a good agreement between nominal and sampled values. The former value is included in the

sampling stage of HM, obtaining a sampled correlation factor of -0.83414. The scatter plot of both approaches can be observed in Fig. 7.11(a), where linear least-squared fittings have been performed and shown with linear functions for both sets of random values. Again, both random sets are in close agreement to each other.

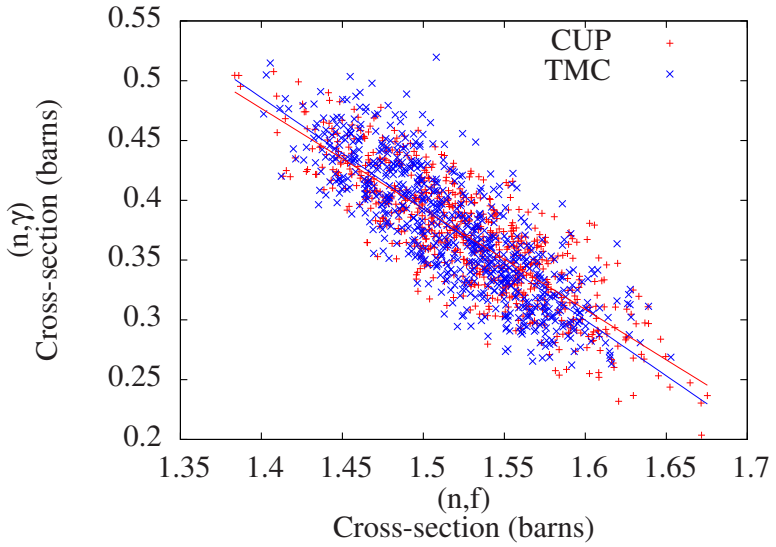

(a). TMC/HM (n,fission)-(n,γ) cross sections

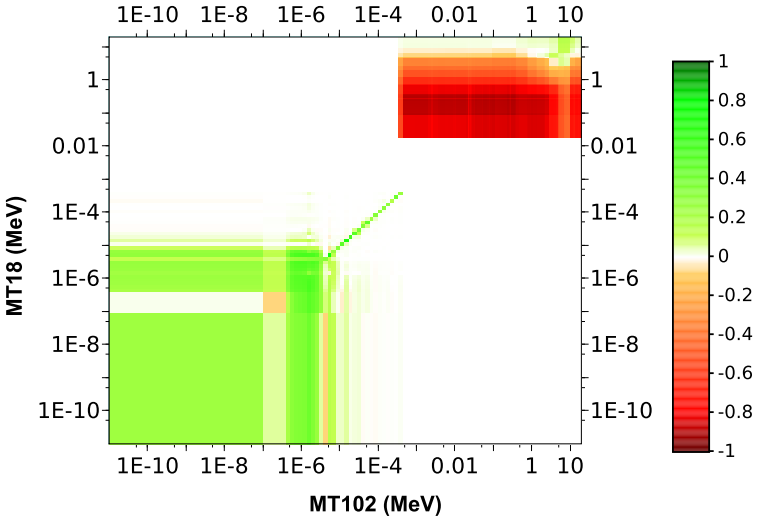

(b). Nominal (n,fission)-(n,γ) correlation matrix

FIGURE 7.11: Comparison of the pair (n,f)-(n,γ) one-group cross sections values of TMC and HM and the correlation matrix in multi-group provided in TENDL-2010 for ^{241}Pu.

After analysing the differences for the main cross sections, ACAB is fed with them. Only the number of atoms during burn-up is followed through Fig. 7.12(a). The ratio of mean values of HM/TMC shows that both values are the same throughout the whole burn-up. When the rel.std.dev. values are observed in Fig. 7.12(b), differences become relevant after 1.05×10^6 s

of burn-up for both approaches. As for ^{239}Pu, below 10^6 s results are meaningless due to the same reason. The ratio HM/TMC for rel.std.dev. shows that HM is 0.95 times the TMC value, so a qualitative agreement is reached. When the percentiles 95 are compared, both of them are close to each other, and their histograms show that both approaches yield very similar PDFs.

Again, the convergence is checked by following the mean value and the rel.std.dev. as a function of number of histories, observing that it is guaranteed with 700 random files.

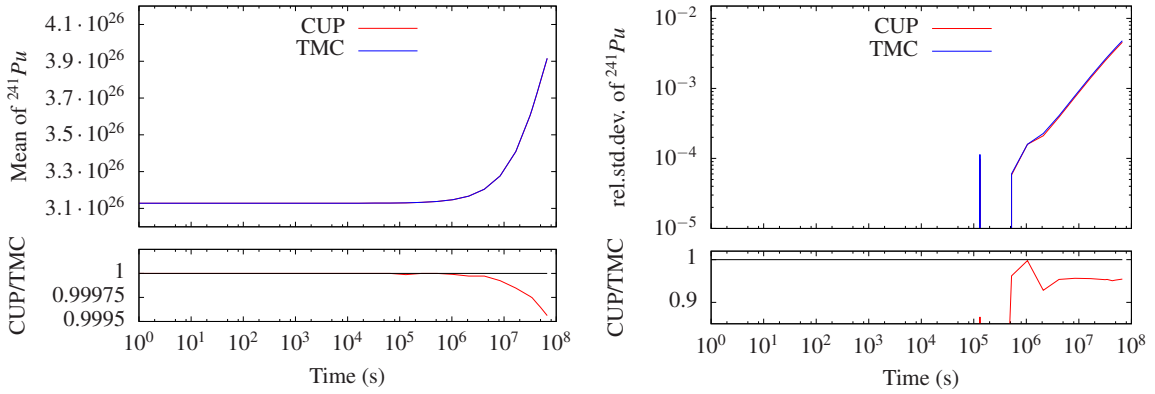

(a). mean value

(b). rel.std.dev.

FIGURE 7.12: Statistics for number of ^{241}Pu atoms during burn-up.

With Table 7.1, the effect of including or not the correlation between (n,fission) and (n,γ) reaction is addressed. When (n,fission) and (n,γ) uncertainties are propagated together considering the cross-correlation ("All reactions" row), a smaller rel.std.dev. is obtained than when these uncertainties are propagated individually (rows "a. (n,fission)" and "b. (n,γ)"). So it reveals the importance of such a negative cross-correlation, which has thus to be taken into account in order to make the HM approach equivalent to TMC. If not included, the HM result goes up to 2.5 times the TMC rel.std.dev. value.

TABLE 7.1: rel.std.dev. values of the number of ^{241}Pu atoms at the end of burn-up.

rel.std.dev.	TMC	HM	HM without cross-correlation
All reactions	0.48%	0.46%	1.14%
a. (n,fission)	0.73%	0.81%	
b. (n,γ)	0.77%	0.75%	

Finally, the sources of differences for the atomic density of ^{241}Pu between the rel.std.dev. of TMC and HM are analysed:

- The bias between mean values of the sampled cross sections from each approach, but as observed before, its effect should be small.
- The bias between rel.std.dev. of the sampled cross sections from each approach, however this effect is negligible since the difference between them does not go above 3% for the most important cross sections.
- The cross-correlations between (n,fission) and (n,γ) reactions have to be taken into account in the HM approach in order to obtain equivalent results to TMC. Once such a correlation is included, it is no longer a source of difference.
- The usage of a different nominal/mean value for the nominal file with covariances from the one obtained from the random files, as described for ^{239}Pu.

7.1.4 Conclusions of the comparison

The comparison of two different Monte Carlo sampling approaches, Total Monte Carlo and Hybrid Method, for nuclear data uncertainty propagation applied to depletion calculations has been performed. For this purpose, the TENDL-2010 library has been used, because it provides random cross-section files and nominal cross section data with covariances based on the random files. With this library, an equivalent working framework is set for comparing TMC and HM.

This comparison has been presented for cross sections of two isotopes: ^{239}Pu and ^{241}Pu, whose uncertainties have been propagated separately using TMC and HM approaches in the EFIT fuel cycle depletion calculation, already addressed in Chapter 6, Sec. 6.2. Differences between HM and TMC random cross section mean values and rel.std.dev. provoke a deviation for the number of atoms during burn-up of the TMC rel.std.dev. from the HM ones. However, such a deviation does not go above 5%. For the case of ^{239}Pu, the histogram obtained from TMC results presents a percentile 95 value higher than the HM one, whereas the rel.std.dev. of HM is greater than of TMC. A large difference between approaches, up to 2.5 times, would be found in ^{241}Pu if cross-correlation between the main reactions, (n,fission) and (n,γ), was not taken into account.

Thus, regarding the issues presented at the beginning of this methodology comparison, the Hybrid Method is almost equivalent to the Total Monte Carlo approach under the proper assumptions: use of the cross section library with covariance information obtained from the random cross section files; and choosing a PDF for sampling cross sections that represents the PDF generated with TMC. However, the Normal PDF is not always the best representation of the TMC approach, and such an assumption could play an important roll in other frameworks such as safety analysis, where the PDF tails of actinides distributions are important for reactivity coefficients or neutron multiplication factor k_{eff}. Therefore, in further studies, different PDFs should be studied and their effects compared, and also in different frameworks in order to check the relevance of choosing one PDF or another. It will be useful to suggest which PDFs should be used to represent the uncertainties of cross section data. Such suggestions could be implemented in the ENDF-6 format.

7.2 Comparison of methodologies: NUDUNA vs Hybrid Method

This comparison allows to assess the importance of taking into account uncertainties in isotopic concentrations, coming mainly from the depletion part, on the transport calculations in burn-up problems. As presented in Chapter 4, the Hybrid Method departs from the assumption of neglecting neutron flux/spectrum uncertainties, taking flux and spectrum as constant in every burn-up step. So, the validity and applicability of such an assumption in burn-up calculations with constant power is also addressed with this comparison. This latter issue can be studied thanks to the NUDUNA capability of including nuclear data uncertainties in both parts, depletion and transport, of a burn-up calculation.

Therefore, both methodologies, NUDUNA and the Hybrid Method, are applied to the same burn-up problem in order to carry out such assessments.

7.2.1 Description of the burn-up problem

The exercise selected is the UAM Benchmark Exercise I-1b TMI-1, described in [Ivanov et al., 2013, Appendix VIII]. It consists in a UQ study on the burn-up problem of a typical PWR pin-cell, whose main specifications are summarised in Fig. 7.13. Here, only Hot Full Power (HFP) conditions are addressed, where the average power density is 33.58 W/gU, and is kept constant during the whole burn-up period of 1825 days. Thus a final burn-up of 61.28 GWd/MTU is achieved. The cross section uncertainties considered in the UQ study are retrieved from SCALE6.0, only for ^{235}U, ^{238}U and ^{239}Pu.

This pin-cell is modelled in SCALE6.0 with HFP conditions, and the burn-up calculation is carried out using the TRITON sequence of SCALE6.0 tool suit with the following parameters: `NITAWL,ADDNUX=2`. Cross section data are retrieved from the nominal ENDF/B-V library of SCALE6.0, since the `NITAWL` option should be switched in order to use NUDUNA random cross section files (see Chapter 3, Section 3.5). The reference calculation with these options for the neutron multiplication factor k_{eff} is presented in Fig. 7.14 which shows the typical PWR pin-cell behaviour.

Only uncertainties in ^{235}U, ^{238}U and ^{239}Pu cross sections are considered for simpleness to assess the different approximations studied here and for being one of the most relevant for burn-up calculations [Ivanov et al., 2013]. Their impact is calculated on k_{eff} and on the

isotopic concentrations of those isotopes given in Table 7.2. They are followed throughout the whole burn-up.

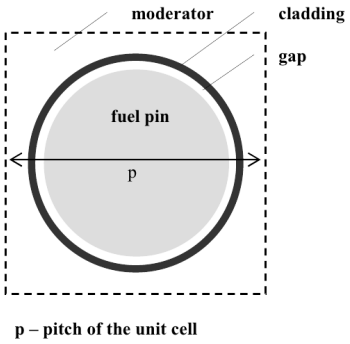

Parameter	Value
Unit cell pitch, [mm]	14.427
Fuel pellet diameter, [mm]	9.391
Fuel pellet material	UO_2
Fuel density, [g/cm^3]	10.283
Fuel enrichment, w/o	4.85
Cladding outside diameter, [mm]	10.928
Cladding thickness, [mm]	0.673
Cladding material	Zircaloy-4
Cladding density, [g/cm^3]	6.55
Gap material	He
Moderator material	H_2O

Parameter / Reactor Condition	HZP	HFP
Fuel Temperature, [K]	551	900
Cladding Temperature, [K]	551	600
Moderator (Coolant) Temperature, [K]	551	562
Moderator (Coolant) Density, [kg/m^3]	766	748.4
Reactor Power ,[MWt]	2.772	2772

FIGURE 7.13: Specifications of the UAM Exercise I-1b TMI-1 modelling a PWR pin-cell. (From [Ivanov et al., 2013])

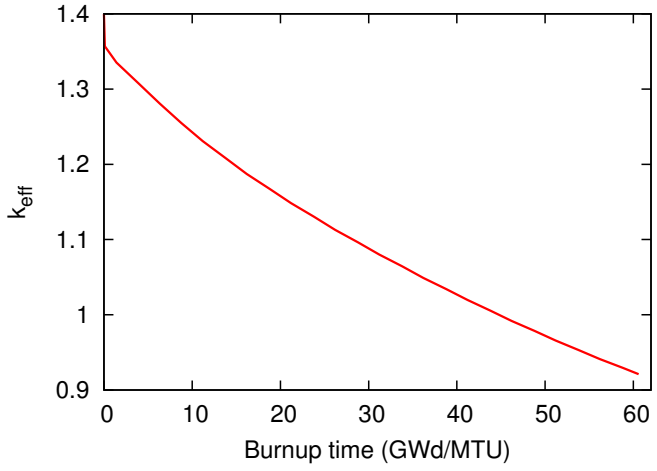

FIGURE 7.14: Evolution of k_{eff} as a function of burn-up, for the UAM Benchmark Exercise I-1b TMI-1 pin-cell. The default ENDF/B-V SCALE6.0 multi-group cross section library is used.

TABLE 7.2: List of isotopes whose concentrations are followed throughout the burn-up process of the UAM Benchmark Exercise I-1b TMI-1 pin-cell.

Light isotopes	^{16}O, ^{90}Sr, ^{95}Mo, ^{99}Tc, ^{109}Ag, ^{103}Rh
	^{106}Ru, ^{133}Cs, ^{134}Cs, ^{137}Cs, ^{135}I, ^{135}Xe
	^{139}La, ^{151}Eu, ^{153}Eu, ^{154}Eu, ^{155}Eu, ^{155}Gd
	^{156}Gd, ^{143}Nd, ^{144}Nd, ^{145}Nd, ^{146}Nd, ^{148}Nd
	^{147}Sm, ^{149}Sm, ^{151}Sm, ^{147}Pm
Heavy isotopes	^{234}U, ^{235}U, ^{236}U, ^{238}U, ^{237}Np, ^{238}Pu
	^{239}Pu, ^{240}Pu, ^{241}Pu, ^{242}Pu, ^{243}Am, ^{244}Cm

7.2.2 Application of the methodologies

7.2.2.1 Application of NUDUNA

As described in Chapter 3, NUDUNA is able to propagate nuclear data uncertainties through complete burn-up problems, taking into account both parts, transport and depletion, at the same time. That is because NUDUNA can generate random cross section data, provided in COVERX files, which are used in both parts of the calculation.

With the TRITON sequence of SCALE6.0, burn-up problems can be tackled, and it can make use of NUDUNA random files. So, random COVERX files are generated for ^{235}U, ^{238}U and ^{239}Pu, and the reference burn-up calculation, described before, is again calculated with every set of random files. For ^{235}U, ^{238}U and ^{239}Pu files, cross section data and fission neutron emission are randomised independently, giving two sets of 200 random files for each isotope. Then, the impact of both parameters in the whole burn-up problem is addressed, and uncertainties on k_{eff} and on isotopic composition are calculated.

Also, NUDUNA can be applied only to the transport part of a burn-up calculation, thanks to one option of the TRITON sequence: `t-newt`; in which transport calculations are performed for a given composition of the fuel. Then, the random files can also be used there for estimating uncertainties only on transport. The composition is extracted from the reference calculation, and again, the same sets of random files are applied at different burn-up points. In this way, uncertainties on isotopic composition are neglected, because no depletion calculation is carried out. Only uncertainty in k_{eff} is thus analysed.

SCALE6.0 uncertainties in COVERX files have been converted into ENDF-6 format, using the nominal values of ENDF/B-VII.1, in order to propagate them with NUDUNA. The usage

of ENDF/B-VII.1 nominal cross section values could lead to differences if compared with the results using ENDF/B-V, however same multi-group cross section values are obtained once ENDF/B-VII.1 is processed to AMPX format. Checks have been carried out to ensure a proper translation between formats.

7.2.2.2 Application of Hybrid Method

The Hybrid Method can only be applied to the depletion part of a burn-up problem, so by default, uncertainties coming from the transport part are not included. This method is used in conjunction with the ACAB depletion code, which requires an specific format for the nuclear data input, different from COVERX. Nevertheless, proper tools/sequences have been developed to use uncertainties in COVERX files (as described in Chapter 4, Sec. 4.3.1.4).

To apply HM to this burn-up problem, using the same input data as NUDUNA, the next points are followed:

1. The same initial composition used in SCALE6.0 is used with ACAB.
2. The same burn-up steps (in which the neutron spectrum is recalculated with the updated composition) and the same sub-steps (divisions of the burn-up step, in which only depletion calculations take place) are used in ACAB as in SCALE6.0.
3. From the SCALE6.0 reference calculation, the neutron spectra in every burn-up step, with their corresponding neutron flux level, are extracted and applied to HM calculations.
4. The same cross section uncertainties are used, using the multi-group approach of HM to generate 500 random cross section files from SCALE6.0 COVERX files. These multi-group cross sections are then collapsed into one-group using the neutron spectra provided with the reference SCALE6.0 calculation for every burn-up step.

Then, once the random one-group cross section files for ACAB have been generated, the depletion calculations can be carried out, and the uncertainty on isotopic compositions is analysed.

7.2.2.3 Differences between applications

No difference has been found between the two different approaches of using NUDUNA to assess the impact of neglecting isotopic composition uncertainties in the transport part of burn-up calculations, since the same code is used and the same sequence, TRITON, is used too. So, the same data processing is performed in both cases. Therefore, it will be a clean assessment of the importance of isotopic composition uncertainties on transport calculations.

Differences between how NUDUNA and HM are applied are investigated. The same cross section data are used and the same uncertainties are propagated, so they are not a source for differences. However, HM uses an already collapsed cross section library processed at a pre-defined temperature of 300K, while NUDUNA provides random cross section data processed at the problem temperature.

Another difference between NUDUNA and HM is that the power of the pin-cell is normalised during SCALE6.0 depletion calculations, that means, the neutron flux level seen by the pin-cell is calculated according to the power normalisation equation. Such a normalisation, given in a general form in Eq. 7.1, states that the power of a system, such as reactor core, fuel assembly or pin-cell, is proportional to the sum of every energy release $E_{i,j}$ due to the different neutron interactions j, calculated by multiplying one-group cross sections $\sigma_{i,j}^{1g}$ of the isotope i, N_i concentrations and total neutron flux ϕ:

$$Power = \phi \sum_i N_i \sum_j \sigma_{i,j}^{1g} E_{i,j}. \tag{7.1}$$

In addition, not only between burn-up steps (where transport calculations provide a different neutron spectrum), but also in every sub-step in TRITON sequence (where only depletion calculations take place), the flux is updated with the composition of the pin-cell through the power normalisation constraint. Such a constraint is not implemented in ACAB, where the flux is kept constant within the same burn-up step. However, HM applies the same neutron flux calculated for each burn-up step given by SCALE6.0.

Therefore, such differences between how NUDUNA and HM are applied to the same problem can disrupt the analysis of the impact of neglecting transport uncertainties.

7.2.3 Neglecting the isotopic concentration uncertainties

NUDUNA is capable of propagating uncertainties in the complete burn-up problem, since the random nuclear data generated are applied to the whole problem. However, one can also perform a limited analysis where the isotopic concentration uncertainties are neglected, that means, only uncertainties on the transport part are addressed. Such an approximation is then studied by applying NUDUNA as described in the previous section, with special focus on the uncertainty contributions coming from cross section and neutron multiplicity data.

7.2.3.1 Propagating cross section uncertainties

The propagated cross sections uncertainties for ^{235}U and ^{239}Pu consist in covariances for total, elastic, (n,γ), (n,2n), fission and inelastic cross sections, plus correlations between elastic-fission, elastic-(n,γ) and (n,γ)-fission reactions. Correlations between cross section reactions of different isotopes are not included, because they have been found of being irrelevant [Cabellos, 2013].

Results of propagating such cross section uncertainties are presented in Fig. 7.15 for ^{235}U, and in Fig. 7.16 for ^{239}Pu. They show uncertainties in k_{eff} and in the isotopic concentrations of ^{235}U and ^{239}Pu induced by ^{235}U and ^{239}Pu cross section uncertainties, respectively. The right panels show the isotopic concentrations and their uncertainties as obtained with the full NUDUNA analyzes. The left panels compare the uncertainty estimates obtained with and without including isotopic concentration uncertainties induced by the depletion step. As can be seen, neglecting the uncertainties of isotopic concentrations leads to a considerable underestimation of the overall uncertainty.

When propagating ^{235}U uncertainties, the impact of isotopic concentration uncertainties becomes relevant above 10 GWd/MTU, and increases with increasing ^{235}U concentration uncertainty. When propagating ^{239}Pu uncertainties, the omission of isotopic concentration uncertainties shows an effect already at the very beginning and reaches a maximum between 20 and 50 GWd/MTU.

The right panels of Fig. 7.15 and 7.16 also show that ^{235}U data uncertainties induce isotopic concentration uncertainties on ^{239}Pu, and vice versa. The reason is that a change in the cross section of one isotope induces changes in neutron flux and spectrum, which modifies

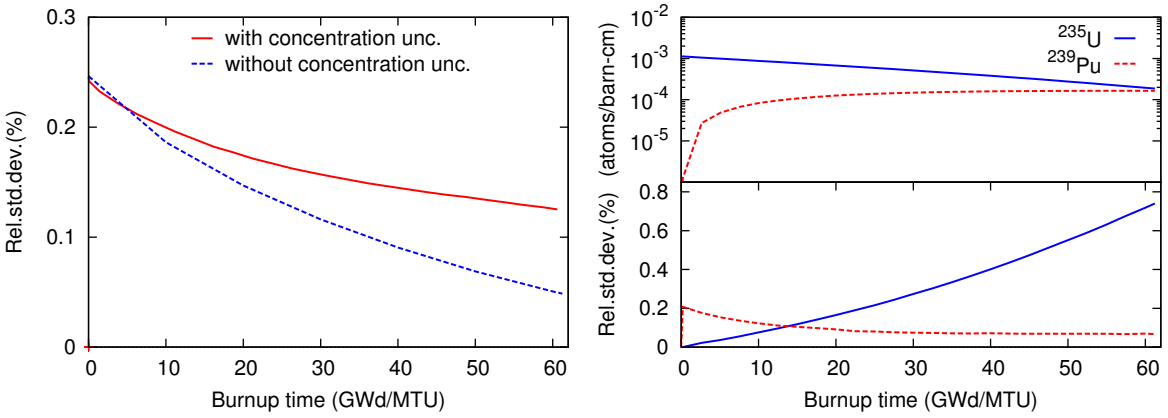

(a). k_{eff} uncertainty *(b).* Concentrations + their uncertainties

FIGURE 7.15: Uncertainties due to ^{235}U cross section uncertainties: the right panel shows concentrations and uncertainties obtained by a complete NUDUNA analysis; the left panel shows a comparison of k_{eff} uncertainties for a complete analysis and for an analysis that neglects isotopic concentration uncertainties.

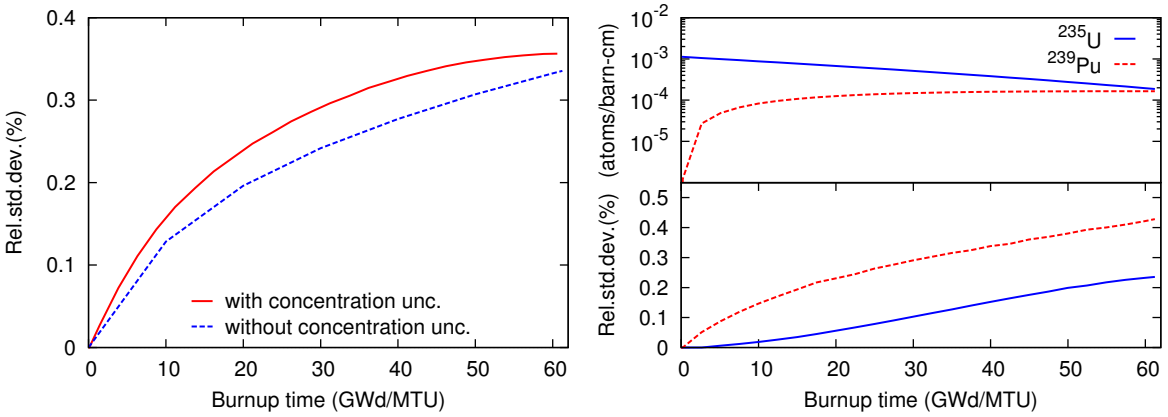

(a). k_{eff} uncertainty *(b).* Concentrations and their uncertainties

FIGURE 7.16: Uncertainties due to ^{239}Pu cross section uncertainties: the right panel shows concentrations and uncertainties obtained by a complete NUDUNA analysis; the left panel shows a comparison of k_{eff} uncertainties for a complete analysis and for an analysis that neglects isotopic concentration uncertainties.

the reaction rates of the other isotope whose nuclear data are not modified. Such induction of uncertainties on other isotope concentrations is provoked mainly through the power normalisation constraint.

7.2.3.2 Impact of fission neutron multiplicities

Fig. 7.17 presents uncertainties induced by fission neutron multiplicity ($\overline{\nu}$) uncertainties. Each panel shows a curve obtained by propagating uncertainties in the whole burn-up problem and a curve obtained by neglecting isotopic number density uncertainties.

A very good agreement between the two approximations for k_{eff} uncertainties is observed. In fact, it shows that $\overline{\nu}$ uncertainties have no impact on the depletion step, and also the implicit impact of $\overline{\nu}$ uncertainties on isotopic compositions via the induced flux uncertainty is negligible. Also, the same result is obtained for ^{238}U $\overline{\nu}$ uncertainties coming from ENDF/B-VII.1.

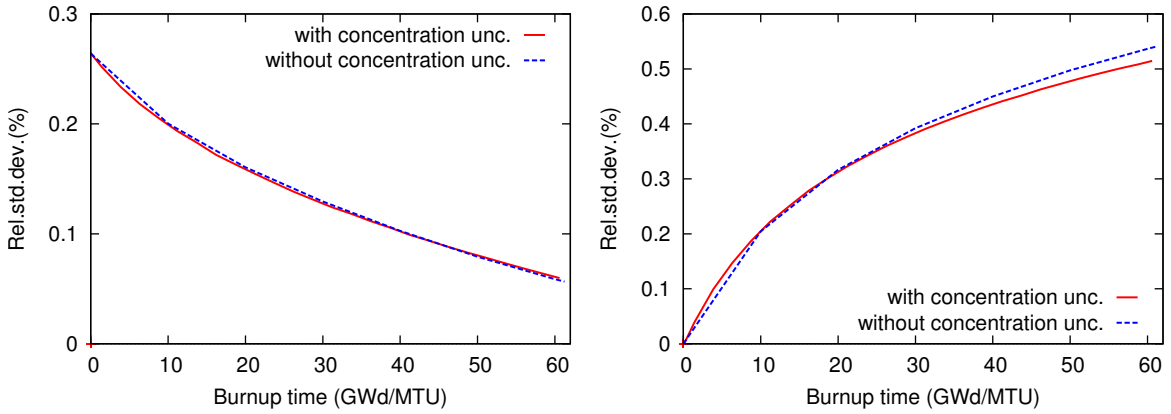

(a). Due to ^{235}U uncertainties

(b). Due to ^{239}Pu uncertainties

FIGURE 7.17: Uncertainties on k_{eff} of the UAM Exercise I-1b TMI-1 benchmark pin-cell induced by fission neutron multiplicity $\overline{\nu}$ uncertainties with and without consideration of concentration uncertainties.

7.2.4 Neglecting neutron flux and spectrum uncertainties

Here, the effect of estimating the uncertainties on isotopic concentrations neglecting neutron flux and spectrum uncertainties, as done by the Hybrid Method, is addressed.

NUDUNA is applied to provide the full uncertainty, HM is used to propagate nuclear data uncertainties only in the depletion step. HM is based on Monte Carlo sampling of nuclear data uncertainties, and for each random draw a complete depletion calculation is performed. However, the flux input is kept at its nominal value, and so no additional transport calculations have to be carried out. Consequently, neutron flux and spectrum uncertainties are not taken into account. Hence, comparing both results the effect of neglecting neutron flux and spectrum uncertainties is assessed.

Neglecting neutron flux and spectrum uncertainties implies that the concentration uncertainty of a given isotope is only influenced by its own cross section uncertainty and by those of isotopes that are part of a transmutation chain that results in the given isotope. Fig. 7.18

presents the dominant contributions to the ^{235}U and ^{236}U concentration uncertainties. Indeed, the ^{235}U concentration addressed in the left panel is not affected by ^{238}U or ^{239}Pu data uncertainties within the HM framework. Propagating also flux uncertainties, as NUDUNA does, leads to sizable contributions of ^{238}U and ^{239}Pu data uncertainties to the ^{235}U concentration uncertainty, as shown by the dashed and dashed-dotted curves in the left panel of Fig. 7.18. So the HM method is not capable to predict the ^{235}U concentration uncertainty since it provides uncertainty estimations much lower than actual ones. The combined effect of propagating at the same time the uncertainties in ^{235}U, ^{238}U and ^{239}Pu cross sections has been also addressed, showing that the total uncertainty on the ^{235}U concentration is a sum of contributions with no counteracting effects. The right panel of Fig. 7.18 shows the ^{236}U concentration uncertainty. This isotopic concentration depends via the ^{235}U(n,γ)^{236}U reaction directly on the ^{235}U cross sections, and HM yields a good result for the contribution of ^{235}U data uncertainties to the ^{236}U concentration uncertainty. Since there are no other isotopes with relevant impact on the ^{236}U concentration uncertainty, it also gives a good result for the total uncertainty of the ^{236}U concentration.

HM is at present not considering in its random sampling the fact that the reactor/fuel assembly/ pin-cell power is fixed. Constraining the flux level to this fixed power after random sampling of the cross sections will induce a variation on the flux level. The implementation of such constraint could possibility lead to an improved HM uncertainty estimate, and future studies should address this topic.

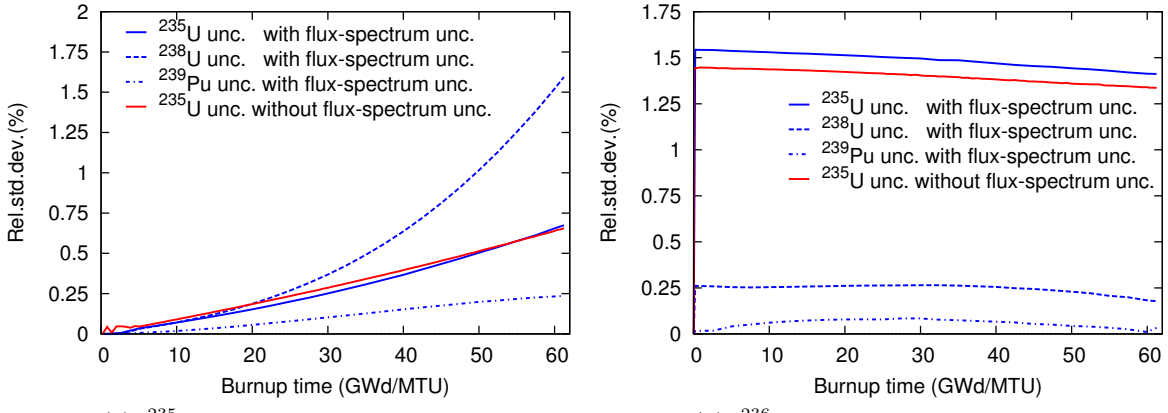

(a). ^{235}U concentration uncertainty *(b).* ^{236}U concentration uncertainty

FIGURE 7.18: Uncertainties of ^{235}U and ^{236}U isotopic concentrations due to ^{235}U, ^{238}U, and ^{239}Pu cross section uncertainties considering or not neutron flux and spectrum uncertainties, obtained with NUDUNA and the Hybrid Method for the UAM Exercise I-1b TMI-1 benchmark pin-cell.

7.2.5 Conclusions

NUDUNA and Hybrid Method have been compared by applying both to a UQ study of a PWR typical pin-cell burn-up problem. Differences between how they are applied to the same problem are found: different cross section structures are used with each method, HM can currently used only a pre-defined SCALE6.0 cross section library processed at a given temperature while NUDUNA provides temperature-dependent random libraries. However, the most important difference is the application of the power normalisation constraint by NUDUNA through the usage of SCALE6.0 TRITON sequence, while HM with ACAB does not.

With NUDUNA, the importance of taking uncertainties on concentrations in transport calculations of burn-up problems is remarked, by comparing the application of NUDUNA to the whole burn-up problem with the application to only the transport part. Without them, underestimations of uncertainties on k_{eff} are observed.

Neglecting neutron flux/spectrum uncertainties, as HM does, may lead to considerable underestimation of the overall concentration uncertainty. However, there are cases where such an approximation is giving good results. Given the gains in computing time by the HM approximation in burn-up problems, future studies might also address applicability criteria of HM such that HM could at least be used to study a limited set of isotopes.

After identifying the power normalisation constraint as an important difference between approaches, its implementation could lead to great improvements of the Hybrid Method. With the power normalisation equation, given in Eq. 7.1, variations of neutron flux will be obtained due to changes in fission cross sections of different isotopes, so the neutron flux will transport fission cross section uncertainties to other isotope concentrations not related by transmutation chains. Therefore, effects of similar order as obtained with NUDUNA can be expected if the power normalisation constraint is implemented in the Hybrid Method.

7.3 Limitations of the Hybrid Method under large spectrum variations

As presented in Chapter 4, Sec. 4.2.1.1 , for the Hybrid Method, one-group cross section uncertainties can only be used when variations of the spectrum between burn-up steps are small enough to maintain a high correlation between one-group cross sections. Additionally, it can be applied even when large variations of the spectrum take place if high correlations exist between cross sections of the energy regions of relevance for the application. This limitation is proved here with the comparison of the one-group cross approach with the multi-group approach, applying both to two hypothetical depletion cases.

These depletion cases consist in the burn-up of the characteristic fuel pin-cell studied in the ESFR fuel cycle (See Chapter 6, Sec. 6.3) in three burn-up steps where the spectrum changes abruptly from one step to the others. Further details are as follow:

- For the first case, the depletion in three burn-up steps uses the neutron flux intensity of the first three ESFR burn-up steps. However, the neutron spectra seen by the fuel cell in each burn-up step are the ones provided in Fig. 7.19. That means first a fast, next an epi-thermal, and finally a thermal spectrum are applied. These results are referred as FS-EPI-TH.
- For the second case, the depletion is as before, but the order of application of spectra is inverted: First a thermal, next an epithermal, and finally a fast spectrum. This case is referred as TH-EPI-FS.

The uncertainties provoked with cross section uncertainties, given in SCALE6.0, on isotopic compositions are analysed. In Table 7.3 and 7.4, uncertainties reached at the end of burn-up are presented for heavy isotopes and fission products, respectively. There, the uncertainty values obtained with the one-group cross section (1g) and multi-group cross section (44g) approaches are very similar, for both depletion cases. Few exceptions arise whose differences are not negligible, and are highlighted in grey: ^{232}U (FS-EPI-TH), ^{244}Pu (TH-EPI-FS), ^{244}Cm (both), ^{248}Cm (FS-EPI-TH), ^{249}Bk (TH-EPI-FS) and ^{249}Cf (TH-EPI-FS).

However, obtaining the same uncertainty at the end of burn-up does not mean that the temporal evolution is the same. For this reason, Fig. 7.20 shows the uncertainty evolution throughout burn-up for a selected set of isotopes. For ^{235}U and ^{238}U, there is almost no

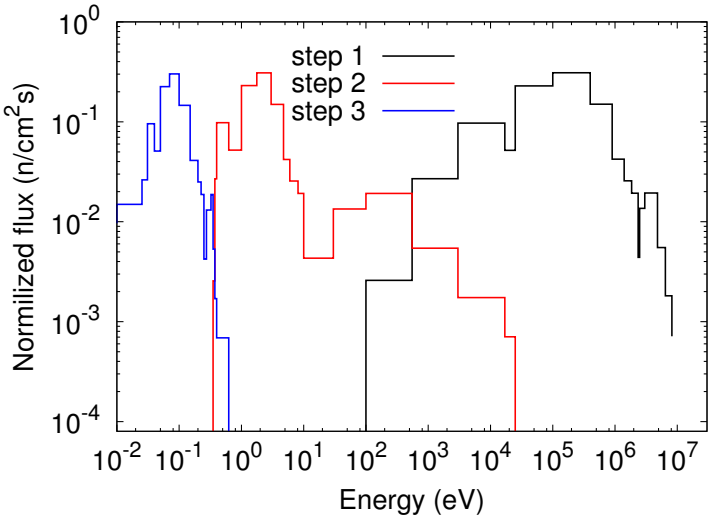

FIGURE 7.19: Neutron spectra seen by the fuel cell for an hypothetical case with large spectrum variations.

differences throughout the whole burn-up. For ^{244}Pu, which has been highlighted before, the differences at the end of burn-up for the TH-EPI-FS case come from a deviation that starts when the spectrum changes from thermal (TH) to epithermal (EPI), and then, such trend continues until the end of burn-up. A singular case occurs for ^{243}Cm, in which large differences are found in the TH-EPI-FS when the spectrum changes from TH to EPI, but the uncertainty reached by both approaches is almost the same at the end of burn-up. The same behaviour of ^{243}Cm is observed also for ^{244}Cm and ^{245}Cm. In the case of ^{248}Cm, the differences at the end of burn-up obtained for FS-EPI-TH are due to the change from EPI to TH spectrum, while for TH-EPI-FS the differences start when the spectrum changes from TH to EPI. The case of ^{249}Bk is very similar to ^{248}Cm, and its behaviour is found also in Cf isotopes: ^{249}Cf, ^{250}Cf, ^{251}Cf and ^{252}Cf.

TABLE 7.3: Uncertainties on the atomic composition of heavy isotopes for the ESFR characteristic fuel cell which sees large neutron spectrum variations between burn-up steps. Cross section uncertainties stored in SCALE6.0 are the only ones propagated.

		FS-EPI-TH			TH-EPI-FS		
Nuclide	N_i (atoms)	N_f - N_i (atoms)	1g (%)	44g (%)	N_f - N_i (atoms)	1g (%)	44g (%)
^{232}U	-	7.70×10^{16}	16.47	13.69	1.44×10^{19}	8.47	8.34
^{233}U	-	1.26×10^{17}	1.74	1.66	8.94×10^{19}	18.99	19.32
^{234}U	-	3.17×10^{22}	14.43	14.05	6.56×10^{24}	4.76	3.99
^{235}U	5.24×10^{26}	-5.23×10^{26}	14.06	13.59	-5.23×10^{26}	5.95	5.27
^{236}U	-	5.34×10^{24}	8.97	7.87	1.88×10^{24}	12.06	10.51
^{237}U	-	2.75×10^{22}	18.69	18.95	3.77×10^{23}	13.55	13.38
^{238}U	2.04×10^{29}	-1.23×10^{29}	1.52	1.28	-1.25×10^{29}	1.61	1.29
^{237}Np	1.65×10^{27}	-1.65×10^{27}	19.82	19.98	-1.64×10^{27}	11.73	11.57
^{238}Np	-	4.00×10^{21}	19.53	19.82	1.94×10^{22}	12.00	11.99
^{239}Np	-	1.22×10^{26}	0.67	1.67	2.15×10^{25}	0.19	1.59
^{238}Pu	1.08×10^{27}	-1.06×10^{27}	15.32	14.96	-1.75×10^{26}	4.30	3.60
^{239}Pu	1.43×10^{28}	-1.41×10^{28}	1.20	1.85	-9.75×10^{27}	0.45	0.80
^{240}Pu	8.89×10^{27}	-8.66×10^{27}	2.98	3.19	-8.66×10^{27}	4.33	4.11
^{241}Pu	2.46×10^{27}	3.69×10^{28}	1.35	1.12	3.01×10^{28}	1.38	1.18
^{242}Pu	3.09×10^{27}	-2.54×10^{27}	8.34	8.45	-2.40×10^{27}	1.50	1.30
^{244}Pu	-	2.41×10^{25}	13.45	12.49	2.28×10^{25}	13.14	10.60
^{241}Am	5.84×10^{27}	-5.80×10^{27}	2.94	2.73	-3.94×10^{27}	1.47	1.24
^{242}Am	-	3.50×10^{24}	3.10	3.02	7.31×10^{23}	4.64	4.55
^{242m}Am	2.30×10^{25}	-2.30×10^{25}	5.49	5.28	-9.61×10^{24}	1.93	1.70
^{243}Am	1.50×10^{27}	-1.37×10^{27}	7.13	7.37	-1.47×10^{27}	3.53	3.48
^{242}Cm	1.92×10^{24}	4.56×10^{26}	15.29	14.88	2.04×10^{26}	3.28	2.84
^{243}Cm	6.69×10^{24}	3.16×10^{24}	20.72	20.33	6.49×10^{24}	12.42	10.31
^{244}Cm	4.89×10^{26}	-1.08×10^{26}	11.80	9.43	-2.66×10^{26}	20.71	17.71
^{245}Cm	1.19×10^{26}	-1.17×10^{26}	7.19	9.05	-6.29×10^{25}	10.33	10.16
^{246}Cm	8.49×10^{24}	3.89×10^{26}	7.63	6.94	3.57×10^{26}	7.84	6.49
^{247}Cm	-	3.17×10^{24}	17.09	17.75	1.94×10^{25}	18.48	20.23
^{248}Cm	-	5.80×10^{25}	16.50	13.93	6.45×10^{25}	15.59	14.59
^{249}Bk	-	8.66×10^{22}	18.84	17.10	1.67×10^{24}	21.90	19.31
^{249}Cf	-	5.38×10^{20}	18.88	17.29	1.28×10^{24}	20.04	17.36
^{250}Cf	-	8.32×10^{22}	21.92	20.62	3.82×10^{23}	20.96	21.20
^{251}Cf	-	1.71×10^{22}	18.43	16.79	1.97×10^{23}	19.65	16.35
^{252}Cf	-	9.60×10^{23}	21.30	19.79	6.05×10^{24}	17.47	15.37

TABLE 7.4: Uncertainties on the atomic composition of fission products for the ESFR characteristic fuel cell which sees large neutron spectrum variations between burn-up steps. Cross section uncertainties stored in SCALE6.0 are the only ones propagated.

		FS-EPI-TH			TH-EPI-FS		
Nuclide	N_i	N_f - N_i	1g	44g	N_f - N_i	1g	44g
	(atoms)	(atoms)	(%)	(%)	(atoms)	(%)	(%)
^{93m}Nb	-	3.06×10^{21}	1.75	1.66	3.98×10^{21}	1.97	1.79
^{94}Nb	-	6.78×10^{21}	6.92	6.16	1.78×10^{22}	2.84	2.77
^{93}Mo	-	2.28×10^{19}	1.59	1.28	1.96×10^{19}	1.56	1.20
^{103}Rh	-	2.14×10^{26}	1.76	1.68	1.25×10^{27}	1.49	1.34
^{107}Pd	-	3.99×10^{27}	1.91	1.69	4.13×10^{27}	1.96	1.38
^{109}Ag	-	2.72×10^{26}	3.23	3.10	4.46×10^{26}	2.27	2.08
^{126}Sn	-	3.13×10^{26}	0.83	0.73	3.25×10^{26}	0.84	0.69
^{126}Sb	-	1.49×10^{24}	4.97	5.47	2.25×10^{23}	12.25	13.62
^{126m}Sb	-	2.92×10^{20}	0.98	1.00	1.54×10^{20}	1.29	0.91
^{129}I	-	1.87×10^{26}	6.43	5.84	7.33×10^{26}	2.23	1.75
^{149}Sm	-	1.41×10^{23}	10.24	11.50	2.01×10^{26}	3.31	3.00
^{150}Sm	-	1.92×10^{26}	8.17	9.49	8.55×10^{26}	11.82	11.00
^{151}Sm	-	1.93×10^{24}	6.21	7.38	1.33×10^{26}	4.30	4.31
^{152}Sm	-	1.21×10^{26}	6.24	7.24	1.87×10^{26}	4.53	4.28
^{151}Eu	-	3.10×10^{19}	6.28	7.52	5.85×10^{23}	4.71	4.54
^{153}Eu	-	7.30×10^{25}	5.89	6.83	9.76×10^{25}	9.42	8.42
^{155}Gd	-	7.97×10^{20}	8.10	8.29	5.30×10^{24}	5.20	6.10

Since a strange behaviour is observed in ^{243}Cm for the TH-EPI-FS case, such a case is studied in more detail. ^{243}Cm is obtained from the neutron capture of ^{242}Cm, and it disappears due to fission and capture reactions mainly. Then, the uncertainty in ^{243}Cm should come from one of these two reactions. The neutron capture of ^{242}Cm carries a large uncertainty, around 30% and 15% in one-group if collapsed with thermal and epithermal spectra, correspondingly. Meanwhile, capture and fission reactions of ^{243}Cm uncertainties are below 7% under both spectra. Furthermore, no differences between the sampled one-group uncertainties obtained from random one-group cross sections and the ones from random multi-group cross sections are found after performing an statistical analysis. So that, this latter issue is discarded as a possible origin for the behaviour of ^{243}Cm in TH-EPI-FS.

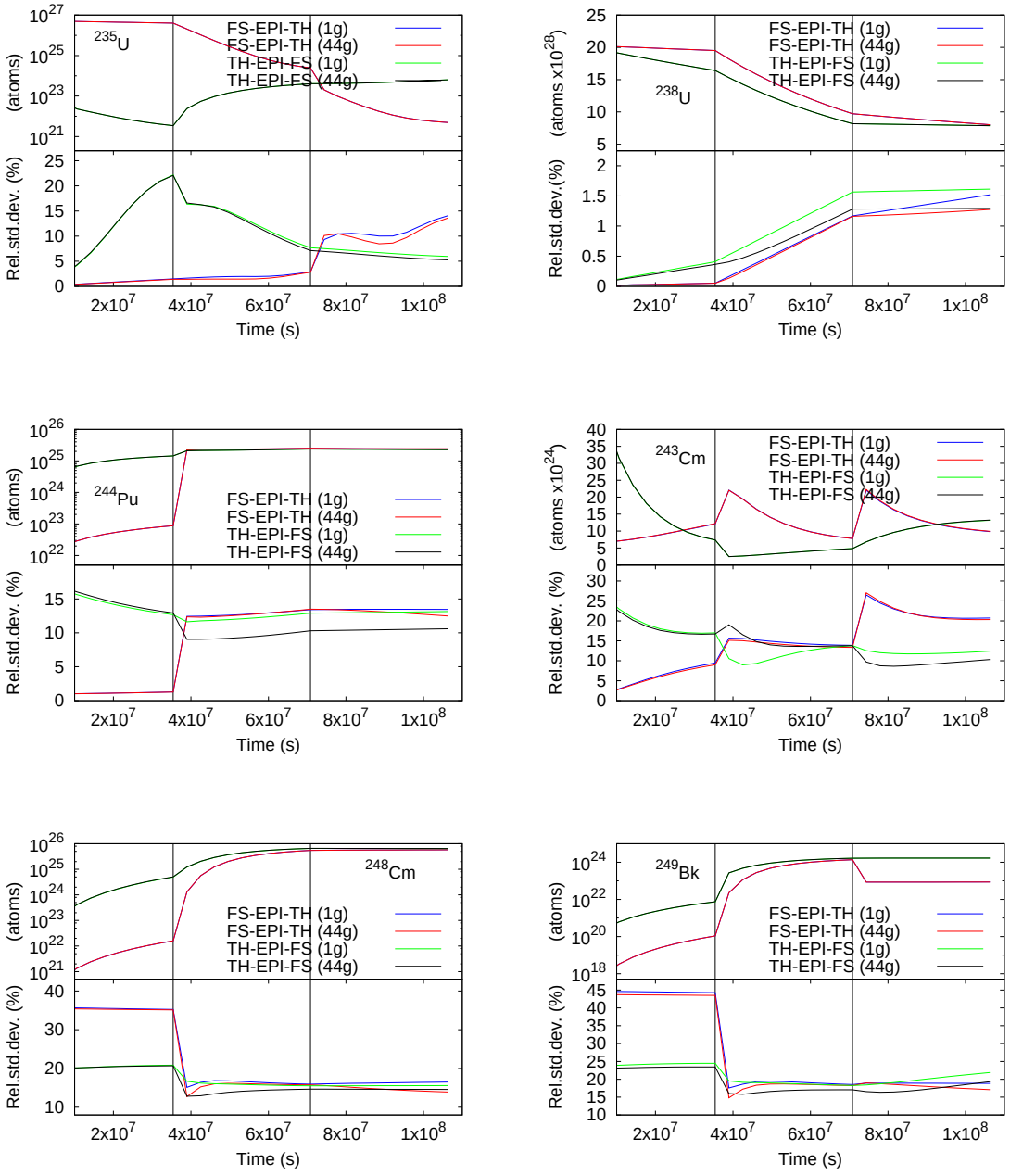

FIGURE 7.20: Evolution of the number of atoms and their uncertainties of a set of selected nuclides due to the usage of one-group (1g) and multi-group (44g) cross section uncertainties with the Hybrid Method for the ESFR characteristic fuel cell which see large neutron spectrum variations between burn-up steps. Uncertainties stored in SCALE6.0 are the only ones propagated.

An extra case for TH-EPI-FS is performed in order to clarify the issue with ^{243}Cm. The same problem is carried out, however, without uncertainties in ^{242}Cm cross sections. The results are shown in Fig. 7.21, observing first that the uncertainty on ^{243}Cm decreases sharply when ^{242}Cm does not carry any uncertainty. Additionally, the strange evolution when the spectrum

changes from thermal to epithermal disappears. However, the trend obtained when switching from epithermal to fast spectrum is again observed, but smaller uncertainties are reached. That means the ^{243}Cm uncertainty is driven by ^{242}Cm, and therefore, the strange behaviour observed in the epithermal step should come from an issue with the neutron capture cross section of ^{242}Cm.

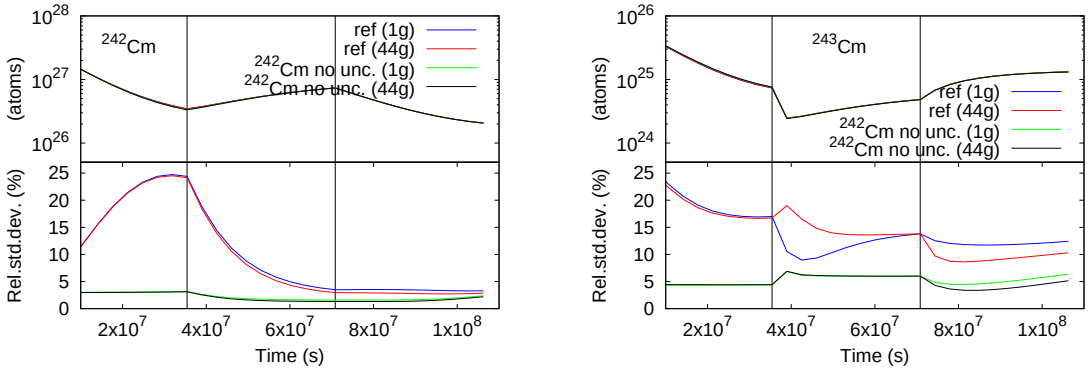

FIGURE 7.21: Evolution of the number of atoms and their uncertainties for ^{242}Cm and ^{243}Cm using one-group (1g) and multi-group (44g) approaches for TH-EPI-FS, comparing with the case in which ^{242}Cm has carries no uncertainties on its cross sections. Uncertainties stored in SCALE6.0 are the only ones propagated.

Using the Hybrid Method with one-group uncertainties with the correlated sampling approach means that cross sections between burn-up steps are completely correlated. However, it could occur that one-group cross sections are not completely correlated when the multi-group approach is used, so it has to be checked in order to prove the equivalence between approaches. Therefore, the one-group cross sections obtained from sampling one-group or multi-group cross sections are compared. Such a comparison is presented in Fig. 7.22, which shows a correlation between TH (thermal) and EPI (epithermal) for cross sections sampled from multi-group uncertainties that does not exist when comparing TH and FS spectra. Hence, one-group uncertainties with correlated sampling will not yield the same results as the multi-group uncertainties for variations of the spectrum from or to TH, or from or to FS.

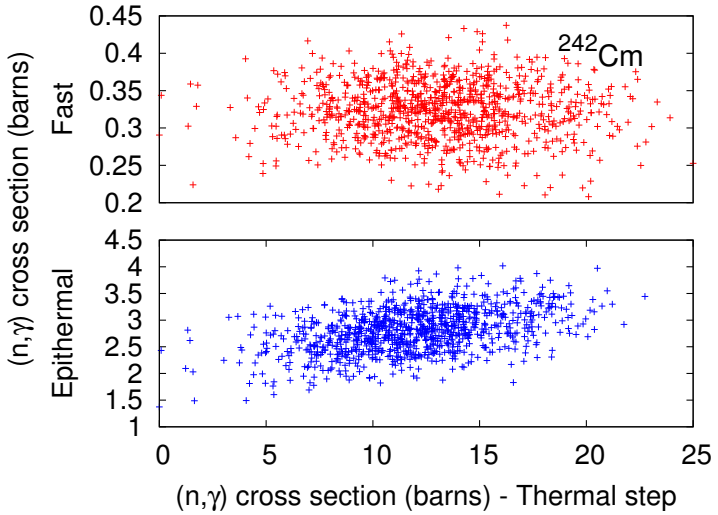

FIGURE 7.22: Scatter plot of random (n,γ) cross sections in 44-groups of ^{242}Cm collapsed into one-group for the different neutron spectra used in TH-EPI-FS case.

Chapter 8

Conclusions and future works

8.1 Conclusions

This thesis presents a methodology for propagating nuclear data uncertainties in depletion calculations, the Hybrid Method, in conjunction with a review of the state-of-the-art of nuclear data and their uncertainties, and uncertainty propagation methodologies.

The Hybrid Method is based on Monte Carlo sampling of nuclear data and its implementation is completely described: from the processing of nuclear data to statistical analysis. Different approaches of the Hybrid Method are presented, depending on which cross section uncertainties are propagated, one-group or multi-group. Improvements have been made to the methodology, such as the use of one-group cross section uncertainties in depletion problems with few/several burn-up steps.

Inconsistencies between independent and cumulative fission yield uncertainties and the lack of covariance (off-diagonal terms) for both gave rise to another development, the implementation of fission yield covariance data generation capability based on a Bayesian/GLS updating scheme, after reviewing the state of the art of methodologies.

Comparisons between other methodologies have been performed in order to analyse the advantages/drawbacks and limitations of the Hybrid method for propagating uncertainties in depletion problems. In particular, the usage of covariance data for propagating uncertainties has been studied, comparing it with the Total Monte Carlo method. The applicability of the Hybrid Method to burn-up problems, which apply the constant power constraint, is studied

in comparison with NUDUNA due to the assumption of neglecting neutron flux/spectrum uncertainties derived from the transport part of burn-up problems. Moreover, the importance of concentration uncertainties in burn-up problems is highlighted.

Once these developments for the Hybrid Method and the generation capability of complete covariance data for fission yield are implemented, they are applied to decay problems and to different advanced reactor fuel cycles.

State-of-the-art of nuclear data and their uncertainties

Nuclear data used in depletion calculations have been reviewed: decay data, fission yields and cross section. The main conclusions regarding uncertainties are presented here.

The revision of decay data is centred on the JEFF-3.1.1 decay library (which is the same data used in JEFF-3.1.2 and JEFF-3.2). It is found that for many isotopes, uncertainties on their decay energies are lacking. This lack has an impact on decay heat calculations related to fission products. Also, uncertainties on branching ratios are not always consistent with a proper update of the uncertainties using the normalisation constraint to one (the sum of branching ratios have to be equal to 1).

The review of fission yield data compiled in JEFF-3.1.1, ENDF/B-VII.1 and JENDL-4.0 reveals that a proper procedure has not yet been developed to assess the uncertainty of fission yields for isotopes with different isomeric states. Furthermore, uncertainties in cumulative and independent fission yields are unrelated by a proper approach such as a Bayesian update scheme (only for ^{239}Pu fission yields in ENDF/B-VII.1), which leads to very large uncertainty values for independent fission yields. Finally, neither of the libraries studied provides covariance data for fission yields, even when important relationships exist between them.

Cross section data uncertainties from EAF libraries (EAF-2007 and EAF-2010) and from SCALE6.0 are analysed, showing two different ways to provide uncertainties: wide energy-groups with no correlations between them, and narrower energy-groups with correlations between them and between reaction cross sections. The latter is the one currently used in major evaluated nuclear data libraries. However, given the lack of data, EAF libraries provide estimations for reaction cross sections that major libraries do not. Comparing cross section uncertainties under different neutron spectra reveals that high energy applications such as ADS-like make use of cross sections with larger uncertainties than other applications such

as Light Water or fusion-type reactors. In fusion applications, even though they are high energy applications, lower uncertainties are found since larger experimental datasets exist in this energy range.

State-of-the-art of methodologies for propagating nuclear data uncertainties

A review of the main codes/tools used for propagating nuclear data uncertainties shows that two main methodologies are applied when transport, depletion or burn-up calculations are tackled: First Order Perturbation theory and Monte Carlo sampling. The former has been implemented and validated for transport calculations, where e.g. criticality is assessed. However, depletion or burn-up problems are not completely well addressed with this methodology because transport and depletion are treated as two problems. Instead, Monte Carlo sampling seems to be the easiest and fastest solution thanks to its easy implementation (use transport/depletion/burn-up codes as black-boxes) and due to its less stringent assumptions, e.g. being able to overcome non-linear effects.

A deep review of two methodologies based on Monte Carlo sampling, Total Monte Carlo and NUDUNA, shows that different sources of nuclear data uncertainties can be used: directly as proposed by evaluators in nuclear data libraries or using experimental data and their uncertainties to generate evaluated nuclear data libraries and basing their uncertainties upon the experimental data and their scattering. Currently, the first approach (using evaluated uncertainties) is the most used, and more implementations are constantly being developed.

Developments with/in the Hybrid Method

The Hybrid Method was the methodology chosen for development and improvement. A review of the first implementation was performed, showing the points to work on. Two approaches have been developed in order to tackle problems with more than one burn-up step: one-group cross section approach with correlated sampling and multi-group cross section approach. Both increase the applicability range of the Hybrid Method to such kinds of problems. Additionally, implementation of tools/sequences for processing different nuclear data formats: COVERX and ENDF6 has been developed. Finally, routines for analysing and post-processing output have been implemented, such as the analysis of the major uncertainty contributors for response functions which are linear combination of others.

Generation of covariance data for fission yields

The generation and use of fission yield covariance data is justified on several grounds: first of all, nuclear data libraries do not provide the uncertainty of such data; secondly, independent and cumulative fission yield are usually inconsistent; and thirdly, in the case of burn-up tracker isotopes, high uncertainty values are obtained if independent fission yield uncertainties are used. This last statement goes against experimental observation of burn-up trackers, which usually carry low uncertainties.

A review of the state-of-the-art of proposed methodologies for generating fission yield covariance data shows that the use of a Bayesian/GLS updating scheme can easily response to such a need. Therefore, it is also implemented within the framework of the Hybrid Method.

Examples of usage are presented for fission yields of thermal ^{235}U and ^{239}Pu fission. Covariance data are generated by updating independent fission yield with data regarding cumulative and mass fission yield. Their impact is later assessed, not only here but also in other works presented within the UAM framework.

Uncertainty Quantification studies

Three different applications are studied with the Hybrid Method.

The first one, the thermal Fission Pulse Decay Heat of ^{235}U and ^{239}Pu, shows the importance of providing decay energy uncertainties for those isotopes of importance for short cooling times. The hypothesis on such uncertainties can completely change results: decay energy uncertainties become more important than fission yield uncertainties. The major contributors are identified, and it is also observed that JEFF-3.1.1 does not have the latest experimental results for decay energy. Fission yield covariance effects are here addressed, showing a sharp reduction in response function uncertainty, not only because of the reduction of the variance values but also because of the negative correlations obtained in the covariance matrices. A comparison with First Order Perturbation theory shows that same results are reached by both methodologies.

In the UQ study on the advanced reactor fuel cycle of EFIT, different response functions are analysed: isotopic composition, decay heat and radiotoxicity. Decay data, fission yield and cross section uncertainties are propagated on all the response functions. Decay uncertainties

have a negligible impact in all response functions, except for very few isotopic concentrations: ^{126}Sb and ^{151}Eu. Meanwhile, fission yield uncertainties are of importance for some fission product concentrations and for ingestion dose (due to ^{133}Xe). Cross section uncertainties are the most relevant source of uncertainty for all the response functions tackled. Uncertainty levels fall within the target accuracies (10%) for decay heat and radiotoxicity whichever library is used (among EAF-2007, EAF-2010 and SCALE6.0). However, for isotopic concentrations of most relevant isotopes, uncertainties fulfil the requirements (5%) only when SCALE6.0 is used. Studying higher burn-ups shows that higher uncertainties are reached, although they remain within target accuracies.

The last UQ study is performed on the ESFR fuel cycle. Only the isotopic composition is analysed, because this exercise is also used for comparing different approaches of the Hybrid Method. It consists in a depletion problem with different burn-up steps where neutron spectrum and flux level change. It reveals the need to use correlated sampling for tackling similar problems, and the same results are obtained when the multi-group approach is applied. Regarding uncertainty values obtained, cross section uncertainties are the most important uncertainty source for isotopic concentrations. Only decay data have an impact, again as in EFIT, on ^{126}Sb and ^{151}Eu. An additional library is used: COMMARA-2.0, its performance being compared with EAF-2010 and SCALE6.0. It yields uncertainties similar to SCALE6.0. Target accuracies (5%) are only achieved with SCALE6.0 and COMMARA-2.0 for major uranic and transuranic.

Comparisons with other methodologies

Comparisons with other methodologies have been carried out in order to evaluate the limitations and assumptions of the Hybrid Method, and also to validate sequences/tools for different nuclear data formats and sampling routines.

The comparison with Total Monte Carlo (TMC) aims to show the equivalence between propagating uncertainties using covariance data and using random files generated by means of TMC. Good agreement is obtained, although different probability density functions for isotopic composition are observed that can change results based on the study of percentiles, such as the case of order statistics. The importance of using covariance data between different reaction cross sections is highlighted: neglecting them leads to overestimations/underestimations.

To assess the limitations of the one-group approach, apart from the UQ study done for ESFR, an additional exercise is proposed. Large spectrum variations take place between different burn-up steps, showing that the one-group approach, even with correlated sampling, cannot yield the same results as the multi-group approach. However, when correlations exist for the relevant cross sections between the different energy regions which are of importance in the application, the one-group approach with correlated sampling can still be applied.

The NUDUNA tool is applied to highlight the importance of taking into account uncertainties in isotopic composition on transport calculations when burn-up problems are overcome. If these uncertainties are neglected, the k_{eff} uncertainty may be underestimated. It is observed that cross section uncertainties can affect other isotope concentrations unrelated with the cross section uncertainties of the isotope treated or through a transmutation chain. Meanwhile, the fission neutron emission does not induce any uncertainty on isotopic concentrations. When NUDUNA results are compared with Hybrid Method results, the effect of neglecting neutron flux/spectrum uncertainties is addressed. Underestimations in concentration uncertainties are obtained for some isotopes, while for others, the Hybrid Method provides a good approximation. Therefore, applicability criteria for applying the Hybrid Method are required when burn-up problems with power constant assumption are tackled.

8.2 Future works

As presented in the previous section, there are several points where further investigations can be carried out.

Regarding the state-of-the-art for nuclear data uncertainties, the performance of major evaluated nuclear data libraries can be compared. It is also important to keep track of new projects regarding nuclear data such as CIELO [Chadwick et al., 2014], which aims to get the best of the major evaluated nuclear data libraries into one evaluation, including covariance information. New libraries with cross section covariances are under development, e.g. new COMMARA versions and the SCALE6.2 covariance library. For UQ tools, new tools or new releases can be investigated, such as SCALE6.2 with SAMPLER, which will be capable of propagating not only cross section uncertainties, but also decay data and fission yield uncertainties.

There is plenty of room for improvements and implementations within the Hybrid Method:

- Implementation of the power normalisation constraint, which will lead to a partial inclusion of neutron flux uncertainties required for a better approximation of burn-up problems with power constant assumption.
- Implementation of sampling multi-group cross sections in arbitrary structure, or the one defined by the structure of the covariance information, in any of the possible formats (mainly ENDF6 or COVERX).
- Research of a methodology to include Hybrid Method results into transport calculations, departing from e.g. the usage of sensitivity coefficients of transport variables to concentrations, as done in [Cabellos, 2013], but accounting for the coupling effect.
- For the sampling sequence, implementation of the sampling of normal and log-normal PDFs correlated variables in order to avoid truncation effects, as proposed in [Žerovnik et al., 2012, Žerovnik et al., 2013].
- Implementation of processing routines which include or modify the temperature effects on cross sections, which could provoke deviation or yield non-precise uncertainty estimations.

For generating fission yield covariance data, comparisons with other methodologies may be performed. However, the main objectives, which were to show evaluators the importance of fission yield covariance data and the current status of inconsistencies between cumulative and independent fission yield uncertainties, have been achieved. Accordingly, it is important to keep track of which methodologies are selected to generate covariance data, and to assess the impact of new evaluations. The impact of fission yield covariance data is currently being assessed in burn-up calculations related to PWR applications, as already mention. Fission yield covariance data are to be used in the new release of SCALE, so comparisons could be carried out.

Comparisons with other methodologies could be made, for example, as done under the UAM framework, in which the Hybrid Method was compared with NUDUNA. However, any further development/implementation in the Hybrid Method should aim to couple transport and depletion parts of burn-up problems. Since CPU-power is becoming cheaper and easier to access, the advantage offered by the Hybrid Method of a faster assessment of the impact of nuclear data uncertainties on depletion calculations when addressing a burn-up problem, is becoming less relevant. Accordingly, it is better to tackle burn-up problems as one entity without any approximation than to assess only one part of it.

Publications, conferences, reports and other works conducted during this thesis

Stays abroad

- **AREVA GmbH, Offenbach, Germany**

  Duration: January 13, 2014 - April 30, 2014

  Supervisor: Axel Hoefer and Oliver Buss (PEPA1-G Radiology & Criticality department)

  Achievements: NUDUNA is a tool for propagating nuclear data uncertainties in transport/depletion/burn-up calculations. The stay in AREVA GmbH was aimed to collaborate with the NUDUNA team (A. Hoefer and O. Buss) for developing a new capability: propagating decay data uncertainties. Works related to the validation of NUDUNA were also performed, specifically the application to burn-up problems. Finally, limitations of the Hybrid Method and other approximations were studied.

- **SCK•CEN - EC-JRC-IRMM, Belgium**

  Duration: August 5, 2012 - November 16, 2012

  Supervisor: Gert Van den Eynde (Head of The Nuclear Systems Physics expert group) - SCK•CEN

  Supervisor: Prof. Peter Schillebeeckx (Nuclear Physics Unit) - EC-JRC-IRMM

  Achievements: The stay at the nuclear research center SCK•CEN was aimed to perform sensitivity analysis of nuclear data for the MYRRHA design (Accelerator Driven System advance reactor). Once the most relevant reactions are determined, comparison

between the major evaluated nuclear data libraries (JEFF, ENDF/B and JENDL) are carried out. Their performance for MYRRHA criticality calculations are analysed and compared. Then, the differences between libraries are studied regarding their performance the previous criticality calculations. Moreover, investigations of the impact of natural carbon thermal capture cross section in graphite-type thermal reactors were conducted. It was found that latest experimental data, already included in ENDF/B-VII.1, provide a significant improvement for the agreement between reactor experimental data and simulations for different benchmarks. Then, it was proposed and accepted a modification of the natural carbon file for the JEFF-3.2 library.

- **NRG (Nuclear Research and consultancy Group), Petten, The Netherlands**
  Duration: September 5, 2011 - December 16, 2011
  Supervisor: Arjan Koning (Senior Consultant).
  Achievements: The stay abroad at NRG Petten, with A.J. Koning and D. Rochman, was aimed to learn the Total Monte Carlo method for propagating nuclear data uncertainties. A comparison between the usage of random files generated with TMC, and the random files coming from covariance data (obtained from previous random files using the Hybrid Method) was performed. Both random files were used for propagating cross section uncertainties in advance reactor fuel cycle, and their results were compared. Good agreement was found.

Publications

Journal Articles

- (2014) L. Fiorito, **C.J. Díez**, O. Cabellos, A. Stankovskiy, G. Van den Eynde, P.E. Labeau , "Fission yield covariance generation and uncertainty propagation through fission pulse decay heat calculation", *Annals of Nuclear Energy*, **69**, July (2014), 331-343.

- (2014) **C.J. Díez**, O. Cabellos, J.S. Martinez , "Impact of Nuclear Data Uncertainties on Advanced Fuel Cycles and their Irradiated Fuel - a Comparison between Libraries", *Nuclear Data Sheets*, **118**, April (2014), 538-541.

- (2014) **C.J. Díez**, O. Cabellos, J.S. Martinez, A. Stankovskiy, G. Van den Eynde, P. Schillebeeckx, J. Heyse, "Analysis of ^{238}Pu and ^{56}Fe Evaluated Data for Use in MYRRHA", *Nuclear Data Sheets*, **118**, April (2014), 516-518.

- (2014) A. Stankovskiy, E. Malambu, G. Van den Eynde, **C.J. Díez**, "Nuclear Data Needs for the Neutronic Design of MYRRHA Fast Spectrum Research Reactor", *Nuclear Data Sheets*, **118**, April (2014), 513-515.

- (2014) J.J. Herrero, R. Ochoa, J.S. Martinez, **C.J. Díez**, N. Garcia-Herranz, O. Cabellos, "Nuclear Data Uncertainty Propagation to Reactivity Coefficients of a Sodium Fast Reactor", *Nuclear Data Sheets*, **118**, April (2014), 535-537.

- (2014) O. Cabellos, V. de Fusco, **C.J. Díez**, J.S. Martinez, E. Gonzalez, D. Cano-Ott, F. Alvarez-Velarde, "Testing JEFF-3.1.1 and ENDF/B-VII.1 Decay and Fission Yield Nuclear Data Libraries with Fission Pulse Neutron Emission and Decay Heat Experiments", *Nuclear Data Sheets*, **118**, April (2014), 472-475.

- (2013) **C.J. Díez**, A. Stankovskiy, E. Malambu, G. Žerovnik, P. Schillebeeckx, G. Van den Eynde, J. Heyse, O. Cabellos. "Review of the ^{nat}C(n,γ) cross section and criticality calculations of the graphite moderated reactor BR1", *Annals of Nuclear Energy* **60** (2013) 210-217.

- (2013) J.S. Martínez, O. Cabellos, **C.J. Díez**, "Methodologies for an improved prediction of the isotopic content in high burnup samples. Application to Vandellós-II reactor core", *Annals of Nuclear Energy* **57** (2013) 199-208.

- (2013) **C.J. Díez**, O. Cabellos, D. Rochman, A.J. Koning, J.S. Martínez, "Monte Carlo uncertainty propagation approaches in ADS burn-up calculations", *Annals of Nuclear Energy*, **54**, (2013) 27-35.

- (2012) **C.J. Díez**, J.J. Herrero, O. Cabellos, J.S. Martínez, "Propagation of Cross-Section Uncertainties in Criticality Calculations in the Framework of UAM-Phase I Using MCNPX-2.7e and SCALE-6.1", *Science and Technology of Nuclear Installations* **2012**, (2013), 10 pages.

- (2012) J.S. Martinez, O. Cabellos, **C.J. Diez**, "Methodologies to assess uncertainties in the tritium production within lithium breeding blankets", *Nukleonika*, **57(1)**, (2012),61-66.

- (2011) O. Cabellos, N. García-Herranz, **C.J. Díez**, R. Alvarez-Cascos, J. Sanz, F. Ogando, P. Sauvan, "Propagation of nuclear data uncertainties in transmutation calculations using ACAB code", *Journal of the Korean Physical Society*, vol. **59**, no. 23, pp. 1268-1271.

Proceedings

- (2011) **C.J. Díez**, O. Cabellos, J.S. Martínez, "Propagation of Nuclear Data Uncertainties using Monte-Carlo Technique in Depletion and Cooling Time Isotopic Predictions", *Proceedings of the International Conference on Mathematics and Computational Methods applied to Nuclear Science and Engineering (M&C2011).*

- (2011) J.S. Martínez, O. Cabellos, **C.J. Díez**, F. Gilfillan, A. Barbas, "Isotopic Prediction Calculation Methodologies: Application to Vandellos-II Reactor Cycles 7-11", *Proceedings of the International Conference on Mathematics and Computational Methods applied to Nuclear Science and Engineering (M&C2011).*

- (2011) O. Cabellos, J.S. Martínez, **C.J. Díez**, "Impact of Nuclear Data Uncertainties in the Phase-1b Benchmark", *Proceedings of the 2011 American Nuclear Society Annual Meeting.*

- (2011) **C.J. Díez**, O. Cabellos, J.S. Martínez, "Analysis of Different Uncertainty Activation Cross Section Data Libraries For LWR, ADS and DEMO Neutron Spectra", *Proceedings of the Workshop on Neutron Cross Section Covariances (NCSC2).*

- (2011) C. Ceresio, O. Cabellos, J.S. Martínez, **C.J. Díez**, "Importance of Nuclear Data Uncertainties in Criticality Calculations", *Proceedings of the Workshop on Neutron Cross Section Covariances (NCSC2).*

- (2011) O. Cabellos, J.S. Martínez, **C.J. Díez**, "Isotopic Uncertainty Assessment due to Nuclear Data Uncertainties in High-Burnup Samples", *Proceedings of the International Conference on Nuclear Criticality 2011 (ICNC 2011).*

- (2011) J.S. Martínez, O. Cabellos, **C.J. Díez**, "Isotopic Prediction Simulations Applied to High Burnups Samples Irradiated in Vandellos-II Reactor Core", *Proceedings of the International Conference on Nuclear Criticality 2011 (ICNC 2011).*

Others

JEF/EFF documents

- (2014) O. Cabellos, D. Piedra, **C.J. Díez**, "Impact of the Fission Yield Covariance Data in Burn-up Calculations", JEF/DOC-1566.
- (2013) **C.J. Díez**, O. Cabellos, L. Fiorito, A. Stankovskiy, G. Van den Eynde, "Generation of Fission Yield covariance data and application to Fission Pulse Decay Heat calculations", JEF/DOC-1520.
- (2012) **C.J. Díez**, "The ^{nat}C(n,g) cross section and its impact on results of criticality calculations on BR1", JEF/DOC-1456.
- (2012) O. Cabellos, V. de Fusco, **C.J. Díez**, J.S. Martinez, D. Cano, E. Gonzalez, F. Alvarez-Velarde,"Calculations of Fission Pulse Neutron Emission: A comparison between JEFF-3.1.1. and ENDF/B-VII.1", JEF/DOC-1435.
- (2011) **O. Cabellos**, **C.J. Díez**, J.S. Martinez, "A Comparison of diffferent Uncertainty Activation Cross-Section Data Libraries: Application to the Prediction Uncertainty in Tritium Production", EFF/DOC-1144.

Project reports/deliverables

- (2011) O. Cabellos, **C.J. Díez**, A.J. Koning, E.M. Gonzalez, "Activation data libraries for Monte Carlo uncertainty propagation in fuel cycle code ACAB", D2.1 Deliverable, ANDES project, Grant Agreement no.: FP7-249671.
- (2013) R.W. Mills, O. Cabellos, **C.J. Díez**, A.J. Koning, E.M. Gonzalez, "Report with transmutation calculations for advanced reactors with new covariance data + updated sensitivity tables", D2.5 Deliverable, ANDES project, Grant Agreement no.: FP7-249671.
- (2013) O. Cabellos, **C.J. Díez**, A.J. Koning, E.M. Gonzalez, "Report on the impact of uncertainties of the fission product nuclear data on the inventory of the irradiated fuel for ACAB ", D2.6 Deliverable, ANDES project, Grant Agreement no.: FP7-249671.

Participation in Conferences, Workshops, Seminars, ...

- **8th OECD LWR UAM Workshop (UAM-8)**, GRS, Garching (Germany), May 14-16, 2014
  With the presentation: "NUDUNA applied to a pin-cell burn-up calculation: UAM Exercise I-1b"

- **International Workshop of Nuclear Data Covariances (CW2014)**, Santa Fe, NM (USA), April 28 - May 1, 2014
  With the presentation: "Impact on Advanced Fuel Cycle and its Irradiated Fuel due to Nuclear Data Uncertainties and Comparison Between Libraries"

- **International Conference on Nuclear Data for Science and Technology (ND2013)**, New York (USA), March 4-8, 2013
  With the presentation: "Impact on Advanced Fuel Cycle and its Irradiated Fuel due to Nuclear Data Uncertainties and Comparison Between Libraries" and with the poster: "Analysis of the Quality of Evaluated Data for Most Relevant Reactions of MYRRHA"

- **6th OECD LWR UAM Workshop (UAM-6)**, KIT, Karlsruhe (Germany), May 9-11, 2012
  With the presentation: "UPM results on PWR Exercise I-2 using MCNPx 2.7e"

- **Workshop on Nuclear Data and Uncertainty Quantification (NDUQ)**, CCFE, Oxfordshire (UK), January 24-25, 2012
  With the presentation: "Comparison of Monte Carlo Uncertainty Propagation Approaches in Activation Calculations"

- **Workshop on Neutron Cross Section Covariances (NCSC2)**, Vienna (Austria), September 14-16, 2011
  With the presentation: "Analysis of Different Uncertainty Activation Cross Section Data Libraries For LWR, ADS and DEMO Neutron Spectra"

- **Workshop on Activation Data EAF 2011**, Prague (Czech Republic), June 01-03, 2011
  With the presentation: "A Comparison of different Uncertainty Activation Cross-Section Data Libraries and collapsed values for different neutron spectra: ADS, FISSION and FUSION"

- **International Conference on Mathematics and Computational Methods applied to Nuclear Science and Engineering (M&C2011)**, Rio de Janeiro (Brazil), May 08-12, 2011

  With the presentation: "Propagation of Nuclear Data Uncertainties in Fuel Cycle Calculations using Monte-Carlo Technique"

Bibliography

[Adams et al., 2009] Adams, B. M., Bohnhoff, W. J., Dalbey, K. R., Eddy, J. P., Eldred, M. S., Gay, D. M., Haskell, K., Hough, P. D., and Swiler, L. P. (2009). DAKOTA, A multilevel parallel object-oriented framework for design optimization, parameter estimation, uncertainty quantification, and sensitivity analysis. Technical Report SAND2010-2183, SNL. Version 5.0 User's Manual, updated Dec 2010 (Version 5.1) updated Nov 2011 (Version 5.2).

[Akiyama et al., 1982a] Akiyama, M., Furuta, K., Ida, T., Sakata, K., and An, S. (1982a). Measurements of beta-ray decay heat of fission products for fast neutron fission of ^{235}U, ^{239}Pu, and ^{233}U. *Journal of the Atomic Energy Society of Japan*, 24(10):803.

[Akiyama et al., 1982b] Akiyama, M., Furuta, K., Ida, T., Sakata, K., and An, S. (1982b). Measurements of gamma-ray decay heat of fission products for fast neutron fission of ^{235}U, ^{239}Pu, and ^{233}U. *Journal of the Atomic Energy Society of Japan*, 24(9):709.

[Algora et al., 2010] Algora, A., Jordan, D., Taín, J. L., Rubio, B., Agramunt, J., Perez-Cerdan, A. B., Molina, F., Caballero, L., Nácher, E., Krasznahorkay, A., Hunyadi, M. D., Gulyás, J., Vitéz, A., Csatlós, M., Csige, L., Äystö, J., Penttilä, H., Moore, I. D., Eronen, T., Jokinen, A., Nieminen, A., Hakala, J., Karvonen, P., Kankainen, A., Saastamoinen, A., Rissanen, J., Kessler, T., Weber, C., Ronkainen, J., Rahaman, S., Elomaa, V., Rinta-Antila, S., Hager, U., Sonoda, T., Burkard, K., Hüller, W., Batist, L., Gelletly, W., Nichols, A. L., Yoshida, T., Sonzogni, A. A., and Peräjärvi, K. (2010). Reactor decay heat in ^{239}Pu: Solving the γ discrepancy in the 4-3000-s cooling period. *Physical Review Letters*, 105(20):202501.

[Álvarez-Velarde et al., 2007] Álvarez-Velarde, F., León, P. T., and González, E. M. (2007). EVOLCODE2, a combined neutronics and burn-up evolution simulation code. In *Proc. 9th Information Exchange Meeting on Actinide and Fission Product P&T*, Nîmes, France.

[Álvarez-Velarde et al., 2009] Álvarez-Velarde, F., Sanz, J., and González, E. M. (2009). Report of the numerical results from the evaluation of the nuclear data sensitivities, priority list and table of required accuracies for nuclear data. Technical Report Deliverable D5.1, Domain DM5 NUDATRA, EUROTRANS Project (FI6W-CT-2004-516520).

[Artioli, 2006] Artioli, C. (2006). Specification for EFIT core and fuel element. Technical Report Deliverable 1.6, Domain DM1 DESIGN, EUROTRANS Project (FI6W-CT-2004-516520).

[Arwade et al., 2010] Arwade, S. R., Moradi, M., and Louhghalam, A. (2010). Variance decomposition and global sensitivity for structural systems. *Engineering Structures*, 32(1):1–10.

[Buss et al., 2011] Buss, O., Hoefer, A., and Neuber, J. (2011). NUDUNA - Nuclear Data Uncertainty Analysis. In *Proc. Int. Conf. on Nuclear Criticality (ICNC 2011)*, Edinburgh, Scotland.

[Cabellos, 2013] Cabellos, O. (2013). Presentation and discussion of the UAM Exercise I-1b: pin-cell burn-up benchmark with the Hybrid Method. *Science and Technology of Nuclear Installations*, 2013. Article ID 790206.

[Cabellos et al., 2014] Cabellos, O., De Fusco, V., Díez, C. J., Martínez, J. S., González, E. M., Cano-Ott, D., and Álvarez-Velarde, F. (2014). Testing JEFF-3.1.1 and ENDF/B-VII.1 decay and fission yield nuclear data libraries with fission pulse neutron emission and decay heat experiments. *Nuclear Data Sheets*, 118(0):472–475.

[Cabellos et al., 2011a] Cabellos, O., Díez, C. J., Koning, A. J., and González, E. M. (2011a). Activation data libraries for Monte Carlo uncertainty propagation in fuel cycle code ACAB. Technical Report Deliverable D2.1, WP2, ANDES Project (FP7-249671).

[Cabellos et al., 2013] Cabellos, O., Díez, C. J., Koning, A. J., and González, E. M. (2013). Report on the impact of uncertainties of the fission product nuclear data on the inventory of the irradiated fuel for ACAB. Technical Report Deliverable D2.6, WP2, ANDES Project (FP7-249671).

[Cabellos et al., 2011b] Cabellos, O., García-Herranz, N., Díez, C. J., Álvarez-Cascos, R., Sanz, J., Ogando, F., and Sauvan, P. (2011b). Propagation of nuclear data uncertainties in transmutation calculations using ACAB code. *Journal of the Korean Physical Society*, 59(23):1268–1271.

[Cacuci, 2003] Cacuci, D. G. (2003). *Sensitivity and uncertainty analysis*. Chapman Hall/CRC, London.

[Ceresio et al., 2011] Ceresio, C., Cabellos, O., Martínez, J. S., and Díez, C. J. (2011). UPM Results BWR-PWR Exercise I-1 by MCNP5 code. Presented at the 5th UAM Workshop, Stockholm, Sweden, 13-15 April.

[Chadwick et al., 2014] Chadwick, M. B., Dupont, E., Bauge, E., Blokhin, A., Bouland, O., Brown, D. A., Capote, R., Carlson, A., Danon, Y., De Saint Jean, C., Dunn, M., Fischer, U., Forrest, R. A., Frankle, S. C., Fukahori, T., Ge, Z., Grimes, S. M., Hale, G. M., Herman, M., Ignatyuk, A., Ishikawa, M., Iwamoto, N., Iwamoto, O., Jandel, M., Jacqmin, R., Kawano, T., Kunieda, S., Kahler, A., Kiedrowski, B., Kodeli, I., Koning, A. J., Leal, L., Lee, Y. O., Lestone, J. P., Lubitz, C., MacInnes, M., McNabb, D., McKnight, R., Moxon, M., Mughabghab, S. F., Noguere, G., Palmiotti, G., Plompen, A., Pritychenko, B., Pronyaev, V., Rochman, D., Romain, P., Roubtsov, D., Schillebeeckx, P., Salvatores, M., Simakov, S., Soukhovitski, E. S., Sublet, J. C., Talou, P., Thompson, I., Trkov, A., Vogt, R., and van der Marck, S. C. (2014). The CIELO collaboration: neutron reactions on ^{1}H, ^{16}O, ^{56}Fe, ^{235,238}U, and ^{239}Pu. *Nuclear Data Sheets*, 118(0):1–25.

[Chadwick et al., 2011] Chadwick, M. B., Herman, M., Obložinský, P., Dunn, M. E., Danon, Y., Kahler, A. C., Smith, D. L., Pritychenko, B., Arbanas, G., Arcilla, R., Brewer, R., Brown, D. A., Capote, R., Carlson, A. D., Cho, Y. S., Derrien, H., Guber, K., Hale, G. M., Hoblit, S., Holloway, S., Johnson, T. D., Kawano, T., Kiedrowski, B. C., Kim, H., Kunieda, S., Larson, N. M., Leal, L., Lestone, J. P., Little, R. C., McCutchan, E. A., MacFarlane, R. E., MacInnes, M., Mattoon, C. M., McKnight, R. D., Mughabghab, S. F., Nobre, G. P. A., Palmiotti, G., Palumbo, A., Pigni, M. T., Pronyaev, V. G., Sayer, R. O., Sonzogni, A. A., Summers, N. C., Talou, P., Thompson, I. J., Trkov, A., Vogt, R. L., van der Marck, S. C., Wallner, A., White, M. C., Wiarda, D., and Young, P. G. (2011). ENDF/B-VII.1 nuclear data for science and technology: cross sections, covariances, fission product yields and decay data. *Nuclear Data Sheets*, 112(12):2887–2996.

[Chadwick et al., 2006] Chadwick, M. B., Obložinský, P., Herman, M., Greene, N. M., McKnight, R. D., Smith, D. L., Young, P. G., MacFarlane, R. E., Hale, G. M., Frankle, S. C., Kahler, A. C., Kawano, T., Little, R. C., Madland, D. G., Moller, P., Mosteller, R. D., Page, P. R., Talou, P., Trellue, H., White, M. C., Wilson, W. B., Arcilla, R., Dunford, C. L.,

Mughabghab, S. F., Pritychenko, B., Rochman, D., Sonzogni, A. A., Lubitz, C. R., Trumbull, T. H., Weinman, J. P., Brown, D. A., Cullen, D. E., Heinrichs, D. P., McNabb, D. P., Derrien, H., Dunn, M. E., Larson, N. M., Leal, L. C., Carlson, A. D., Block, R. C., Briggs, J. B., Cheng, E. T., Huria, H. C., Zerkle, M. L., Kozier, K. S., Courcelle, A., Pronyaev, V., and van der Marck, S. C. (2006). ENDF/B-VII.0: next generation evaluated nuclear data library for nuclear science and technology. *Nuclear Data Sheets*, 107(12):2931–3060.

[Chiba, 2007] Chiba, G. (2007). ERRORJ - A code to process neutron-nuclide reaction cross section covariance, version 2.3. Technical Report JAEA-Data/Code 2007-007, JAEA.

[Crouch, 1977] Crouch, E. A. C. (1977). Fission-product yields from neutron-induced fission. *Atomic Data and Nuclear Data Tables*, 19(5):417–532.

[CSEWG, 2012] CSEWG (2012). ENDF-6 Formats Manual. Data formats and procedures for the Evaluated Nuclear Data Files ENDF/B-VI and ENDF/B-VII. Technical Report BNL-90365-2009 Rev.2, ENDF-102, BNL.

[Cullen, 2012] Cullen, D. E. (2012). *PREPRO 2012: 2012 ENDF/B Pre-processing Codes*. report IAEA-NDS-39, Rev. 15.

[Dagpunar, 1988] Dagpunar, J. (1988). *Principles of random variate generation*. Oxford science publications. Clarendon Press.

[Dickens et al., 1981] Dickens, J. K., Love, T. A., McConnell, J. W., and Peelle, R. W. (1981). Fission-product energy release for times following thermal-neutron fission of Plutonium-239 and Plutonium-241 between 2 and 14,000 s. *Nuclear Science and Engineering*, 78(2):126–146.

[Díez et al., 2014a] Díez, C. J., Buss, O., Porsch, A. H. D., and Cabellos, O. (2014a). Comparison of nuclear data uncertainty propagation methodologies for PWR burn-up simulations. Submitted on July 29 2014 to *Annals of Nuclear Energy*.

[Díez et al., 2011] Díez, C. J., Cabellos, O., and Martínez, J. S. (2011). Propagation of nuclear data uncertainties in fuel cycle calculations using Monte Carlo technique. In *Proc. Int. Conf. on Mathematics and Computational Methods Applied to Nuclear Science and Engineering (M&C 2011)*, Rio de Janeiro, RJ, Brazil.

[Díez et al., 2012] Díez, C. J., Cabellos, O., and Martínez, J. S. (2012). Analysis of different uncertainty activation cross section data libraries for LWR, ADS and DEMO neutron spectra. *EPJ Web of Conferences*, 27:00005.

[Díez et al., 2014b] Díez, C. J., Cabellos, O., and Martínez, J. S. (2014b). Impact of nuclear data uncertainties on advanced fuel cycles and their irradiated fuel – a comparison between libraries . *Nuclear Data Sheets*, 118(0):538–541.

[Díez et al., 2014c] Díez, C. J., Cabellos, O., and Martínez, J. S. (2014c). Nuclear data uncertainty propagation in depletion calculations using cross section uncertainties in one-group or multi-group. Accepted for publishing on June 29 2014 in *Nuclear Data Sheets*.

[Díez et al., 2014d] Díez, C. J., Cabellos, O., Martínez, J. S., Stankovskiy, A., Van den Eynde, G., Schillebeeckx, P., and Heyse, J. (2014d). Analysis of ^{238}Pu and ^{56}Fe evaluated data for use in MYRRHA. *Nuclear Data Sheets*, 118(0):516–518.

[Díez et al., 2013a] Díez, C. J., Cabellos, O., Rochman, D., Koning, A. J., and Martínez, J. S. (2013a). Monte Carlo uncertainty propagation approaches in ADS burn-up calculations. *Annals of Nuclear Energy*, 54(0):27–35.

[Díez et al., 2013b] Díez, C. J., Herrero, J. J., Cabellos, O., and Martínez, J. S. (2013b). Propagation of cross-section uncertainties in criticality calculations in the framework of UAM-Phase I using MCNPX-2.7e and SCALE-6.1. *Science and Technology of Nuclear Installations*, 2013. Article ID 380284.

[Díez et al., 2013c] Díez, C. J., Stankovskiy, A., Malambu, E., Žerovnik, G., Schillebeeckx, P., Van den Eynde, G., Heyse, J., and Cabellos, O. (2013c). Review of the $^{\mathrm{nat}}$C(n,γ) cross section and criticality calculations of the graphite moderated reactor BR1. *Annals of Nuclear Energy*, 60(0):210–217.

[Dossantos-Uzarralde, 2008] Dossantos-Uzarralde, P. J.and Guittet, A. (2008). A Polynomial Chaos Approach for Nuclear Data Uncertainties Evaluations. *Nuclear Data Sheets*, 109(12):2894–2899.

[Dunford, 2008] Dunford, C. L. (2008). *ENDF Utility Codes Release 6.13*. OECD/NEA Data Bank USCD1214/05.

[England and Rider, 1994] England, T. R. and Rider, B. F. (1994). Evaluation and compilation of fission product yields. Technical Report LA-UR-94-3106, ENDF-349, LANL.

[Fiorini and Vasile, 2011] Fiorini, G. L. and Vasile, A. (2011). European Commission – 7th Framework Programme: The Collaborative Project on European Sodium Fast Reactor (CP ESFR). *Nuclear Engineering and Design*, 241(9):3461–3469.

[Fiorito et al., 2014] Fiorito, L., Díez, C. J., Cabellos, O., Stankovskiy, A., Van den Eynde, G., and Labeau, P. E. (2014). Fission yield covariance generation and uncertainty propagation through fission pulse decay heat calculation. *Annals of Nuclear Energy*, 69(0):331–343.

[Forrest, 2007] Forrest, R. A. (2007). The European Activation File: EAF-2007 neutron-induced cross section library. Technical Report UKAEA FUS 534, EURATOM/UKAEA Fusion Association.

[Forrest et al., 2008] Forrest, R. A., Kopecky, J., and Koning, A. J. (2008). Revisions and improvement of neutron capture cross sections for EAF-2009 and validation of TALYS calculations. Technical Report UKAEA FUS 546, UKAEA.

[García-Herranz et al., 2010] García-Herranz, N., Cabellos, O., Álvarez-Velarde, F., Sanz, J., González, E. M., and Juan, J. (2010). Nuclear data requirements for the ADS conceptual design EFIT: Uncertainty and sensitivity study. *Annals of Nuclear Energy*, 37(11):1570–1579.

[García-Herranz et al., 2008] García-Herranz, N., Cabellos, O., Sanz, J., Juan, J., and Kuijper, J. C. (2008). Propagation of statistical and nuclear data uncertainties in Monte Carlo burn-up calculations. *Annals of Nuclear Energy*, 35(4):714–730.

[Gauld et al., 2010] Gauld, I. C., Ilas, G., Murphy, B. D., and Weber, C. F. (2010). Validation of SCALE 5 decay heat predictions for LWR spent nuclear fuel. Technical Report NUREG/CR-6972, ORNL.

[Gentle, 2003] Gentle, J. E. (2003). *Random number generation and Monte Carlo methods*. Springer, New York, 2nd edition.

[Ghanem and Red-Horse, 1999] Ghanem, R. and Red-Horse, J. (1999). Propagation of probabilistic uncertainty in complex physical systems using a stochastic finite element approach. *Physica D: Nonlinear Phenomena*, 133(1–4):137–144.

[Gilli, 2013] Gilli, L. (2013). *Uncertainty quantification in reactor physics using adjoint/perturbation techniques and adaptive spectral methods*. A thesis, Delft University of Technology, Delft, The Netherlands.

[Haldar and Mahadevan, 2000] Haldar, A. and Mahadevan, S. (2000). *Probability, reliability, and statistical methods in engineering design*. John Wiley, New York.

[Hardy et al., 1977] Hardy, J. C., Carraz, L. C., Jonson, B., and Hansen, P. G. (1977). The essential decay of pandemonium: A demonstration of errors in complex beta-decay schemes. *Physics Letters B*, 71(2):307–310.

[Herman et al., 2011] Herman, M. W., Obložinský, P., Mattoon, C. M., Pigni, M., Hoblit, S., Mughabghab, S. F., Sonzogni, A. A., Talou, P., Chadwick, M. B., Hale, G. M., Kahler, A. C., Kawano, T., Little, R. C., and Young, P. G. (2011). COMMARA-2.0 neutron cross section covariance library. Technical Report BNL-94830-2011, BNL.

[IAEA, 1974] IAEA (1974). Fission Product Nuclear Data (FPND). Technical Report IAEA-169, IAEA.

[IAEA, 2001] IAEA (2001). Compilation and evaluation of fission yield nuclear data. Technical Report IAEA-TECDOC-1168, IAEA.

[Isotalo and Aarnio, 2011] Isotalo, A. E. and Aarnio, P. A. (2011). Comparison of depletion algorithms for large systems of nuclides. *Annals of Nuclear Energy*, 38(2–3):261–268.

[Ivanov et al., 2013] Ivanov, K., Avramova, M., Kamerow, S., Kodeli, I., Sartori, E., Ivanov, E., and Cabellos, O. (2013). Benchmarks for uncertainty analysis in modelling (UAM) for the design, operation and safety analysis of LWRs. Technical Report NEA/NSC/-DOC(2013)7, OECD/NEA.

[JAERI, 2013] JAERI (2013). JENDL-4.0u website. `http://wwwndc.jaea.go.jp/jendl/j40/update/`.

[James, 1987] James, M. (1987). A review of libraries of fission product yields. In *Proc. of a Specialists Meeting on Data for Decay Heat Predictions*, NEACRP-L; 302 / NEANDC; 245-U, page 69, Studsvik, Sweden.

[James et al., 1991] James, M. F., Mills, R. W., and Weaver, D. R. (1991). A new evaluation of fission product yields and the production of a new library (UKFY2) of independent and cumulative yields. Part I. Methods and outline of the evaluation. Technical Report AEA-TRS-1015.

[Katakura, 2003] Katakura, J. I. (2003). A new set of parameters for 5 Gaussian fission yields systematics. In *Proc. Int. Conf. on Nuclear Criticality Safety (ICNC2003)*, Tokai-mura, Japan.

[Katakura, 2012] Katakura, J. I. (2012). JENDL FP Decay Data File 2011 and Fission Yields Data File 2011. Technical Report JAEA-Data/Code 2011-025, JAEA.

[Katakura, 2013] Katakura, J. I. (2013). Uncertainty analyses of decay heat summation calculations using JENDL, JEFF, and ENDF files. *Journal of Nuclear Science and Technology*, 50(8):799–807.

[Katakura et al., 2001] Katakura, J. I., Yoshida, T., Oyamatsu, K., and Tachibana, T. (2001). JENDL FP Decay Data File 2000. Technical Report JAERI-1343, JAERI.

[Kawano and Chadwick, 2013] Kawano, T. and Chadwick, M. B. (2013). FPY data evaluation for ENDF/B-VII.1. In *WPEC - Subgroup 37 Kick-off meeting*, NEA, Issy-les-Moulineaux, France.

[Kellet et al., 2009] Kellet, M. A., Bersillon, O., and Mills, R. W. (2009). The JEFF-3.1/-3.1.1 radioactive decay data and fission yields sub-libraries. Technical Report JEFF Report 20, OECD/NEA Data Bank.

[Kinsey, 1979] Kinsey, R. (1979). ENDF-102, data formats and procedures for the Evaluated Nuclear Data File, ENDF. Technical Report BNL-50496 2nd Edition, BNL. revised by B. Magurno (Nov 1983).

[Kodeli, 2008] Kodeli, I. (2008). *SUSD3D*. NEA Data Bank NEA-1628/03.

[Kodeli, 2010] Kodeli, I. (2010). *ANGELO-LAMBDA*. NEA Data Bank NEA-1798/03.

[Koning et al., 2011] Koning, A. J., Bauge, E., Dean, C. J., Dupont, E., Fischer, U., Forrest, R. A., Jacqmin, R., Leeb, H., Kellett, M. A., Mills, R. W., Nordborg, C., Pescarini, M., Rugama, Y., and Rullhusen, P. (2011). Status of the JEFF nuclear data library. *Journal of the Korean Physical Society*, 59(23):1057–1062.

[Koning et al., 2009] Koning, A. J., Hilaire, S., and Duijvestijn, M. (2009). *TALYS-1.2: A nuclear reaction program*. NRG.

[Koning et al., 2013a] Koning, A. J., Hilaire, S., and Goriely, S. (2013a). *TALYS-1.6: A nuclear reaction program*. NRG.

[Koning and Rochman, 2008a] Koning, A. J. and Rochman, D. (2008a). TENDL-2008: Consistent TALYS-based evaluated nuclear data library including covariance data. Technical Report JEF/DOC-1262, OECD/NEA Data Bank.

[Koning and Rochman, 2008b] Koning, A. J. and Rochman, D. (2008b). TENDL-2008: TALYS-based evaluated nuclear data library. `http://www.talys.eu/tendl-2008/`.

[Koning and Rochman, 2008c] Koning, A. J. and Rochman, D. (2008c). Towards sustainable nuclear energy: Putting nuclear physics to work. *Annals of Nuclear Energy*, 35(11):2024–2030.

[Koning and Rochman, 2009a] Koning, A. J. and Rochman, D. (2009a). TENDL-2009: Consistent TALYS-based evaluated nuclear data library including covariance data. Technical Report JEF/DOC-1310, OECD/NEA Data Bank.

[Koning and Rochman, 2009b] Koning, A. J. and Rochman, D. (2009b). TENDL-2009: TALYS-based evaluated nuclear data library. `http://www.talys.eu/tendl-2009/`.

[Koning and Rochman, 2010] Koning, A. J. and Rochman, D. (2010). TENDL-2010: TALYS-based evaluated nuclear data library. `ftp://ftp.nrg.eu/pub/www/talys/tendl2010/tendl2010.html`.

[Koning and Rochman, 2012] Koning, A. J. and Rochman, D. (2012). Modern nuclear data evaluation with the TALYS code system. *Nuclear Data Sheets*, 113(12):2841–2934.

[Koning et al., 2013b] Koning, A. J., Rochman, D., van der Marck, S. C., Kopecky, J., Sublet, J. C., Pomp, S., Sjostrand, H., Forrest, R., Bauge, E., Henriksson, H., Cabellos, O., Goriely, S., Leppanen, J., Leeb, H., Plompen, A., and Mills, R. W. (2013b). TENDL-2013: TALYS-based evaluated nuclear data library. `www.talys.eu/tendl-2013.html`.

[Little et al., 2008] Little, R. C., Kawano, T., Hale, G. D., Pigni, M. T., Herman, M., Obložinský, P., Williams, M. L., Dunn, M. E., Arbanas, G., Wiarda, D., McKnight, R. D., McKamy, J. N., and Felty, J. R. (2008). Low-fidelity Covariance Project. *Nuclear Data Sheets*, 109(12):2828–2833.

[MacFarlane and Kahler, 2010] MacFarlane, R. E. and Kahler, A. C. (2010). Methods for processing ENDF/B-VII with NJOY. *Nuclear Data Sheets*, 111(12):2739 – 2890.

[Madland and England, 1976] Madland, D. G. and England, T. R. (1976). Distribution of independent fission-product yields to isomeric states. Technical Report LA-6595-MS, LANL.

[Madland and Nix, 1982] Madland, D. G. and Nix, J. R. (1982). New calculation of prompt fission neutron spectra and average prompt neutron multiplicities. *Nuclear Science and Engineering*, 81:213–271.

[Marsaglia and Tsang, 2004] Marsaglia, G. and Tsang, W. W. (2004). The 64-bit universal RNG. *Statistics & Probability Letters*, 66(2):183–187.

[Mattoon et al., 2012] Mattoon, C. M., Brown, D., and Elliott, J. B. (2012). Covariance applications with Kiwi. *EPJ Web of Conferences*, 27:00002.

[McLane and CSEWG, 1996] McLane, V. and CSEWG (1996). ENDF-201 ENDF/B-VI Summary documentation supplement I, ENDF/HE-VI summary documentation. Technical Report BNL-NCS-17541, ENDF-201, BNL.

[Mills, 1995] Mills, R. W. (1995). *Fission product yield evaluation.* A thesis, University of Birmingham, Birmingham, UK.

[Mills, 2013] Mills, R. W. (2013). WPEC subgroup 37 Description. In *WPEC - Subgroup 37 Kick-off meeting*, NEA, Issy-les-Moulineaux, France.

[Mills et al., 2013] Mills, R. W., Cabellos, O., Díez, C. J., Koning, A. J., and González, E. M. (2013). Report with transmutation calculations for advanced reactors with new covariance data + updated sensitivity tables. Technical Report Deliverable D2.5, WP2, ANDES Project (FP7-249671).

[Musgrove et al., 1973] Musgrove, A. R., Cook, J. L., and Trimble, G. D. (1973). Prediction of unmeasured fission product yields. In *IAEA Panel on Fission Product Nuclear Data*, volume IAEA-169 2, page 163, Bologna, Italy.

[OECD/NEA Data Bank, 2012] OECD/NEA Data Bank (2012). JEFF-3.1.2 Evaluated Data Library - Neutron data. `http://www.oecd-nea.org/dbforms/data/eva/evatapes/jeff_31/JEFF312/`.

[OECD/NEA Data Bank, 2014] OECD/NEA Data Bank (2014). JEFF-3.2 Evaluated Data Library - Neutron data. `http://www.oecd-nea.org/dbforms/data/eva/evatapes/jeff_32/`.

[ORNL, 2009] ORNL (2009). *SCALE: A modular code system for performing standardized computer analysis for licensing evaluation.* ORNL/TM-2005/39, Version 6.0.

[Otuka et al., 2011] Otuka, N., Dunaeva, S., Dupont, E., Schwerer, O., and Blokhin, A. (2011). The role of the nuclear reaction data centres in experimental nuclear data knowledge sharing. *Journal of the Korean Physical Society*, 59(23):1292–1297.

[Pelowitz, 2008] Pelowitz, D. B. (2008). MCNPX Users Manual. Technical Report LA-CP-07-1473, LANL.

[Pigni et al., 2013] Pigni, M. T., Gauld, I. C., Williams, M. L., Havluj, F., Wiarda, D., and Ilas, G. (2013). Applications of decay data and fission product yield covariance matrices in uncertainty quantification on decay heat. In *WPEC - Subgroup 37 Kick-off meeting*, NEA, Issy-les-Moulineaux, France.

[Rimpault et al., 2002] Rimpault, G., Plisson, D., Tommasi, J., Jacqmin, R., Rieunier, J. M., Verrier, D., and Biron, D. (2002). The ERANOS code and data system for fast reactor neutronic analyses. In *Proc. Int. Conf. PHYSOR 2002: Conference on the New Frontiers of Nuclear Technology*, pages 7–10, Seoul, Korea.

[Rineiski, 2011] Rineiski, A. (2011). Synthesis of options to optimize feedback coefficients. Technical Report SP2.1.3. Deliverable 1, CP-ESFR Project, Contract Number 232658.

[Rochman and Koning, 2010] Rochman, D. and Koning, A. J. (2010). TENDL-2010: Reaching completeness and accuracy. Technical Report JEF/DOC-1349, OECD/NEA Data Bank.

[Rochman et al., 2014] Rochman, D., Zwermann, W., van der Marck, S. C., Koning, A. J., Sjöstrand, H., Helgesson, P., and Krzykacz-Hausmann, B. (2014). Efficient use of Monte Carlo: Uncertainty propagation. *Nuclear Science and Engineering*, 177(3):337–349.

[Rudstam, 1992] Rudstam, G. (1992). Isomeric yields in fission. In *Fission Product Nuclear Data*, pages 271–287, Tokai, Japan. OECD. NEA/NSC/DOC(92)9.

[Salvatores et al., 2008] Salvatores, M., Aliberti, G., Dunn, M., Hogenbirk, A., Ignatyuk, A., Ishikawa, M., Kodeli, I., Koning, A. J., McKnight, R., Mills, R. W., Obložinský, P., Palmiotti, G., Plompen, A., Rimpault, G., Rugama, Y., Talou, P., and Yang, W. S. (2008). Uncertainty and target accuracy assessment for innovative systems using recent covariance data evaluations. Technical Report NEA/WPEC-26, OECD/NEA.

[Santamarina et al., 2009] Santamarina, A., Bernard, D., Blaise, P., Coste, M., Courcelle, A., Huynh, T. D., Jouanne, C., Leconte, P., Litaize, O., Mengelle, S., Noguère, G., Ruggiéri, J.-M., Sérot, O., Tommasi, J., Vaglio, C., and Vidal, J.-F. (2009). The JEFF-3.1.1 Nuclear Data Library. Technical Report JEFF Report 22, OECD/NEA Data Bank.

[Sanz et al., 2008] Sanz, J., Cabellos, O., and García-Herranz, N. (2008). *ACAB-2008: ACtivation ABacus code V2008*. OECD/NEA Data Bank NEA-1839.

[Schier and Couchell, 1997] Schier, W. A. and Couchell, G. P. (1997). Beta and gamma decay heat measurements between 0.1 s and 50,000 s for neutron fission of ^{235}U, ^{238}U, and ^{239}Pu: Final report. Technical Report DOE/ER/40723-4, USDOE.

[Schmidt, 2013] Schmidt, K. H. (2013). A new evaluation method based on covariances from the GEF model. In *WPEC - Subgroup 37 Kick-off meeting*, NEA, Issy-les-Moulineaux, France.

[Schmidt and Jurado, 2010] Schmidt, K. H. and Jurado, B. (2010). General model description of fission observables. Technical Report EFNUDAT. `http://www.cenbg.in2p3.fr/IMG/pdf_final_efnudat_report2.pdf`.

[Schmidt and Jurado, 2012] Schmidt, K. H. and Jurado, B. (2012). Prompt-neutron and prompt-gamma emission from a general description of the fission process. Technical Report JEF/DOC-1423, OECD/NEA Data Bank.

[Serot et al., 2005] Serot, O., Wagemans, C., and Heyse, J. (2005). New results on Helium and Tritium gas production from ternary fission. *AIP Conference Proceedings*, 769(1):857–860.

[Shibata et al., 2011] Shibata, K., Iwamoto, O., Nakagawa, T., Iwamoto, N., Ichihara, A., Kunieda, S., Chiba, S., Furutaka, K., Otuka, N., Ohasawa, T., Murata, T., Matsunobu, H., Zukeran, A., Kamada, S., and Katakura, J. I. (2011). JENDL-4.0: A new library for nuclear science and engineering. *Journal of Nuclear Science and Technology*, 48(1):1–30.

[Shibata et al., 2002] Shibata, K., Kawano, T., Nakagawa, T., Iwamoto, O., Katakura, J. I., Fukahori, T., Chiba, S., Hasegawa, A., Murata, T., Matsunobu, H., Ohsawa, T., Nakajima, Y., Yoshida, T., Zukeran, A., Kawai, M., Baba, M., Ishikawa, M., Asami, T., Watanabe, T., Watanabe, Y., Igashira, M., Yamamuro, N., Kitazawa, H., Yamano, N., and Takano, H. (2002). Japanese Evaluated Nuclear Data Library version 3 revision-3: JENDL-3.3. *Journal of Nuclear Science and Technology*, 39(11):1125–1136.

[Sobol, 2001] Sobol, I. M. (2001). Global sensitivity indices for nonlinear mathematical models and their Monte Carlo estimates. *Mathematics and Computers in Simulation*, 55(1–3):271–280.

[Stankovskiy et al., 2014] Stankovskiy, A., Malambu, E., Van den Eynde, G., and Díez, C. J. (2014). Nuclear data needs for the neutronic design of MYRRHA fast spectrum research reactor. *Nuclear Data Sheets*, 118(0):513–515.

[Sublet et al., 2010] Sublet, J.-C., Packer, L. W., Kopecky, J., Forrest, R. A., Koning, A. J., and Rochman, D. (2010). The European Activation File: EAF-2010 neutron-induced cross section library. Technical Report CCFE-R (10) 05, CCFE.

[Sublet et al., 2012] Sublet, J.-C. C., Eastwood, J. W., and Morgan, J. G. (2012). The FISPACT-II User Manual. Technical Report CCFE-R(11)11 Issue 3, CCFE.

[Suyama and Mochizuki, 2005] Suyama, K. and Mochizuki, H. (2005). Effect of neutron induced reactions of Neodymium-147 and 148 on burnup evaluation. *Journal of Nuclear Science and Technology*, 42(7):661–669.

[Talou, 2007] Talou, P. (2007). Prompt fission neutrons calculations in the Madland-Nix model. Technical Report LA-UR-07-8168, LANL.

[Tobias, 1980] Tobias, A. (1980). Decay heat. *Progress in Nuclear Energy*, 5(1):1–93.

[Tobias, 1989] Tobias, A. (1989). Derivation of decay heat benchmarks for U235 and Pu239 by a least squares fit to measured data. Technical Report RD/B–6210/R89, CEGB.

[Tuli, 1995] Tuli, J. K. (1995). Nuclear Wallet Cards. Technical report, BNL. Fifth edition.

[Venard et al., 2009] Venard, C., Santamarina, A., Leclainche, A., and Mounier, C. (2009). The RIB tool for the determination of computational bias and associated uncertainty in the CRISTAL criticality-safety package. In *Proc. 2009 Nuclear Criticality Safety Division (NCSD 2009) Topical Meeting on Realism, Robustness and the Nuclear Renaissance*, Richland, WA, USA.

[Wahl, 1985] Wahl, A. C. (1985). Nuclear-charge distribution near symmetry for thermal-neutron-induced fission of ^{235}U. *Physical Review C*, 32:184–194.

[Wahl, 1988] Wahl, A. C. (1988). Nuclear-charge distribution and delayed-neutron yields for thermal-neutron-induced fission of ^{235}U, ^{233}U, and ^{239}Pu and for spontaneous fission of ^{252}Cf. *Atomic Data and Nuclear Data Tables*, 39(1):1–156.

[Wahl, 2002] Wahl, A. C. (2002). Systematics of fission-product yields. Technical Report LA-13928, LANL.

[Wiarda and Dunn, 2008] Wiarda, D. and Dunn, M. E. (2008). PUFF-IV: A code for processing ENDF uncertainty data into multigroup covariance matrices. Technical Report ORNL/TM-2006/147/R1, ORNL.

[Wieselquist et al., 2013] Wieselquist, W., Zhu, T., Vasiliev, A., and Ferroukhi, H. (2013). PSI methodologies for nuclear data uncertainty propagation with CASMO-5M and MCNPX: Results for OECD/NEA UAM Benchmark Phase I. *Science and Technology of Nuclear Installations*, 2013. Article ID 549793.

[Wong et al., 2005] Wong, C. P. C., Malang, S., Sawan, M., Smolentsev, S., Majumdar, S., Merrill, B., Sze, D. K., Morley, N., Sharafat, S., and Dagher, M. (2005). Assessment of first wall and blanket options with the use of liquid breeder. *Fusion Science and Technology*, 47(3):502–509.

[X-5 Monte Carlo Team, 2003] X-5 Monte Carlo Team (2003). MCNP – A General Monte Carlo N-Particle transport code. Technical Report LA-CP-03-0245, LANL. Version 5.

[Žerovnik et al., 2012] Žerovnik, G., Trkov, A., and Kodeli, I. A. (2012). Correlated random sampling for multivariate normal and log-normal distributions. *Nuclear Instruments and Methods in Physics Research Section A: Accelerators, Spectrometers, Detectors and Associated Equipment*, 690(0):75–78.

[Žerovnik et al., 2013] Žerovnik, G., Trkov, A., Smith, D. L., and Capote, R. (2013). Transformation of correlation coefficients between normal and lognormal distribution and implications for nuclear applications. *Nuclear Instruments and Methods in Physics Research Section A: Accelerators, Spectrometers, Detectors and Associated Equipment*, 727(0):33–39.

[Zhu et al., 2014] Zhu, T., Rochman, D., Vasiliev, A., Ferroukhi, H., Wieselquist, W., and Pautz, A. (2014). Comparison of two approaches for nuclear data uncertainty propagation in MCNPX for selected fast spectrum critical benchmarks. *Nuclear Data Sheets*, 118(0):388–391.

[Zwermann et al., 2009] Zwermann, W., Krzykacz-Hausmann, B., Gallner, L., and Pautz, A. (2009). Influence of nuclear covariance data on reactor core calculations. In *Proc. Second Int. Workshop on Nuclear Data Evaluation for Reactor Applications (WONDER 2009)*, pages 99–104, Cadarache, France.

[Zwermann et al., 2012] Zwermann, W., Krzykacz-Hausmann, B., Gallner, L., Pautz, A., and Velkov, K. (2012). Aleatoric and epistemic uncertainties in sampling based nuclear data

uncertainty and sensitivity analyses. In *Proc. Int. Conf. PHYSOR 2012: Conference on Advances in Reactor Physics - Linking Research, Industry, and Education*, Knoxville, TN, USA.